November 2020

U/Pb Zircon Ages of Felsic Veins in the Sawtooth Metamorphic Complex, Idaho, U.S.A: Implications for Magmatism and Vein Source

Kyle Tollefson
Louisiana State University and Agricultural and Mechanical College

U/PB ZIRCON AGES OF FELSIC VEINS IN THE SAWTOOTH METAMORPHIC COMPLEX, IDAHO, U.S.A: IMPLICATIONS FOR MAGMATISM AND VEIN SOURCE

A Thesis

Submitted to the Graduate Faculty of the
Louisiana State University and
Agricultural and Mechanical College
in partial fulfillment of the
requirements for the degree of
Master of Science

in

The Department of Geology and Geophysics

by
Kyle Tollefson
B.S., University of Wisconsin – Eau Claire, 2017
December 2020

ACKNOWLEDGMENTS

I would like to thank my advisor Dr. Barbara Dutrow who provided the scientific context and samples for this project as well as helped me secure funding. Also, for her support, motivation, and for teaching me the many soft skills needed to become a great scientist. She pushed me to be the best I could be and taught me the skills necessary to succeed in my future endeavors. I would also like to thank my other committee members Dr. Darrell Henry and Dr. Adam Forte who provided their invaluable expertise regarding the conceptual aspects of my project

I thank Andrew Webb for assistance with polishing thin sections as well as help with setting up the equipment and instruments needed for heavy mineral separation. I thank Dr. Peter Horvath for help with the electron microprobe data collection. I thank Meridith Miska for her help in mounting and polishing the zircon pucks needed for U-Pb geochronology as well as for helping with SEM imaging of the zircons. A special thanks to Dr. Andreas Möller from University of Kansas, for collecting the U-Pb isotope data of the zircons and reducing the data during the unprecedented Covid-19 pandemic. A special thanks as well to Dr. Paul Mueller who provided expertise with U-Pb zircon data reduction and interpretation of zircon ages.

Financial support for this project was provided by the American Federation of Mineralogical Societies to Dr. Dutrow. I would also like to thank the LSU Department of Geology and Geophysics for awarding me a graduate teaching assistantship that provided financial support during my graduate studies.

TABLE OF CONTENTS

LIST OF TABLES

LIST OF FIGURES

ABSTRACT

Veins associated with igneous activity provide numerous insights into the geologic history of an area. The Sawtooth Metamorphic Complex (SMC) in Idaho is a roof pendent of high-grade rocks cross-cut by numerous felsic veins of unknown age and source. Obtaining U/Pb zircon geochronology of these veins can facilitate understanding the ages of magmatism in the region, their source, when nearby batholiths were juxtaposed to the SMC, and provide additional insights into the geologic evolution of the area. Each potential source of these veins has a distinct age: the Sawtooth batholith (ca. 47 Ma), the Idaho batholith (98-53 Ma), an anatectic melt associated with aluminous gneisses in the complex (>100 Ma), an undefined later melting and/or hydrothermal event (<43 Ma), or a combination of the these. In each of these potential sources, plagioclase optical cathodoluminescence (OM-CL) responses are obtained to determine any correlation with vein source and as an alternative proxy to ages.

U/Pb ages of zircons were obtained for six vein samples spatially separated around the SMC. The ages range from 72.3 ± 1.2 Ma to 131.0 ± 2.2 Ma. Two samples contained zircons with inherited cores, with ages ranging from 317 ± 7 Ma to 1803 ± 55 Ma. Vein emplacement ages, determined by youngest ages, range from 75.5 ± 0.6 Ma to 101 ± 1 Ma. Zircon formation ages indicate an extended period of magmatism occurred episodically for at least 49 Ma. inherited core ages indicate incorporation of rocks containing Proterozoic and Ordovician-aged zircons. Vein emplacement ages are consistent with the Idaho batholith time frame suggesting the SMC was juxtaposed to the Idaho batholith before vein emplacement.

Evaluation of OM-CL responses show that green plagioclase CL responses are characteristic of the Idaho batholith. Green is observed in ten of thirteen samples. This suggests that age and plagioclase CL color correlate for the Idaho batholith. This correlation suggests that OM-CL

plagioclase responses may be a useful proxy for source in the absence of geochronology. This study contributes new U/Pb zircon age data in a region that is poorly understood.

CHAPTER I. INTRODUCTION

Veins are found in many rocks and form from magmatic melts and hydrothermal solutions initiated from a variety of igneous (intrusion) or metamorphic (anatectic) processes. As such, veins are significant because they yield insight into the magmatic, metamorphic, structural, and/or tectonic evolution of the region (e.g. Bons et al., 2012; Kylander-Clark and Hacker, 2014). Emplacement of veins is controlled by far field processes such as the stress, strain, pressure, and temperature, and near field processes such as fluid composition, distance from the source, and crystallization paths. Minerals and structural indicators found within the veins may record these processes as well as the relative and absolute timing of vein emplacement (Bons et al., 2012). In felsic veins, zircon is likely. Zircons without any inherited component or the overgrowth rims on inherited cores reflect the emplacement age of veins. Inherited zircon cores within veins serve as a probe into subsurface geology (e.g. Gaschnig et al., 2008; Gaschnig et al., 2013). Thus, mineralogy, source and age of veins provide additional constraints on the geologic history of a region.

Within the Sawtooth Metamorphic Complex (SMC), a roof pendant of high-grade rocks located near Stanley, Idaho, numerous veins crosscut the metamorphic lithologies (Dutrow, personal communication). Thus, this area is optimally suited for vein-related studies. The SMC roof pendant is unique in the region because most basement rocks in the area are unavailable due to the pervasive magmatism of the Idaho batholith and Challis magmatic province.

The purpose of this study is to (1) characterize the mineralogy of select veins crosscutting the SMC, (2) obtain U/Pb zircon age dates on a subset of these veins, (3) evaluate chemical and optical signatures as a proxy for vein source, (4) determine the likely source of the veins, and (5) relate the source of the veins to the geologic evolution of the area.

Studying these veins within the SMC complements existing metamorphic studies in the area and could provide insights into the age and extent of previous magmatism, potential rocks in the subsurface, relative timing of metamorphism in the complex, as well as buoyancy and weakening of rocks which impact uplift and tectonic processes.

CHAPTER II. BACKGROUND

First mapped as undifferentiated Precambrian metamorphic rocks (Reid, 1963), the Sawtooth Metamorphic Complex (SMC) is located within the Sawtooth Range of Idaho, U.S.A. (Fig. 1). The complex is bounded by the Atlanta lobe of the Idaho batholith on the south and west, the Sawtooth batholith to the north, and the Sawtooth Fault to the east (e.g. Dutrow et al., 1995; Metz, 2010; Reid, 1963; Thackray et al., 2013) (Fig. 2).

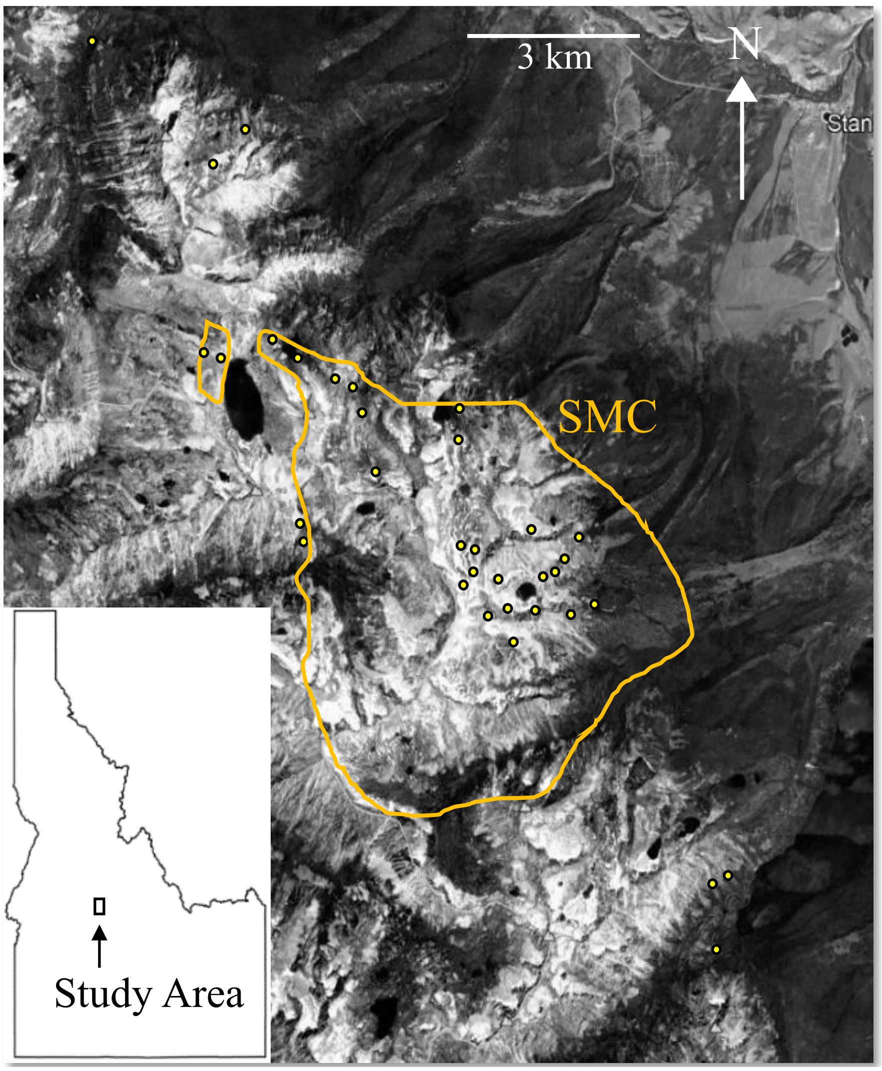

Figure 1. Google Earth map showing location of the Sawtooth Metamorphic Complex (SMC) and samples for this study (yellow circles). Extent of the complex from B. Dutrow (personal communication) and based on Metz (2010).

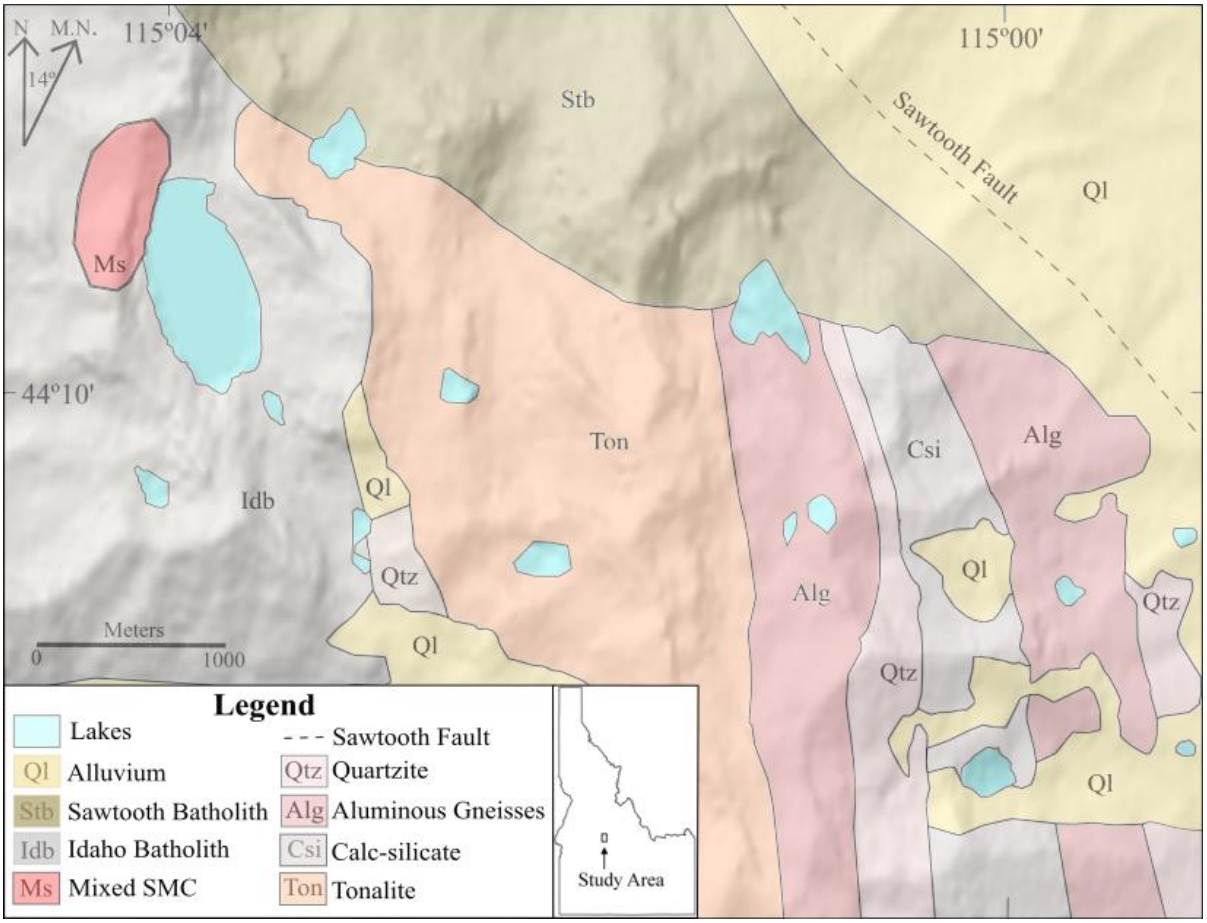

Figure 2. Geologic map showing major lithologies within the Sawtooth Metamorphic Complex and surrounding units. Modified from Bergeron (2012).

Later studies characterized the lithologies of the SMC to contain a series of high-grade metamorphic rocks that include aluminous gneisses, amphibolites, calc-silicate gneisses, marbles, metapsammites, and quartzofeldspathic gneisses as major units (e.g. Metz, 2010).

At least three deformational and two metamorphic events are recorded in the calc-silicate gneisses (Fukai and Dutrow, 2017). Mineral assemblages and textures combined with geothermobarometry in the aluminous gneisses indicate clock-wise P-T-t paths that suggest the SMC experienced burial to mid-lower crust depths and exhumation within a collisional tectonic setting (e.g. Smith, 2016). Some garnet-bearing rocks within the SMC are migmatites (Metz, 2010) and retain evidence of anatectic melting. The interpreted residual melt has rare potassium

feldspar suggesting an earlier melting episode extracted this component from the garnet-bearing rocks (Smith, 2016).

Within the SMC, there are numerous felsic veins (Fig. 3) that vary in size from centimeter-scale to tens-of-meters (e.g. Ma et al., 2017). These veins occur as concordant lenses between SMC lithologies (Metz, 2010) and as discordant veins that cross-cut outcrop-scale banding and foliation (Fukai, 2013). The veins are not restricted to a single lithology or area. Felsic veins are quartz bearing, so if enough zirconium is present, zircon will crystallize. These felsic veins are suggested to have formed in the presence of hydrous fluids and an oxidizing environment (personal communication, Paul Mueller) which impacts zircon chemistry. In an oxidizing environment U^{6+} is mobile while Th remains immobile (e.g. Keppler and Wyllie,

Figure 3. Photos of the numerous felsic veins crosscutting the metamorphic rocks within the SMC. The veins range in width from centimeter to tens of meters and are fine grained to pegmatitic. (Photo Credit: B. Dutrow).

1991). An oxidizing environment results in zircon grains with high U and low Th during vein crystallization. Therefore, a low Th/U ratio is indicative of zircon growth during crystallization of these felsic veins in the SMC (Rubatto, 2002).

A portion of a previous study by Ma (2015), looked at granitic and gabbroic intrusions within the SMC to constrain the timing of tectonic processes as well as gain insight to the sub-SMC crust. Ma determined the granitic intrusions to be part of four separate phases of magmatism that occurred at ca.120 Ma, ca. 97-96 Ma, ca. 91-87 Ma, and ca. 84-73 Ma. However, for a subset of samples procured from Ma, U/Pb zircon vein crystallization ages have an age range of 77 ± 1 Ma to 101 ± 1 Ma (Tab .1). These intrusions were hypothesized to be sourced by magma injection from beneath the SMC or by in-situ anatectic melting of aluminous gneisses, which Ma found both to be plausible sources for the intrusions.

Table 1. Locations and ages of Ma (2015) samples

Sample Number/unit	**Latitude (N)**	**Longitude (W)**	**Age ± 2σ**
MC13ST-05	44°08.494’	115°00.023’	
MC13ST-14	44°08.455’	115°00.299’	77 ± 1 Ma
MC13ST-18	44°08.566’	114°59.223’	92 ± 1 Ma
MC14ST-04	44°09.248’	115°00.017’	92 ± 1 Ma
MC14ST-08	44°09.174’	114°59.395’	99 ± 1 Ma
MC14ST-10	44°08.485’	115°00.587’	84 ± 1 Ma
MC14ST-12	44°08.492’	115°00.450’	101 ± 1 Ma
MC14ST-13	44°08.493’	114°59.470’	95 ± 1 Ma

2.1. Sawtooth Batholith

To the northeast and south, the Sawtooth batholith (STB) bounds the SMC. The STB is associated with the intrusive suites of the Challis volcanic field which range in age from 51 to 43 Ma (Armstrong et al., 1977; Gaschnig et al., 2010). The intrusive suites include the pink granite

suite consisting of granite and the quartz monzodiorite suite consisting of granite, granodiorite, quartz monzodiorite, diorite, and gabbro (Armstrong et al., 1977; Bennett and Knowles, 1985; Lewis and Kiilsgaard, 1991; Reid, 1963).

The pink granite suite is characterized by distinct pink perthitic alkali feldspars (Fig. 4) and by its subequal amounts of alkali feldspar, quartz, and plagioclase (Kiilsgaard et al., 1970; Lewis and Kiilsgaard, 1991; Reid, 1963). The pink granite suite also contains minor hornblende, biotite, muscovite, and accessory zircon, apatite, titanite, allanite, ilmenite, and magnetite (Kiilsgaard et al., 1970; Lewis and Kiilsgaard, 1991; Reid, 1963). This pink granite suite is a two feldspar subsolvus granite, but also contains perthitic alkali feldspar.

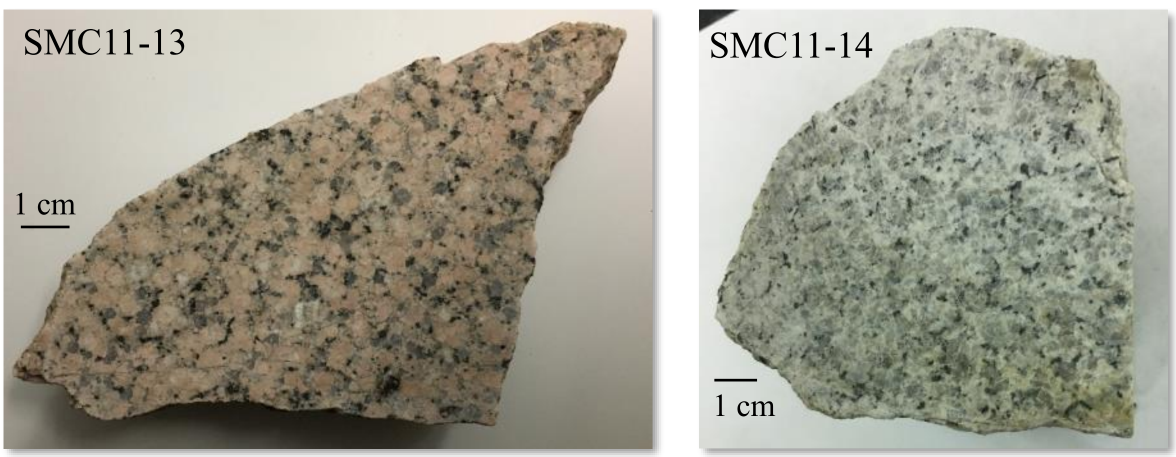

Figure 4. Photographs of hand samples showing distinct differences between the Sawtooth batholith (SMC11-13) and Idaho batholith (SMC11-14). For additional information see (Dutrow et al., 2014).

The quartz monzodiorite suite is characterized by variable proportions of plagioclase, quartz, alkali feldspar, hornblende, and biotite (Kiilsgaard and Lewis, 1985; Lewis and Kiilsgaard, 1991). The quartz monzodiorite suite also contains accessory apatite, titanite, allanite, and zircon (Kiilsgaard and Lewis, 1985; Lewis and Kiilsgaard, 1991).

The STB is comprised of the pink granite suite (Fig. 4) (e.g. Reid, 1963). U/Pb zircon ages of two samples near the SMC give crystallization dates of 47.1 ± 0.7 Ma and 46.6 ± 0.6 Ma

(Dutrow et al., 2014). Another sample of STB collected farther from the SMC than the previous two samples gives an U/Pb zircon crystallization date of 44.9 ± 1.0 Ma (Gaschnig et al., 2010).

2.2. Idaho Batholith

To the west, the Idaho batholith (IB) bounds the SMC. The IB covers a large region in Idaho and is comprised of a northern Bitterroot lobe and southern Atlanta lobe. The SMC is within the Atlanta lobe which contains lithologies of tonalite, hornblende-biotite granodiorite, porphyritic granodiorite, biotite granodiorite, muscovite-biotite granite, and leucocratic granite (Kiilsgaard and Lewis, 1985). The tonalite contains major biotite and quartz, minor alkali feldspar, hornblende, and accessory titanite, allanite, apatite, magnetite, and zircon (Kiilsgaard and Lewis, 1985). It is gray, medium-to-coarse grained and dark gray with some alteration of feldspar into sericite (Kiilsgaard and Lewis, 1985).

The hornblende-biotite granodiorite is characterized by the presence of hornblende and contains major quartz, plagioclase, alkali feldspar, and biotite with accessory titanite and allanite (Kiilsgaard and Lewis, 1985). It is gray to dark gray and has weak to prominent foliation (Kiilsgaard and Lewis, 1985).

The porphyritic granodiorite is characterized by feldspar megacrysts and contains major quartz, plagioclase, alkali feldspar, biotite, minor hornblende, and accessory titanite, apatite, allanite, and zircon (Kiilsgaard and Lewis, 1985; Reid, 1963). It is medium to coarse grained, typically foliated, contains moderate to pervasive feldspars altered to sericite, and pervasive biotite altered to chlorite (Kiilsgaard and Lewis, 1985; Reid, 1963).

The biotite granodiorite is characterized by predominant plagioclase with lesser alkali feldspar and quartz (Kiilsgaard and Lewis, 1985; Reid, 1963). The biotite granodiorite contains minor biotite and accessory muscovite, hornblende, allanite, titanite, opaques, and zircon

(Kiilsgaard and Lewis, 1985; Reid, 1963). It is light gray, medium to coarse grained, and contains pervasive sericite from feldspar alteration and chlorite from biotite alteration (Kiilsgaard and Lewis, 1985; Reid, 1963).

The muscovite-biotite granite is characterized by igneous muscovite (Kiilsgaard and Lewis, 1985). The muscovite-biotite granite contains major quartz, alkali feldspar, plagioclase, minor biotite, and local garnet (Kiilsgaard and Lewis, 1985). It is light gray and medium to coarse grained (Kiilsgaard and Lewis, 1985).

The leucocratic granite is characterized by its white to light gray color (Kiilsgaard and Lewis, 1985; Reid, 1963). The leucocratic granite contains sub-equal amounts of plagioclase, alkali feldspar, and quartz with minor biotite, local garnet, accessory magnetite, allanite, apatite, and zircon (Kiilsgaard and Lewis, 1985; Reid, 1963). It is fine to medium grained and contains moderate sericite altered from feldspars and chlorite altered from biotite (Kiilsgaard and Lewis, 1985; Reid, 1963).

The differing lithologies that make up the Atlanta lobe of the IB, range in age from ca. 98 to 64 Ma (Gaschnig et al., 2010; Kiilsgaard and Lewis, 1985). However, the only lithologies observed near the SMC are porphyritic granodiorite, biotite granodiorite, and leucocratic granite (Reid, 1963). Four samples of IB collected near the SMC are grey in hand specimen (Fig. 4), with one having an U/Pb zircon crystallization age of 85.0 ± 2.4 Ma (Dutrow et al., 2014) and the three others having U/Pb crystallization ages of 92 ± 1 Ma, 92 ± 1 Ma, and 89 ± 1 Ma (Ma, 2015). Gaschnig and colleagues (2013) conducted a study on inherited zircon cores found within the IB. In this study they separated the Atlanta lobe of the IB into a northern and southern portion. In the southern portion, inherited core ages formed two major peaks at 2550 Ma and 670 Ma. For the northern portion of the Atlanta lobe, the majority of inherited core ages range from

2000 to 1000 Ma, containing peaks at 1700 to 1600 Ma and 1500 to 1400 Ma. Two cores of Ordovician age were also found in the Northern Atlanta lobe.

2.3. Potential Felsic Vein Sources

Within the SMC region, several possibilities exist for the source of the felsic veins that crosscut the complex. Each of these sources is characterized by a distinct age range and each source contains feldspars. Potential sources for these veins include: (1) The STB. If sourced by the STB, veins will have crystallization ages of ca. 47 Ma (Dutrow et al., 2014).

(2) The Atlanta lobe of the IB. If sourced by the IB, veins will have crystallization ages within the range of ca. 98 to 64 Ma (Gaschnig et al., 2010; Kiilsgaard and Lewis, 1985).

(3) Anatectic melt derived from melting of aluminous gneisses. These conditions would have occurred near the peak of metamorphism, prior to exhumation. Peak metamorphic conditions for the aluminous gneisses occurred at a minimum depth of 22.5 km (Smith, 2016). The Idaho batholith which is found at the same elevations as the aluminous gneisses, has a maximum emplacement depth of its base at 18 km (Hyndman, 1981). To create the current day configuration of the Idaho batholith and aluminous gneisses, anatectic melts would have had to form at a depth greater than 22.5 km and then experience exhumation to a depth shallower than 18 km before emplacement of the Idaho batholith. Therefore, if anatectic melts are the vein sources, veins will have crystallization ages older than the Idaho batholith (~100 Ma).

(4) Another (unidentified) melting and/or hydrothermal event. Hydrothermal alteration has occurred throughout Idaho and could be a potential source of veining (Criss et al., 1991). An unidentified event would be suggested by an age unrelated to the proposed sources above.

(5) Multiple of these events. If there are multiple sources for these veins, age data for each event would be present.

2.4. Optical Microscope Cathodoluminescence (OM-CL)

Optical microscope cathodoluminescence (OM-CL) is a fast, powerful technique which elucidates textures not observed in plain-polarized light (PPL) or cross-polarized light (XPL). Cathodoluminescence occurs when the sample is excited by energetic electrons and generates photons in the visible light range. These responses can be indicative of structural defects or trace elements within the minerals (Tab. 2) (e.g. Geake et al., 1973; Götze, 2012; Götze et al., 2013; Marfunin, 1979). Plagioclase has a wide range of color responses in CL which make it a useful mineral to detect differences among samples (Götze, 2012). Previous studies have tested whether these differing CL color responses could be used to determine the provenance of that feldspar grain (e.g. Scholonek and Augustsson, 2016).

Table 2. Suggested trace element CL activators for feldspars from (Goetze, 2012).

CL Color	***Suggested Activator***
Purple	Eu^{2+} Cu^{2+}
Dark Blue	Al-O^{-}-Al center Al-O-Ti
Light Blue	$O^{—}Si…M^{+}$
Green-Yellow	Mn^{2+}
Red	Fe^{3+}

2.5. Zirconium Saturation Temperature

Calculating the zircon solubility in crustal melts is dependent on the zirconium content of the melt, the composition, and the temperature (Watson and Harrison, 1983). Therefore, determining whole rock major and trace elements allows for the calculation of the zirconium saturation temperature (Boehnke et al., 2013). If zirconium saturation is attained, zircon will form.

Zirconium saturation temperatures have been used to determine minimum (zirconium undersaturated magmas) and maximum (zirconium saturated magmas) magma temperatures as well as to understand preservation of inheritance within rock samples (Miller et al., 2003). If a rock sample has no zircon inheritance, the calculated zirconium saturation temperature can also be used as the temperature of crystallization (Miller et al., 2003).

CHAPTER III. METHODS

To characterize the veins mineralogy, textures, and ages, several optical and analytical methods were used. Veins were made into thin sections for petrographic studies to determine the mineral assemblages, textures, and rock types of all veins. Select vein samples had zircons separated to obtain U/Pb age dates. Potential vein sources in the region all have distinct age ranges allowing for use of vein age as a source proxy. Feldspar mineral chemistry and optical cathodoluminescence plagioclase responses were evaluated as potential proxies of vein source by comparison of potential source samples to that of veins with undetermined source.

3.1. Sample Selection

Samples of lithologies that are possible vein sources as well as vein samples of undetermined source were selected for optical, mineralogical, and geochronologic study. Samples starting with LF or SMC were collected previously by B. Dutrow from 2011 through 2016. Thin sections of samples with known U/Pb ages, collected by Ma (2015), were available for petrographic and cathodoluminescent plagioclase response analyses. Samples starting with MC##ST were collected by Chong Ma from 2013 through 2014. Samples studied were selected to ensure a large spatial distribution (Tab. 3). Samples with previously obtained whole rock geochemical data with zirconium values were selected to calculate zirconium saturation temperatures. Two samples displaying differing OM-CL plagioclase responses were chosen for mineral chemical analysis. A subset of samples with sufficient material were selected for U/Pb zircon geochronology.

Table 3. Location data for all samples.

Sample Number/unit	Latitude (N)	Longitude (W)
Sawtooth Batholith		
LF-12	N.D.	N.D.
SMC11-012	44°01.138’	114°56.427’
SMC11-013	44°06.047’	114°57.670’
SMC13-39	44°12.772’	115°03.923’
SMC13-42	44°12.510’	115°04.257’
Idaho Batholith		
SMC11-014a	44°06.056’	114°57.566’
MC14ST-19	44°09.278’	115°03.085’
MC14ST-21	44°09.147’	115°03.081’
MC14ST-25	44°05.510’	114°57.557’
Leucocratic Granite Phase of IB		
SMC15-05	44°10.323’	115°14.715’
Anatectic Melts		
SMC12-111	44°08.491’	115°00.454’
SMC12-116	44°08.482’	115°00.444’
SMC12-117	44°08.504’	115°00.432’
SMC14-48c	44°08.777’	115°00.522’
SMC15-41	44°08.786’	115°00.954’

LF and SMC samples collected by B. Dutrow.

Sample Number/unit	Latitude (N)	Longitude (W)
Vein Samples		
SMC11-30	N.D.	N.D.
SMC13-05	44°10.554’	115°02.692’
SMC13-31	44°09.051’	115°00.801’
SMC13-132	44°08.513’	115°00.438’
SMC14-09	44°08.842’	114°59.757’
SMC14-11	44°10.262’	115°01.018’
SMC14-26	44°09.994’	115°01.019’
SMC14-40	44°09.048’	115°01.005’
SMC14-43	44°09.765’	115°02.176’
SMC14-44	44°10.258’	115°02.313’
SMC14-47	44°10.964’	115°03.458’
SMC14-61	44°10.829’	115°04.397’
SMC14-62	44°10.769’	115°04.147’
SMC14-112	44°08.294’	115°00.355’
SMC15-03	44°10.523’	115°02.504’
SMC16-09	44°08.927’	114°59.599’
SMC16-22	44°10.790’	115°03.140’
SMC16-34	44°08.863’	115°00.845’

MC##ST samples collected by C. Ma.

3.2. Optical Petrography

Polished thin sections of 19 felsic veins of unknown source were prepared for petrographic analyses at Wagner Petrographic in Lindon, UT, and at Louisiana State University. In addition, 8 thin sections from veins of unknown source as well as 14 from potential vein sources were used (collected by Barbara Dutrow and Chong Ma).

Petrographic analyses and point counting of samples were completed on a Leica petrographic microscope fitted with a PELCON automatic point counter stage. Optical petrography was used to examine mineral phases, textures, modal proportions as well as record any samples adequate for use in U/Pb zircon geochronology. Due to plagioclase coronas representing residual melt (Smith, 2016) and not accurately representing the mineral modes of the removed melt, anatectic melt samples were not analyzed petrographically in this study.

Petrographic study of anatectic melts has been completed by Hoffmann (2016) and Smith (2016). To determine the rock classification, three-hundred points were counted with a 1mm spacing for each sample. Normalized point count values were used to determine rock name via the IUGS QAPF classification for plutonic rocks (e.g. Le Bas and Streckeisen, 1991).

For determining a likely source of veins by petrography, samples of known source were compared to vein samples of unknown source. Sawtooth batholith and Idaho batholith samples, as well as the residual of anatectic melts, served as known source reference materials with distinct petrographic characteristics of each source. These distinct characteristics were then compared to vein samples of unknown source to determine similarities that suggest a likely vein source.

3.3. Optical Microscope Cathodoluminescence (OM-CL)

OM-CL observations and imaging of polished and uncoated thin sections were completed in the OPI lab in the Department of Geology and Geophysics at Louisiana State University on a Leica DM 2700P petrographic microscope fitted with a cold cathode Reliotron stage and Leica DFC 7000T low light camera. An electron beam voltage of ~-10kV and beam current of 0.2-0.5 mA was used and the Reliotron stage was under vacuum at 25-40 mTorr. The total amount of light collection varied per sample. After photographing the CL responses of samples, image processing was completed using FastStone image software. Image processing was used to adjust brightness and contrast but did not alter the observed color. Image processing also enhanced textures not seen in optical microscope observations. PPL, XPL and CL photos were taken of the same area. Observed CL colors were matched to a Munsell color chart for distinction (Fig. 5).

Primarily, feldspar OM-CL responses and observed textures were the targeted observations. The observed OM-CL color responses and textures of potential source samples were compared to determine distinct OM-CL characteristics for each potential source.

3.4. Zirconium Saturation Temperature

Whole rock geochemistry of both major and trace elements used for zirconium saturation temperature calculations were based on data obtained in previous work (Dutrow et al., 2014; Ma, 2015). Zirconium saturation temperature calculations used the equation of Boehnke et al. (2013). Calculated zirconium saturation temperatures of the Idaho batholith and Sawtooth batholith were compared for each batholith and to veins of unknown source.

3.5. Backscatter Electron (BSE) Imaging and Electron Microprobe Analysis (EMPA)

Two vein samples of unknown source were imaged using backscatter electrons (BSE) and feldspars analyzed. Data were collected using wavelength dispersive spectrometry (WDS) on the JEOL JXA-8230 Electron Superprobe, housed in the Chevron's Geomaterials lab at LSU's Department of Geology & Geophysics and the Shared Instrumentation Facility. BSE image gray levels are a function of the mean atomic weight and can reveal compositional zoning and/or alteration within minerals. Based on these images, targeted feldspar analysis points were chosen to avoid alteration and to traverse areas of compositional zoning. Analytical points were taken along plagioclase and alkali feldspar rim-rim traverses to determine compositional zoning.

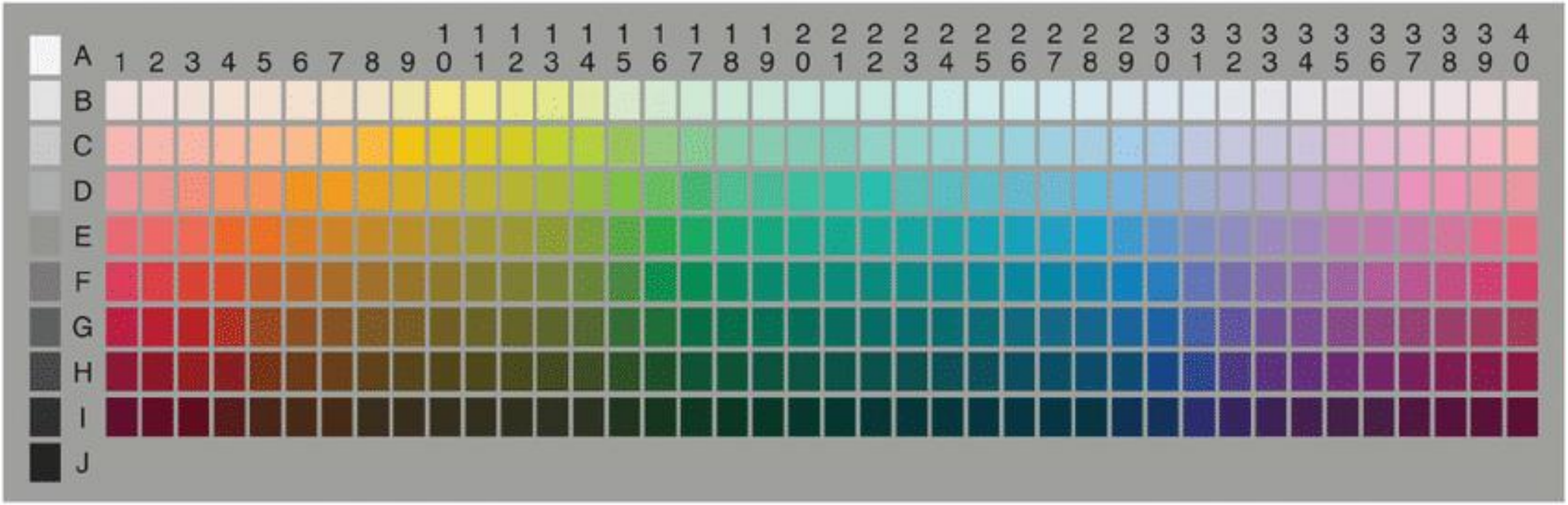

Bright Blue	Moderate Blue	Dark Blue	Bright Green	Moderate Green	Dark Green	Yellowish Green	Yellow	Pink	Red	Brown	Neon Orange	Neon Green
28C 29C 30C	29F 30F	30G 30H	15C 15D	13F 14F	15F 15G	12C 13C	10C 11C	1D 2D	3F 4F 3G	10F 10G	4E 5E	14C

Figure 5. Table of CL colors with Munsell color chart used for reference. Chart taken from (Vejdemo-Johansson et al., 2014).

Operating conditions of the EMPA included an accelerating voltage of 15 kV, a probe current of 20 nA, and a defocused 5 μm electron-beam diameter. Alkali and plagioclase feldspars were analyzed for Si, Al, Fe, Ca, Ba, Na, and K using well-characterized mineral standards (Tab. 4). Fe had a 40 second count time on the peak and 20 second count time on the background. Ba had a 60 second count time on the peak and 30 second count time on the background. All other analyzed elements had a 20 second count time on the peak and 10 second count time on the background. Instrument drift and data quality were examined by measuring multiple secondary standards as unknowns.

Structural formulae were calculated using an excel program (D. Henry, personal communication) that normalized the weight-percent oxide analyses to atoms per formula unit (apfu) based on eight oxygen atoms. Analyses with a total oxide weight percent of below 99% or above 101% were omitted.

Table 4. Standards used for Feldspar EMP analyses

Element Analyzed	**Mineral Standard**
Si	Toronto albite
Al	Toronto plagioclase
Fe	Toronto almandine
Ca	Toronto plagioclase
Ba	Toronto barite
Na	Toronto albite
K	Toronto sanidine

3.6. Heavy Mineral Separation and Imaging

Six samples of felsic veins of unknown source and one sample from a unit mapped as the leucocratic granite phase of the IB (Field notes, B. Dutrow) were chosen for U/Pb zircon geochronologic studies. Each sample had a minimum amount of 3.5 kg (3 kg for heavy mineral separation, 400 g for future whole rock geochemistry work, and 100 g as a hand sample for observations) of rock material.

Rock samples were trimmed to be free of alteration, then crushed, and sieved so all grains were of less than 177 micrometers in size. Vein samples were cut into slabs to minimize contamination and washed with tap water to remove foreign rock particles. Slabs were disaggregated using a jaw crusher and pulverized using a disc grinder within the LSU's Department of Geology & Geophysics rock lab. Crushing was continued until all the material passed through an 80-mesh sieve. The sieved material was then rinsed in tap water and baked at 100 C° overnight. The jaw crusher, disc grinder, and sieves were cleaned with soap and water, rinsed with acetone, and dried between samples to prevent cross contamination.

After the sieved material was dry, a hand magnet was used to remove magnetic grains and metal shavings from the machines used in the disaggregation process. Next the sample was passed through a Frantz magnetic separator multiple times with different front slope, side slope, and amps settings (Tab. 5). The final "non-magnetic" mineral separates were density separated using lithium metatungstate (ρ=2.95 g/mL) to concentrate heavy minerals i.e. zircon. Separated "heavies" were then rinsed with distilled and deionized water.

Table 5. Frantz magnetic separator settings for each sample run

Run	Down Slope	Side Slope	Amps
1	Hand Magnet		
2	10°	10°	0.4
3	10°	10°	1.2
4	10°	3°	Max amps

Zircons were handpicked under a binocular microscope based on optical properties and morphology. Picked zircons were mounted in epoxy blanks with FC-1 (Duluth Gabbro) standards and polished at the University of Florida Center for Isotope Geoscience. Polished pucks were imaged on a Zeiss scanning electron microscope (SEM) at the University of Florida separately using BSE imaging and CL imaging to observe zoning patterns, core and overgrowth relationships and alteration features. SEM-BSE and CL imaging were used to determine the

growth textures of zircons and target analysis points. Imaging and targeted analyses allow for dating of the crystallization age (i.e. magmatic zircons), potentially metamorphic events (i.e. metamorphic overgrowths), and inherited core ages.

3.7. LA-ICP-MS and U/Pb Ages

To obtain U/Pb ages for zircons, U/Pb isotopic analyses of zircon cores and overgrowths were performed at the University of Kansas using the LA-ICP-MS method. Mounted zircon crystals were ablated with a Photon Machines Analyte G2 193nm ArF excimer laser coupled to a Thermo Scientific Element 2 high resolution sector-field ICP-MS. Due to samples having ten times the typical uranium content, spot size was set at 15 µm (Personal communication, Andreas Möller). Fractionation and drift calibration were corrected by using GJ1 zircon (608.5 ± 0.4 Ma) (Jackson et al., 2004) as a calibration standard. Calibration was checked using secondary standards of FCT (28.196 ± 0.038 Ma) (Fish Canyon Tuff) (Wotzlaw et al., 2013), Plesovice (337.13 ± 0.37 Ma) (Sláma et al., 2008), and FC-1 (1099.0 ± 0.6 Ma) (Duluth Gabbro) (Paces and Miller Jr, 1993).

Data reduction was completed using VizualAge data reduction scheme (Petrus et al., 2012) for Iolite software (Hellstrom et al., 2008; Paton et al., 2011; Paton et al., 2010). Reduced ages were corrected for Pb-loss, inheritance, and common Pb (Personal communication, Andreas Möller and Paul Mueller).

Age data were separated into inherited cores and vein crystallization dates by age difference. Large clusters of continuous young dates represent vein crystallization data and few older discontinuous dates represent inherited core data. Statistical analysis could not be completed on inherited core dates due to the small amount of data. Therefore, inherited core dates with <5% discordance are used as acceptable ages.

Reduced $^{206}Pb/^{238}U$ vein crystallization ages were plotted versus $^{206}Pb/^{238}U$ to $^{207}Pb/^{235}U$ discordance to determine if age and discordance were correlated. If no correlation was present, reduced age data were filtered to a discordance of <1% and a Th/U ratio of <0.01 (Pers. Comm. Paul Mueller). The mean age and 2σ were calculated and all dates outside of the calculated 2σ were discarded. Of the resulting dates, the ten youngest were plotted as kernel density estimates (KDEs) using Density Plotter 8.5 (Vermeesch, 2012) to determine age groupings. The youngest age grouping was plotted on a Terra-Wasserburg diagram and weighted mean plot using IsoplotR (Abramson, 1982; Botev et al., 2010; Ludwig, 1998; Ludwig, 2003; Vermeesch, 2012, 2018). Mean ages, 2σ, and 2 s.e.m (standard error of the mean) were calculated for the youngest age group determined by the KDE plots. Calculated ages <1000 Ma are reported as $^{206}Pb/^{238}U$ ages and calculated ages >1000 Ma are reported as $^{207}Pb/^{206}Pb$ ages based on (Bruguier et al., 2001).

To determine potential sources for the veins, vein crystallization ages were compared with the age ranges of potential sources. To determine potential sources of inheritance, core ages were compared to age dates of inherited cores within the IB reported by Gaschnig and colleagues (2013) as well as detrital zircon ages from SMC metapsammites reported by Ma (2015).

CHAPTER IV. RESULTS

Forty-one samples including five Sawtooth batholith, four Idaho batholith, the residual of five anatectic melts, one sample of a unit mapped as the leucocratic granite phase of the IB, and twenty-six veins of unknown source from throughout the SMC were examined via petrographic analyses and OM-CL. Two samples were examined for feldspar mineral chemistry and seven samples had U/Pb zircon geochronology performed (Tab. 6, see also Appendix A.).

Table 6. Methods used on each sample.

Sample Number	**Petrography**	**OM-CL**	**Whole rock Geochemistry**	**Zirconium Saturation Temperature**	**EMPA**	**U/Pb Zircon Geochronology**
			Sawtooth Batholith			
LF-12	x	x	D	x		
SMC11-012	x	x	D	x		D
SMC11-013	x	x	D	x		D
SMC13-39	x	x	D	x		
SMC13-42	x	x	D	x		
			Idaho Batholith			
SMC11-014	x	x	D	x		D
MC14ST-19	x	x	M	x		M
MC14ST-21	x	x	M	x		M
MC14ST-25	x	x	M	x		M
			Idaho Batholith Leucocratic Granite Phase			
SMC15-05	x	x				x
			Anatectic Melts			
SMC12-111	SH	x				
SMC12-116	SH	x				
SMC12-117	SH	x				
SMC14-48c	SH	x				
SMC15-41	SH	x				

x=This study D=(Dutrow, 2014) M=(Ma,2015) SH=(Smith, 2016; Hoffman, 2016)

(table cont'd.)

Sample Number	Petrography	OM -CL	Whole rock Geochemistry	Zirconium Saturation Temperature	EMPA	U/Pb Zircon Geochronology
			Vein Samples			
SMC11-30	x	x				
SMC13-05	x	x				
SMC13-31	x	x				
SMC13-132	x	x	D	x	x	x
SMC14-09	x	x				x
SMC14-11	x	x				x
SMC14-26	x	x				
SMC14-40	x	x				
SMC14-43	x	x				x
SMC14-44	x	x				
SMC14-47	x	x				
SMC14-61	x	x				
SMC14-62	x	x				
SMC14-112	x	x				
SMC15-03	x	x				
SMC16-09	x	x				x
SMC16-22	x	x				x
SMC16-34	x	x			x	
			Vein Samples from Ma (2015)			
MC13ST-05	x	x	M	x		
MC13ST-14	x	x	M	x		M
MC13ST-18	x	x	M	x		M
MC14ST-04	x	x				M
MC14ST-08	x	x	M	x		M
MC14ST-10	x	x	M	x		M
MC14ST-12	x	x	M	x		M
MC14ST-13	x	x	M	x		M

x=This study D=(Dutrow, 2014) M=(Ma,2015) SH=(Smith, 2016; Hoffman, 2016)

4.1. Sawtooth Batholith Samples

Five Sawtooth batholith samples were analyzed in this study. STB samples are easily identified in the field because of their coarse grain size and pink color. STB samples in this study are two feldspar biotite-bearing granites with minor hornblende in four of five samples (Tab. 7). Accessory minerals include variable amounts of apatite, magnetite, and zircon. Secondary minerals include variable amounts of epidote, chlorite, hematite, and sericite. Samples are medium-to-coarse grained and contain pervasive perthitic alkali feldspars (Fig. 6). Myrmekitic texture is present in one sample. Hand specimens are pink-colored and coarse grained (Fig. 4).

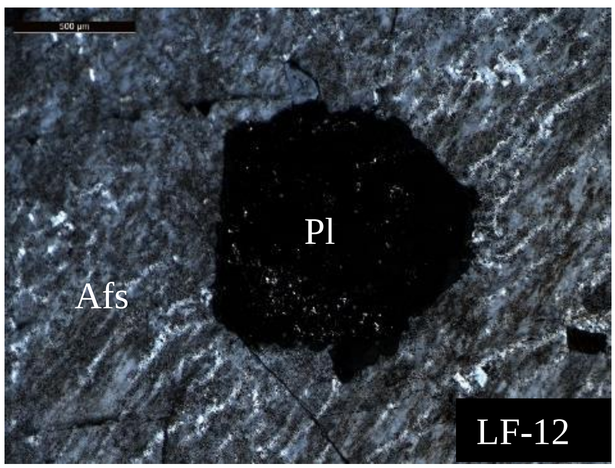

Figure 6. Cross polarized photomicrographs of STB sample LF-12 showing perthitic texture. Scalebar equals 500 microns.

Plagioclase in Sawtooth batholith samples luminesces pink, red, brown, neon green, moderate green, dark-green, and neon orange (Tab. 8). All five STB samples contain albite exsolution with pink OM-CL responses. All samples display pink albite exsolution, however, only four of five STB samples contain plagioclase grains with a pink response (Fig. 7). These four samples also contain plagioclase with brown OM-CL responses; thus, the majority of samples contain plagioclase grains with both pink and/or brown responses. The one sample without pink and/or brown plagioclase responses displays neon orange, neon green and dark green responses (Fig. 7, SMC11-12) which contrasts with the four other samples. This sample is

Table 7. Rock type (based on modes), mineralogy, and textures observed.

Sample Number	Rock Type	Primary Minerals									Alterations					Textures	
		Afs	**Pl**	**Qz**	**Aln**	**Ap**	**Bt**	**Hbl**	**Mag**	**Zrn**	**Czo**	**Ep**	**Chl**	**Hem**	**Ser**	**Perthite**	**Myrmekite**
Sawtooth Batholith																	
LF-12	Monzo-Granite	X	X	X		X	X	X	X	X			X		X	Pe	
SMC11-012	Monzo-Granite	X	X	X			X		X				X	X	X	Pe	
SMC11-013	Syeno-Granite	X	X	X			X	X	X				X	X		Pe	Pe
SMC13-39	Monzo-Granite	X	X	X			X	X	X	X		X	X		X	Pe	
SMC13-42	Syeno-Granite	X	X	X		X	X	X	X	X		X	X	X	X	Pe	
Idaho Batholith																	
SMC11-014a	Granodiorite	X	X	X		X	X		X	X			X		X	Mi	Mo
MC14ST-19	Granodiorite	X	X	X		X	X	X		X	X		X		X	Mi	Mo
MC14ST-21	Granodiorite	X	X	X	X	X	X		X	X	X		X		X	Mi	Mo
MC14ST-25	Granodiorite	X	X	X		X	X		X	X			X		X	Mi	Mi
Leucocratic Phase of Idaho Batholith																	
SMC15-05	Granodiorite	X	X	X	X	X	X		X	X	X	X	X		X	Mi	Mi
Vein Samples																	
MC13ST-05	Monzo-Granite	X	X	X		X	X		X	X	X	X	X	X	X	Mi	
MC13ST-14	Monzo-Granite	X	X	X		X	X		X	X			X		X	Mi	Mo
MC13ST-18	Granodiorite	X	X	X	X	X	X			X	X				X	Mi	
MC14ST-04	Monzo-Granite	X	X	X			X		X	X	X		X		X	Mi	
MC14ST-08	Granodiorite	X	X	X			X		X		X		X	X	X		
MC14ST-10	Granodiorite	X	X	X	X	X	X			X			X		X	Mi	Mi
MC14ST-12	Granodiorite	X	X	X		X	X		X						X		Pe
MC14ST-13	Monzo-Granite	X	X	X		X	X		X	X		X	X		X	Mi	Mo

Mi=Minor Mo=Moderate Pe=Pervasive
Mineral abbreviations from Whitney and Evans (2010).

(table cont'd.)

Sample Number	Rock Type	Primary Minerals									Secondary Minerals					Textures	
		Afs	Pl	Qz	Aln	Ap	Bt	Hbl	Mag	Zrn	Czo	Ep	Chl	Hem	Ser	Perthite	Myrmekite
Vein Samples																	
SMC11-30	Monzo-Granite	X	X	X			X		X				X		X	Mi	Mi
SMC13-05	Granodiorite	X	X	X			X		X	X			X	X	X	Mo	Mi
SMC13-31	Syeno-Granite	X	X	X			X						X		X	Pe	
SMC13-132	Monzo-Granite	X	X	X			X			X	X		X		X	Mi	Pe
SMC14-09	Granodiorite	X	X	X	X	X	X		X	X			X		X	Mi	Mo
SMC14-11	Monzo-Granite	X	X	X			X		X	X			X		X	Pe	
SMC14-26	Monzo-Granite	X	X	X			X		X	X			X	X	X	Mi	Mo
SMC14-40	Monzo-Granite	X	X	X										X	X	Mo	Mi
SMC14-43	Monzo-Granite	X	X	X					X	X				X	X	Mo	
SMC14-44	Monzo-Granite	X	X	X		X	X	X	X	X	X		X		X	Mo	
SMC14-47	Monzo-Granite	X	X	X					X	X					X	Pe	
SMC14-61	Granodiorite	X	X	X	X		X		X	X			X		X	Mi	Mi
SMC14-62	Granodiorite	X	X	X			X		X	X			X		X	Mi	
SMC14-112	Syeno-Granite	X	X	X			X		X		X		X		X	Pe	Mi
SMC15-03	Syeno-Granite	X	X	X			X		X	X			X		X	Pe	
SMC16-09	Monzo-Granite	X	X	X			X			X			X		X	Pe	
SMC16-22	Granodiorite	X	X	X		X		X	X	X					X	Mi	
SMC16-34	Granodiorite	X	X	X		X	X		X	X			X	X	X	Mi	Mi

Mi=Minor Mo=Moderate Pe=Pervasive
Mineral abbreviations from Whitney and Evans (2010).

Table 8. Observed textures, plagioclase OM-CL responses, and alkali feldspar OM-CL responses.

Sample Number	**Plagioclase Response**	**Alkali Feldspar Response**	**Textures**
		Sawtooth Batholith	
LF-12	Pink, brown, and moderate green	Moderate blue with pink albite exsolution	Perthite and highly altered plagioclase cores
SMC11-012	Neon orange, neon green, dark green, and pink	Dark blue with pink albite exsolution	Perthite
SMC11-013	Pink and brown	Dark blue with pink albite exsolution	Perthite and highly altered plagioclase cores
SMC13-39	Pink, red, and brown	Moderate to dark blue with pink albite exsolution	Perthite and highly altered plagioclase cores
SMC13-42	Pink, red, and brown	Moderate blue with pink albite exsolution	
		Idaho Batholith	
SMC11-014a	Bright green and moderate green	Moderate blue and dark blue	Oscillatory zoned plagioclase and myrmekite
MC14ST-19	Moderate green and brown	Bright blue and moderate blue	Myrmekite
MC14ST-21	Moderate green and brown	Bright blue, moderate blue, and red	Myrmekite and red zonation in alkali feldspar
MC14ST-25	Bright green and moderate green	Moderate blue and dark blue	Oscillatory zoned plagioclase
		Leucocratic Phase of Idaho Batholith	
SMC15-05	Moderate green, brown, and red	Bright blue and red with oscillatory zoning	Oscillatory zoned alkali feldspar and myrmekite. Highly altered plagioclase cores
		Anatectic Melts	
SMC12-111	Moderate green and brown	Bright blue and moderate blue	Myrmekite
SMC12-116	Yellowish green and moderate blue	Bright blue	Myrmekite
SMC12-117	Yellowish green and moderate blue		
SMC14-48c	Bright Blue		
SMC15-41	Yellowish green and moderate blue		

(table cont'd.)

Sample Number	Plagioclase Response	Alkali Feldspar Response	Textures
		Vein Samples	
MC13ST-05	Brown	Bright blue, moderate blue, and red	Red zoning in alkali feldspar
MC13ST-14	Moderate green and moderate blue	Bright blue and moderate blue	
MC13ST-18	Moderate green and moderate blue	Moderate blue	
MC14ST-04	Moderate green and moderate blue	Moderate blue	
MC14ST-08	Moderate green and moderate blue	Bright blue	
MC14ST-10	Bright green		Twin plane alteration
MC14ST-12	Moderate green and moderate blue		Myrmekite and twin plane alteration
MC14ST-13	Moderate green and brown	Bright blue and dark blue	Myrmekite
SMC11-30	Moderate green, moderate blue, and brown	Bright blue	
SMC13-05	Pink, bright green, neon orange, and red	Bright blue and moderate blue	Highly altered sample
SMC13-31	Brown	Bright blue	
SMC13-132	Bright green and brown	Bright blue and moderate blue	Twin plane alteration
SMC14-09	Brown and red	Moderate blue and dark blue	Myrmekite
SMC14-11	Moderate green and brown	Dark blue	Twin plane alteration
SMC14-26	Bright blue, brown, and red	Moderate blue	
SMC14-40	Moderate blue, brown, and red	Bright blue	
SMC14-43	Moderate green, red, and orange	Bright blue and moderate blue	highly altered sample
SMC14-44	Brown and red	Moderate blue and red	highly altered sample
SMC14-47	Moderate green, pink, and red	Bright blue and red with pink albite exsolution	Perthite

(table cont'd.)

Sample Number	Plagioclase Response	Alkali Feldspar Response	Textures
		Vein Samples	
SMC14-61	Moderate green, brown, and red	Bright blue, moderate blue, and red with oscillatory zoning	Oscillatory zoned alkali feldspar and highly altered plagioclase cores
SMC14-62	Moderate green, brown, and red	Moderate blue zoned with red and pink albite exsolution	Zoned alkali feldspar and perthite. Highly altered plagioclase cores
SMC14-112	Bright green and moderate blue	Bright blue and moderate blue	
SMC15-03	Moderate green, brown, and pink	Moderate blue with pink albite exsolution	Perthite and highly altered plagioclase cores
SMC16-09	Brown	Bright to moderate blue	
SMC16-22	Yellow	Moderate blue	
SMC16-34	Moderate green and brown	Bright blue, moderate blue, and red with oscillatory zoning	Oscillatory zoned alkali feldspar

located the furthest south of all STB samples and is the furthest from the SMC. A moderate green plagioclase response was also observed in a single grain of a sample with pink and/or brown responses. Alkali feldspar luminesces moderate blue and dark blue (Tab. 8). Three of five samples contain moderate blue alkali feldspar response and three of five samples contain dark blue alkali feldspar responses. Pervasively sericitized plagioclase cores are common and perthitic texture is observed in all samples.

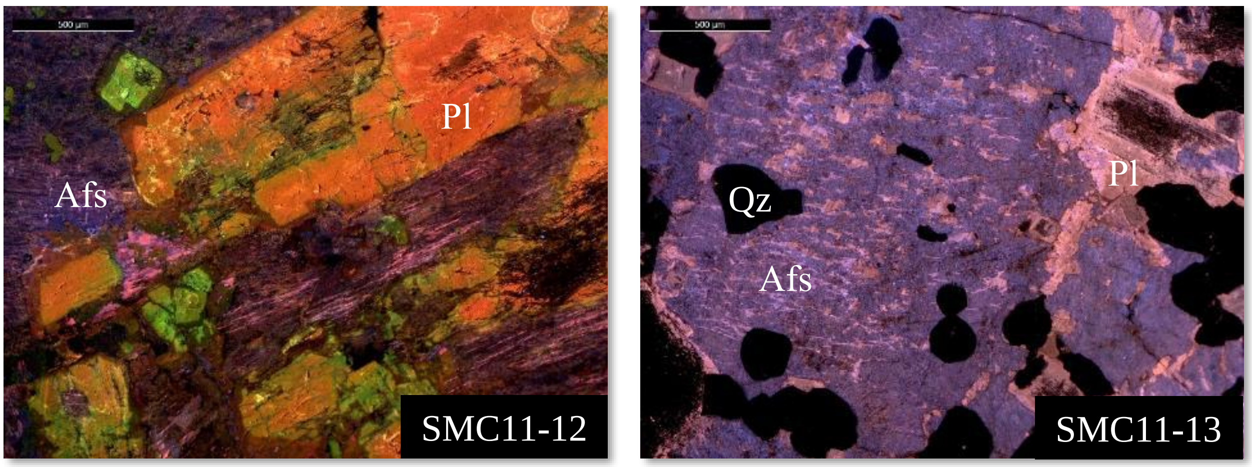

Figure 7. OM-CL photographs of STB samples SMC11-12 and SMC11-13 showing distinct colors of plagioclase CL response: SMC11-12: neon orange, neon green, dark green. SMC11-13: pink plagioclase and perthite within alkali-feldspar (blue). Note highly altered cores observed. Scale bar equals 500 micrometers.

4.2. Idaho Batholith Samples

Four Idaho batholith samples were analyzed in this study. Samples were identified by their mineralogy combined with sample location and U/Pb ages (Dutrow et al., 2014; Ma, 2015). All samples are biotite-bearing granodiorites; one sample contains minor hornblende (Tab. 7). Additional minor minerals include variable amounts of allanite, apatite, magnetite, and zircon. Secondary minerals include clinozoisite, chlorite and sericite. Samples are medium grained, display minor perthite and variable amounts of myrmekite (Fig. 8). Hand specimens are light gray and medium grained (Fig. 4).

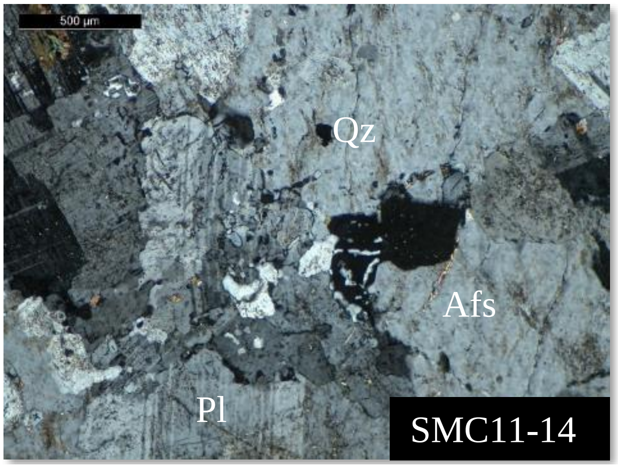

Figure 8. Cross polarized photomicrographs of IB sample SMC11-14 showing myrmekitic texture. Scale bar equals 500 micrometers.

Plagioclase in Idaho batholith samples luminesces light green, moderate green, and brown (Tab. 8). All four IB samples contain plagioclase grains with a moderate green OM-CL response (Fig. 9). Two samples also contain plagioclase with light green CL response and the other two contain dark green plagioclase. Oscillatory zoned plagioclase is observed two of the four samples. Alkali feldspar luminesces bright blue, moderate blue, dark blue, and in some cases, red (Tab. 8). Such color contrasts highlight textural features such as myrmekite which is observed in three of four samples.

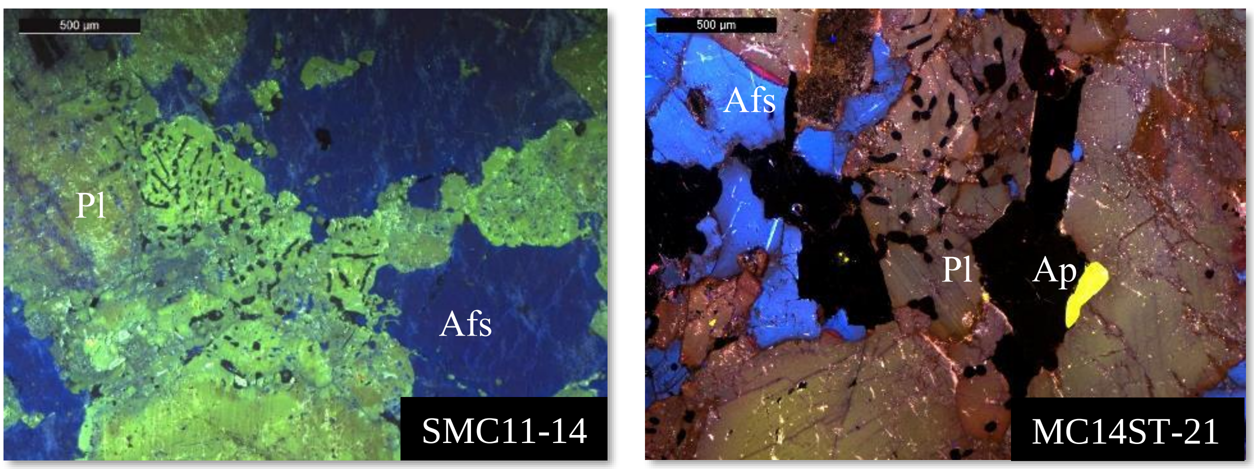

Figure 9. OM-CL image of IB sample SMC11-14 and MC14ST-21 displaying bright green and moderate green plagioclase responses. Myrmekite texture also observed. Cores and altered rims are apparent. Alkali feldspar luminesces blue. Apatite luminescence yellow. Scale bar equals 500 micrometers.

4.3. Anatectic Melt Samples

Five anatectic melt samples were analyzed in this study. Remnants of anatectic melt are preserved in the samples as plagioclase-rich coronas surrounding garnets in the high grade metamorphic rock (Smith, 2016). These coronas largely lack alkali feldspar and primarily contain plagioclase with quartz and biotite.

Plagioclase in anatectic melt samples luminesces bright green, moderate green, bright blue, moderate blue, and brown (Tab. 8). Three of five samples have plagioclase response colors of bright green and/or moderate blue (Fig. 10). Alkali feldspar luminesces deep blue (Tab. 8). Alkali feldspar is rare in coronas and only found in two of the five samples. Within these two samples, myrmekitic texture is also observed.

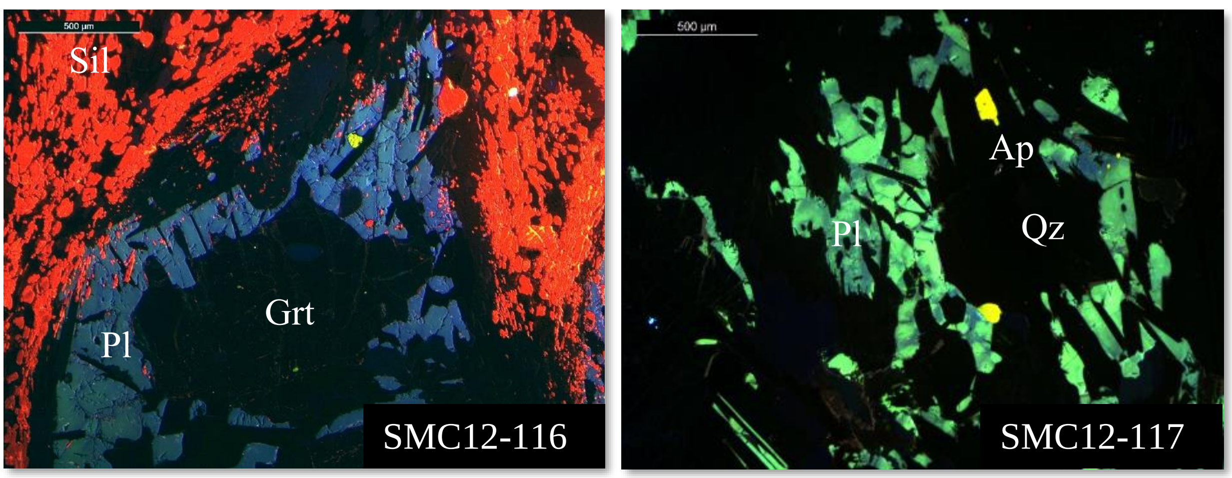

Figure 10. OM-CL photographs of anatectic melt residual showing distinct plagioclase CL responses: 12-116: moderate blue. SMC12-117: plagioclase is yellowish green and moderate blue. Sillimanite luminesces red. Apatite luminesces yellow. Quartz and garnet non-luminescent for these dwell times. Photos: Barbara Dutrow

4.4. Distinct Optical Characteristics of Potential Vein Sources

By comparing distinct plagioclase CL characteristics of each known source to unknown veins, possible provenance can be explored. Distinct characteristics of STB samples are pink color in hand specimen, syeno-granitic composition, pervasive perthite observed as pink albite exsolution in OM-CL, and OM-CL plagioclase responses of pink, neon green, and neon orange.

Distinct characteristics of IB samples are gray color in hand specimen, granodioritic composition, myrmekitic texture and plagioclase OM-CL responses of bright green and moderate green, and red zoned alkali feldspar observed in OM-CL. Distinct characteristics of anatectic melts include plagioclase OM-CL responses of yellowish green, bright blue, and moderate-turquoise blue.

4.5. Vein Samples of Unknown Source

Twenty-seven vein samples were analyzed in this study by thin section. Three are syeno-granites, thirteen are monzo-granites, and eleven are granodiorites (Tab. 7). Likely sources are identified based on petrographic analyses, OM-CL plagioclase colors, and for a subset of samples, U/Pb zircon geochronology.

Veins with a syeno-granite (QAP) composition

Three syeno-granite samples are biotite syeno-granites with variable amounts of accessory magnetite and zircon. Secondary minerals include variable amounts of chlorite, sericite, and clinozoisite. Samples are coarse grained with pervasive perthite and variable amounts of myrmekite.

Plagioclase in these samples luminesces bright green, moderate green, moderate blue, brown, and pink (Tab. 8). Brown plagioclase response is found in two of the three samples and is the only color in multiple samples. Alkali feldspar luminesces bright blue and moderate blue. Perthite and highly altered plagioclase cores are observed in one sample.

Veins with a monzo-granite (QAP) composition

Ten of the monzo-granite samples are biotite monzo-granites and three are leucocratic monzo-granites. One of these sample contains trace hornblende. Minor minerals include variable amounts of magnetite, allanite, apatite, and zircon. Secondary minerals include variable amounts

of chlorite, hematite, sericite, clinozoisite, and epidote. Samples are fine-to-coarse grained and contain little to abundant perthite. Six samples contain myrmekite.

Plagioclase in these thirteen monzo-granite samples luminesces bright green, moderate green, bright blue, moderate blue, brown, red and pink (Tab. 8). Moderate green and/or brown plagioclase responses are most prevalent and are found in all thirteen samples. Alkali feldspar luminesces bright blue, moderate blue, dark blue, and red (Tab. 8). Perthite, myrmekite, and twin plane alteration are observed but are rare.

Veins with a granodiorite (QAP) composition

Ten biotite granodiorites occur within this grouping with one hornblende granodiorite. Minor minerals include variable amounts of allanite, apatite, magnetite, and zircon. Secondary minerals include variable amounts of clinozoisite, epidote, chlorite, hematite, and sericite. Samples are fine-to-coarse grained with variable amounts of perthite and myrmekite.

Plagioclase in the granodiorite samples luminesces bright green, moderate green, moderate blue, brown, red, pink, yellow, and neon orange (Tab. 8). The most prevalent observed plagioclase response was moderate green which occurred in eight of the eleven samples. Alkali feldspar luminesces bright blue, moderate blue, dark blue, and red (Tab. 8). Oscillatory zoning in alkali feldspar is observed in four of the eleven samples. Myrmekite and twin plane alteration are present but rarely observed.

4.6. Zirconium Saturation Temperatures

Major element compositions and trace zirconium content of sixteen samples previously analyzed (Dutrow et al., 2014; Ma, 2015) were used to determine zirconium saturation temperatures (Boehnke et al., 2013) (Tab. 9). Five Sawtooth batholith samples have zirconium

saturation temperatures ranging from 658 to 737 °C with an average of 688 ± 32 °C (1σ), three Idaho batholith samples have a temperature range of 592 to 693 °C with an average temperature

Table 9. Calculated zirconium saturation temperatures based on (Boehnke et al., 2013).

	Sawtooth Batholith					Idaho Batholith		
Sample	LF-12	SMC 11-12	SMC 11-13	SMC 13-39	SMC 13-42	SMC 11-14	MC14 ST-19	MC14 ST-25
SiO2	72.13	78.24	73.79	71.04	71.20	71.12	67.45	73.74
TiO2	0.25	0.13	0.16	0.21	0.28	0.26	0.56	0.13
Al2O3	15.60	10.83	13.77	15.80	14.54	15.34	16.02	14.81
Fe2O3	2.18	2.04	2.04	1.61	2.48	2.04	3.72	0.91
MnO	0.03	0.06	0.04	0.01	0.03	0.03	0.05	0.01
MgO	0.23	0.02	0.02	0.17	0.22	0.27	1.42	0.12
CaO	0.60	0.25	0.28	0.63	0.66	2.13	4.25	1.19
Na2O	3.23	3.50	4.01	3.25	3.48	4.07	3.54	3.85
K2O	7.05	4.88	6.05	6.93	5.77	3.88	2.83	5.22
P2O5	0.04	0.00	0.00	0.04	0.04	0.04	0.16	0.02
Total	101.32	99.95	100.16	99.69	98.69	99.19	100.00	100.00
Trace								
Zr (in PPM)	67	105	164	62	86	103	38	67
Zr T(°C)	663	695	737	658	687	693	592	659

Whole rock geochemical data taken from Dutrow et al. (2014) and Ma (2015).

VEIN SAMPLES

Sample	MC13 ST-05	MC13 ST-14	MC13 ST-18	MC14 ST-08	MC14 ST-10	MC14 ST-12	MC14 ST-13	SMC 13-132
Composition	MGr	MGr	Grd	Grd	Grd	Grd	MGr	MGr
SiO2	80.24	73.90	67.14	75.42	76.15	77.22	70.63	74.77
TiO2	0.01	0.18	0.67	0.08	0.12	0.15	0.10	0.10
Al2O3	13.66	14.63	17.66	14.78	14.19	13.95	16.11	14.90
Fe2O3	0.82	1.48	1.86	0.68	0.90	1.37	0.67	0.25
MnO	0.17	0.03	0.00	0.00	0.00	0.00	0.00	0.00
MgO	0.00	0.21	1.28	0.08	0.18	0.24	0.12	0.17
CaO	0.83	1.50	4.81	3.91	3.08	2.16	0.65	1.29
Na2O	6.23	5.19	5.50	4.70	4.89	3.18	2.36	3.50
K2O	2.02	3.07	0.89	0.32	0.47	1.66	9.27	5.33
P2O5	0.02	0.02	0.20	0.03	0.02	0.07	0.08	0.03
Total	104.00	100.22	100.01	100.00	100.00	100.00	99.99	100.34
Trace								
Zr (in PPM)	181	63	76	42	117	46	17	90
Zr T(°C)	748	648	638	614	708	659	552	690

Whole rock geochemical data taken from Dutrow et al. (2014) and Ma (2015).

MGr = Monzo-granite   Grd = Granodiorite

of 648 ± 51 °C (1σ), four veins of unknown source are granodiorites and have a temperature range from 614 to 708 °C with an average temperature of 655 ± 40 °C (1σ), and four veins of unknown source belonging to the monzo-granite grouping have a temperature range from 552 to 748 °C with an average temperature of 659 ± 83 °C (1σ).

4.7. Feldspar Mineral Chemistry

Two vein samples of unknown source with differing rock type and plagioclase OM-CL response colors were chosen for feldspar mineral chemical analysis. SMC13-132 is a coarse grained monzo-granite with bright green and brown plagioclase in OM-CL and plagioclase twin planes show alteration in CL. SMC16-34 is medium-grained granodiorite with moderate green and brown plagioclase in OM-CL and contains oscillatory zoned alkali feldspar observed in CL.

SMC13-132

Three plagioclase grains and three alkali feldspar grains were analyzed to determine core to rim compositional differences and to determine minor elements that might give rise to the CL signature. Plagioclase cores have a compositional range of $(Na_{0.73\text{-}0.97}Ca_{0.15\text{-}0.24}K_{0.01\text{-}0.02})(Si_{2.75\text{-}2.98}Al_{1.02\text{-}1.25})O_8$ and rims have a range of $(Na_{0.94\text{-}0.96}Ca_{0.02\text{-}0.04}K_{0.00\text{-}0.01})(Si_{2.96\text{-}2.97}Al_{1.04\text{-}1.04})O_8$ (Appendix C, Tab. 10). Anorthite content decreases from core to rim correlating to a change in plagioclase CL color (Appendix C, Fig. 11). Only one alkali feldspar data point taken from a core was reliable and had a composition of $(K_{0.91}Na_{0.07}Ba_{0.02})(Si_{2.96}Al_{1.05})O_8$ (Appendix C, Tab. 11).

SMC16-34

OM-CL displayed compositional zoning in the feldspars. Thus, five plagioclase grains and nine alkali feldspar grains were analyzed in this sample to determine core-to-rim compositional differences. Plagioclase cores have a compositional range of

$(Na_{0.85-0.98}Ca_{0.04-0.14}K_{0.01-0.01})(Si_{2.84-2.93}Al_{1.07-1.16})O_8$ and rims have a range of $(Na_{0.86-0.93}Ca_{0.03-0.07}K_{0.01-0.01})(Si_{2.84-2.92}Al_{1.03-1.08})O_8$ (Appendix C, Tab. 12). Anorthite content decreases from core to rim correlating to a change in plagioclase CL color (Appendix C, Fig. 12). Alkali feldspar cores have a compositional range of $(K_{0.90-0.94}Na_{0.07-0.10}Ba_{0.01-0.02})(Si_{2.96-2.99}Al_{1.00-1.04})O_8$ and rims have a range of $(K_{0.90-0.94}Na_{0.07-0.09}Ba_{0.01-0.03})(Si_{2.94-2.99}Al0_{0.99-1.06})O_8$ (Appendix C, Tab. 13).

Table 10. Mineral chemistry of plagioclase feldspar cores and rims for sample SMC13-132.

	CORE RANGE		CORE AVERAGE	RIM RANGE		RIM AVERAGE
SiO2	62.32	68.64	64.13	68.30	68.37	68.34
Al2O3	20.00	24.08	23.03	20.28	20.42	20.35
FeO	0.00	0.03	0.01	0.00	0.02	0.01
CaO	0.46	5.09	3.90	0.71	0.88	0.80
BaO	0.00	0.04	0.03	0.01	0.01	0.01
Na2O	8.52	11.57	9.40	11.21	11.39	11.30
K2O	0.11	0.40	0.21	0.07	0.16	0.11
Total	100.30	100.91	100.71	100.85	100.98	100.92
Structural Formula Based on 8 Oxygens						
T (iv) site: Si	2.75	2.98	2.81	2.96	2.97	2.96
Al	1.02	1.25	1.19	1.04	1.04	1.04
T site total	4.00	4.01	4.00	4.00	4.00	4.00
Fe2+	0.00	0.00	0.00	0.00	0.00	0.00
Ca	0.02	0.24	0.18	0.03	0.04	0.04
Ba	0.00	0.00	0.00	0.00	0.00	0.00
Na	0.73	0.97	0.80	0.94	0.96	0.95
K	0.01	0.02	0.01	0.00	0.01	0.01
M-site total	0.98	1.00	0.99	0.99	1.00	0.99
Feldspar Components						
albite (mol%)	73.61	97.12	80.29	94.97	96.27	95.62
anorthite (mol%)	2.11	24.08	18.47	3.33	4.14	3.73
orthoclase (mol%)	0.64	2.27	1.19	0.38	0.88	0.63
celsian (mol%)	0.01	0.07	0.04	0.01	0.02	0.01

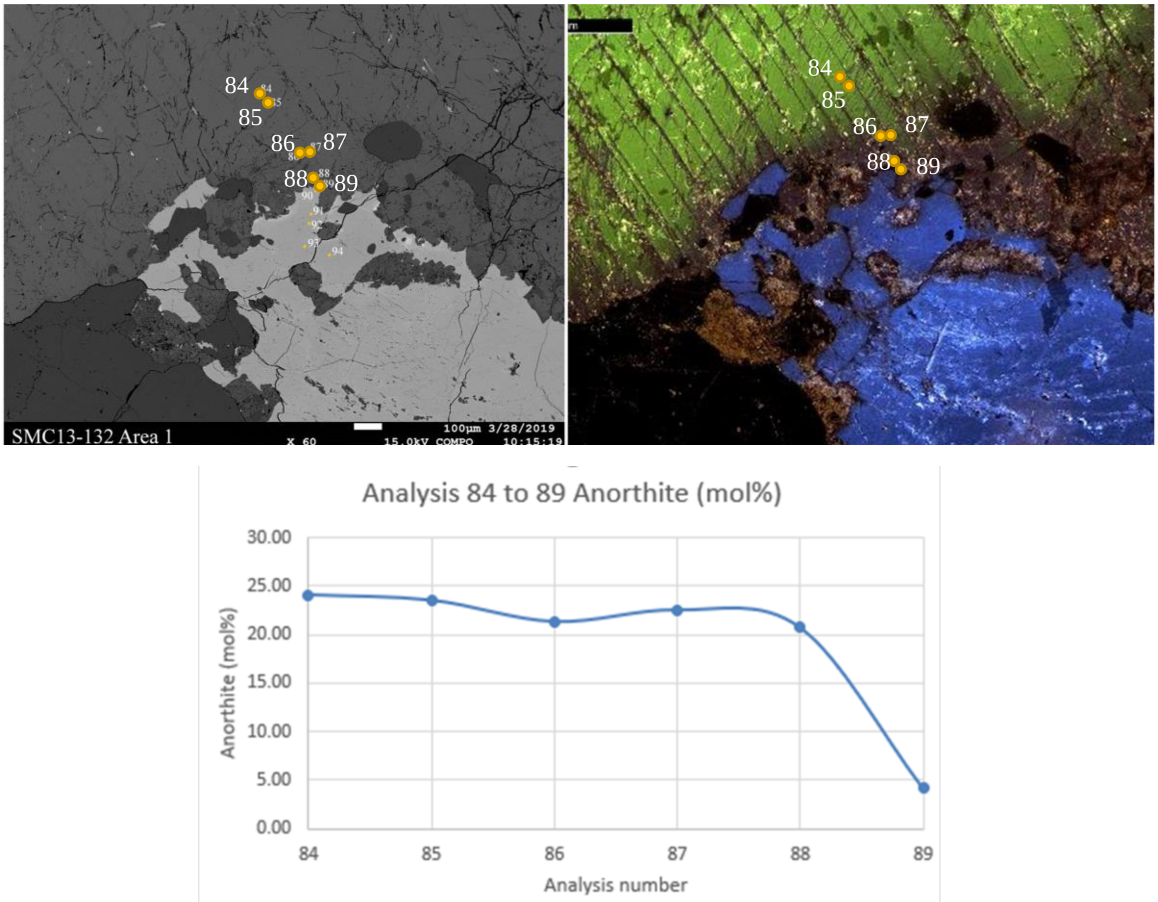

Figure 11. (Top) BSE image of SMC13-132 showing the location of EMPA analysis points in relation to the plagioclase CL color at each location. (Bottom) Graph of anorthite content per analysis point. Points traverse plagioclase CL color change from green (core) to brown (rim).

Table 11. Mineral chemistry of Alkali feldspar cores and rims for sample SMC13-132.

	CORE RANGE		CORE AVERAGE	RIM RANGE		RIM AVERAGE
SiO2	62.99	62.99	62.99			
Al2O3	18.98	18.98	18.98			
FeO	0.00	0.00	0.00			
CaO	0.00	0.00	0.00			
BaO	1.14	1.14	1.14			
Na2O	0.76	0.76	0.76			
K2O	15.25	15.25	15.25			
Total	99.11	99.11	99.11			
Structural Formula Based on 8 Oxygens						
T (iv) site: Si	2.96	2.96	2.96			
Al	1.05	1.05	1.05			
T site total	4.01	4.01	4.01			
Fe2+	0.00	0.00	0.00			
Ca	0.00	0.00	0.00			
Ba	0.02	0.02	0.02			
Na	0.07	0.07	0.07			
K	0.91	0.91	0.91			
M-site total	1.00	1.00	1.00			
Feldspar Components						
albite (mol%)	6.86	6.86	6.86			
anorthite (mol%)	0.00	0.00	0.00			
orthoclase (mol%)	91.04	91.04	91.04			
celsian (mol%)	2.09	2.09	2.09			

Table 12. Mineral chemistry of plagioclase feldspar cores and rims for sample SMC16-34.

	CORE RANGE		CORE AVERAGE	RIM RANGE		RIM AVERAGE
SiO2	63.93	66.22	65.48	63.84	66.72	68.35
Al2O3	20.41	22.19	21.66	20.07	20.86	22.11
FeO	0.00	0.04	0.01	0.00	0.01	0.03
CaO	0.84	2.89	2.33	0.71	1.45	2.86
BaO	0.00	0.04	0.01	0.00	0.02	0.04
Na2O	10.07	11.47	10.44	10.11	10.91	11.49
K2O	0.13	0.22	0.16	0.12	0.16	0.20
Total	99.03	100.99	100.10	99.11	100.13	100.86
Structural Formula Based on 8 Oxygens						
T (iv) site: Si	2.84	2.93	2.88	2.84	2.92	2.97
Al	1.07	1.16	1.12	1.03	1.08	1.16
T site total	4.00	4.00	4.00	4.00	4.00	4.01
Fe2+	0.00	0.00	0.00	0.00	0.00	0.00
Ca	0.04	0.14	0.11	0.03	0.07	0.14
Ba	0.00	0.00	0.00	0.00	0.00	0.00
Na	0.85	0.98	0.89	0.86	0.93	0.97
K	0.01	0.01	0.01	0.01	0.01	0.01
M-site total	0.99	1.04	1.01	0.99	1.00	1.02
Feldspar Components						
albite (mol%)	85.69	95.11	88.20	85.93	92.27	95.62
anorthite (mol%)	3.84	13.54	10.88	3.24	6.79	13.39
orthoclase (mol%)	0.69	1.22	0.90	0.65	0.90	1.14
celsian (mol%)	0.00	0.06	0.02	0.00	0.03	0.06

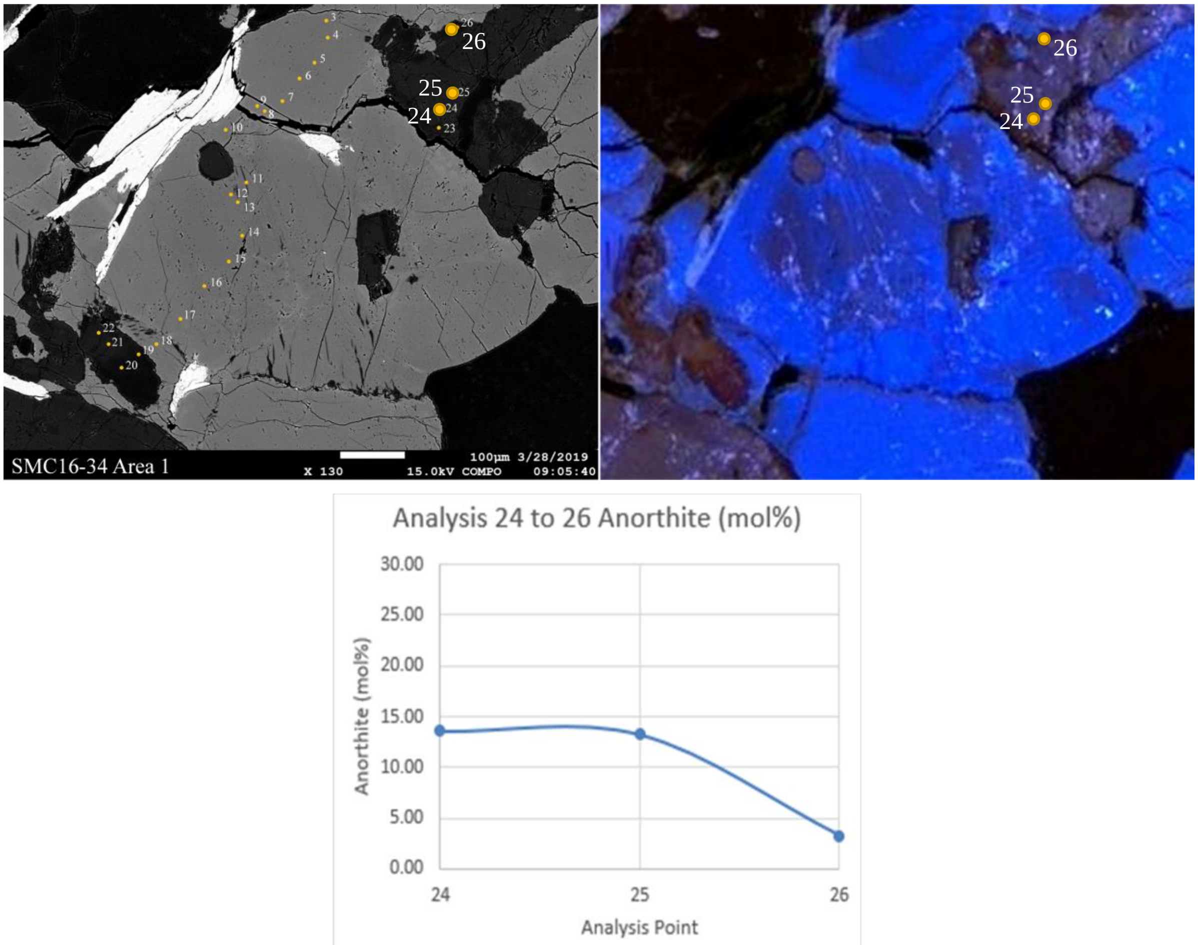

Figure 12. (Top) BSE image of SMC16-34 showing the location of EMPA analysis points in relation to the plagioclase CL color at each location. (Bottom) Graph of anorthite content per analysis point. Points traverse plagioclase CL color change from brown (core) to red (rim).

Table 13. Mineral chemistry of alkali feldspar cores and rims for sample SMC16-34.

	CORE RANGE		CORE AVERAGE	RIM RANGE		RIM AVERAGE
SiO2	63.29	65.31	64.00	62.39	64.73	63.54
Al2O3	18.45	18.96	18.73	18.13	19.10	18.75
FeO	0.00	0.04	0.01	0.00	0.20	0.04
CaO	0.00	0.01	0.00	0.00	0.02	0.00
BaO	0.33	0.85	0.65	0.53	1.77	1.04
Na2O	0.76	1.07	0.89	0.77	0.97	0.87
K2O	15.08	16.01	15.46	14.91	16.05	15.38
Total	99.04	100.97	99.75	99.02	100.67	99.63
Structural Formula Based on 8 Oxygens						
T (iv) site: Si	2.96	2.99	2.97	2.94	2.99	2.97
Al	1.00	1.04	1.03	0.99	1.06	1.03
T site total	3.99	4.01	4.00	3.98	4.01	4.00
Fe2+	0.00	0.00	0.00	0.00	0.01	0.00
Ca	0.00	0.00	0.00	0.00	0.00	0.00
Ba	0.01	0.02	0.01	0.01	0.03	0.02
Na	0.07	0.10	0.08	0.07	0.09	0.08
K	0.90	0.94	0.92	0.90	0.94	0.92
M-site total	1.00	1.02	1.01	1.00	1.04	1.01
Feldspar Components						
albite (mol%)	6.84	9.35	7.88	6.94	8.78	7.74
anorthite (mol%)	0.00	0.05	0.01	0.00	0.09	0.02
orthoclase (mol%)	89.46	91.68	90.92	88.94	91.85	90.34
celsian (mol%)	0.61	1.57	1.19	0.93	3.24	1.89

4.8. U/Pb Zircon Geochronology

U/Pb zircon age dates were obtained for seven vein samples of unknown source. These data served as a calibration for, and test of, the validity of OM-CL plagioclase responses as a source proxy. Analyses points targeted both the inherited cores and the overgrowths of the zircon grains to determine the age of the latest overgrowth as well as the original crystallization age (Appendix F). Discordance calculated for ages <1000 Ma are reported as $^{207}Pb/^{235}U$ ages versus $^{206}Pb/^{238}U$ ages and discordance calculated for ages >1000 Ma are reported as $^{207}Pb/^{206}Pb$ versus $^{206}Pb/^{238}U$ ages based on (Bruguier et al., 2001). Of the seven samples, only one sample, SMC14-43, had a high percentage (25 of 38 analyses) of zircon grains with discordance over

5%. Appendix E contains all the data. A brief overview of analyzed samples is presented subsequently.

Sample SMC13-132 is a coarse-grained biotite monzo-granite (QAP) with accessory zircon. Secondary minerals include clinozoisite, chlorite, and sericite. The sample contains minor perthite and pervasive myrmekitic texture. Zircon grains show no zonation in BSE images and no response in SEM-CL images (Fig. 13), which is characteristic of metamict zircons. Uranium content ranges from 12020 ± 830 ppm to 1080 ± 300 ppm and thorium ranges from 2022 ± 30 ppm to 107 ± 8 ppm (Tab. 14).

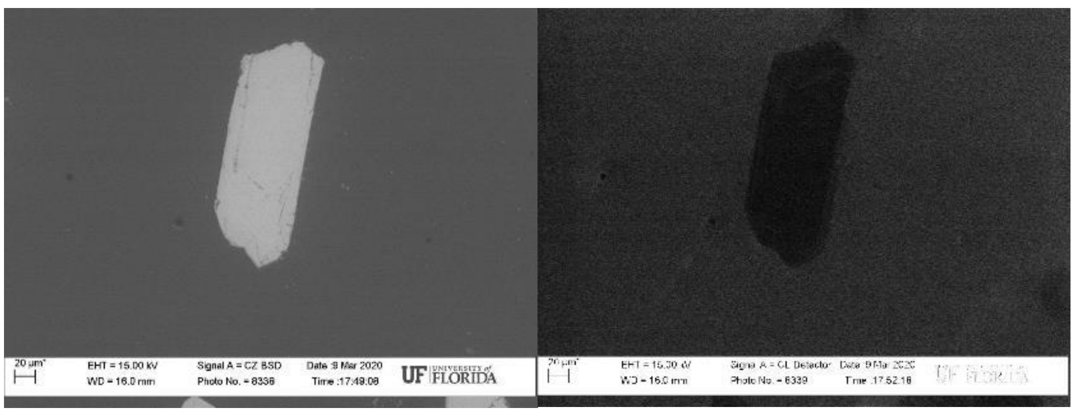

Figure 13. SMC13-132 BSE image showing no zonation and SEM-CL image showing no CL response.

Table 14. Uranium and thorium content of zircons.

Sample	Uranium Content (ppm)	Thorium Content (ppm)
SMC13-132	12020 ± 830 ppm to 1080 ± 300 ppm	2022 ± 30 ppm to 107 ± 8 ppm
SMC14-09	1752 ± 52 ppm to 303 ± 26 ppm	182 ± 5 ppm to 24 ± 2 ppm
SMC14-11	13610 ± 940 ppm to14 ± 1 ppm	1930 ± 240 ppm to 3 ± 1 ppm
SMC14-43	20800 ± 2900 ppm to 1560 ± 190 ppm	7310 ± 800 ppm to 40 ± 8 ppm
SMC15-05	5520 ± 250 ppm to 45 ± 10 ppm	3320 ± 230 ppm to 24 ± 4 ppm
SMC16-09	5650 ± 240 ppm to 235 ± 7 ppm	132 ± 5 ppm to 18 ± 1 ppm
SMC16-22	8230 ± 580 ppm to 17 ± 1 ppm	2110 ± 350 ppm to 3 ± 1 ppm

Data from forty-one zircon spot analyses, give $^{206}Pb/^{238}U$ ages of ca. 84.0 ± 1.5 Ma to 105.3 ± 1.3 Ma for analyses with <5% discordance (Appendix E, Tab. 15). Plotting the filtered data results in a calculated $^{206}Pb/^{238}U$ mean age of 87.4 ± 0.4 Ma (2s.e.m.). These ten data points were also plotted on a Tera-Wasserburg Concordia diagram and give an intercept age of 87.4 ± 0.4 Ma (MSWD = 0.99) and the weighted mean age of 87.4 ± 0.5 Ma (MSWD = 1.18) (Fig. 14).

Table 15. Vein crystallization age, inherited core dates, date range, and outlier ages.

Sample	Age date	Inherited Core Dates	Date Range (<5% Discord.)	Outliers (r)=rim (c)=core
SMC13-132	87.4 ± 0.4 Ma		84.0 ± 1.5 Ma – 105.3 ± 1.3 Ma	
SMC14-09	93.9 ± 0.5 Ma		92.8 ± 1.5 Ma – 96.5 ± 1.6 Ma	60.7 Ma ± 1.1 Ma (r) 103.0 Ma ± 2.1 Ma (c) 119.0 Ma ± 2.8 Ma (c)
SMC14-11	80.6 ± 0.7 Ma	1322 ± 42 Ma, 1386 ± 56 Ma, 1454 ± 39 Ma, 1803 ± 55 Ma	78.2 ± 1.5 Ma – 107.3 ± 5.1 Ma	
SMC14-43	75.5 ± 0.6 Ma		72.3 ± 1.4 Ma – 85.0 ± 1.7 Ma	101.0 ± 1.8 Ma (c)
SMC15-05	79.2 ± 1.2 Ma	576 ± 9 Ma, 597 ± 19 Ma, 641 ± 10 Ma, 686 ± 15 Ma, 715 ± 11 Ma	71.4 ± 1.2 Ma – 100.7 ± 5.1 Ma	121.0 ± 2.7 Ma (c)
SMC16-09	86.5 ± 0.5 Ma		85.8 ± 1.9 Ma – 131.2 ± 2.2 Ma	
SMC16-22	80.3 ± 0.6 Ma	317 ± 7 Ma, 446 ± 7 Ma, 666 ± 13 Ma, 1074 ± 49 Ma, 1194 ± 72 Ma, 1238 ± 45 Ma, 1503 ± 26 Ma	79.4 ± 1.3 Ma – 102.3 ± 2.7 Ma	109.3 ± 2.9 Ma (c) 112.1 ± 2.1 Ma (c)

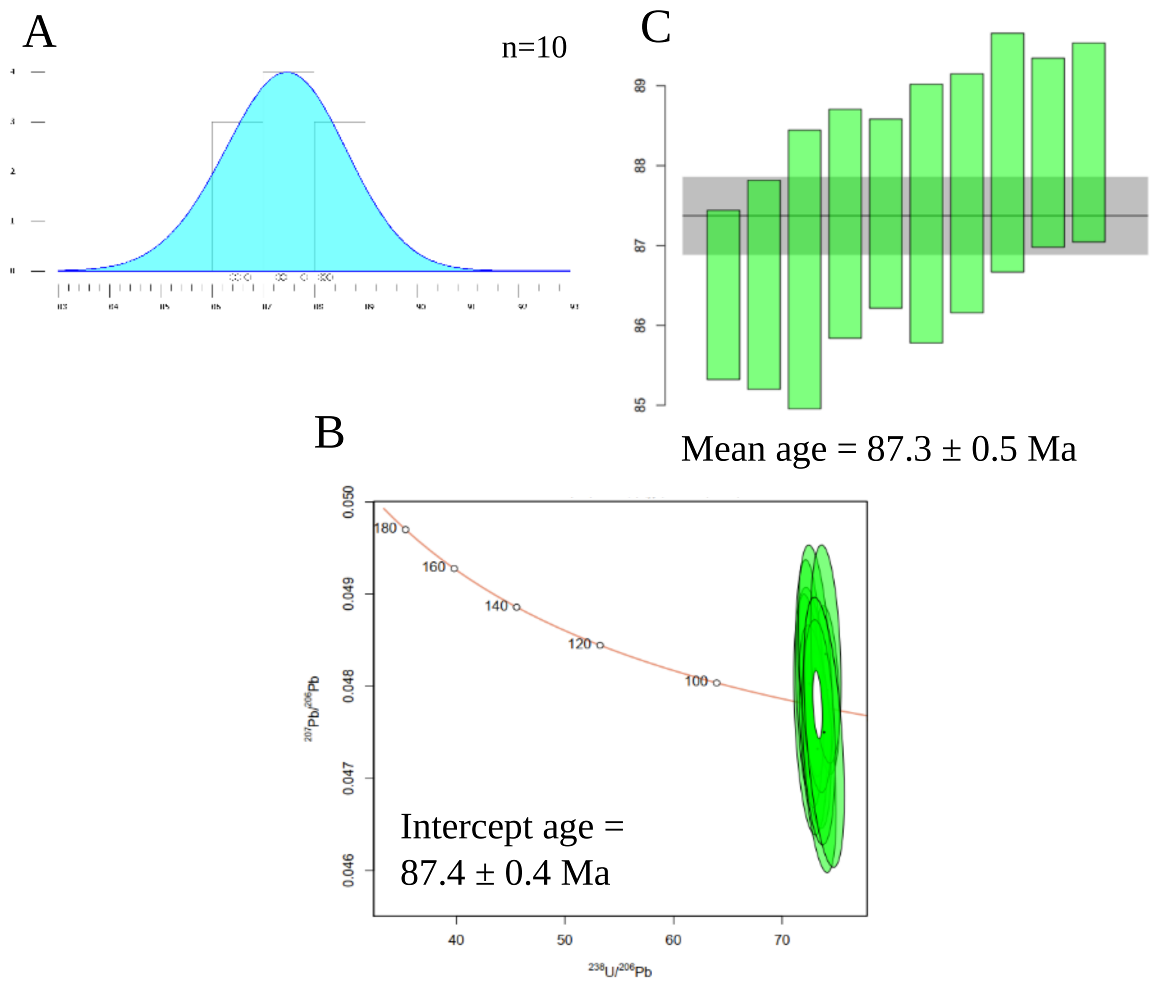

Figure 14. SMC13-132. (A) KDE showing age grouping used for calculating a mean age of 87.4 ± 0.4 Ma (2s.e.m.). Circles are ages plotted without error and n= total number of dates used. (B) Terra-Wasserburg Concordia diagram showing intercept age of 87.4 ± 0.4 Ma. (C) Weighted mean plot showing calculated mean age of 87.4 ± 0.5 Ma. Error bars are shown at 2 s.e.m.

Sample SMC14-09 is a coarse-grained biotite granodiorite (QAP) with accessory allanite, apatite, magnetite, and zircon. Secondary minerals include chlorite and sericite. The sample contains minor perthite and some myrmekitic texture. Zircon grains show no zonation in BSE images, however SEM-CL images show zonation with inherited cores and overgrowths in

multiple zircons. One such examples is shown in Fig. 15. Uranium content ranges from 1752 ± 52 ppm to 303 ± 26 ppm and thorium ranges from 182 ± 5 ppm to 24 ± 2 ppm (Tab. 14).

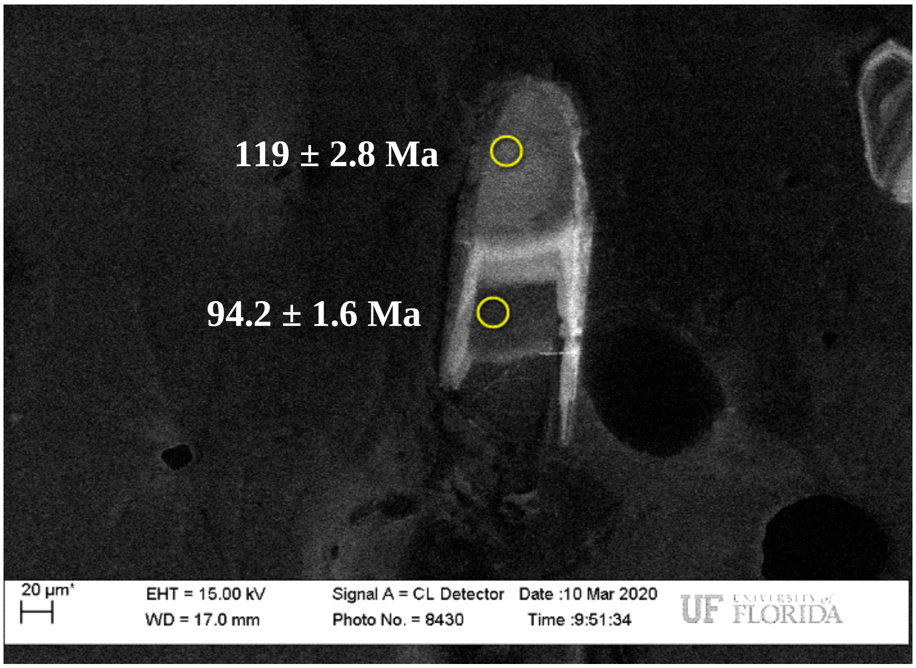

Figure 15. SEM-CL image of SMC14-09 zircon grain with ages indicated. Orientation of zircon in epoxy resulted in uneven polish and laser drilling to core age domain on upper point.

Data from forty-eight zircon spot analyses with <5% discordance give $^{206}Pb/^{238}U$ dates of ca. 92.8 ± 1.5 Ma to 96.5 ± 1.6 Ma (Appendix E, Tab. 15). Outlier dates included ca. 60.7 Ma ± 1.1 Ma, 103.0 Ma ± 2.1 Ma, and 119.0 Ma ± 2.8 Ma. Plotting the filtered data results in a calculated $^{206}Pb/^{238}U$ mean age of 93.9 ± 0.3 Ma (2s.e.m.). These ten data points were also plotted on a Tera-Wasserburg Concordia diagram and give an intercept age of 94.0 ± 0.5 Ma (MSWD = 0.22) and the weighted mean age of 93.9 ± 0.6 Ma (MSWD = 0.33) (Fig. 16).

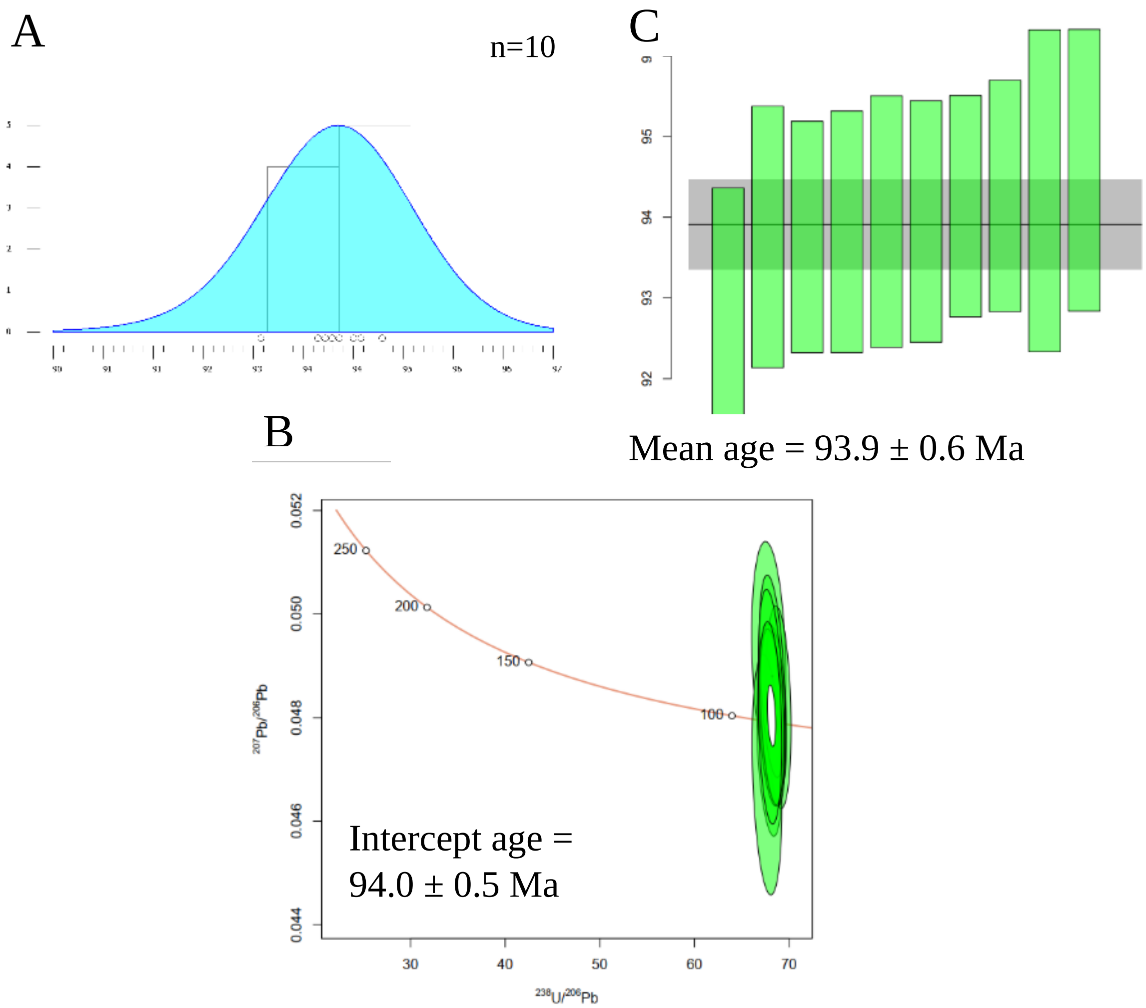

Figure 16. SMC14-09. (A) KDE showing age grouping used for calculating a mean age of 93.9 ± 0.3 Ma (2s.e.m.). Circles are ages plotted without error and n= total number of dates used. (B) Terra-Wasserburg Concordia diagram showing intercept age of 94.0 ± 0.5 Ma. (C) Weighted mean plot showing calculated mean age of 93.9 ± 0.6 Ma. Error bars are shown at 2 s.e.m.

Sample SMC14-11 is a coarse-grained biotite-bearing monzo-granite (QAP) with accessory zircon. Secondary minerals include chlorite and sericite. The sample contains pervasive perthite. Zircon grains show no zonation in BSE images and hard to distinguish zonation in some SEM-CL images. Some grains look metamict in SEM-CL however, multiple images show clear zonation with inherited cores and overgrowths (Fig. 17). Uranium content

ranges from 13610 ± 940 ppm to14 ± 1 ppm and thorium ranges from 1930 ± 240 ppm to 3 ± 1 ppm (Tab. 14).

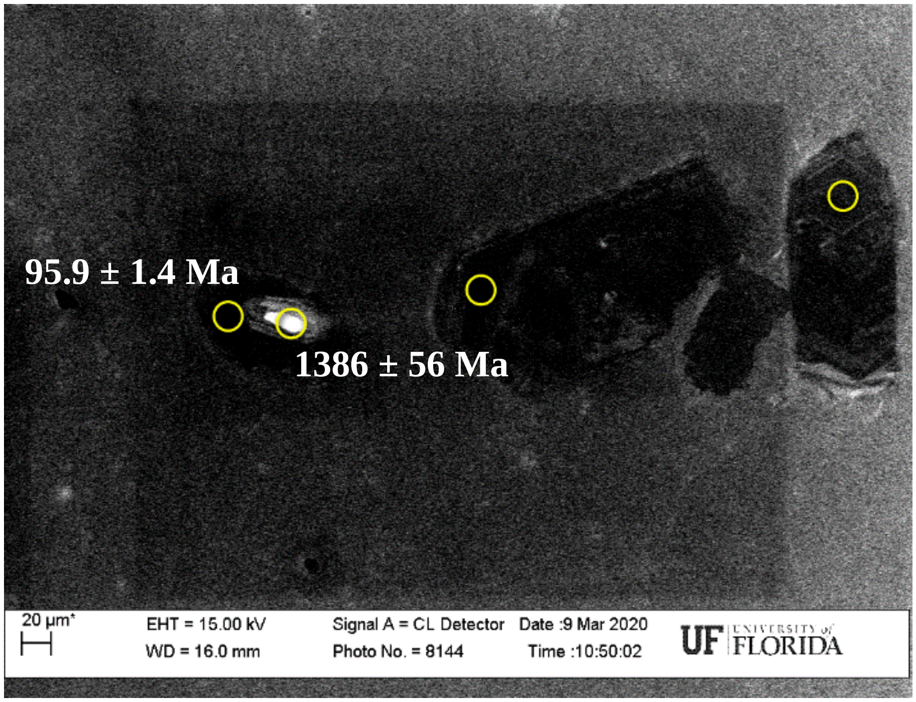

Figure 17. SEM-CL image of SMC14-11 zircon grain with rim (black) and core (white) ages indicated.

Data from sixty-three zircon spot analyses with <5% discordance give $^{206}Pb/^{238}U$ ages of ca. 78.2 ± 1.5 Ma to 107.3 ± 5.1 Ma (Appendix E, Tab. 15). $^{207}Pb/^{206}Pb$ core ages are ca. 1322 ± 42 Ma, 1386 ± 56 Ma, 1454 ± 39 Ma, and 1803 ± 55 Ma. Plotting the filtered data results in a calculated $^{206}Pb/^{238}U$ mean age 80.6 ± 0.7 Ma (2s.e.m.). These five data points were also plotted on a Tera-Wasserburg Concordia diagram and give an intercept age 80.6 ± 0.6 Ma (MSWD = 1.40) and the weighted mean age of 80.5 ± 0.8 Ma (MSWD = 1.47) (Fig. 18).

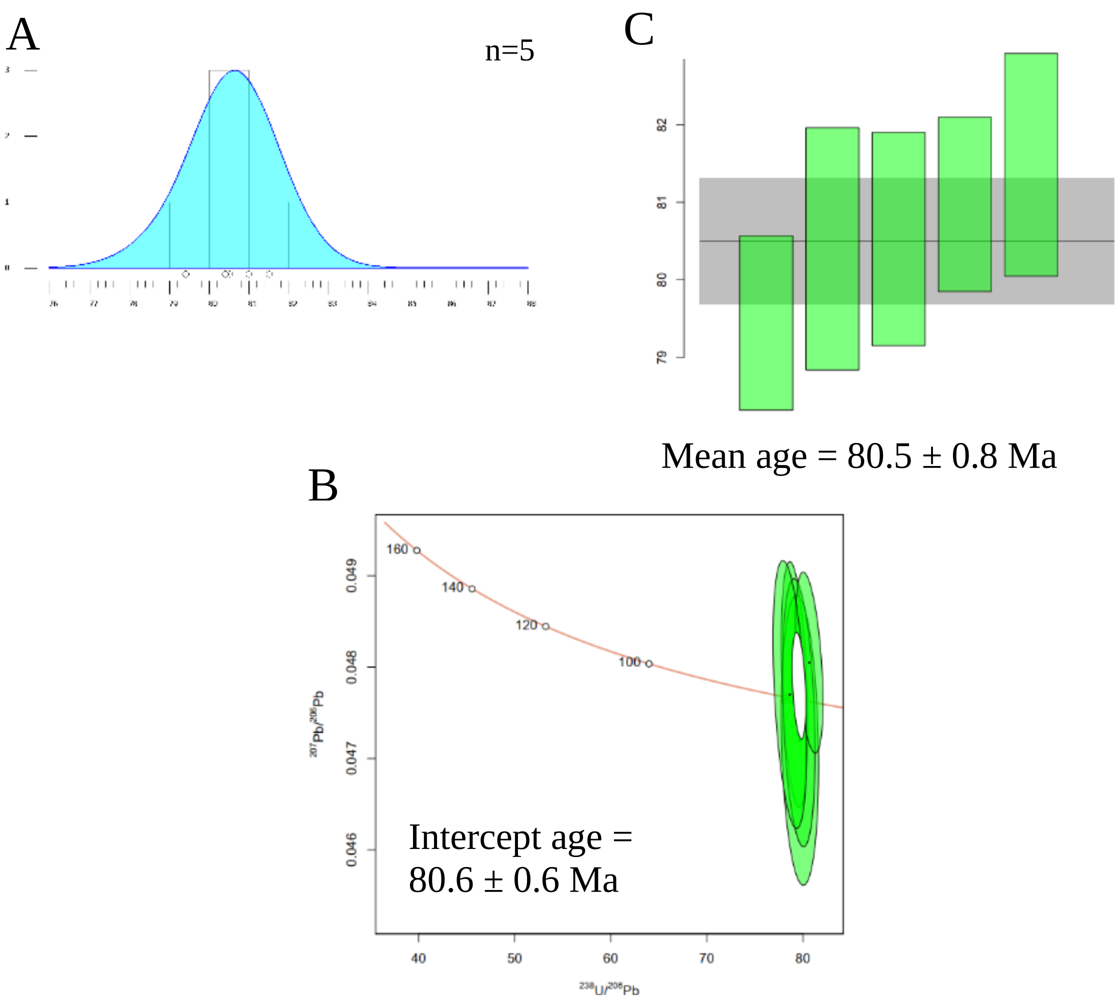

Figure 18. SMC14-11. (A) KDE showing age grouping used for calculating a mean age of 80.6 ± 0.7 Ma (2s.e.m.). Circles are ages plotted without error and n= total number of dates used. (B) Terra-Wasserburg Concordia diagram showing intercept age of 80.6 ± 0.6 Ma. (C) Weighted mean plot showing calculated mean age of 80.5 ± 0.8 Ma. Error bars are shown at 2 s.e.m.

Sample SMC14-43 is a fine grained leucocratic monzo-granite (QAP) with accessory zircon. Secondary minerals include hematite and sericite. The sample contains some myrmekitic texture. Zircon grains show no zonation in BSE images and are completely black in SEM-CL images (Fig. 19). Uranium content ranges from 20800 ± 2900 ppm to 1560 ± 190 ppm and thorium ranges from 7310 ± 800 ppm to 40 ± 8 ppm (Tab. 14).

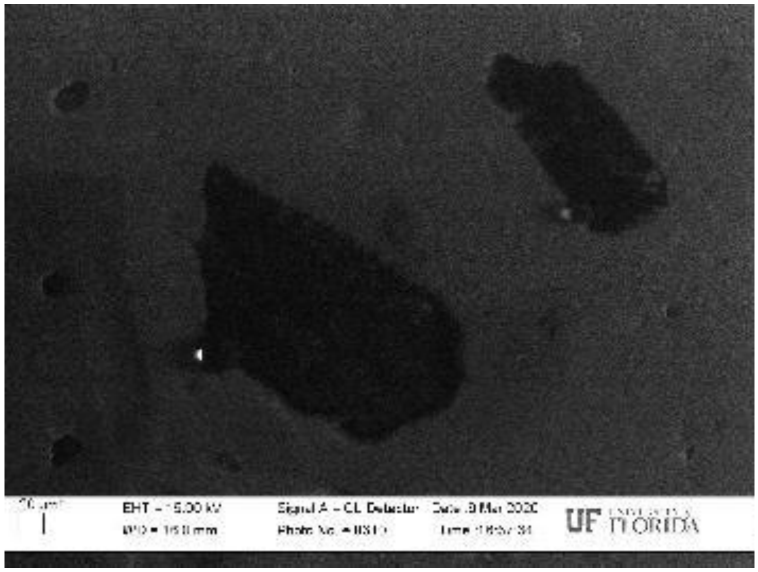

Figure 19. SMC14-43 SEM-CL image showing no CL response.

Data from thirty-four zircon spot analyses give $^{206}Pb/^{238}U$ ages of ca. 72.3 ± 1.4 Ma to 85.0 ± 1.7 Ma with an outlier of ca. 101.0 ± 1.7 Ma for analyses with <5% discordance (Appendix E, Tab. 15). Only thirteen age dates have discordance <5%. Therefore, the ten youngest age dates with <5% and Th/U ratio of <0.1 were plotted on a KDE to determine the best fitting age grouping (Fig. 20). Six age dates formed a consistent grouping and were used for calculating the mean age and error of vein crystallization. For these six age dates, the calculated $^{206}Pb/^{238}U$ mean age and 2s.e.m. were 75.5 ± 0.6 Ma. These six data points were also plotted on a Tera-Wasserburg Concordia diagram and give an intercept age of 76.1 ± 0.6 Ma (MSWD = 3.00) and the weighted mean is 75.8 ± 0.8 Ma (MSWD = 1.91) (Fig. 20).

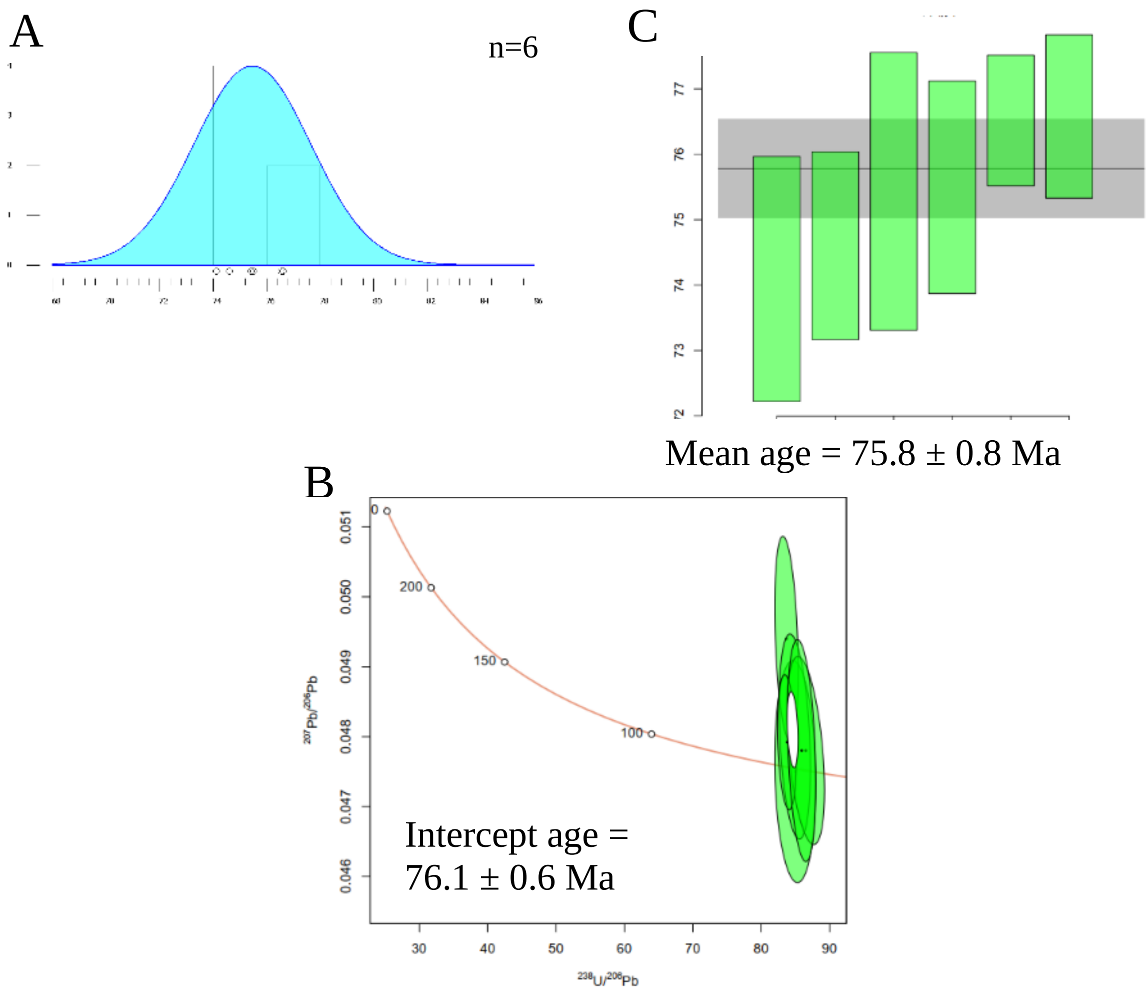

Figure 20. SMC14-43. (A) KDE showing age grouping used for calculating a mean age of 75.5 ± 0.6 Ma (2s.e.m.). Circles are ages plotted without error and n= total number of dates used. (B) Terra-Wasserburg Concordia diagram showing intercept age of 76.1 ± 0.6 Ma. (C) Weighted mean plot showing calculated mean age of 75.8 ± 0.8 Ma. Error bars are shown at 2 s.e.m.

Sample SMC15-05 is a medium-grained biotite granodiorite (QAP) with accessory allanite, apatite, magnetite, and zircon. Secondary minerals include clinozoisite, epidote, chlorite, and sericite. The sample contains minor perthite and minor myrmekitic textures. Zircon grains show no zonation in BSE images. Some grains look metamict in SEM-CL however, images show clear zonation with inherited cores and overgrowths apparent in multiple zircons (Fig. 21).

Uranium content ranges from 5520 ± 250 ppm to 45 ± 10 ppm and thorium ranges from 3320 ± 230 ppm to 24 ± 4 ppm (Tab. 14).

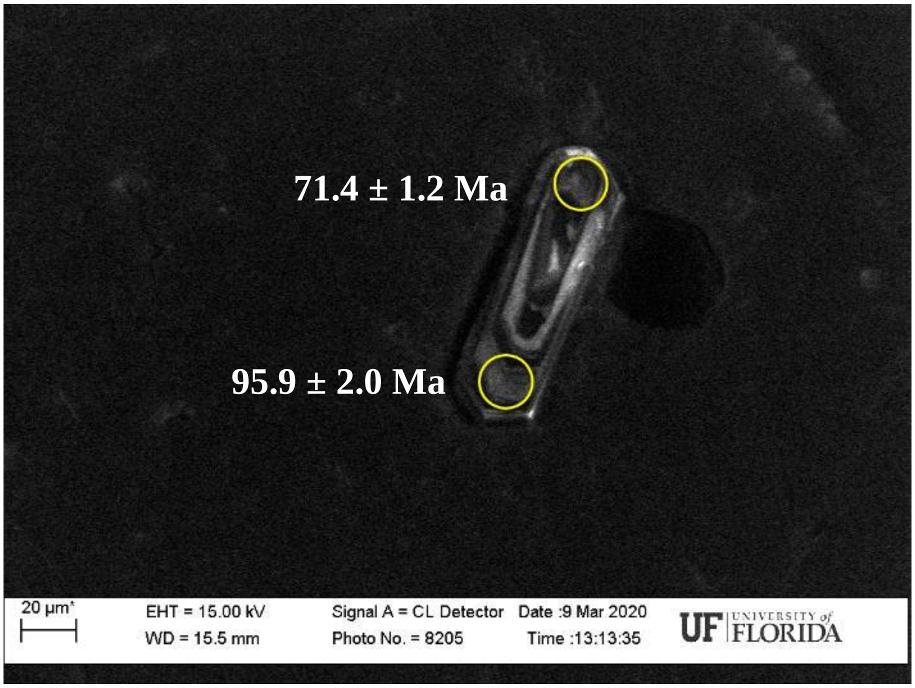

Figure 21. SEM-CL image of SMC15-05 zircon grain with ages indicated.

Data from thirty-two zircon spot analyses with <5% discordance give $^{206}Pb/^{238}U$ dates of ca. 71.4 ± 1.2 Ma to 100.7 ± 5.1 Ma with one date of ca. 121.0 ± 2.7 Ma (Appendix E, Tab. 15). $^{206}Pb/^{238}U$ core ages are ca. 576 ± 9 Ma, 597 ± 19 Ma, 641 ± 10 Ma, 686 ± 15 Ma, and 715 ± 11 Ma. Plotting the filtered data results in a calculated $^{206}Pb/^{238}U$ mean age 79.2 ± 1.2 Ma (2s.e.m.). These eight data points were also plotted on a Tera-Wasserburg Concordia diagram and give an intercept age 79.5 ± 1.4 Ma (MSWD = 2.90) and the weighted mean age of 79.5 ± 1.3 Ma (MSWD = 5.10) (Fig. 22).

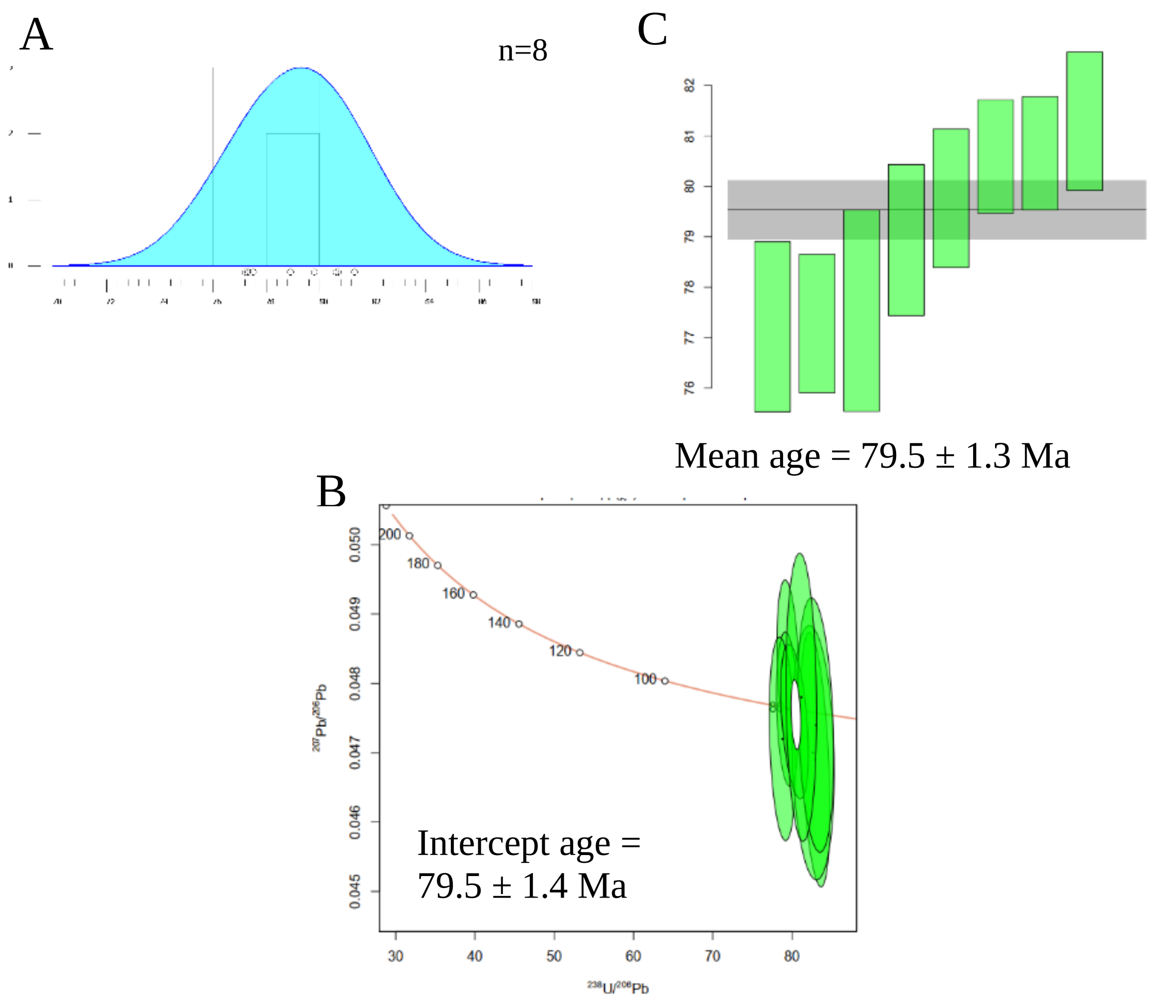

Figure 22. SMC15-05. (A) KDE showing age grouping used for calculating a mean age of 79.2 ± 1.2 Ma (2s.e.m.). Circles are ages plotted without error and n= total number of dates used. (B) Terra-Wasserburg Concordia diagram showing intercept age 79.5 ± 1.4 Ma. (C) Weighted mean plot showing calculated mean age of 79.5 ± 1.3 Ma. Error bars are shown at 2 s.e.m.

Sample SMC16-09 is a coarse-grained biotite-bearing monzo-granite (QAP) with accessory zircon. Secondary minerals include chlorite and sericite. The sample contains pervasive perthite. Zircon grains show no zonation in BSE images, however SEM-CL images show clear zonation with inherited cores and overgrowths (Fig.23). Uranium content ranges from 5650 ± 240 ppm to 235 ± 7 ppm and thorium ranges from 132 ± 5 ppm to 18 ± 1 ppm (Tab. 14).

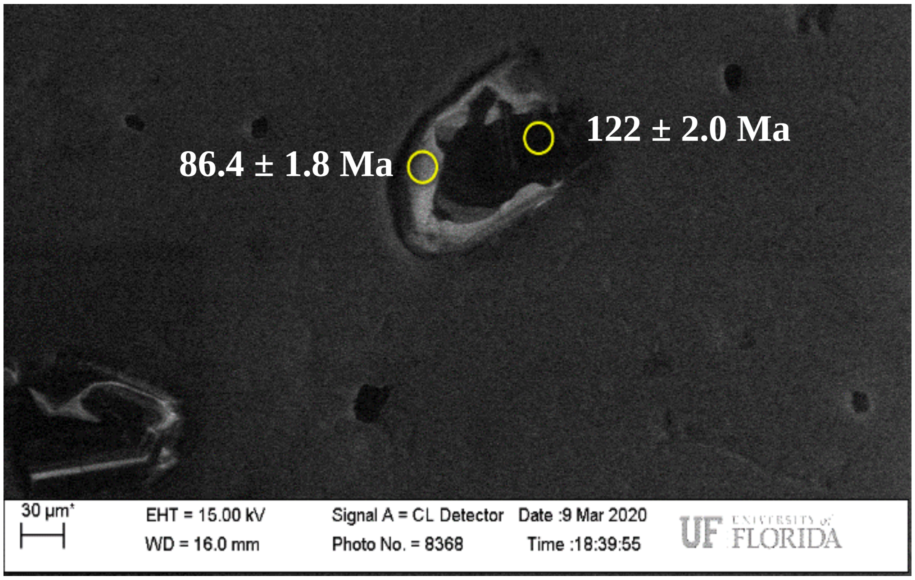

Figure 23. SEM-CL image of SMC16-09 zircon grain with ages indicated.

Data from thirty-nine zircon spot analyses give $^{206}Pb/^{238}U$ ages of ca. 85.8 ± 1.9 Ma to 131.2 ± 2.2 Ma for analyses with <5% discordance (Appendix E, Tab. 12). A wide dispersion of ten youngest dates (ca. 86 to 108 Ma) is observed for low discordances (<1%). Therefore, to narrow the dispersion, the discordance filter was raised to <3% which resulted in the ten youngest age dates having an age dispersion of 85.8 ± 1.9 Ma to 91.3 Ma ± 1.8 Ma. These ten ages were plotted on a KDE to determine the best fitting age grouping. Six age dates were used for calculating the mean age and error of vein crystallization. For these six age dates, the calculated $^{206}Pb/^{238}U$ mean age and 2s.e.m. were 86.5 ± 0.5 Ma. Plotting these six data points on a Tera-Wasserburg Concordia diagram and give an intercept age of 86.7 ± 0.7 Ma (MSWD = 0.42) and the weighted mean is 86.7 ± 0.6 Ma (MSWD = 1.4) (Fig. 24).

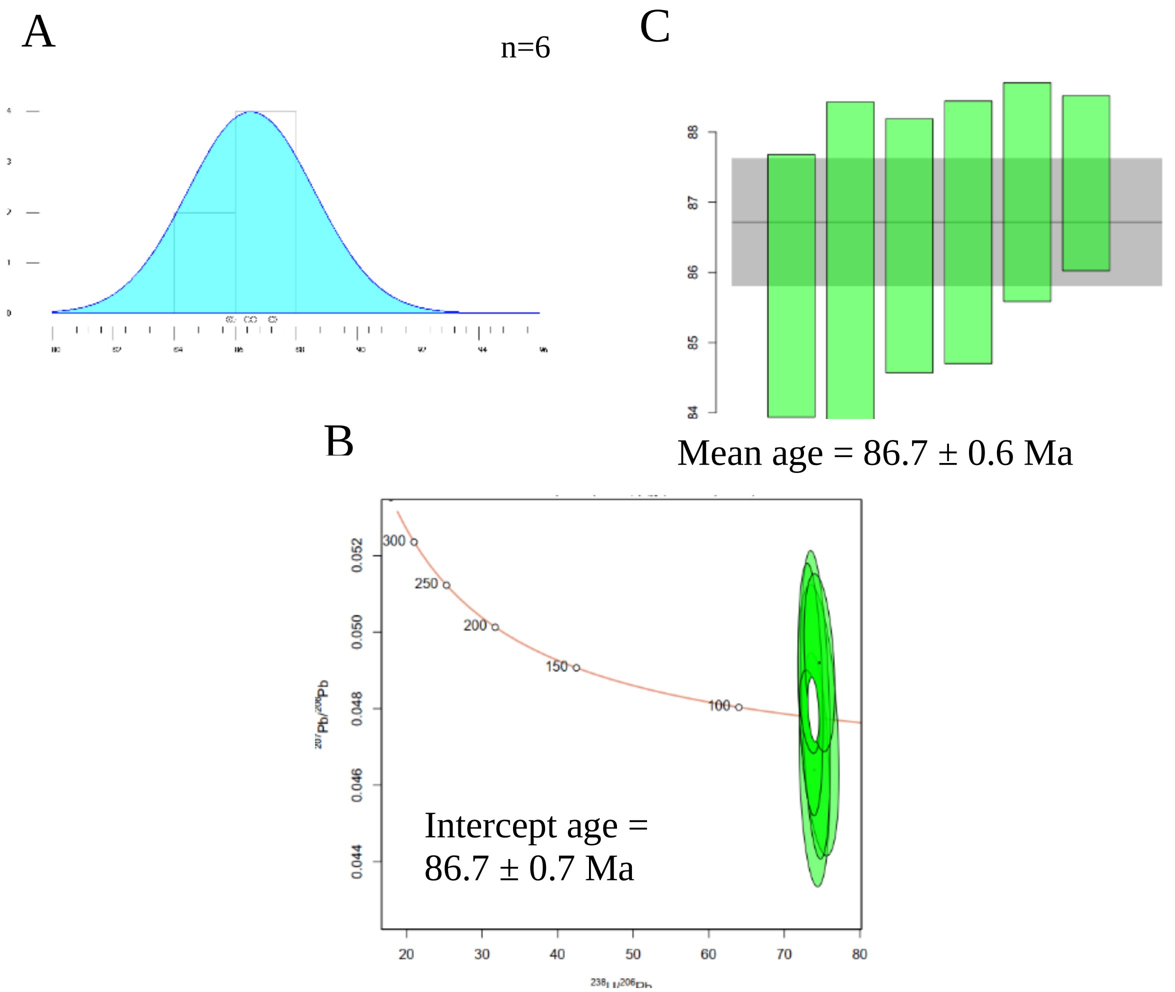

Figure 24. SMC16-09. (A) KDE showing age grouping used for calculating a mean age of 86.5 ± 0.5 Ma (2s.e.m.). Circles are ages plotted without error and n= total number of dates used. (B) Terra-Wasserburg Concordia diagram showing intercept age of 86.7 ± 0.7 Ma. (C) Weighted mean plot showing calculated mean age of 86.7 ± 0.6 Ma Error bars are shown at 2 s.e.m.

Sample SMC16-22 is a coarse-grained hornblende granodiorite (QAP) with accessory apatite, magnetite, and zircon. Sericite is the only secondary mineral observed. This sample contains minor perthite. Zircon grains show no zonation in BSE images. Some grains look metamict in SEM-CL, however, images show clear zonation with inherited cores and overgrowths apparent in multiple zircons (Fig. 25). Uranium content ranges from 8230 ± 580 ppm to 17 ± 1 ppm and thorium ranges from 2110 ± 350 ppm to 3 ± 1 ppm (Tab. 14).

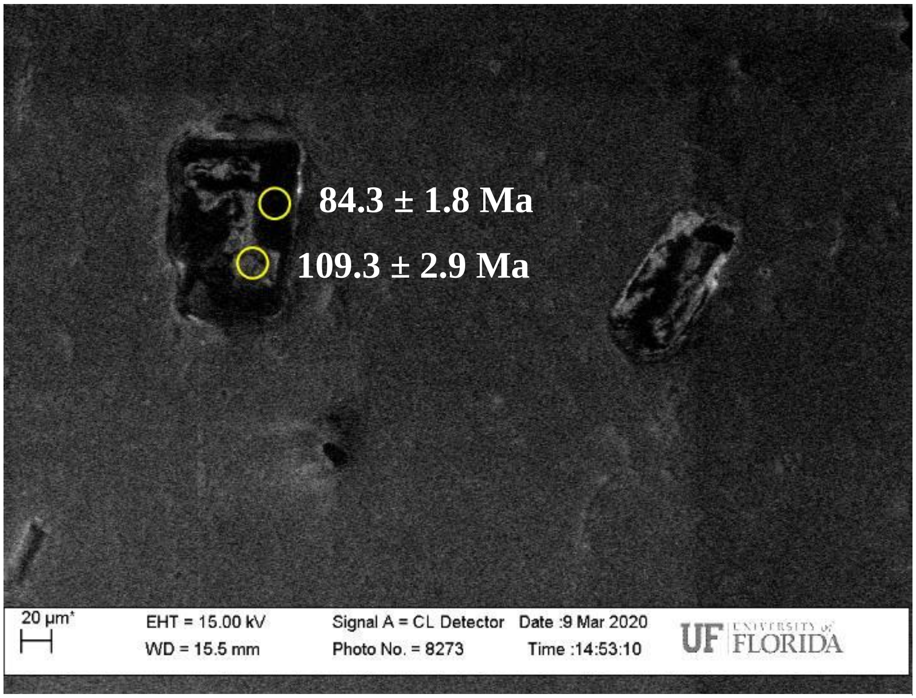

Figure 25. SEM-CL image of SMC16-22 zircon grain with ages indicated.

Data from fifty-seven zircon spot analyses with <5% discordance give $^{206}Pb/^{238}U$ ages of ca. 79.4 ± 1.3 Ma to 102.3 ± 2.7 Ma (Appendix E, Tab. 15). Outliers include ca. 109.3 ± 2.9 Ma and 112.1 ± 2.1 Ma. Analyses also give $^{206}Pb/^{238}U$ core ages are ca. 317 ± 7 Ma, 446 ± 7 Ma, and 666 ± 13 Ma, 1074 ± 49 Ma, 1194 ± 72 Ma, 1238 ± 45 Ma, and1503 ± 26 Ma. Plotting the filtered data results in a calculated $^{206}Pb/^{238}U$ mean age 80.3 ± 0.6 Ma (2s.e.m.). These seven data points were also plotted on a Tera-Wasserburg Concordia diagram and give an intercept age 80.5 ± 0.6 Ma (MSWD = 0.81) the weighted mean age of 80.4 ± 0.8 Ma (MSWD = 1.18) (Fig. 26).

The sample of the leucocratic granite phase of the IB, SMC15-05 has a crystallization age of 79.2 ± 1.2 Ma (2s.e.m.) with inherited core ages of 576 ± 9 Ma, 597 ± 19 Ma, 641 ± 10 Ma, 686 ± 15 Ma, and 715 ± 11 Ma (Appendix E, Tab. 15).

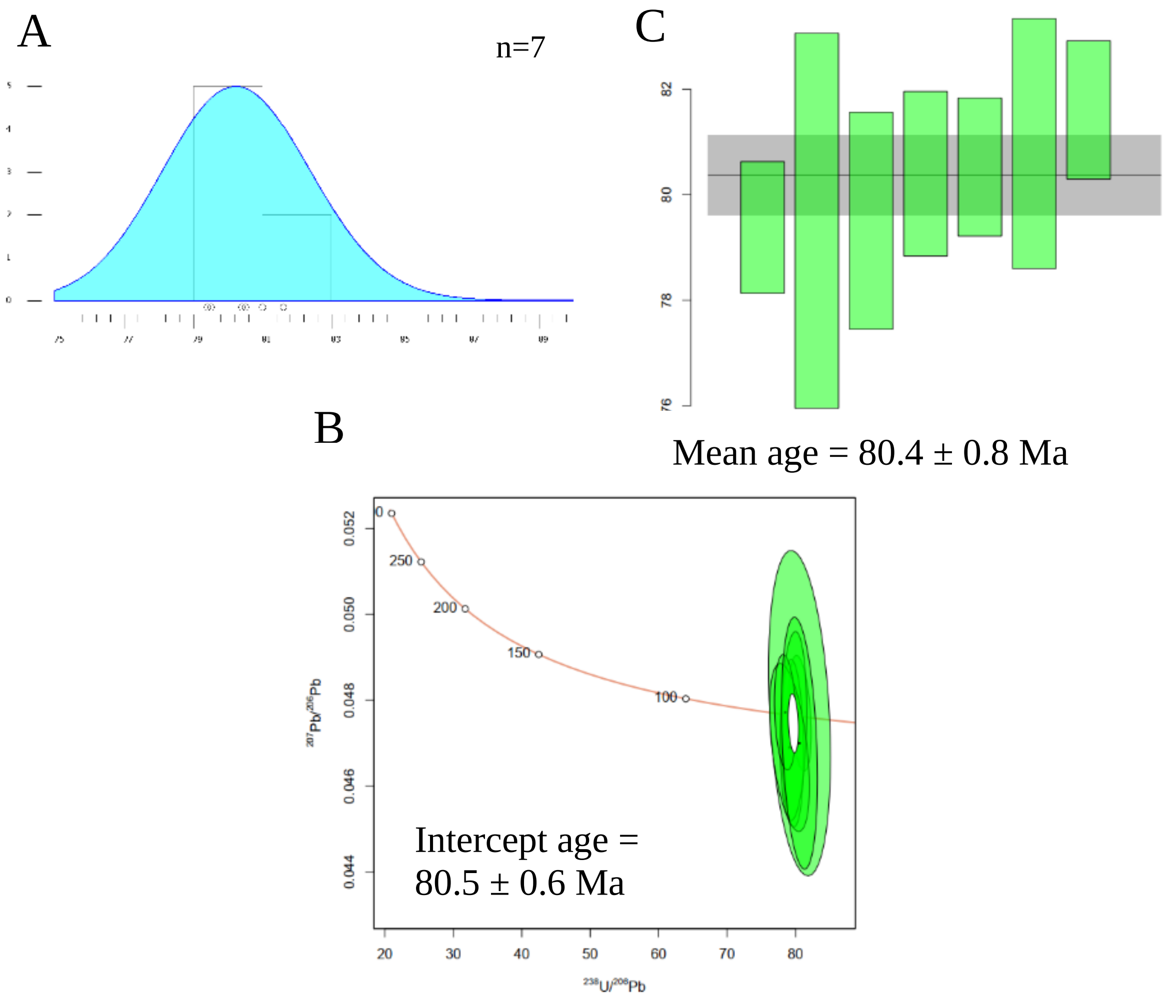

Figure 26. SMC16-22. (A) KDE showing age grouping used for calculating a mean age of 80.3 ± 0.6 Ma (2s.e.m.). Circles are ages plotted without error and n= total number of dates used. (B) Terra-Wasserburg Concordia diagram showing intercept age of 80.5 ± 0.6 Ma. (C) Weighted mean plot showing calculated mean age of 80.4 ± 0.8 Ma Error bars are shown at 2 s.e.m.

Vein samples analyzed here have crystallization ages that range in age from 75.5 ± 0.6 Ma to 93.9 ± 0.5 Ma (2s.e.m.). In addition, numerous inherited cores are present, and include ages of 1322 ± 42 Ma, 1386 ± 56 Ma, 1454 ± 39 Ma, and 1803 ± 55 Ma in SMC14-11, 317 ± 7 Ma, 446 ± 7 Ma, 666 ± 13 Ma, 1074 ± 49 Ma, 1194 ± 72 Ma, 1238 ± 45 Ma, and 1503 ± 26 Ma in SMC16-22 (Appendix E, Tab. 15).

CHAPTER V. DISCUSSION

Vein samples analyzed for U/Pb zircon geochronology include three biotite-bearing monzo-granites (QAP), one biotite granodiorite (QAP), one leucocratic monzo-granite (QAP), and one hornblende-bearing granodiorite (QAP). A biotite-bearing granodiorite (QAP) (SMC15-05) sampled from a vein mapped as the leucocratic granite phase of the IB (Field notes, B. Dutrow) was also dated. With a U/Pb age date of 79.2 ± 1.2 Ma and a biotite-bearing granodiorite (QAP) composition, this suggests that SMC15-05 is a phase of the IB and therefore can be used as a reference for IB potential source material for OM-CL plagioclase response comparisons. OM-CL plagioclase colors of this sample (SMC15-05) are moderate green, brown, red, and orange. Moderate green is the distinct color for this source (IB). Brown, red, and orange OM-CL plagioclase responses are also observed in the STB, suggesting that these colors are not distinct responses for either the IB or STB.

For the six vein samples, zircon dates with <5% discordance and < 0.1 U/Th ratio give a range from 72.3 ± 1.2 Ma to 131.0 ± 2.2 Ma (Tab. 15). This range of zircon formation ages suggests that these veins may reflect multiple generations of igneous activity in the area. In addition, this suggests that an extended period of magmatism occurred in this region for at least 49 Ma.

Vein crystallization ages, (calculated using the youngest age peak) for six SMC vein samples, have a range from 75.5 ± 0.6 Ma to 93.9 ± 0.5 Ma (Tab.15). Supplementing these samples by seven samples from Ma (2015) gives an age range of 75.5 ± 0.6 Ma to 101 ± 1 Ma. These ages are consistent with IB crystallization ages (Gaschnig et al., 2010; Kiilsgaard and Lewis, 1985). This consistency suggests the IB was juxtaposed to the SMC before the onset of vein emplacement.

The difference in the oldest age of zircon formation (131.0 ± 2.2 Ma) and vein crystallization onset (101 ± 1 Ma) indicates that magmatism and zircon formation was taking place for ca. 30 Ma before the onset of vein formation.

Inherited zircon cores were observed in two (SMC14-11, SMC16-22) of the six vein samples analyzed in this study (Appendix D). Inherited core ages ranged from 317 ± 7 Ma to 1803 ± 55 Ma and include one Paleoproterozoic age, seven Mesoproterozoic age, one Neoproterozoic age, one Ordovician age, and one Pennsylvanian age.

Inherited zircon cores may provide insight into the likely basement/sub-SMC rocks in the region. While ages are younger than the xenocrystic 1.7 – 1.8 Ga zircon found in Cretaceous-Eocene granitoids (Foster et al., 2006; Gaschnig et al., 2008), the data here suggest rocks containing Proterozoic, Ordovician, and Pennsylvanian zircons were tapped for melting or assimilated during magma ascent.

The majority of inherited core ages found in these two vein samples fall within the range of inherited core ages found in Atlanta lobe IB rocks (Gaschnig et al., 2013). Gaschnig and colleagues found the northern Atlanta lobe of the IB to contain inherited cores with the majority of ages ranging from 2000 to 1000 Ma, with peaks at 1700 to 1600 Ma and 1500 to 1400 Ma. Two cores of Ordovician age were also found. The source material of Proterozoic inherited cores was considered to be Neoproterozoic metasedimentary rocks found near this region (Lewis et al., 2007; Lewis et al., 2010). The Ordovician inherited cores were suggested to be from plutons just east and north of the northern Atlanta lobe (Lund et al., 2010). The majority of inherited core ages in SMC veins range between 2000 and 1000 Ma with no apparent peaks. With one inherited core that is Ordovician in age the SMC inherited cores match the age distribution in Gaschnig et. al. (2013), suggesting they may have similar sources.

In the thirteen vein samples with thin sections and U/Pb zircon ages (this study and Ma, 2015), OM-CL plagioclase colors include bright green, moderate green, brown, moderate blue, red, orange, and yellow. Bright and moderate green plagioclase colors are predominant (occurring in ten samples) and are consistent with OM-CL plagioclase responses observed in IB samples. A caveat, however, is that five of these ten samples also contain a moderate blue-colored plagioclase consistent with responses observed in AM. This suggests that, while plagioclase can be consistent with IB sources, some IB plagioclase shows a color consistent with anatectic melts. Brown, red, and orange are found in multiple potential sources and cannot be directly linked to a distinct source and are, therefore, not diagnostic. Yellow is observed in one vein sample but not observed in the potential source samples. However, only a few samples of each potential source were examined; with additional samples additional colors might be apparent. Ten of thirteen vein samples exhibiting OM-CL plagioclase responses matching IB source samples indicates that, in these samples, plagioclase OM-CL responses and age correlate (Tab. 16).

Extending the CL color and age information to veins without age determinations suggests that veins exhibiting the distinct OM-CL plagioclase responses can be attributed to potential sources. Bright green and/or moderate green colors are consistent with the IB. Veins with pink plagioclase OM-CL are inferred to be STB and veins with turquoise green and/or blue responses are inferred to be AM. However, no samples with pink or blue plagioclase have ages, thus making them the highest priority for future geochronology.

Twelve vein samples without age dates contain OM-CL plagioclase responses that suggest specific sources. Three of the twelve contain moderate green, consistent with the IB, two contain blue plagioclase consistent with AM, and one contains pink plagioclase consistent with the STB (Tab. 16). Two veins display both green and blue plagioclase which are distinct to the

Table 16. Samples with OM-CL Plagioclase colors, age dates, and likely source determined by OM-CL.

Sample Unit	Sample Number	Distinct OM-CL Plagioclase Color	Age ± (2σ)	Likely Source by OM-CL	Likely Source with Addition of Petrography
Leucocratic Granite Phase of IB	SMC15-05	Green and Orange	79.2 ± 1.2 Ma	IB	IB
Age Dated Veins	SMC13-132	Green	87.4 ± 0.4 Ma	IB	IB
	SMC14-09	Brown	93.9 ± 0.5 Ma	IB	IB
	SMC14-11	Yellow	80.6 ± 0.7 Ma	ND	ND
	SMC14-43	Green and Orange	75.5 ± 0.6 Ma	IB	IB
	SMC16-09	Brown	86.5 ± 0.5 Ma	ND	ND
	SMC16-22	Yellow	80.3 ± 0.6 Ma	ND	IB
Veins Without Age Dates	SMC11-30	Green and Blue		IB or AM	IB or AM
	SMC13-05	Green, Pink, and Orange		IB or STB	IB
	SMC13-31	Brown		ND	STB
	SMC14-26	Blue		AM	AM
	SMC14-40	Blue		AM	AM
	SMC14-44	Brown		ND	ND
	SMC14-47	Green and Pink		IB or STB	IB or STB
	SMC14-61	Green		IB	IB
	SMC14-62	Green		IB	IB
	SMC14-112	Green and Blue		IB or AM	STB
	SMC15-03	Green		STB	STB
	SMC16-34	Green		IB	IB
Ma's Vein Samples	MC13ST-05	Brown		ND	ND
	MC13ST-14	Green and Blue	77 ± 1 Ma*	IB or AM	IB or AM
	MC13ST-18	Green and Blue	92 ± 1 Ma*	IB or AM	IB
	MC14ST-04	Green and Blue	92 ± 1 Ma*	IB or AM	IB or AM
	MC14ST-08	Green and Blue	99 ± 1 Ma*	IB or AM	IB
	MC14ST-10	Green	84 ± 1 Ma*	IB	IB
	MC14ST-12	Green and Blue	101 ± 1 Ma*	IB or AM	IB
	MC14ST-13	Green	95 ± 1 Ma*	IB	IB

* = ages from (Ma, 2015)   ND = Not determined (OM-CL or petrography not distinct to a source)

IB and AM (Tab. 16). An additional two samples contain both green and pink plagioclase which are distinct colors for the IB and STB (Tab. 16). Two veins contain plagioclase with colors that do not match any potential source.

A potential reason for a single sample matching multiple sources could be due to post crystallization overprinting of primary plagioclase CL responses by altering fluids. Overprinting by altering fluids results in vein samples having single plagioclase grains with a primary plagioclase color distinct to one source observed with a secondary overprinting plagioclase response that matches the distinct color of another source. Pervasive overprinting causes difficulty in distinguishing the primary from the secondary CL responses and results in assigning multiple likely sources to a single sample.

Several caveats of the CL method should be taken into account. OM-CL feldspar imaging is a qualitative method, thus making a direct comparison between samples more difficult than a quantitative method. For example, distinguishing between both groupings of a color and differing shades within a color group can be difficult, especially if OM-CL work is performed with differing operating conditions or by multiple investigators whose perception of color may differ (e.g. bright green vs moderate green). Only a small subset of potential source rocks has been imaged. With the IB composed of numerous intrusions (e.g. Gaschnig et al., 2010), more samples are needed to characterize the variability in the region.

A partial solution is to quantify the CL response by using spectroscopic methods. Use of OM-CL spectrum can distinguish two samples with the same OM-CL response (e.g. both Al-O-Al centers and REEs cause a blue OM-CL response in plagioclase (Götze, 2012; Götze et al., 1999). This method is another approach to improve sample matching and will allow for use of cathodoluminescent activators to categorize samples.

Rock classification for samples of the two potential vein source batholiths include syeno-granitic, monzo-granitic, and granodioritic. The STB was found to have both syeno-granites (QAP) and monzo-granites (QAP). The IB was found to only have granodiorites (QAP). The six age-dated veins of this study and seven added from Ma (2015) include (five) monzo-granites (QAP) and (six) granodiorites (QAP). Due to STB samples and IB aged veins both including monzo-granites (QAP), this indicates that monzo-granites (QAP) are not distinct to one potential source. Therefore, only granodiorites (QAP) are distinctly found in the IB and only syeno-granites (QAP) are distinctly found in the STB, matching previous work in the region (Bennett, 1980; Bennett and Knowles, 1985; Kiilsgaard and Lewis, 1985; Reid, 1963).

Veins without age dates include five of twelve samples that are monzo-granites, four that are granodiorites likely sourced by the IB, and three that are syeno-granites likely sourced by the STB (Tab. 16). Adding the likely source determinations by rock composition to the likely vein sources determined by OM-CL plagioclase responses reduces the number of likely sources per sample and determines a likely source for samples. Two vein samples of unknown age had multiple likely vein sources reduced to a single likely source and one sample with an undetermined likely source by OM-CL plagioclase response had one determined by sample composition (Tab. 16). However, of the seven samples with likely sources determined by composition one did not match either of the likely sources as determined by OM-CL plagioclase responses. A potential reason could be due to the composition of the final melt evolving from the source.

Evaluating the spatial distribution of veins of unknown source shows no distinct locations. The Sawtooth batholith and anatectic melt sources show no apparent grouping. However, the Idaho batholith shows grouping in the east-central portion of the SMC (Fig. 27).

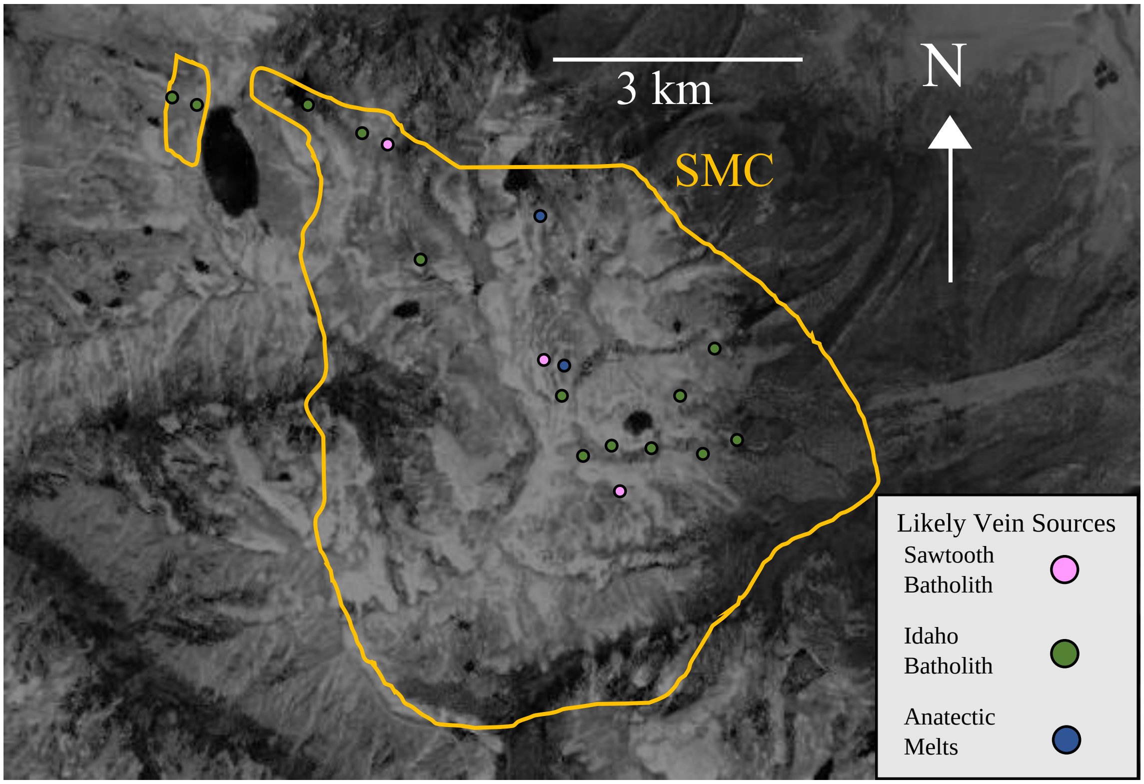

Figure 27. Google earth map of SMC showing the likely source of all veins of unknown source.

Zirconium saturation temperatures calculated for samples have an overlapping range of temperatures: STB of 658 to 737 °C with an average of 688 ± 32 °C (1σ) and a range for the IB of 592 to 693 °C with an average of 648 ± 51 °C (1σ). Thus, the zirconium saturation temperature averages are within error and are not helpful to determine potential sources.

Major element chemistry of samples analyzed by EMP have a decrease in anorthite content from core to rim with change in OM-CL plagioclase responses from green to brown (SMC13-132) and brown to red (SMC16-34, Fig. 11, 12). Rims of grains with quenched luminescence correspond to lower anorthite content. This chemical change suggests that calcium may have been leached in an altering fluid. SMC13-132 contains blue alteration on plagioclase

rims suggesting potential rare earth elements (Götze et al., 1999). SMC16-34 contains dark red alteration on plagioclase rims suggesting oxidation of Fe^{2+} to Fe^{3+} by altering fluids (Geake et al., 1973).

Major element feldspar mineral chemistry does correlate to OM-CL plagioclase responses. However, luminescence is caused by trace elements and not the major elements which were measured for feldspar mineral chemistry. This suggests that alteration of the rims of compositionally zoned plagioclase by fluids that mobilize calcium results in the apparent observed major element correlation to OM-CL plagioclase response.

CHAPTER VI. CONCLUSIONS

U/Pb ages of zircons found in the six felsic samples studied here from spatially throughout the SMC have an age range of 72.3 ± 1.2 Ma to 131.0 ± 2.2 Ma. Such a range in ages indicates that pulses of magmatism occurred in this area for at least 49 million years, beginning by 131 Ma. Vein crystallization ages give an age range of 75.5 ± 0.6 Ma to 101 ± 1 Ma, indicating 26 Ma of vein emplacement. These ages are consistent with those of IB emplacement and suggest the SMC was likely juxtaposed near the IB at that onset of vein formation.

Inherited zircon cores (317 ± 7 Ma to 1803 ± 55 Ma) from the six veins have ages throughout the Proterozoic, with a few ages in the Ordovician and Pennsylvanian. This range indicates melting or assimilation of older zircons with Proterozoic, Ordovician, and Pennsylvanian ages.

OM-CL plagioclase responses correlate with U/Pb geochronology data for the IB. This correlation indicates that for select samples, plagioclase OM-CL responses provide a first order approximation to a possible source in the absence of geochronology.

APPENDIX A. PETROGRAPHIC REPORTS

SAMPLE: LF-12

Last update: 2/26/20

Petrographer: Kyle Tollefson

LOCATION: 44°09.765N, 115°02.176W
COLLECTOR: Barbara Dutrow

DATE COLLECTED:

AGE DATE:

ROCK TYPE: Hornblende-bearing Biotite Monzo-Granite

MEGASCOPIC DESCRIPTION: Leucocratic, white, coarse-grained granitoid chiefly composed of microcline megacrysts within matrix of plagioclase, quartz, and minor biotite.
===
MINERAL ASSEMBLAGES: (Point counted modes)

Plagioclase (22%) [0.25-6 mm] Anhedral to subhedral grains exhibiting albite twinning and major seritization**.**

Microcline (40%) [5-10 mm] Subhedral to euhedral megacrysts with pervasive perthitic intergrowths. Grains also exhibit carlsbad twinning and major sericite alteration.

Quartz (28.3%) [0.25-4 mm] Subhedral to euhedral grains with slight sweeping extinction.

Biotite (9.3%) [<2.5 mm] Anhedral to subhedral laths with brown to green pleochroism and birds eye extinction. Grains exhibit pervasive chloritization.

Hornblende (tr%) [<0.2-1 mm] Subhedral to euhedral grains with red to brown pleochroism and simple twinning.

Apatite (tr%) [<0.125 mm] Euhedral colorless grains with moderate relief and 1st order birefringence.

Sericite (tr%) [<0.1 mm] Subhedral colorless laths exhibiting high birefringence.

Magnetite (tr%) [<0.25 mm] Anhedral opaque grains exhibiting brownish-grey, isotropic, and pitted nature in reflective light.

Chlorite (tr%) [0.1-2.5 mm] Subhedral green laths replacing biotite.

Zircon (tr%) [<0.125 mm] Euhedral colorless grains with high relief and high birefringence.
===

TEXTURES: Hypidiomorphic porphyritic texture dominated by microcline megacrysts in a matrix of, plagioclase, quartz, and biotite, respectively. Microcline has pervasive perthitic exsolution.

ALTERATION: Pervasive metasomatic/hydrothermal alteration from biotite to chlorite and plagioclase to sericite/muscovite.

OPTICAL CATHODOLUMINESCENCE

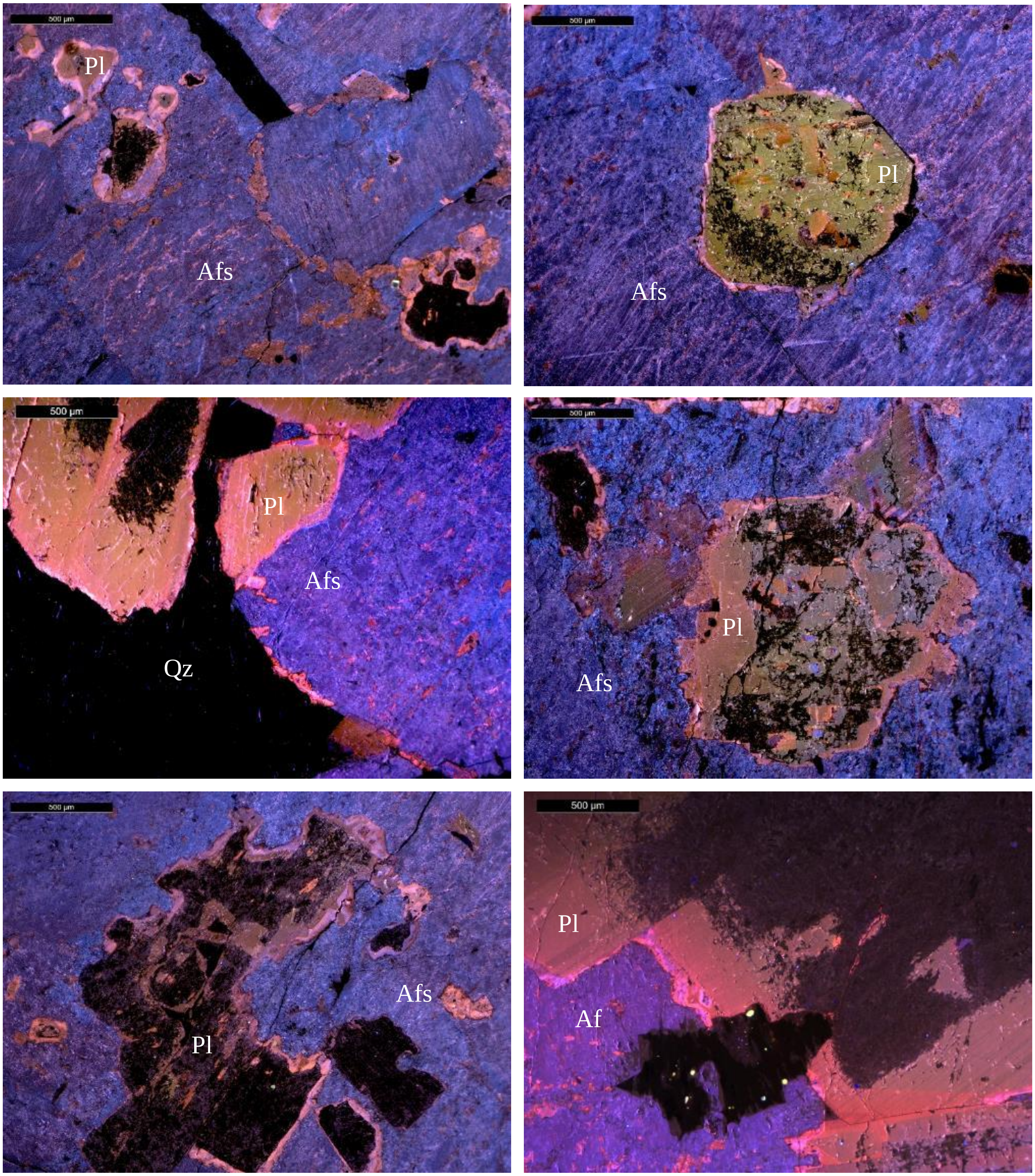

Mineral abbreviations taken from (Whitney and Evans, 2010). Moderate blue alkali feldspar with pervasive pink albite exsolution (perthite). Highly altered (sericitized) cores of plagioclase ranging in color from pink to brown.

COMMENTS AND INTERPRETATION:

Based on the QAP ratio of 31.34:44.30:24.36of the likely primary magmatic minerals, this rock is best classified as Hornblende-bearing Biotite Monzo-Granite with secondary alteration to muscovite/sericite and chlorite. The fact that the alkali-feldspar and plagioclase from separate phenocrysts implies that the granite is a subsolvus granite.

The magmatic paragenetic sequence is likely (Plagioclase) > (Microcline + quartz) > (Biotite + opaques) and then hydrothermal alteration to muscovite/sericite + chlorite.

Following the crystallization of the igneous minerals there are a series of subsolidus changes to the minerals. Post-crystallization deformation likely generated the quartz deformations features and allowed access to aqueous fluids associated with alteration.

Pervasive perthitic microcline, cl responses of pervasive pink albite exsolution, and sample location suggest this sample is part of the Sawtooth Batholith.

SAMPLE: SMC 11-12

Last update: 2/26/20

Petrographer: Kyle Tollefson

LOCATION: 44°01.138N, 114°56.427W
COLLECTOR: Barbara Dutrow

DATE COLLECTED: July 21st 2011

AGE DATE: 47.18 +0.54 Ma

ROCK TYPE: Muscovite-bearing Biotite Monzo-Granite

MEGASCOPIC DESCRIPTION: Leucocratic, white, coarse-grained phaneritic granitoid chiefly composed of microcline, plagioclase, and quartz with minor biotite.
===
MINERAL ASSEMBLAGES: (Point counted modes)

Plagioclase (20%) [0.1-1 mm] Subhedral to euhedral grains exhibiting albite twinning and minor seritization.

Microcline (35%) [0.1-3 mm] Anhedral to subhedral grains exhibiting pervasive perthite and major seritization.

Quartz (40%) [0.125-3.75 mm] Anhedral to subhedral grains exhibiting minor sweeping extinction and checkerboard extinction.

Biotite (5%) [0.25-3 mm] Anhedral to subhedral laths exhibiting brown to green pleochroism, birds eye extinction, and minor chloritization.

Sericite (0.3%) [0.1 mm] Anhedral to **s**ubhedral colorless laths exhibiting high birefringence.

Hematite (tr%) [0.1 mm] Anhedral to subhedral opaque grains with red rims.

Magnetite (tr%) [0.075 mm] Subhedral to euhedral opaque grains exhibiting brownish-grey, isotropic, and a pitted nature in reflective light.

Chlorite (tr%) [0.1-0.75 mm] Subhedral green laths replacing biotite.
===

TEXTURES: Allotriomorphic coarse-grained texture dominated by microcline, plagioclase, quartz, and biotite, respectively. Microcline exhibits pervasive perthite texture.

ALTERATION: Minor metasomatic/hydrothermal alteration from biotite to chlorite and plagioclase to sericite/muscovite.

OPTICAL CATHODOLUMINESCENCE

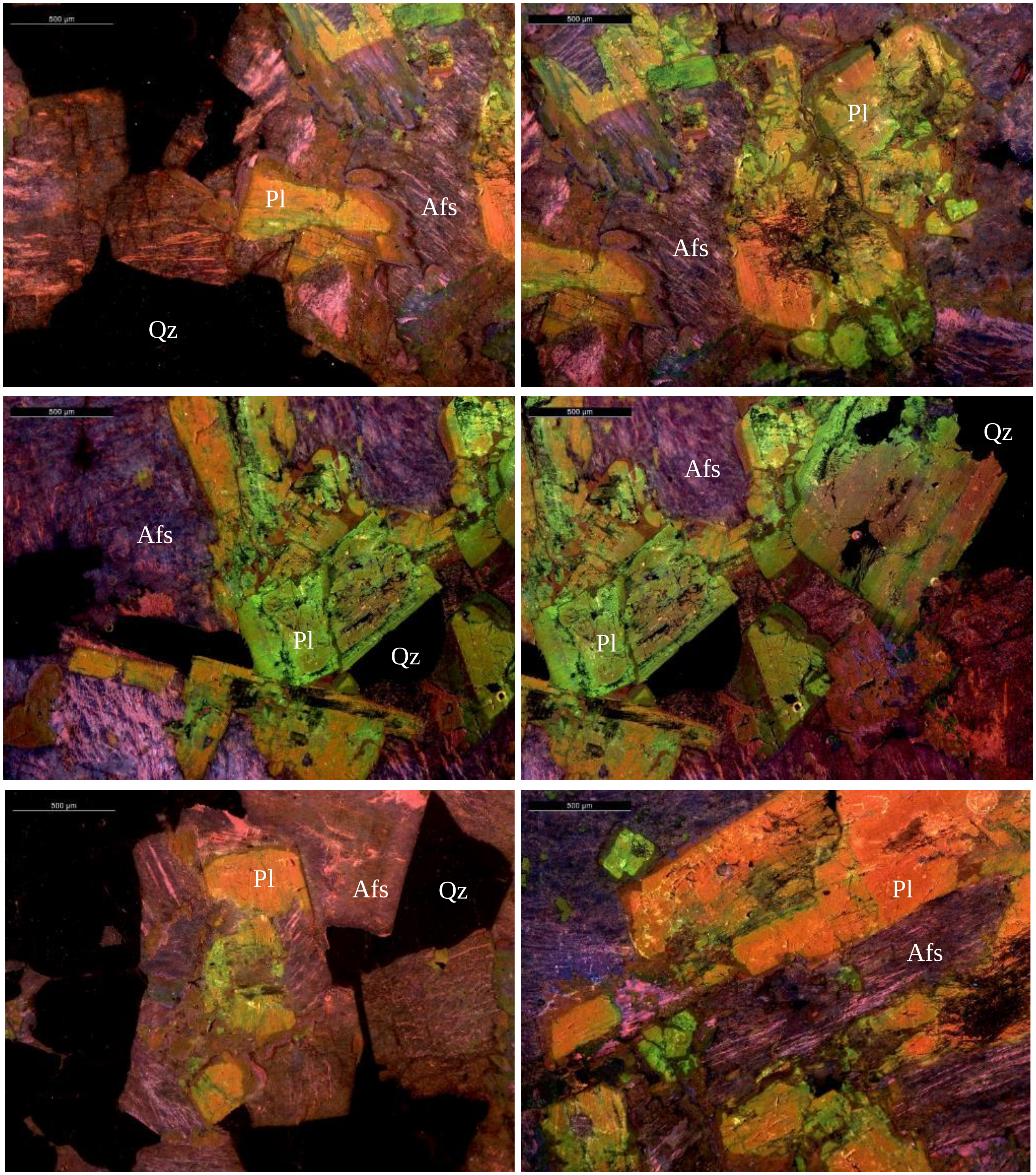

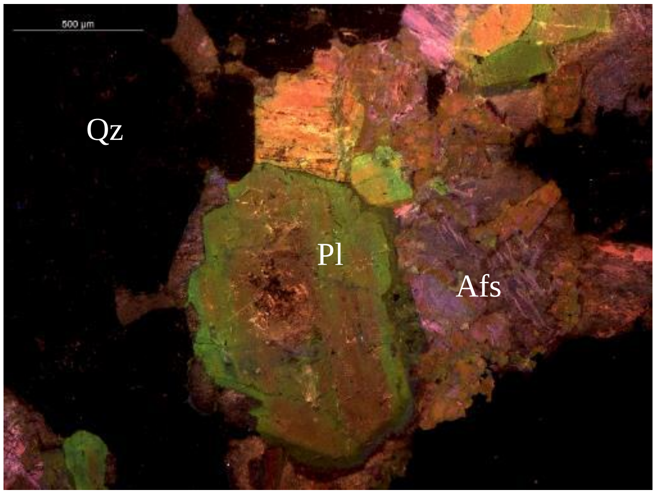

Mineral abbreviations taken from (Whitney and Evans, 2010). Moderate blue alkali feldspar with pervasive pink albite exsolution (perthite). Plagioclase ranging in color from neon orange to neon green.

COMMENTS AND INTERPRETATION:

Based on the QAP ratio of 42.11:36.84:21.05of the likely primary magmatic minerals, this rock is best classified as Muscovite-bearing Biotite Monzo-Granite with secondary alteration to muscovite/sericite and chlorite. The fact that the alkali-feldspar and plagioclase from separate phenocrysts implies that the granite is a subsolvus granite.

The magmatic paragenetic sequence is likely (plagioclase+opaques) > (microcline + quartz) and then hydrothermal alteration to muscovite/sericite + chlorite.

Following the crystallization of the igneous minerals there are a series of subsolidus changes to the minerals. Post-crystallization deformation likely generated the quartz deformations features and allowed excess to aqueous fluids associated with alteration.

An age date of 47.18 +0.54 Ma, pervasive perthitic microcline, neon orange plagioclase CL responses, and sample location suggest this sample is part of the Sawtooth Batholith.

SAMPLE: SMC 11-13

Last update: 2/26/20

Petrographer: Kyle Tollefson

LOCATION: 44°06.047N, 114°57.670W
COLLECTOR: Barbara Dutrow

DATE COLLECTED: July 22nd 2011

AGE DATE: 46.50+0.48 Ma

ROCK TYPE: Hornblende Biotite-bearing Syeno-Granite

MEGASCOPIC DESCRIPTION: Leucocratic, white, coarse-grained granitoid chiefly composed of microcline phenocrysts in a matrix of plagioclase, and quartz with minor biotite.

===

MINERAL ASSEMBLAGES: (Point counted modes)

Plagioclase (11%) [0.1-2 mm] Anhedral to subhedral grains exhibiting albite twinning and moderate seritization.

Microcline (52.7%) [0.5-5 mm] Anhedral grains exhibiting pervasive perthite, carlsbad twinning, and major seritization. pervasive myrmekites or graphic texture of plagioclase-quartz develop at margins with plagioclase.

Quartz (33%) [0.5-2, 0.025-0.1 mm] Anhedral to subhedral grains exhibiting minor sweeping extinction.

Biotite (3.3%) [0.25-2 mm] Anhedral to subhedral laths exhibiting brown to reddish brown pleochroism, birds eye extinction, and minor chloritization.

Hornblende (tr%) [0.4 mm] Subhedral to euhedral grains exhibiting red to beige pleochroism.

Hematite (tr%) [0.4 mm] Euhedral opaque to dark red grains.

Magnetite (tr%) [0.5-0.25 mm] Anhedral to subhedral opaque grains exhibiting brownish-grey, isotropic, and a pitted nature in reflective light.

Chlorite (tr%) [0.05 mm] Subhedral green laths replacing biotite.

===

TEXTURES: Allotriomorphic porphyritic texture dominated by microcline megacrysts in a plagioclase, quartz, and biotite matrix, respectively. Microcline exhibits pervasive perthite texture. Microcline, plagioclase, and quartz exhibit myrmekitic texture.

ALTERATION: Moderate metasomatic/hydrothermal alteration from biotite to chlorite and plagioclase to sericite/muscovite.

OPTICAL CATHODOLUMINESCENCE

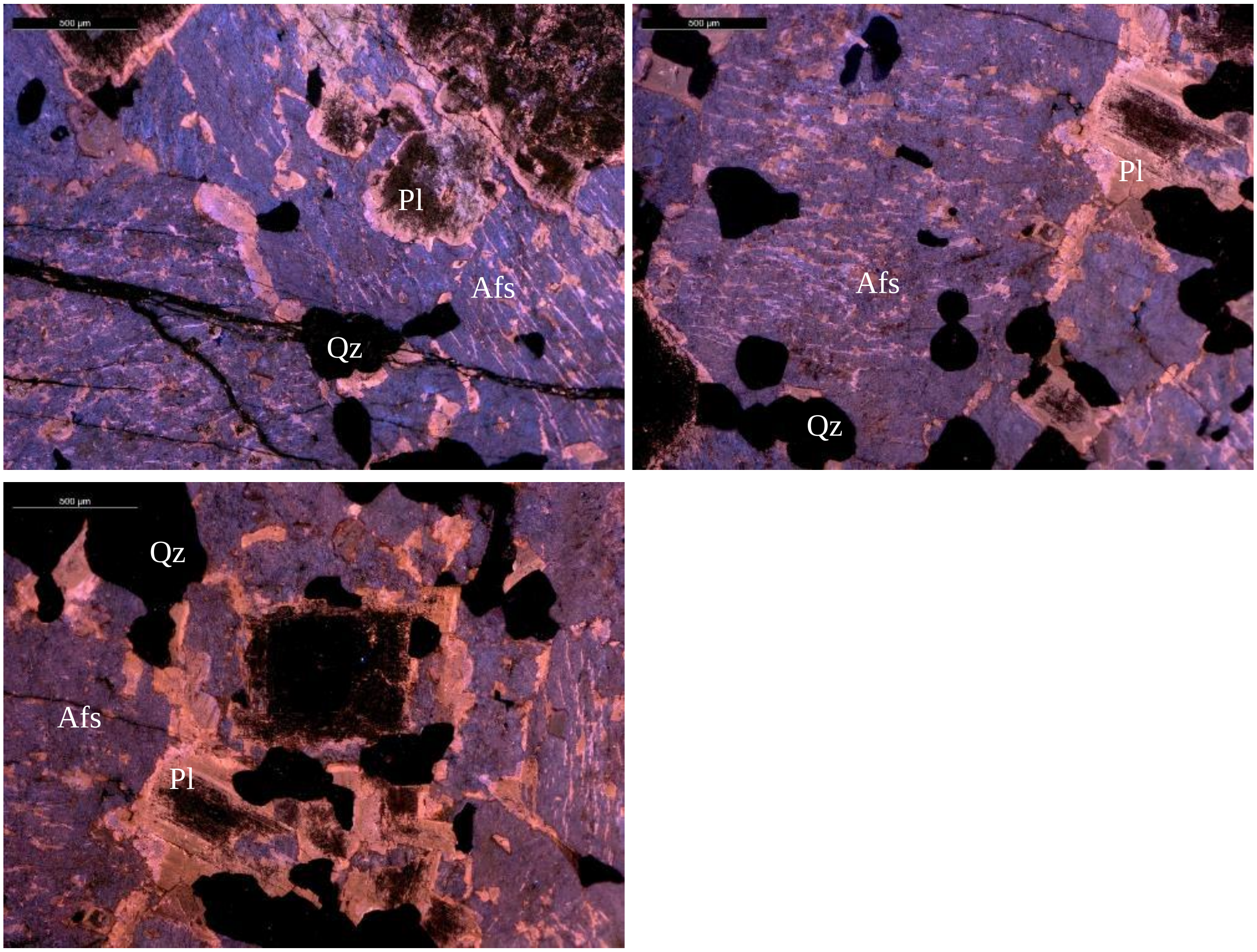

Mineral abbreviations taken from (Whitney and Evans, 2010). Moderate blue alkali feldspar with pervasive pink albite exsolution (perthite). Highly altered (seritized) cores of plagioclase ranging in color from pink to brown.

COMMENTS AND INTERPRETATION:

Based on the QAP ratio of 34.13:54.50:11.38 of the likely primary magmatic minerals, this rock is best classified as Hornblende Biotite-bearing Syeno-Granite with secondary alteration to muscovite/sericite and chlorite. The fact that the alkali-feldspar and plagioclase from separate phenocrysts implies that the granite is a subsolvus granite.

The magmatic paragenetic sequence is likely (Hornblende) > (plagioclase+opaques) > (microcline + quartz) and then hydrothermal alteration to muscovite/sericite + chlorite.

Following the crystallization of the igneous minerals there are a series of subsolidus changes to the minerals. Post-crystallization deformation likely generated the quartz deformations features and allowed excess to aqueous fluids associated with alteration.

An age date of 46.50+0.48 Ma, Syeno-Granite classification, pervasive perthitic microcline, pink plagioclase and pervasive albite exsolution CL responses, and sample location suggest this sample is part of the Sawtooth Batholith.

SAMPLE: SMC 13-39

Last update: 2/26/20

Petrographer: Kyle Tollefson

LOCATION: 44°12.772N, 115°03.923W
COLLECTOR: Barbara Dutrow

DATE COLLECTED: July 14th 2013

AGE DATE:

ROCK TYPE: Hornblende Biotite-bearing Monzo-Granite

MEGASCOPIC DESCRIPTION: Leucocratic, white, coarse-grained phaneritic granitoid chiefly composed of microcline, plagioclase, and quartz with minor biotite.
==
MINERAL ASSEMBLAGES: (Point counted modes)

Plagioclase (22.7%) [0.1-10 mm] Subhedral grains exhibiting albite twinning and moderate seritization.

Microcline (30.7%) [0.25-9 mm] Subhedral grains exhibiting pervasive perthite, and moderate seritization.

Quartz (43%) [0.1-7.5 mm] Anhedral to subhedral grains exhibiting minor sweeping extinction.

Biotite (3.7%) [0.1-1.75 mm] Subhedral laths exhibiting brown to green pleochroism, birds eye extinction, and major chloritization.

Hornblende (tr%) [0.3 mm] Subhedral grains exhibiting dark reddish brown pleochroism.

Magnetite (tr%) [<0.75 mm] Anhedral to subhedral opaque grains exhibiting brownish-grey, isotropic, and a pitted nature in reflective light.

Sericite (tr%) [<0.1 mm] Subhedral colorless laths exhibiting high birefringence.

Epidote (tr%) [<0.1 mm] Subhedral light green grains exhibiting moderate relief and high birefringence.

Chlorite (tr%) [0.05-0.2 mm] Subhedral green laths replacing biotite.

Zircon (tr%) [<0.1 mm] Euhedral colorless grains with high relief and high birefringence.
==

TEXTURES: Hypidiomorphic coarse-grained texture dominated by microcline, plagioclase, quartz, and biotite, respectively. Microcline exhibits perthite texture.

ALTERATION: Moderate metasomatic/hydrothermal alteration from biotite to chlorite and plagioclase to sericite/muscovite.

OPTICAL CATHODOLUMINESCENCE

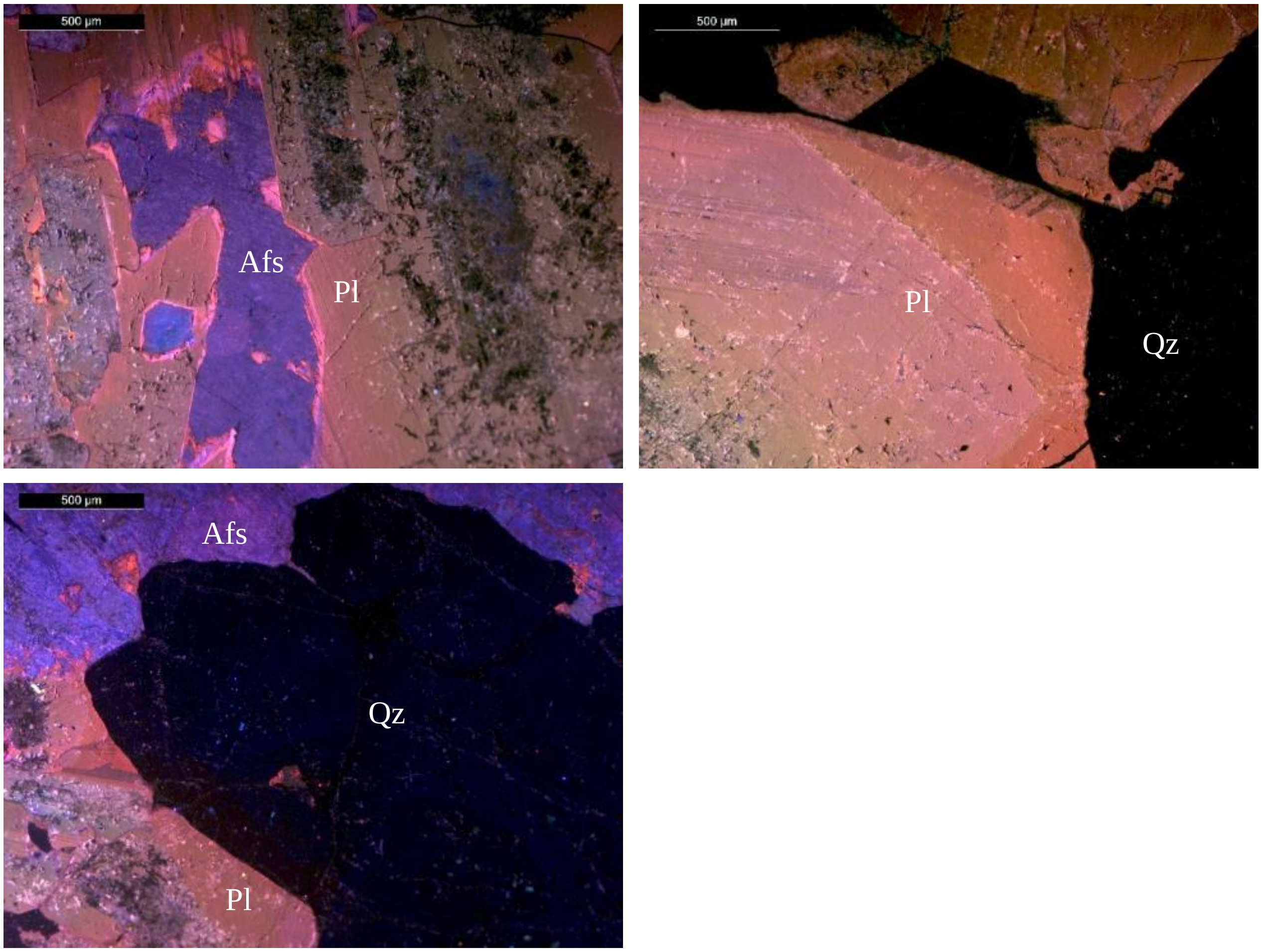

Mineral abbreviations taken from (Whitney and Evans, 2010). Moderate to dark blue alkali feldspar with pervasive pink albite perthite. Brow to red/pink plagioclase with highly altered cores.

COMMENTS AND INTERPRETATION:

Based on the QAP ratio of 44.61:31.85:23.55 of the likely primary magmatic minerals, this rock is best classified as Hornblende Biotite-bearing Monzo-Granite with secondary alteration to muscovite/sericite and chlorite. The fact that the alkali-feldspar and plagioclase from separate phenocrysts implies that the granite is a subsolvus granite.

The magmatic paragenetic sequence is likely (Plagioclase + microcline) > (Biotite + opaques) > (quartz) and then hydrothermal alteration to muscovite/sericite + chlorite.

Following the crystallization of the igneous minerals there are a series of subsolidus changes to the minerals. Post-crystallization deformation likely generated the quartz deformations features and allowed excess to aqueous fluids associated with alteration.

Pervasive perthitic microcline and sample location suggest this sample is part of the Sawtooth Batholith.

SAMPLE: SMC 13-42

Last update: 2/26/20

Petrographer: Kyle Tollefson

LOCATION: 44°12.510N, 115°04.257W
COLLECTOR: Barbara Dutrow

DATE COLLECTED: July 14th 2013

AGE DATE:

ROCK TYPE: Hornblende-bearing Biotite Syeno-Granite

MEGASCOPIC DESCRIPTION: Leucocratic, white, medium-grained phaneritic granitoid chiefly composed of microcline, plagioclase, and quartz with minor biotite.
===
MINERAL ASSEMBLAGES: (Point counted modes)

Plagioclase (18.7%) [0.1-10 mm] Subhedral grains exhibiting albite twinning and major seritization.

Microcline (48.7%) [0.25-9 mm] Subhedral to euhedral grains exhibiting pervasive perthite, carlsbad twinning, and moderate seritization.

Quartz (27.7%) [0.1-7.5 mm] Anhedral to subhedral grains exhibiting minor sweeping extinction.

Biotite (5%) [0.1-2 mm] Subhedral laths exhibiting brown to green pleochroism, birds eye extinction, and major chloritization.

Hornblende (tr%) [0.2-0.75 mm] Subhedral grains exhibiting dark reddish brown to brown pleochroism.

Magnetite (tr%) [<0.75 mm] Anhedral to subhedral opaque grains exhibiting brownish-grey, isotropic, and a pitted nature in reflective light.

Sericite (tr%) [<0.1 mm] Subhedral colorless laths exhibiting high birefringence.

Hematite (tr%) [<0.5] Anhedral opaque grains with red rims.

Epidote (tr%) [<0.1 mm] Subhedral light green grains exhibiting moderate relief and high birefringence.

Apatite (tr%) [<0.1 mm] Subhedral colorless grains with moderate relief and 1st order birefringence.

Chlorite (tr%) [0.1-1.5 mm] Subhedral green laths replacing biotite.

Zircon (tr%) [<0.1 mm] Euhedral colorless grains with high relief and high birefringence.
===

TEXTURES: Hypidiomorphic medium-grained texture dominated by microcline, plagioclase, quartz, and biotite, respectively. Microcline exhibits perthite texture.

ALTERATION: Pervasive metasomatic/hydrothermal alteration from biotite to chlorite and plagioclase to sericite/muscovite.

OPTICAL CATHODOLUMINESCENCE

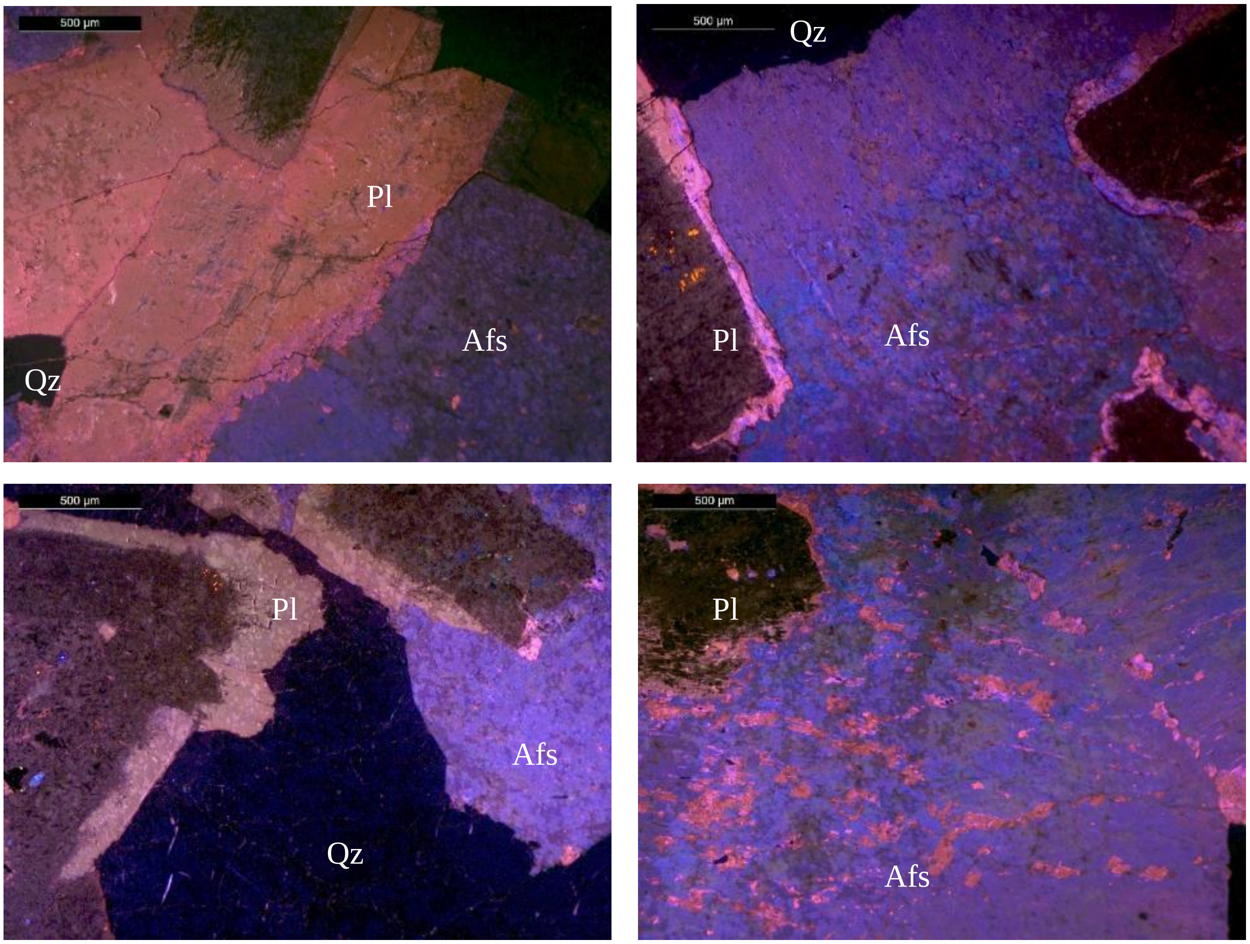

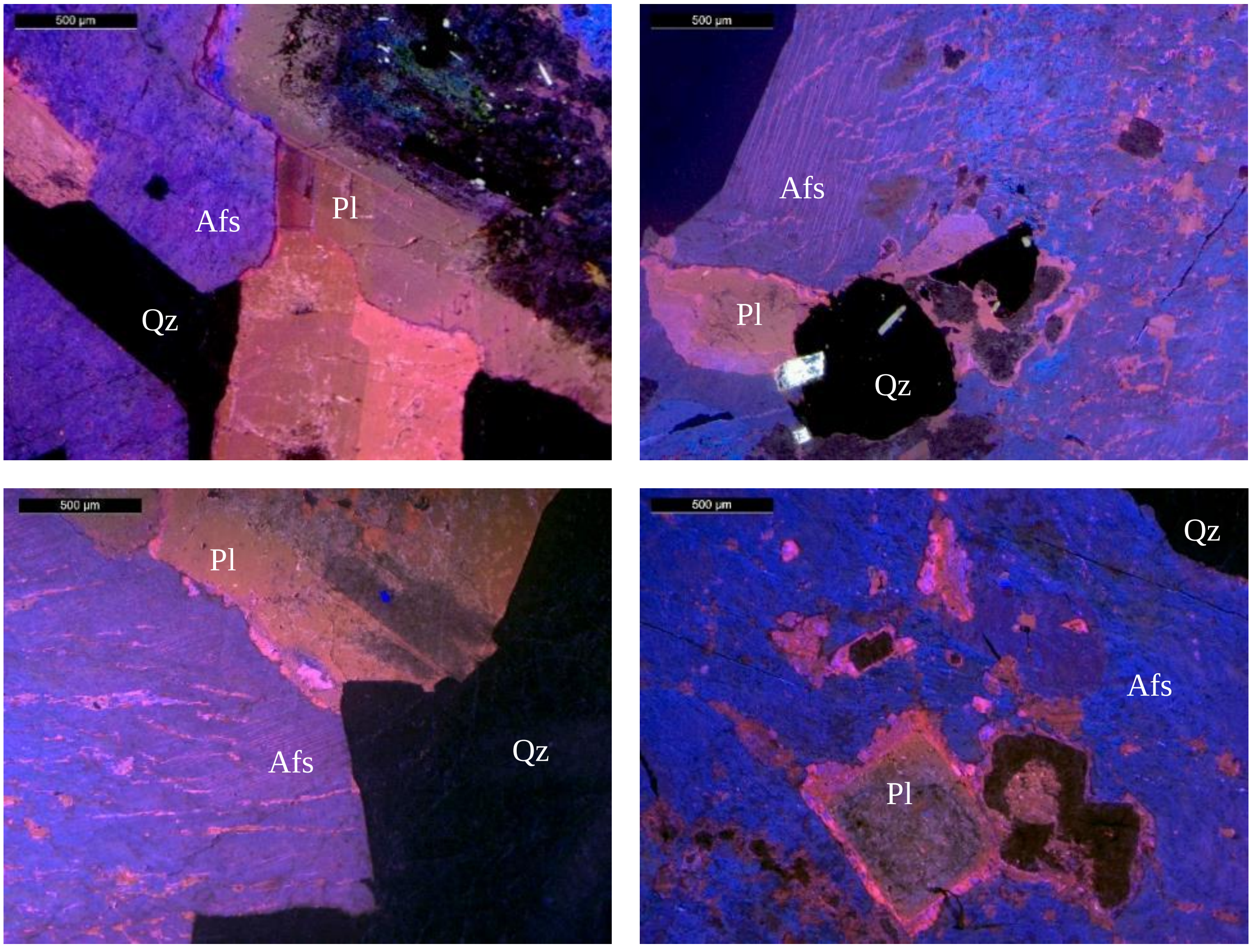

Mineral abbreviations taken from (Whitney and Evans, 2010). Moderate to dark blue alkali feldspar with pervasive pink albite perthite. Brown to pink/red plagioclase with highly altered cores.

COMMENTS AND INTERPRETATION:

Based on the QAP ratio of 29.13:51.21:19.66 of the likely primary magmatic minerals, this rock is best classified as Hornblende-bearing Biotite Syeno-Granite with secondary alteration to muscovite/sericite and chlorite. The fact that the alkali-feldspar and plagioclase from separate phenocrysts implies that the granite is a subsolvus granite.

The magmatic paragenetic sequence is (Plagioclase + microcline) > (Biotite + opaques) > (quartz) and then hydrothermal alteration to muscovite/sericite + chlorite.

Following the crystallization of the igneous minerals there are a series of subsolidus changes to the minerals. Post-crystallization deformation likely generated the quartz deformations features and allowed excess to aqueous fluids associated with alteration.

Syeno-Granite classification, pervasive perthitic microcline, and sample location suggest this sample is part of the Sawtooth Batholith.

SAMPLE: SMC 11-14

Last update: 2/26/20

Petrographer: Kyle Tollefson

LOCATION: 44°06.056N, 114°57.566W
COLLECTOR: Barbara Dutrow

DATE COLLECTED: July 22nd 2011

AGE DATE: 85.00+2.4 Ma

ROCK TYPE: Biotite-bearing Granodiorite

MEGASCOPIC DESCRIPTION: Leucocratic, white, medium-grained phaneritic equigranular granitoid chiefly composed of microcline, plagioclase, and quartz with minor biotite.
===
MINERAL ASSEMBLAGES: (Point counted modes)

Plagioclase (42.3%) [0.3-2 mm] Subhedral to euhedral grains exhibiting albite twinning and moderate seritization.

Microcline (21.7%) [0.1-5 mm] Anhedral to subhedral grains exhibiting minor perthite and minor seritization. Moderate myrmekites of plagioclase-quartz develop at margins with plagioclase.

Quartz (32%) [0.1-3 mm] Anhedral grains exhibiting minor sweeping extinction.

Biotite (3.3%) [0.05-0.75 mm] Anhedral to subhedral laths exhibiting brown to reddish brown pleochroism, birds eye extinction, and minor chloritization.

Sericite (tr%) [<0.1 mm] Subhedral colorless laths exhibiting high birefringence.

Apatite (tr%) [<0.1 mm] Anhedral to subhedral colorless grains with moderate relief and 1st order birefringence.

Magnetite (tr%) [0.05-0.25 mm] Anhedral opaque grains exhibiting brownish-grey, isotropic, and a pitted nature in reflective light.

Chlorite (tr%) [0.1 mm] Subhedral green laths replacing biotite.

Zircon (tr%) [<0.05 mm**]** Euhedral colorless grains with high relief and high birefringence.
===

TEXTURES: Allotriomorphic medium-grained equigranular texture dominated by microcline, plagioclase, quartz, and biotite, respectively. Microcline exhibits minor perthite. Microcline, plagioclase, and quartz exhibit myrmekitic texture.

ALTERATION: Minor metasomatic/hydrothermal alteration from biotite to chlorite and plagioclase to sericite/muscovite.

OPTICAL CATHODOLUMINESCENCE

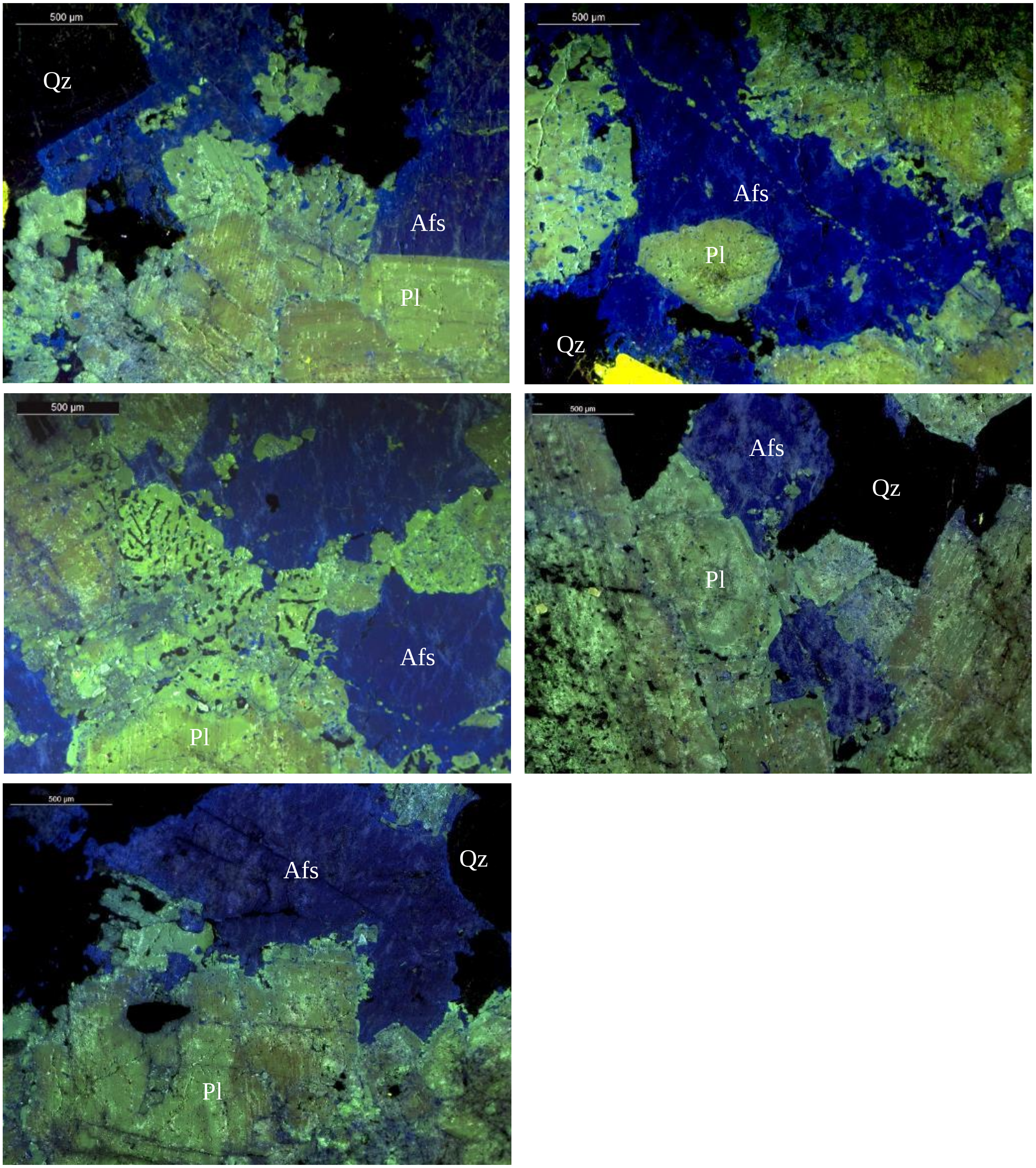

Mineral abbreviations taken from (Whitney and Evans, 2010). Dark blue alkali feldspar and moderate to dark green plagioclase. Oscillatory zoning present in plagioclase and myrmekitic texture observed.

COMMENTS AND INTERPRETATION:

Based on the QAP ratio of 33.33:22.60:44.06 of the likely primary magmatic minerals, this rock is best classified as Muscovite Biotite-bearing Granodiorite with secondary alteration to muscovite/sericite and chlorite. The fact that the alkali-feldspar and plagioclase from separate phenocrysts implies that the granite is a subsolvus granite.

The magmatic paragenetic sequence is likely (plagioclase) > (biotite + opaques) > (Microcline + quartz) and then hydrothermal alteration to muscovite/sericite + chlorite.

Following the crystallization of the igneous minerals there are a series of subsolidus changes to the minerals. Post-crystallization deformation likely generated the quartz deformations features and allowed excess to aqueous fluids associated with alteration.

An age date of 85.00+2.4 Ma, Granodiorite classification, myrmekitic texture, green plagioclase with oscillatory zoning CL responses, and sample location suggest this sample is part of the Idaho Batholith.

SAMPLE: MC14ST-19

Last update: 2/26/20

Petrographer: Kyle Tollefson

LOCATION: 44°09.278N, 115°03.085W
COLLECTOR: Chong Ma

DATE COLLECTED:

AGE DATE: 92±1Ma

ROCK TYPE: Hornblende-bearing Biotite Granodiorite

MEGASCOPIC DESCRIPTION: Leucocratic, white, medium-grained phaneritic granitoid chiefly composed of microcline, plagioclase, and quartz with minor biotite.
==

MINERAL ASSEMBLAGES: (Point counted modes)

Plagioclase (35.3%) [0.25-8 mm] Anhedral to subhedral grains exhibiting albite twinning and moderate seritization.

Microcline (19%) [0.25-2.5 mm] Anhedral to subhedral grains exhibiting, minor perthite, and minor seritization. Moderate myrmekites of plagioclase-quartz develop at margins with plagioclase.

Quartz (36%) [0.25-8 mm] Anhedral to subhedral grains exhibiting moderate sweeping extinction.

Biotite (6.7%) [0.1-5 mm] Subhedral laths exhibiting brown to green pleochroism, birds eye extinction, and minor chloritization.

Sericite (1.7%) [<0.5 mm] Subhedral colorless laths exhibiting high birefringence.

Apatite (tr%) [<0.25 mm] Subhedral colorless grains with moderate relief and 1st order birefringence.

Clinozoisite (tr%) [0.01-1 mm] Anhedral to subhedral colorless grains with moderate relief and lst order birefringence.

Hornblende (1.3%) [1-5 mm] Subhedral to euhedral grains exhibiting green to brown pleochroism and 60-120 clevage.

Chlorite (tr%) [0.1-0.75 mm] Subhedral green laths replacing biotite.

Zircon (tr%) [<0.1 mm] Euhedral colorless grains with high relief and high birefringence.
==

TEXTURES: Hypidiomorphic medium-grained texture dominated by microcline, plagioclase, quartz, and biotite, respectively. Microcline exhibits minor perthite. Microcline, plagioclase, and quartz exhibit myrmekitic texture.

ALTERATION: Minor metasomatic/hydrothermal alteration from biotite to chlorite and plagioclase to sericite/muscovite.

OPTICAL CATHODOLUMINESCENCE

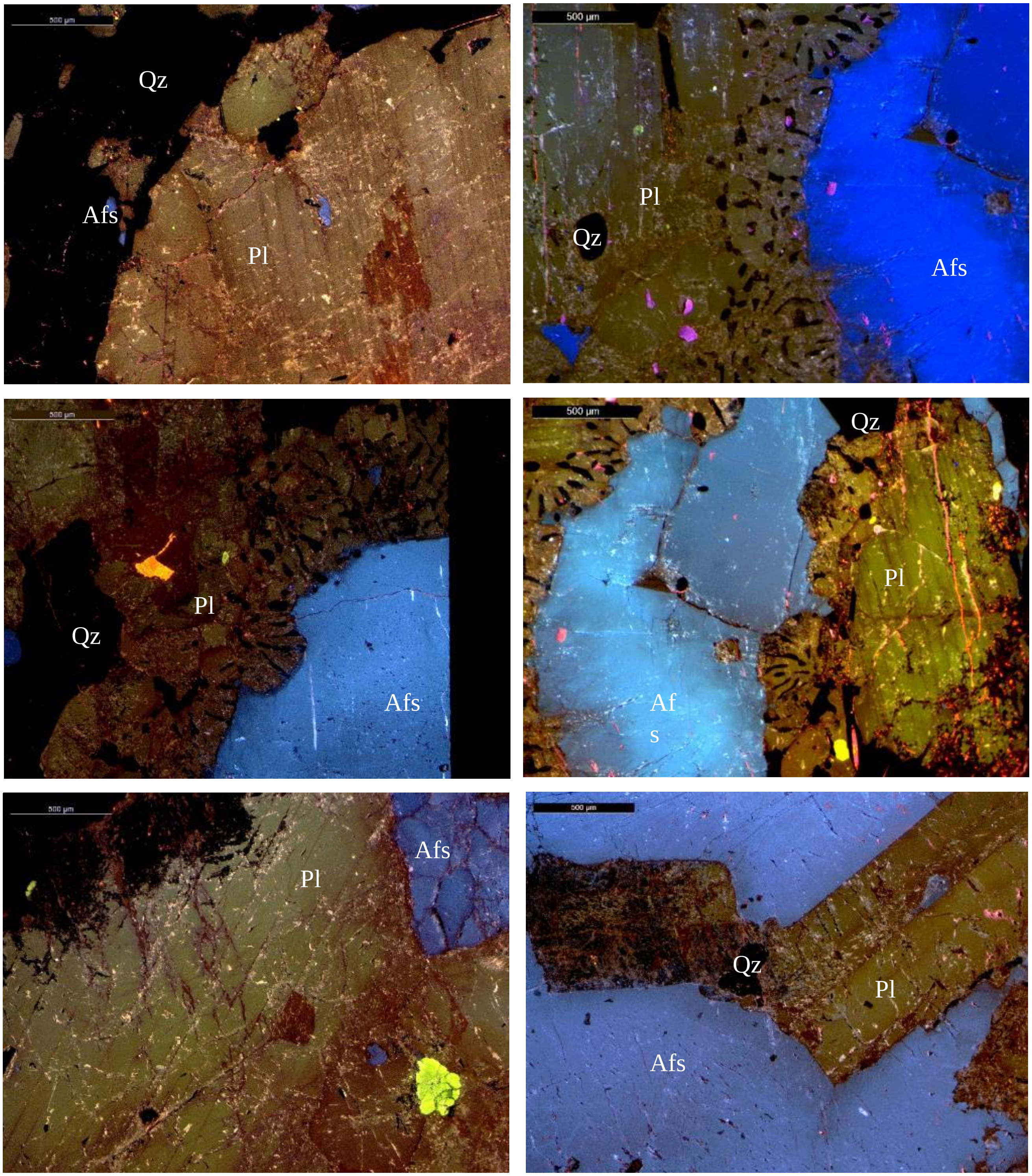

Mineral abbreviations taken from (Whitney and Evans, 2010). Moderate to dark blue alkali feldspar and moderate to brown plagioclase. Myrmekitic texture and carbonate minerals observed.

COMMENTS AND INTERPRETATION:
Based on the QAP ratio of 39.87:21.04:39.09 of the likely primary magmatic minerals, this rock is best classified as Hornblende-bearing Biotite Granodiorite with secondary alteration to muscovite/sericite and chlorite. The fact that the alkali-feldspar and plagioclase from separate phenocrysts implies that the granodiorite is subsolvus.

The magmatic paragenetic sequence is likely (Plagioclase) > (Biotite) > (Microcline + quartz) and then hydrothermal alteration to muscovite/sericite + chlorite.

Following the crystallization of the igneous minerals there are a series of subsolidus changes to the minerals. Post-crystallization deformation likely generated the quartz deformations features and allowed excess to aqueous fluids associated with alteration.

An age date of 92±1 Ma, Granodiorite classification, minor perthitic microcline, myrmekitic texture, and sample location suggest this sample is part of the Idaho Batholith.

SAMPLE: MC14ST-21

Last update: 2/26/20

Petrographer: Kyle Tollefson

LOCATION: 44°09.147N, 115°03.081W
COLLECTOR: Chong Ma

DATE COLLECTED:

AGE DATE: 92±1 Ma

ROCK TYPE: Biotite Granodiorite

MEGASCOPIC DESCRIPTION: Leucocratic, white, medium-grained phaneritic granitoid chiefly composed of microcline, plagioclase, and quartz with folitated biotite.
===
MINERAL ASSEMBLAGES: (Point counted modes)

Plagioclase (33%) [0.2-2.5 mm] Subhedral grains exhibiting albite twinning and moderate seritization.

Microcline (15%) [0.1-4 mm] Anhedral to subhedral grains exhibiting minor perthite, and moderate seritization. Moderate myrmekites of plagioclase-quartz develop at margins with plagioclase.

Quartz (40%) [0.01-8 mm] Anhedral to subhedral grains exhibiting major sweeping extinction and checkerboard extinction. Recrystallized quartz.

Biotite (11.7%) [0.2-1.5 mm] Subhedral laths with dark brown to tan pleochroism, birds eye extinction, and minor chloritization. Biotites are foliated suggesting magma flow or syndeformational crystallization.

Sericite (0.7%) [<0.5 mm] Subhedral colorless laths exhibiting high birefringence.

Clinozoisite (tr%) [<1 mm] Anhedral colorless grains with moderate relief and lst order birefringence.

Allanite (tr%) [<0.3 mm] Anhedral to subhedral light brown grains exhibiting high relief and 1st order birefringence.

Apatite (tr%) [<0.2 mm] Subhedral colorless grains with moderate relief and 1st order birefringence.

Magnetite (tr%) [<0.1 mm] Subedral opaque grains exhibiting brownish-grey, isotropic, and a pitted nature in reflective light.

Chlorite (tr%) [0.2 mm] Subhedral green laths replacing biotite.

Zircon (tr%) [<0.1 mm] Euhedral colorless grains with high relief and high birefringence.
===

TEXTURES: Allotriomorphic medium-grained texture dominated by microcline, plagioclase, quartz, and biotite, respectively. Microcline exhibiting minor perthite texture. Microcline, plagioclase, and quartz exhibit myrmekitic texture. Recrystallization in the quartz indicates post-crystallization deformation.

ALTERATION: Moderate metasomatic/hydrothermal alteration from biotite to chlorite and plagioclase to sericite/muscovite.

OPTICAL CATHODOLUMINESCENCE

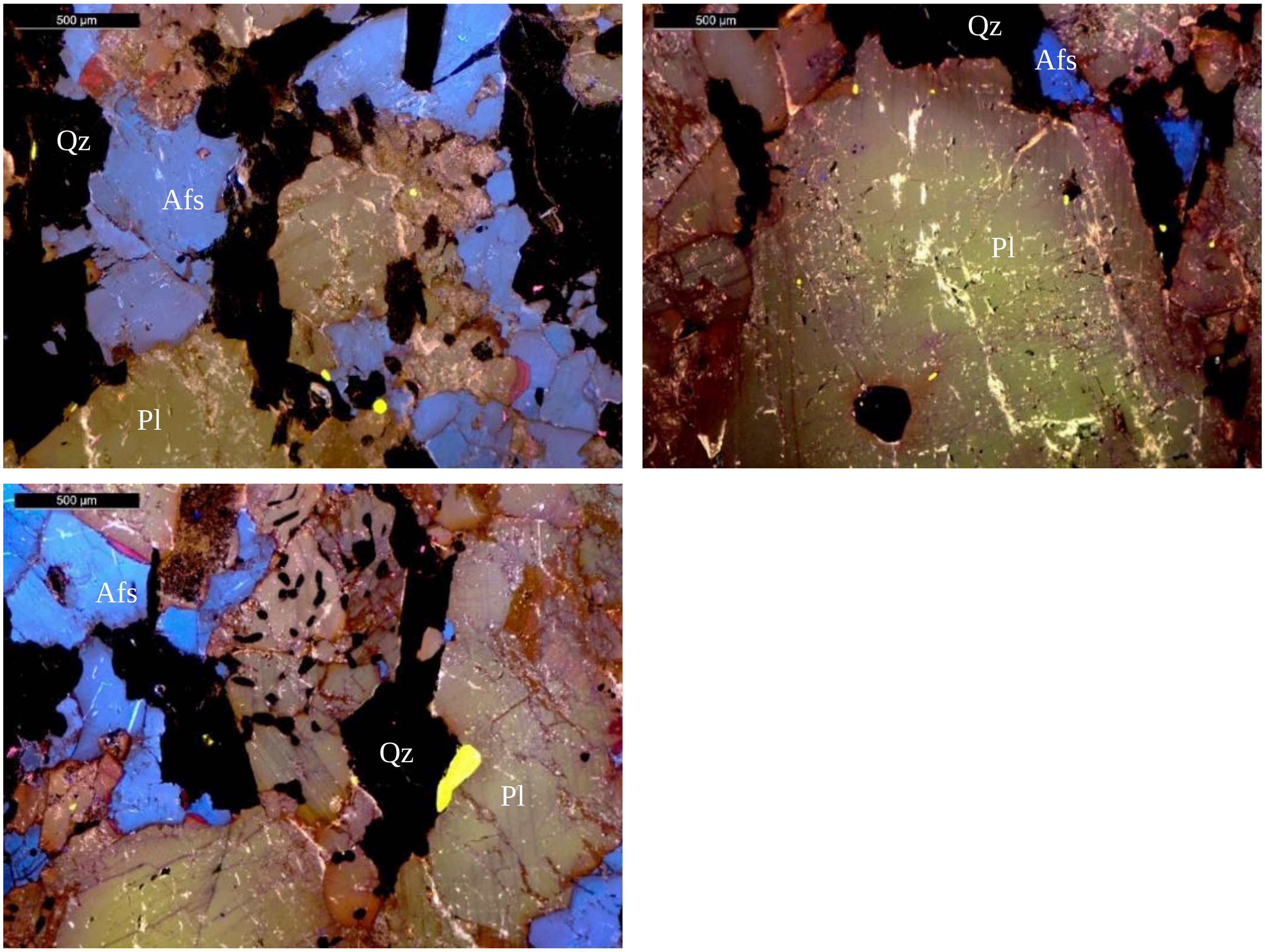

Mineral abbreviations taken from (Whitney and Evans, 2010). Bright blue alkali feldspar with red zonation. Moderate green and brown plagioclase. Myrmekitic texture observed.

COMMENTS AND INTERPRETATION:

Based on the QAP ratio of 45.45:17.05:37.50of the likely primary magmatic minerals, this rock is best classified as Biotite Granodiorite with secondary alteration to muscovite/sericite and chlorite. The fact that the alkali-feldspar and plagioclase from separate phenocrysts implies that the granite is a subsolvus granite.

The magmatic paragenetic sequence is likely (Plagioclase) > (Biotite) > (Microcline + quartz) and then hydrothermal alteration to muscovite/sericite + chlorite.

Biotites are foliated suggesting magma flow or syndeformational crystallization. Following the crystallization of the igneous minerals there are a series of subsolidus changes to the minerals. Post-crystallization deformation likely generated the quartz deformations features and allowed excess to aqueous fluids associated with alteration.

An age date of 92±1 Ma, Granodiorite classification, minor perthitic microcline, myrmekitic texture, and sample location suggest this sample is part of the Idaho Batholith.

SAMPLE: MC14ST-25

Last update: 2/26/20

Petrographer: Kyle Tollefson

LOCATION: 44°05.510N, 114°57.557W
COLLECTOR: Chong Ma

DATE COLLECTED:

AGE DATE: 89±1 Ma

ROCK TYPE: Biotite-bearing Granodiorite

MEGASCOPIC DESCRIPTION: Leucocratic, white, medium-grained phaneritic granitoid chiefly composed of microcline, plagioclase, and quartz with minor biotite.
==
MINERAL ASSEMBLAGES: (Point counted modes)

Plagioclase (39%) [0.5-2.5 mm] Anhedral to subhedral grains exhibiting faint albite twinning and moderate seritization.

Micocline (18%) [0.25-1.5 mm] Anhedral to subhedral grains exhibiting minor perthite and moderate seritization. Minor myrmekites of plagioclase-quartz develop at margins with plagioclase.

Quartz (41%) [0.25-4.5 mm] Anhedral grains exhibiting minor sweeping extinction.

Biotite (1%) [<0.5 mm] Subhedral laths exhibiting light brown to brown pleochroism, birds eye extinction, and moderate chloritization.

Sericite (0.3%) [<1.75 mm] Subhedral colorless laths exhibiting high birefringence.

Magnetite (tr%) [0.05-0.4 mm] Anhedral to euhedral opaque grains exhibiting brownish-grey, isotropic, and a pitted nature in reflective light.

Apatite (tr%) [<0.125 mm] Anhedral to subhedral colorless grains with moderate relief and 1st order birefringence.

Chlorite (tr%) [0.05 mm] Subhedral green laths replacing biotite.

Zircon (tr%) [<0.2 mm] Euhedral colorless grains with high relief and high birefringence.
==

TEXTURES: Allotriomorphic medium-grained texture dominated by microcline, plagioclase, quartz, and biotite, respectively. Microcline, plagioclase, and quartz exhibit myrmekitic texture.

ALTERATION: Moderate metasomatic/hydrothermal alteration from biotite to chlorite and plagioclase to sericite/muscovite.

OPTICAL CATHODOLUMINESCENCE

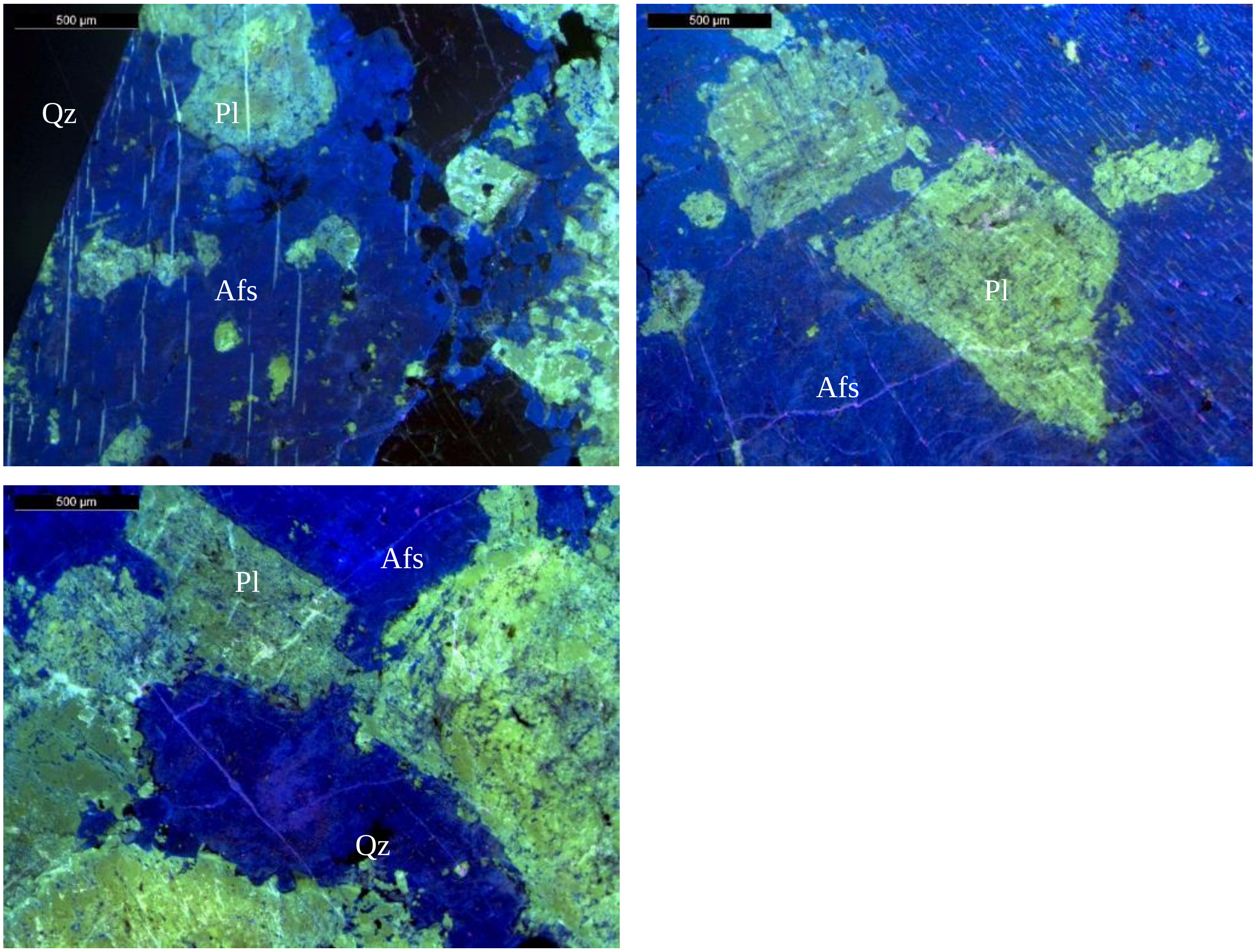

Mineral abbreviations taken from (Whitney and Evans, 2010). Dark blue alkali feldspar and moderate to dark green plagioclase. Oscillatory zoning present in plagioclase.

COMMENTS AND INTERPRETATION:

Based on the QAP ratio of 41.84:18.37:39.80of the likely primary magmatic minerals, this rock is best classified as Biotite-bearing Granodiorite with secondary alteration to muscovite/sericite and chlorite. The fact that the alkali-feldspar and plagioclase from separate phenocrysts implies that the granodiorite is subsolvus.

The magmatic paragenetic sequence is likely (Plagioclase) > (Biotite + opaques) > (Microcline + quartz) and then hydrothermal alteration to muscovite/sericite + chlorite.

Following the crystallization of the igneous minerals there are a series of subsolidus changes to the minerals. Post-crystallization deformation likely generated the quartz deformations features and allowed excess to aqueous fluids associated with alteration.

An age date of 89±1 Ma, Granodiorite classification, myrmekitic texture, green plagioclase with oscillatory zoning in CL, and sample location suggest this sample is part of the Idaho Batholith.

SAMPLE: MC13ST-05

Last update: 2/26/20

Petrographer: Kyle Tollefson

LOCATION: 44°08.494N, 115°00.023W
COLLECTOR: Chong Ma

DATE COLLECTED:

AGE DATE: 78±4 Ma

ROCK TYPE: Biotite-bearing Monzo-Granite

MEGASCOPIC DESCRIPTION: Leucocratic, white, medium-grained phaneritic granitoid chiefly composed of microcline, plagioclase, and quartz with minor biotite.
===
MINERAL ASSEMBLAGES: (Point counted modes)

Plagioclase (20%) [0.05-4 mm] Anhedral to subhedral grains exhibiting kink structures (deformed albite twinning) and major seritization.

Microcline (36%) [0.1-5 mm] Anhedral to subhedral grains exhibiting tartan twinning/ minor perthite and moderate seritization.

Quartz (43%) [0.05-8 mm] Anhedral grains exhibiting major sweeping extinction. Recrystallized quartz.

Biotite (0.7%) [0.1-2.25 mm] Subhedral laths with green to brown pleochroism and major chloritization.

Magnetite (tr%) [<0.2 mm] Subhedral to euhedral opaque grains exhibiting brownish-grey, isotropic, and a pitted nature in reflective light.

Sericite (tr%) [<0.5 mm] Subhedral colorless laths exhibiting high birefringence.

Clinozoisite (tr%) [<0.1 mm] Anhedral colorless grains with moderate relief and lst order birefringence.

Epidote (tr%) [<0.1 mm] Subhedral pale green grains with moderate relief and high birefringence.

Apatite (tr%) [<0.2 mm] Subhedral to euhedral colorless grains with moderate relief and 1st order birefringence.

Hematite (tr%) [<0.1 mm] Anhedral opaque grains with red edges.

Chlorite (tr%) [0.1-1 mm] Subhedral green laths replacing biotite.

Zircon (tr%) [<0.1 mm] Euhedral colorless grains with high relief and high birefringence.
===

TEXTURES: Allotriomorphic medium-grained texture dominated by microcline, plagioclase, quartz, and biotite, respectively. Microcline has perthitic exsolution. The kink banding in plagioclase and recrystallization in the quartz indicates post-crystallization deformation

ALTERATION: Pervasive metasomatic/hydrothermal alteration from biotite to chlorite, plagioclase to sericite/muscovite.

OPTICAL CATHODOLUMINESCENCE

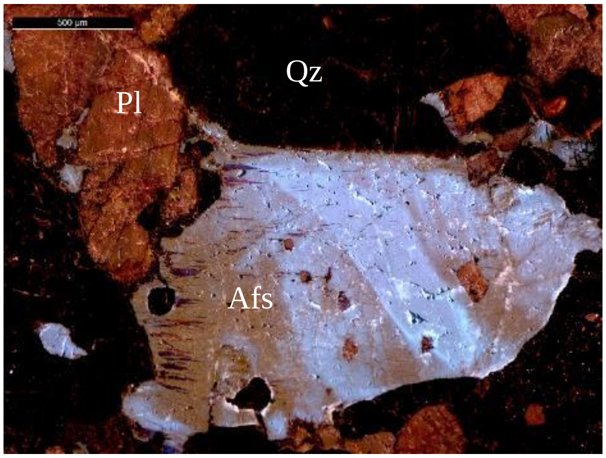

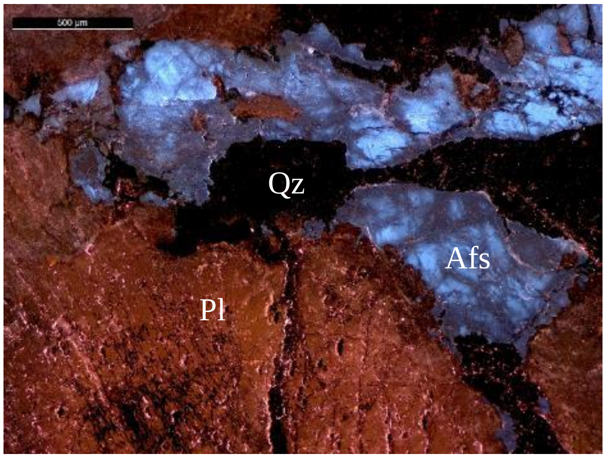

Mineral abbreviations taken from (Whitney and Evans, 2010). Light to moderate blue alkali feldspar with extensive red alteration (Fe^{3+} from fluids) and brown plagioclase with extensive alteration.

COMMENTS AND INTERPRETATION:
Based on the QAP ratio of 43.43:36.36:20.20of the likely primary magmatic minerals, this rock is best classified as Biotite-bearing Monzo-Granite with secondary alteration to muscovite/sericite and chlorite. The fact that the alkali-feldspar and plagioclase from separate phenocrysts implies that the granodiorite is subsolvus.
The magmatic paragenetic sequence is likely (Plagioclase) > (Biotite) > (Microcline + quartz) and then hydrothermal alteration to muscovite/sericite + chlorite.

Following the crystallization of the igneous minerals there are a series of subsolidus changes to the minerals. Post-crystallization deformation likely generated the plagioclase deformation bands, quartz deformation features and allowed access to aqueous fluids associated with alteration.

An age date of 78±4 Ma, and red zonation in CL suggest this sample is part of the Idaho Batholith.

SAMPLE: MC13ST-14

Last update: 2/26/20

Petrographer: Kyle Tollefson

LOCATION: 44°08.455N, 115°00.299W
COLLECTOR: Chong Ma

DATE COLLECTED:

AGE DATE: 77±1 Ma

ROCK TYPE: Biotite–bearing Monzo-Granite

MEGASCOPIC DESCRIPTION: Leucocratic, white, coarse-grained phaneritic granitoid chiefly composed of microcline, plagioclase, and quartz with minor biotite and muscovite.
===
MINERAL ASSEMBLAGES: (Point counted modes)

Plagioclase (23.3%) [0.2-12 mm] Subhedral exhibiting kink structures (deformed albite twinning) and moderate seritization.

Microcline (38.7%) [0.1-6 mm] Anhedral to subhedral grains exhibiting tartan twinning, minor perthite, and moderate seritization. Moderate myrmekites of plagioclase-quartz develop at margins with plagioclase.

Quartz (33.3%) [0.05-8 mm] Anhedral grains exhibiting moderate sweeping extinction. Resorption/ recrytsallization boundaries.

Biotite (4.3%) [0.1-5 mm] Anhedral to subhedral laths with green to brown pleochroism, birds eye extinction, and moderate chloritization.

Sericite (0.3%) [0.05-0.75 mm] Subhedral colorless laths exhibiting high birefringence.

Magnetite (tr%) [<0.2 mm] Subhedral opaque grains exhibiting brownish-grey, isotropic, and a pitted nature in reflective light.

Apatite (tr%) [<0.1 mm] Subhedral to euhedral colorless grains with moderate relief and 1st order birefringence.

Chlorite (tr%) [0.1-1 mm] Subhedral green laths replacing biotite.

Zircon (tr%) [<0.05 mm] Euhedral colorless grains with high relief and high birefringence.
===
TEXTURES: Allotriomorphic coarse-grained texture dominated by microcline, plagioclase, quartz, and biotite, respectively. Microcline, plagioclase, and quartz exhibit myrmekitic texture. The kink banding in plagioclase and recrystallization in the quartz indicates post-crystallization deformation.

ALTERATION: Moderate metasomatic/hydrothermal alteration from biotite to chlorite and plagioclase to sericite/muscovite.

OPTICAL CATHODOLUMINESCENCE

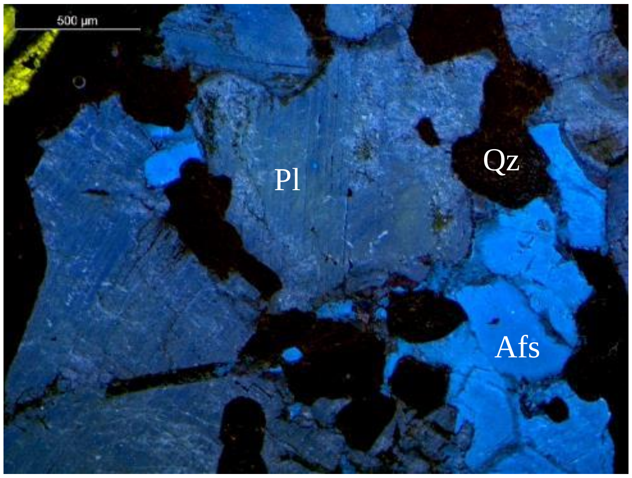

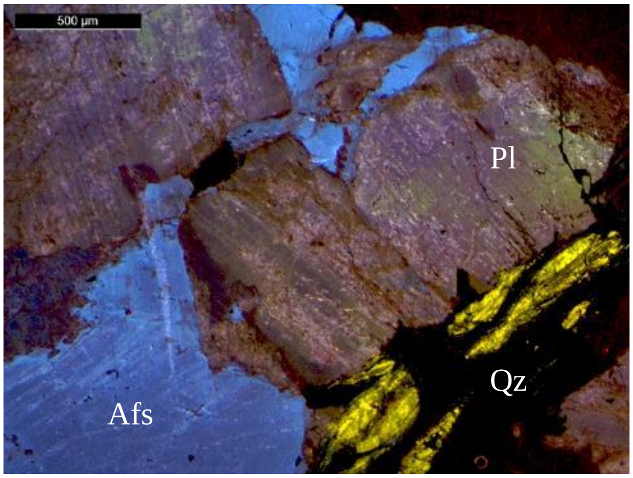

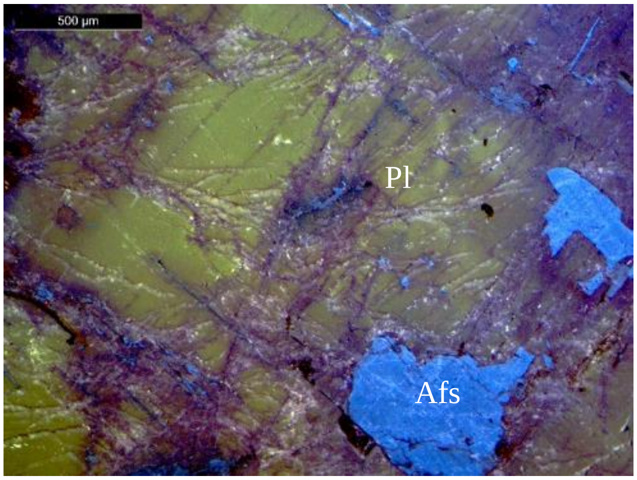

Mineral abbreviations taken from (Whitney and Evans, 2010). Moderate blue alkali feldspar and moderate green plagioclase altered blue. Yellow apatite also present.

COMMENTS AND INTERPRETATION:

Based on the QAP ratio of 34.94:40.61:24.45 of the likely primary magmatic minerals, this rock is best classified as Biotite–bearing Monzo-Granite with secondary alteration to muscovite/sericite and chlorite. The fact that the alkali-feldspar and plagioclase from separate phenocrysts implies that the granite is a subsolvus granite.

The magmatic paragenetic sequence is likely (Plagioclase) > (Biotite + opaques) > (microcline + quartz) and then hydrothermal alteration to muscovite/sericite + chlorite.

Following the crystallization of the igneous minerals there are a series of subsolidus changes to the minerals. Post-crystallization deformation likely generated the plagioclase deformation bands, quartz deformations features, and allowed access to aqueous fluids associated with alteration.

An age date of 77±1 Ma, myrmekitic texture, and moderate green plagioclase CL responses suggest this sample is part of the Idaho Batholith.

SAMPLE: MC13ST-18

Last update: 2/26/20

Petrographer: Kyle Tollefson

LOCATION: 44°08.566N, 114°59.223W
COLLECTOR: Chong Ma

DATE COLLECTED:

AGE DATE: 92±1Ma

ROCK TYPE: Allanite-bearing Biotite Granodiorite

MEGASCOPIC DESCRIPTION: Leucocratic, white, equigranular, medium-grained phaneritic granitoid chiefly composed of orthoclase, plagioclase, and quartz with minor biotite.
==
MINERAL ASSEMBLAGES: (Point counted modes)

Plagioclase (28%) [0.1-2.5 mm] Subhedral grains exhibiting albite twinning and minor seritization.

Microcline (12%) [0.1-2.5 mm] Anhedral to subhedral grains exhibiting minor perthite.

Quartz (50%) [0.1-2.5 mm] Anhedral grains exhibiting minor sweeping extinction.

Biotite (9%) [0.05-0.75 mm] Subhedral to euhedral laths with light brown to moderate brown pleochroism and birds eye extinction.

Apatite (tr%) [<0.1 mm] Subhedral colorless grains with moderate relief and 1st order birefringence.

Allanite (5%) [0.01-0.5 mm] Subhedral to euhedral equant grains with brown to reddish brown pleochroism, high relief, and high birefringence.

Clinozoisite (tr%) [<0.1 mm] Anhedral to subhedral colorless grains with moderate relief and lst order birefringence.

Zircon (tr%) [<0.1 mm] Euhedral colorless grains with high relief and high birefringence.
==

TEXTURES: Hypidiomorphic medium-grained, equigranular texture dominated by microcline, plagioclase, quartz, and biotite, respectively. Microcline has minor perthitic exsolution.

ALTERATION: Minor metasomatic/hydrothermal alteration from plagioclase to sericite/muscovite.

OPTICAL CATHODOLUMINESCENCE

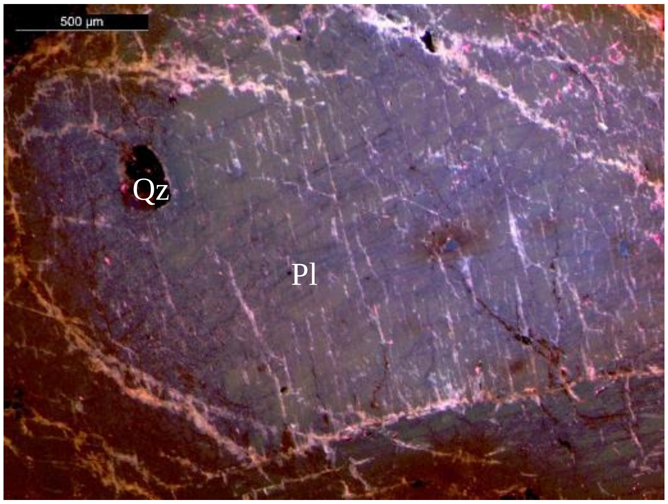

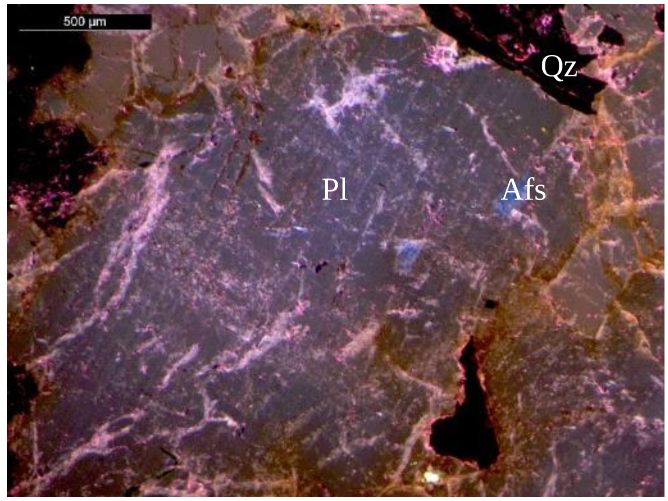

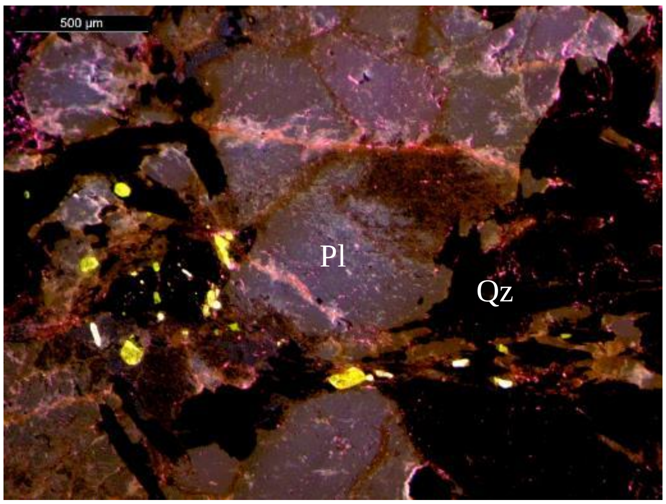

Mineral abbreviations taken from (Whitney and Evans, 2010). Moderate blue alkali feldspar with moderate green and moderate blue plagioclase.

COMMENTS AND INTERPRETATION:

Based on the QAP ratio of 55.56:13.33:31.11of the likely primary magmatic minerals, this rock is best classified as Allanite-bearing Biotite Granodiorite with secondary alteration to muscovite/sericite. The fact that the alkali-feldspar and plagioclase from separate phenocrysts implies that the granite-granodiorite subsolvus.

The magmatic paragenetic sequence is likely (Plagioclase) > (Biotite) > (Microcline + quartz) and then hydrothermal alteration to muscovite/sericite.

An age date of 92±1 Ma, Granodiorite classification, minor perthitic microcline, and moderate green plagioclase CL responses suggest this sample is part of the Idaho Batholith.

SAMPLE: MC14ST-04

Last update: 2/26/20

Petrographer: Kyle Tollefson

LOCATION: 44°09.248N, 115°00.017W
COLLECTOR: Chong Ma

DATE COLLECTED:

AGE DATE: 92±1 Ma

ROCK TYPE: Biotite-bearing Monzo-Granite

MEGASCOPIC DESCRIPTION: Leucocratic, white, medium-grained phaneritic granitoid chiefly composed of microcline, plagioclase, and quartz with minor biotite.
==
MINERAL ASSEMBLAGES: (Point counted modes)

Plagioclase (16.3%) [0.01-6 mm] Subhedral grains exhibiting albite twinning and minor seritization.

Microcline (25.3%) [0.1-5 mm] Anhedral to subhedral grains exhibiting pericline twinning and minor perthite.

Quartz (54.7%) [0.01-4 mm] Anhedral grains exhibiting major sweeping extinction. Recrystallized quartz.

Biotite (3%) [<0.75 mm] Subhedral to euhedral laths with light brown to brown pleochroism, birds eye extinction, and moderate chloritization. Biotites are foliated suggesting-magma flow or syndeformational crystallization.

Clinozoisite (tr%) [<0.1 mm] Anhedral to subhedral colorless grains with moderate relief and lst order birefringence.

Magnetite (tr%) [<0.05 mm] Subhedral to euhedral opaque grains exhibiting brownish-grey, isotropic, and a pitted nature in reflective light.

Chlorite (tr%) [0.1-0.25 mm] Subhedral green laths replacing biotite.

Zircon (tr%) [<0.05 mm] Euhedral colorless grains with high relief and high birefringence.
==

TEXTURES: Allotriomorphic medium-grained texture dominated by microcline, plagioclase, quartz, and biotite, respectively. Grains are aligned, visible in biotite. Recrystallization in the quartz indicates post-crystallization deformation.

ALTERATION: Minor metasomatic/hydrothermal alteration from biotite to chlorite and plagioclase to sericite/muscovite.

OPTICAL CATHODOLUMINESCENCE

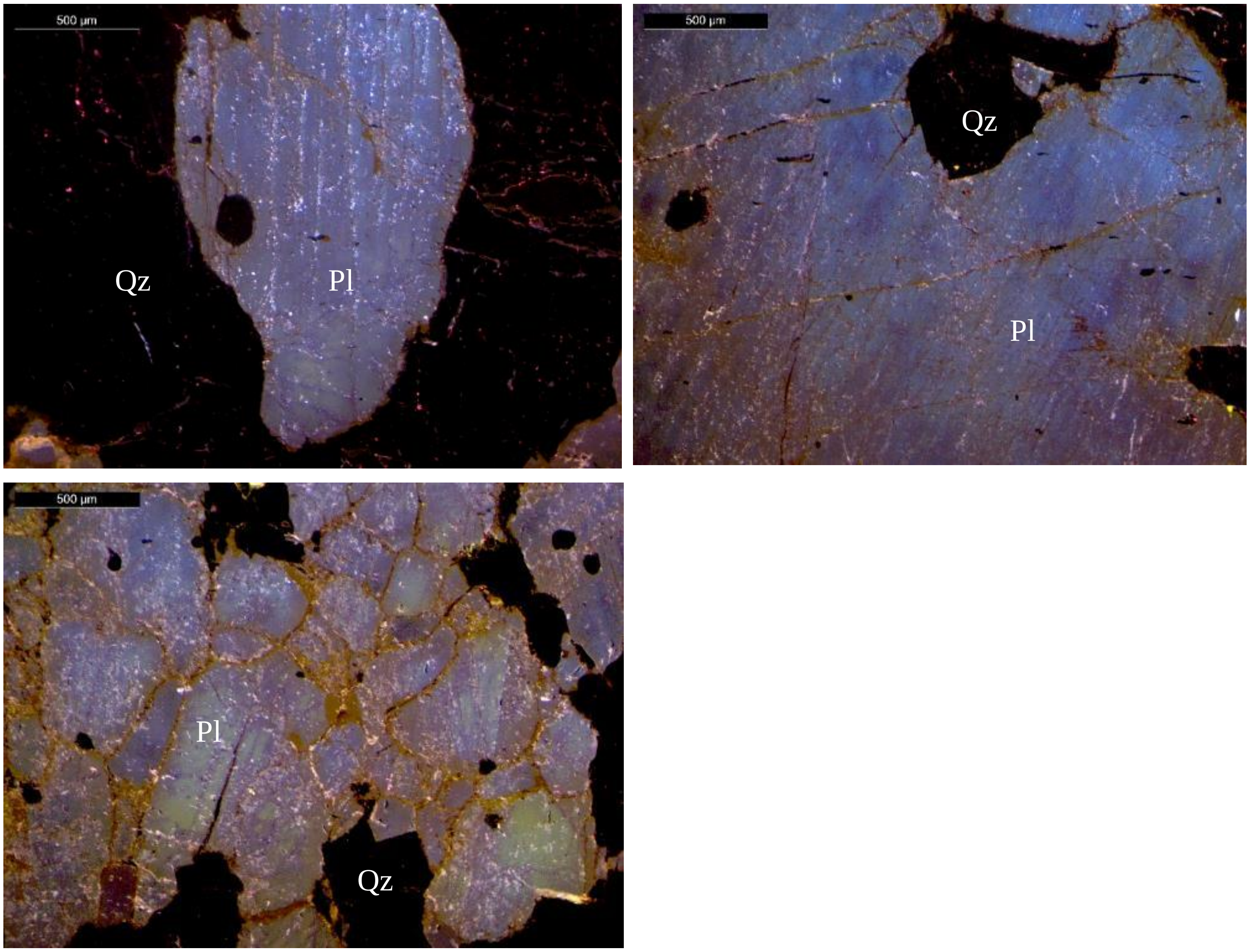

Mineral abbreviations taken from (Whitney and Evans, 2010). Moderate blue alkali feldspar, moderate green and moderate blue plagioclase.

COMMENTS AND INTERPRETATION:

Based on the QAP ratio of 56.80:26.27:16.93 of the likely primary magmatic minerals, this rock is best classified as Biotite-bearing Monzo-Granite with secondary alteration to muscovite/sericite and chlorite. The fact that the alkali-feldspar and plagioclase from separate phenocrysts implies that the granite-granodiorite is subsolvus.

The magmatic paragenetic sequence is likely (Plagioclase) > (Biotite) > (Microcline + Quartz) and then hydrothermal alteration to muscovite/sericite + chlorite.

Biotites are foliated suggesting-magma flow or syndeformational crystallization. Following the crystallization of the igneous minerals there are a series of subsolidus changes to the minerals. Post-crystallization deformation likely generated the quartz deformations features and allowed excess to aqueous fluids associated with alteration.

An age date of 92±1 Ma and moderate green plagioclase CL responses suggest this sample is part of the Idaho Batholith.

SAMPLE: MC14ST-08

Last update: 2/26/20

Petrographer: Kyle Tollefson

LOCATION: 44°09.174N, 114°59.395W
COLLECTOR: Chong Ma

DATE COLLECTED:

AGE DATE: 99±1 Ma

ROCK TYPE: Biotite-bearing Granodiorite

MEGASCOPIC DESCRIPTION: Leucocratic, white with reddish-orange alterations, fine-grained phaneritic granitoid chiefly composed of microcline, plagioclase, and quartz with minor biotite.
==
MINERAL ASSEMBLAGES: (Point counted modes)

<u>Plagioclase</u> (40%) [0.25-2 mm] Subhedral grains exhibiting albite twinning and minor seritization.

<u>Microcline</u> (20%) [0.2-0.5 mm] Subhedral grains exhibiting pericline twinning and minor seritization.

<u>Quartz</u> (40%) [0.1-4 mm] Anhedral to subhedral grains exhibiting minor sweeping extinction.

<u>Biotite</u> (0.7%) [<0.25 mm] Subhedral laths with brown to green pleochroism, birds eye extinction, and moderate chloritization.

<u>Sericite</u> (tr%) [<0.1 mm] Subhedral to euhedral colorless laths exhibiting high birefringence.

<u>Clinozoisite</u> (tr%) [<0.01 mm] Anhedral colorless grains with moderate relief and lst order birefringence.

<u>Magnetite</u> (tr%) [<0.1 mm] Subhedral to euhedral opaque grains exhibiting brownish-grey, isotropic, and a pitted nature in reflective light.

<u>Hematite</u> (tr%) [<0.05 mm] Anhedral opaque grains with red rims. Found filling fractures and along grain boundaries.

<u>Chlorite</u> (tr%) [0.1 mm] Subhedral green laths replacing biotite.
==

TEXTURES: Hypidiomorphic fine-grained texture dominated by microcline, plagioclase, quartz, and biotite, respectively.

ALTERATION: Moderate metasomatic/hydrothermal alteration from biotite to chlorite, plagioclase to sericite/muscovite, and precipitation of hematite.

OPTICAL CATHODOLUMINESCENCE

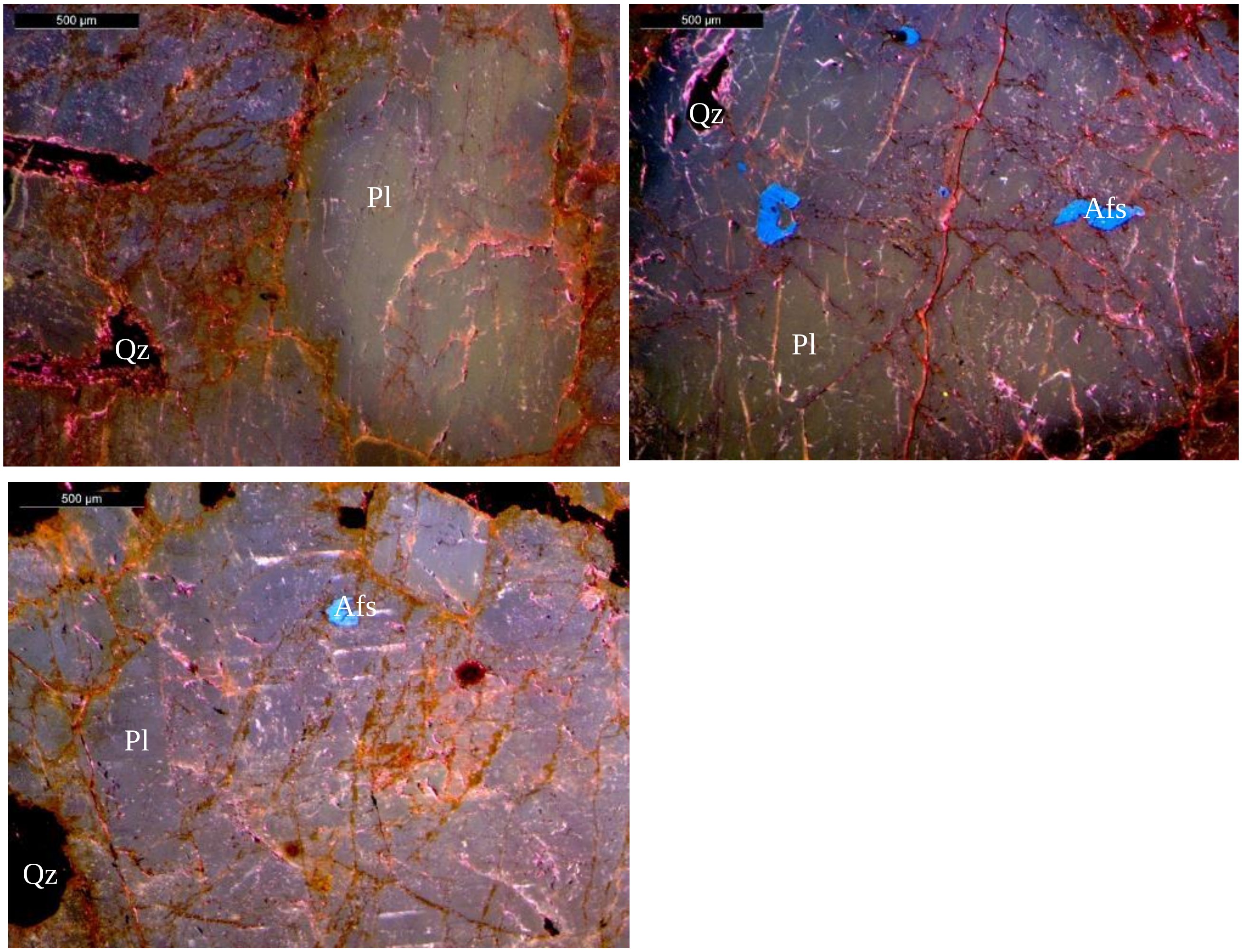

Mineral abbreviations taken from (Whitney and Evans, 2010). Bright blue alkali feldspar with moderate green and moderate blue plagioclase.

COMMENTS AND INTERPRETATION:

Based on the QAP ratio of 40.00:20.00:40.00of the likely primary magmatic minerals, this rock is best classified as Biotite-bearing Granodiorite with secondary alteration to muscovite/sericite and chlorite. The fact that the alkali-feldspar and plagioclase from separate phenocrysts implies that the granite-granodiorite is subsolvus.

The magmatic paragenetic sequence is likely (Plagioclase) > (Biotite) > (microcline + quartz) and then hydrothermal alteration to muscovite/sericite + chlorite.

Post-crystallization deformation likely allowed excess to aqueous fluids associated with alteration and precipitation of hematite.

An age date of 99±1 Ma, Granodiorite classification, and moderate green plagioclase CL responses suggest this sample is part of the Idaho Batholith.

SAMPLE: MC14ST-10

Last update: 2/26/20

Petrographer: Kyle Tollefson

LOCATION: 44°08.485N, 115°00.587W
COLLECTOR: Chong Ma

DATE COLLECTED:

AGE DATE: 84±1Ma

ROCK TYPE: Biotite-bearing Granodiorite

MEGASCOPIC DESCRIPTION: Leucocratic, white, medium-grained phaneritic granitoid chiefly composed of microcline, plagioclase, and quartz with minor biotite.
==

MINERAL ASSEMBLAGES: (Point counted modes)

Plagioclase (35.3%) [0.1-8 mm] Anhedral to subhedral grains exhibiting albite twinning and moderate seritization.

Microcline (13%) [0.25-4 mm] Subhedral grains exhibiting faint pericline twinning, minor perthite, and moderate seritization. Minor myrmekites of plagioclase-quartz develop at margins with plagioclase.

Quartz (45.3%) [0.05-6 mm] Anhedral grains exhibiting major sweeping extinction and checkerboard extinction. Recrystallized quartz.

Biotite (3.3%) [<0.5 mm] Anhedral to subhedral laths exhibiting brown to green pleochroism, birds eye extinction, and major chloritization.

Sericite (3%) [0.1-3 mm] Subhedral colorless laths exhibiting high birefringence.

Magnetite (tr%) [<0.15 mm] Anhedral to subhedral opaque grains exhibiting brownish-grey, isotropic, and a pitted nature in reflective light.

Allanite (tr%) [<0.1 mm] Subhedral light brown grains exhibiting high relief and 1st order birefringence.

Apatite (tr%) [<0.1 mm] Subhedral colorless grains with moderate relief and 1st order birefringence.

Chlorite (tr%) [0.1-1 mm] Subhedral green laths replacing biotite.

Zircon (tr%) [<0.15 mm] Euhedral colorless grains with high relief and high birefringence.
===

TEXTURES: Hypidiomorphic medium-grained texture dominated by microcline, plagioclase, quartz, and biotite, respectively. Microcline, plagioclase, and quartz exhibit myrmekitic texture. Recrystallization in the quartz indicates post-crystallization deformation.

ALTERATION: Moderate metasomatic/hydrothermal alteration from biotite to chlorite and plagioclase to sericite/muscovite.

OPTICAL CATHODOLUMINESCENCE

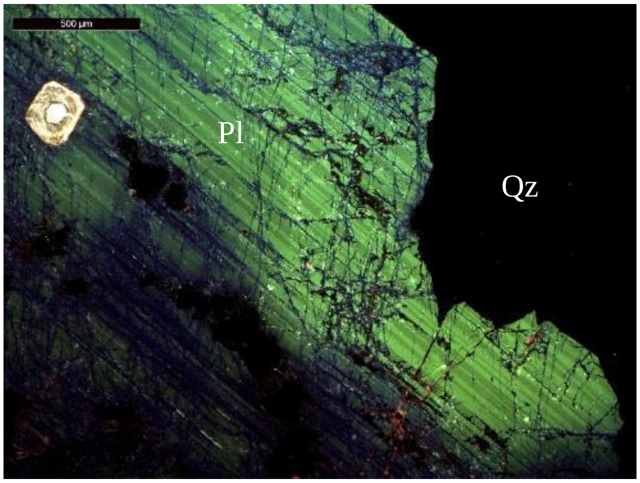

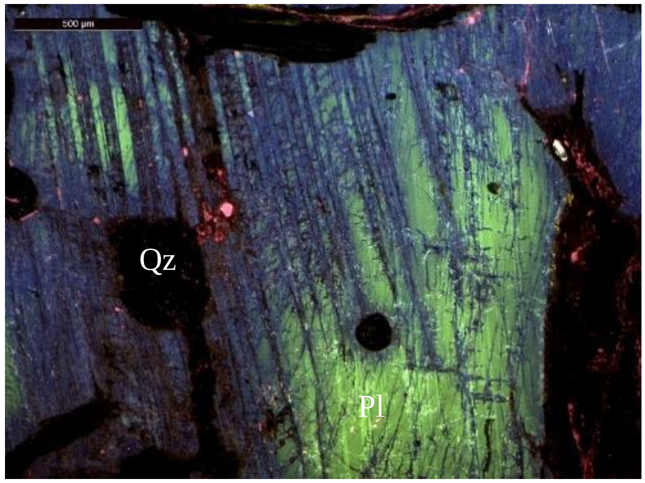

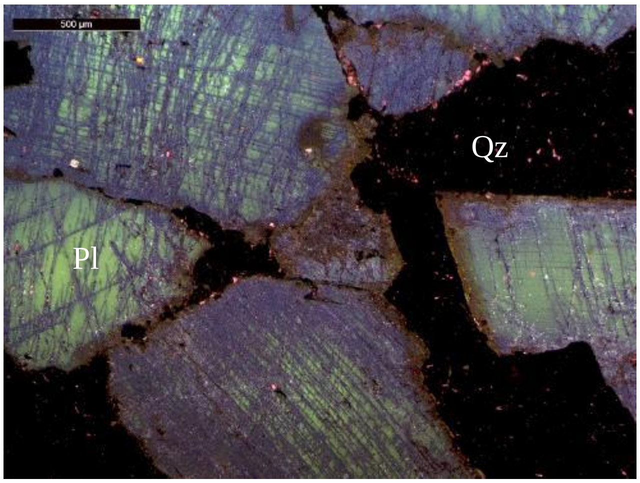

Mineral abbreviations taken from (Whitney and Evans, 2010). Moderate green plagioclase.

COMMENTS AND INTERPRETATION:

Based on the QAP ratio of 48.40:13.89:37.71 of the likely primary magmatic minerals, this rock is best classified as Biotite-bearing Granodiorite with secondary alteration to muscovite/sericite and chlorite. The fact that the alkali-feldspar and plagioclase from separate phenocrysts implies that the granodiorite is subsolvus.

The magmatic paragenetic sequence is likely (Plagioclase) > (Biotite) > (microcline + quartz) and then hydrothermal alteration to muscovite/sericite + chlorite.

Following the crystallization of the igneous minerals there are a series of subsolidus changes to the minerals. Post-crystallization deformation likely generated the quartz deformations features and allowed excess to aqueous fluids associated with alteration.

An age date of 84±1 Ma, Granodiorite classification, myrmekitic texture, and moderate green plagioclase CL responses, suggest this sample is part of the Idaho Batholith.

SAMPLE: MC14ST-12

Last update: 2/26/20

Petrographer: Kyle Tollefson

LOCATION: 44°08.492N, 115°00.450W
COLLECTOR: Chong Ma

DATE COLLECTED:

AGE DATE: 101±1 Ma

ROCK TYPE: Biotite-bearing Granodiorite

MEGASCOPIC DESCRIPTION: Leucocratic, white, medium-grained phaneritic granitoid chiefly composed of orthoclase, plagioclase, and quartz with minor biotite.
==

MINERAL ASSEMBLAGES: (Point counted modes)

Plagioclase (30%) [0.1-2.6 mm] Subhedral grains exhibiting albite twinning and moderate seritization.

Microcline (14.7%) [0.2-4 mm] Subhedral grains exhibiting moderate seritization. Pervasive myrmekites of plagioclase-quartz develop at margins with plagioclase.

Quartz (40%) [0.01-5 mm] Anhedral to subhedral grains exhibiting minor sweeping extinction. Recrystallized quartz.

Biotite (1.3%) [<0.25 mm] Subhedral laths with tan to brown pleochroism and birds eye extinction. Biotites are foliated suggesting magma flow or syndeformational crystallization.

Sericite (12.7%) [0.1-2.5 mm] Euhedral colorless laths exhibiting high birefringence.

Apatite (tr%) [<0.1 mm] subhedral, clear, mod relief, low birefringence

Clinozoisite (tr%) [<0.5 mm] Anhedral colorless grains with moderate relief and lst order birefringence.

Magnetite (tr%) [<0.1 mm] Subhedral to euhedral opaque grains exhibiting brownish-grey, isotropic, and a pitted nature in reflective light.
==

TEXTURES: Allotriomorphic medium-grained texture dominated by microcline, plagioclase, quartz, and biotite, respectively. Microcline, plagioclase, and quartz exhibit myrmekitic texture. Recrystallization in the quartz indicates post-crystallization deformation.

ALTERATION: Minor metasomatic/hydrothermal alteration from plagioclase to sericite/muscovite.

OPTICAL CATHODOLUMINESCENCE

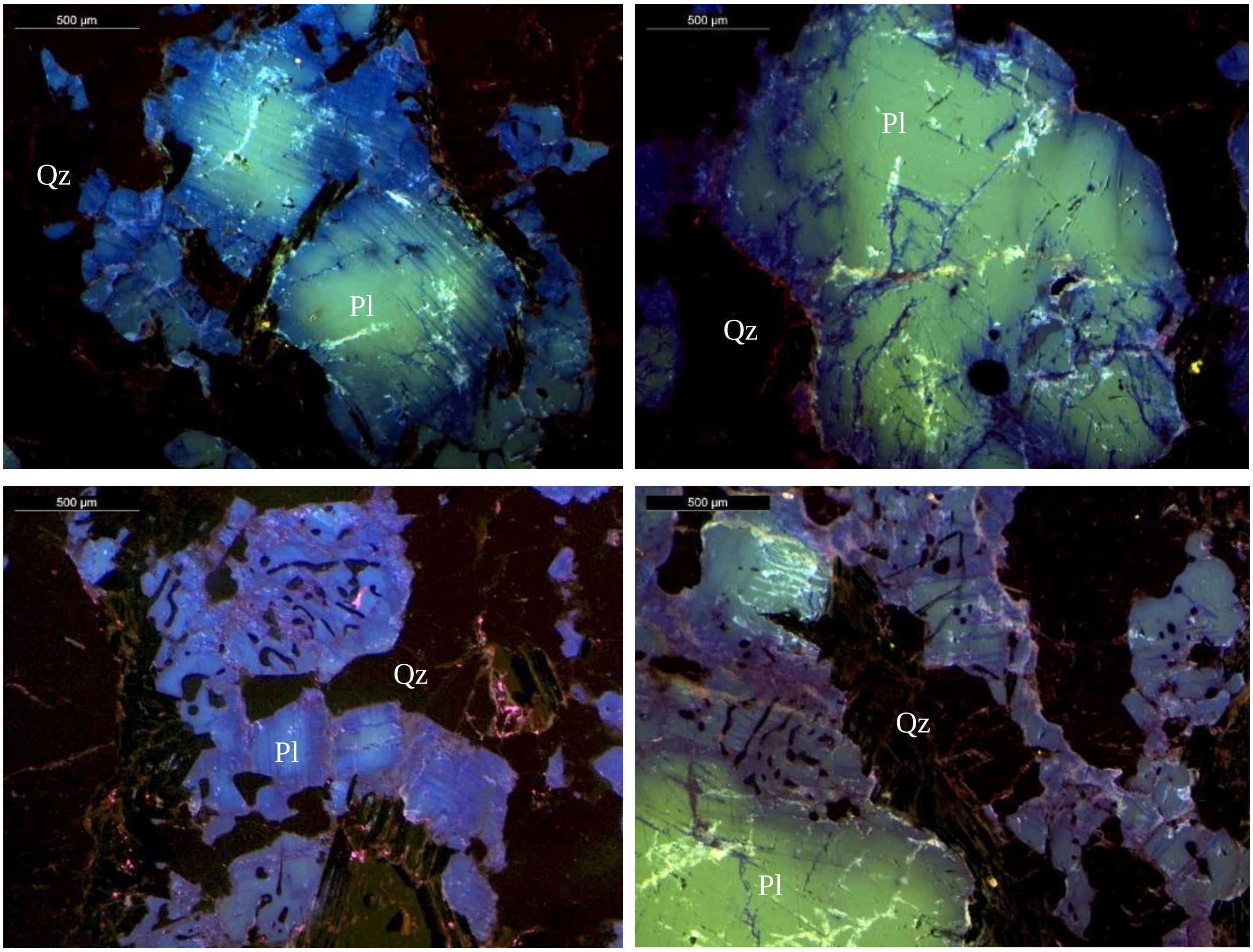

Mineral abbreviations taken from (Whitney and Evans, 2010). Moderate blue alkali feldspar with moderate green and moderate blue plagioclase. Myrmekitic texture observed.

COMMENTS AND INTERPRETATION:

Based on the QAP ratio of 47.23:17.36:35.42of the likely primary magmatic minerals, this rock is best classified as Biotite-bearing Muscovite Granodiorite with secondary alteration to muscovite/sericite. The fact that the alkali-feldspar and plagioclase from separate phenocrysts implies that the granite is a subsolvus granite.

The magmatic paragenetic sequence is likely (Plagioclase) > (Biotite + opaques) > (microcline + quartz) and then hydrothermal alteration to muscovite/sericite.

Biotites are foliated suggesting magma flow or syndeformational crystallization. Following the crystallization of the igneous minerals there are a series of subsolidus changes to the minerals. Post-crystallization deformation likely generated the quartz deformations features and allowed excess to aqueous fluids associated with alteration.

An age date of 101±1 Ma, Granodiorite classification, myrmekitic texture, and moderate green plagioclase CL responses suggest this sample is part of the Idaho Batholith.

SAMPLE: MC14ST-13

Last update: 2/26/20

Petrographer: Kyle Tollefson

LOCATION: 44°08.493N, 114°59.470W
COLLECTOR: Chong Ma

DATE COLLECTED:

AGE DATE: 95±1 Ma

ROCK TYPE: Biotite-bearing Monzo-Granite

MEGASCOPIC DESCRIPTION: Leucocratic, white, medium-grained phaneritic granitoid chiefly composed of microcline, plagioclase, and quartz with minor biotite.
==

MINERAL ASSEMBLAGES: (Point counted modes)

Plagioclase (25%) [0.1-5 mm] Subhedral grains exhibiting faint albite twinning and moderate seritization.

Microcline (43%) [0.25-10 mm] Anhedral to subhedral grains exhibiting tartan twinning, minor perthite, and minor seritization. Moderate myrmekites of plagioclase-quartz develop at margins with plagioclase.

Quartz (28.3%) [0.01-7 mm] Anhedral to subhedral grains exhibiting minor sweeping extinction and checkerboard extinction. Recrystallized quartz.

Biotite (4.7%) [0.1-2 mm] Subhedral laths exhibiting dark brown to tan pleochroism, birds eye extinction, and minor chloritization. Biotites found interstitial to feldspars and quartz.

Apatite (tr%) [0.1-0.4 mm] Subhedral colorless grains with moderate relief and 1st order birefringence.

Magnetite (tr%) [<0.3 mm] Anhedral to subedral opaque grains exhibiting brownish-grey, isotropic, and a pitted nature in reflective light.

Epidote (tr%) [0.05 mm] Subhedral colorless grains exhibiting high relief and high birefringence.

Sericite (tr%) [<0.1] Subhedral colorless laths exhibiting high birefringence.

Chlorite (tr%) [0.1 mm] Subhedral green laths replacing biotite.

Zircon (tr%) [<0.02 mm] Euhedral colorless grains with high relief and high birefringence.

TEXTURES: Hypidiomorphic medium-grained texture dominated by microcline, plagioclase, quartz, and biotite, respectively. Microcline exhibits minor perthite texture. Microcline, plagioclase, and quartz exhibit myrmekitic texture. Recrystallization in the quartz indicates post-crystallization deformation.

ALTERATION: Minor metasomatic/hydrothermal alteration from biotite to chlorite and plagioclase to sericite/muscovite.

OPTICAL CATHODOLUMINESCENCE

Mineral abbreviations taken from (Whitney and Evans, 2010). Bright blue alkali feldspar and moderate

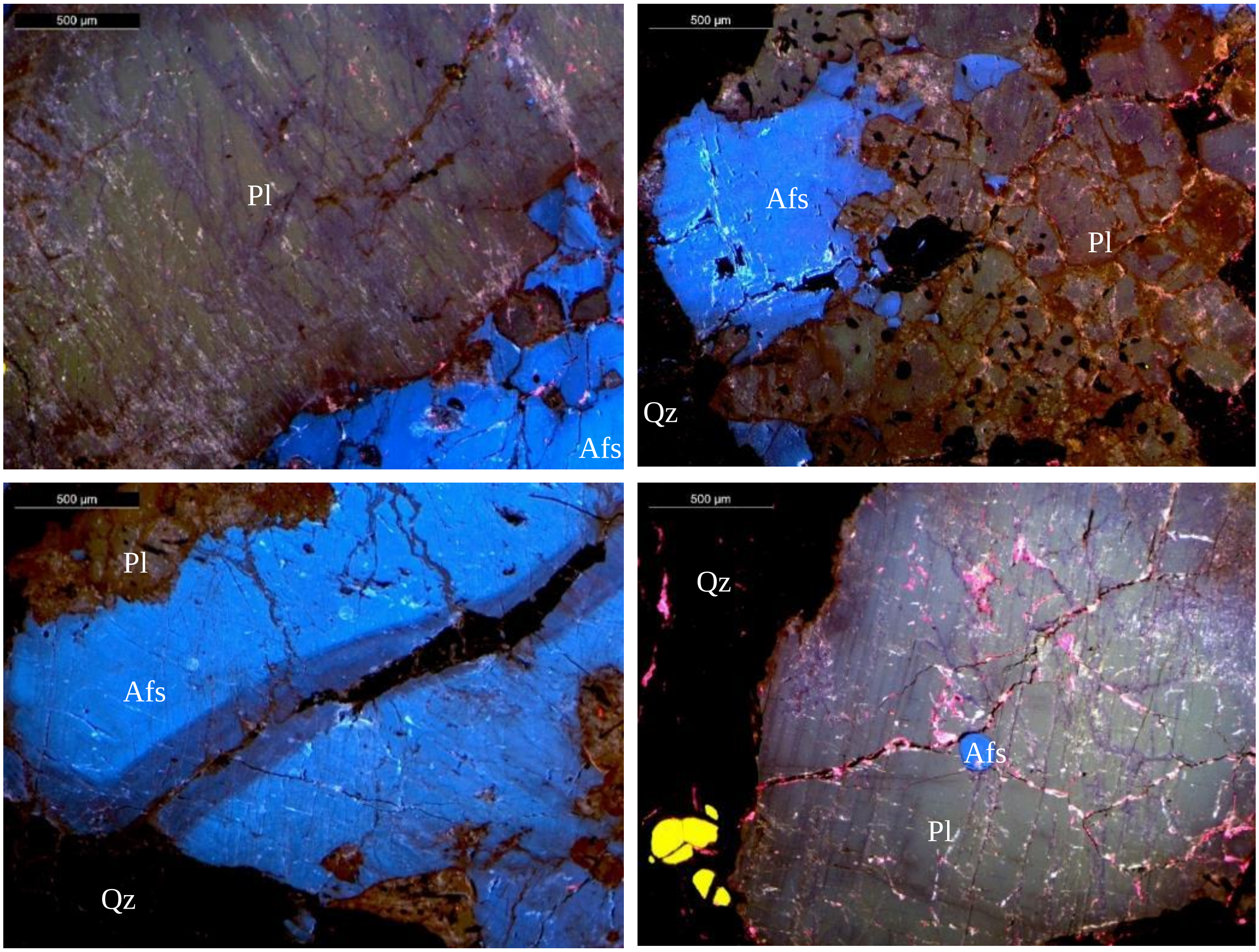

blue. Moderate green, brown, and moderate blue plagioclase. Carbonates and myrmekitic texture observed.

COMMENTS AND INTERPRETATION:

Based on the QAP ratio of 29.39:44.65:25.96 of the likely primary magmatic minerals, this rock is best classified as Biotite-bearing Monzo-Granite with secondary alteration to muscovite/sericite and chlorite. The fact that the alkali-feldspar and plagioclase from separate phenocrysts implies that the granite is a subsolvus granite.

The magmatic paragenetic sequence is likely (Plagioclase) > (Biotite + opaques) > (Microcline + quartz) and then hydrothermal alteration to muscovite/sericite + chlorite.

Following the crystallization of the igneous minerals there are a series of subsolidus changes to the minerals. Post-crystallization deformation likely generated the quartz deformations features and allowed excess to aqueous fluids associated with alteration.

An age date of 95±1 Ma, myrmekitic texture, perthitic microcline, and moderate green plagioclase CL responses suggest this sample is part of the Idaho Batholith.

SAMPLE: SMC11-30

Last update: 2/26/20

Petrographer: Kyle Tollefson

LOCATION:
COLLECTOR: Barbara Dutrow

DATE COLLECTED:

AGE DATE:

ROCK TYPE: Biotite-bearing Monzo-Granite

MEGASCOPIC DESCRIPTION: Leucocratic, white, coarse-grained phaneritic granitoid chiefly composed of microcline, plagioclase, and quartz with minor biotite.
==
MINERAL ASSEMBLAGES: (Point counted modes)

Plagioclase (22.3%) [0.2-10 mm] Anhedral to subhedral grains exhibiting albite twinning and major seritization.

Microcline (34.3%) [0.1-14 mm] Anhedral to subhedral grains exhibiting tartan twinning, minor perthite, and minor seritization. Minor myrmekites of plagioclase-quartz develop at margins with plagioclase.

Quartz (42.3%) [0.01-4 mm] Anhedral grains exhibiting moderate sweeping extinction. Recrystallized quartz.

Biotite (1%) [0.2-1.5 mm] Subhedral laths exhibiting brown to green pleochroism, birds eye extinction, and moderate chloritization.

Sericite (tr%) [0.1-1.75 mm] Subhedral colorless laths exhibiting high birefringence.

Magnetite (tr%) [<0.2 mm] Anhedral to subhedral opaque grains exhibiting brownish-grey, isotropic, and a pitted nature in reflective light.

Chlorite (tr%) [0.1-1 mm] Subhedral green laths replacing biotite.
==

TEXTURES: Allotriomorphic coarse-grained texture dominated by microcline, plagioclase, quartz, and biotite, respectively. Microcline exhibits minor perthite texture. Microcline, plagioclase, and quartz exhibit myrmekitic texture. Recrystallization in the quartz indicates post-crystallization deformation.

ALTERATION: Moderate metasomatic/hydrothermal alteration from biotite to chlorite and plagioclase to sericite/muscovite.

OPTICAL CATHODOLUMINESCENCE

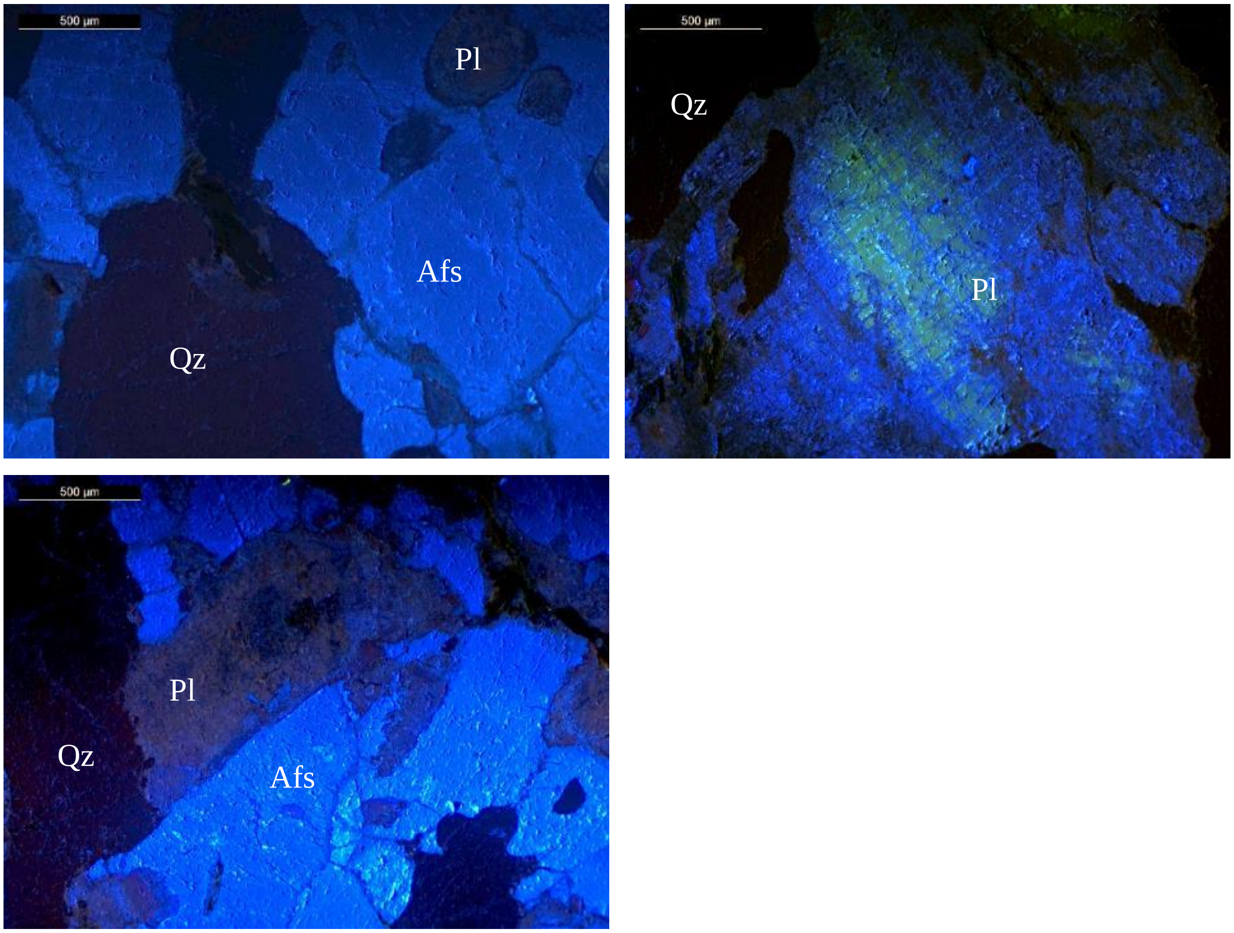

Mineral abbreviations taken from (Whitney and Evans, 2010). Bright blue alkali feldspar with moderate green and brown plagioclase.

COMMENTS AND INTERPRETATION:

Based on the QAP ratio of 42.77:34.68:22.55 of the likely primary magmatic minerals, this rock is best classified as Biotite-bearing Monzo-Granite with secondary alteration to muscovite/sericite and chlorite. The fact that the alkali-feldspar and plagioclase from separate phenocrysts implies that the granodiorite is subsolvus.

The magmatic paragenetic sequence is likely (Plagioclase + microcline) > (Biotite + opaques) > (quartz) and then hydrothermal alteration to muscovite/sericite + chlorite.

Following the crystallization of the igneous minerals there are a series of subsolidus changes to the minerals. Post-crystallization deformation likely generated the quartz deformations features and allowed excess to aqueous fluids associated with alteration.

Moderate green and moderate blue plagioclase CL responses and no other distinct characteristics suggest this sample is sourced by the Idaho batholith or anatectic melts.

SAMPLE: SMC 13-05

Last update: 2/26/20

Petrographer: Kyle Tollefson

LOCATION: 44°10.554N, 115°02.692W
COLLECTOR: Barbara Dutrow

DATE COLLECTED: June 27th 2013

AGE DATE:

ROCK TYPE: Biotite Granodiorite

MEGASCOPIC DESCRIPTION: Leucocratic, white, coarse-grained phaneritic granitoid chiefly composed of microcline, plagioclase, and quartz with minor biotite.
==
MINERAL ASSEMBLAGES: (Point counted modes)

Plagioclase (40.3%) [0.25-6 mm] Anhedral to subhedral grains exhibiting albite twinning and major seritization.

Microcline (6.7%) [0.25-7 mm] Anhedral to subhedral grains exhibiting moderate perthite, and moderate seritization. Minor myrmekites of plagioclase-quartz develop at margins with plagioclase.

Quartz (46.3%) [0.05-7 mm] Anhedral grains exhibiting minor sweeping extinction. Recrystallized quartz.

Biotite (6%) [0.1-2.5 mm] Anhedral to subhedral laths exhibiting brown to green pleochroism, birds eye extinction, and major chloritization.

Sericite (0.7%) [0.1-0.5 mm] Subhedral colorless laths exhibiting high birefringence.

Hematite (tr%) [<0.25 mm] Anhedral to euhedral opaque grains with red rims.

Magnetite (tr%) [<0.1 mm] Anhedral to subhedral opaque grains exhibiting brownish-grey, isotropic, and a pitted nature in reflective light.

Chlorite (tr%) [0.1-3 mm] Subhedral green laths replacing biotite.

Zircon (tr%) [<0.2 mm] Euhedral colorless grains with high relief and high birefringence.
==

TEXTURES: Allotriomorphic coarse-grained texture dominated by microcline, plagioclase, quartz, and biotite, respectively. Microcline exhibits perthite texture. Microcline, plagioclase, and quartz exhibit myrmekitic texture. Recrystallization in the quartz indicates post-crystallization deformation.

ALTERATION: Pervasive metasomatic/hydrothermal alteration from biotite to chlorite and plagioclase to sericite/muscovite.

OPTICAL CATHODOLUMINESCENCE

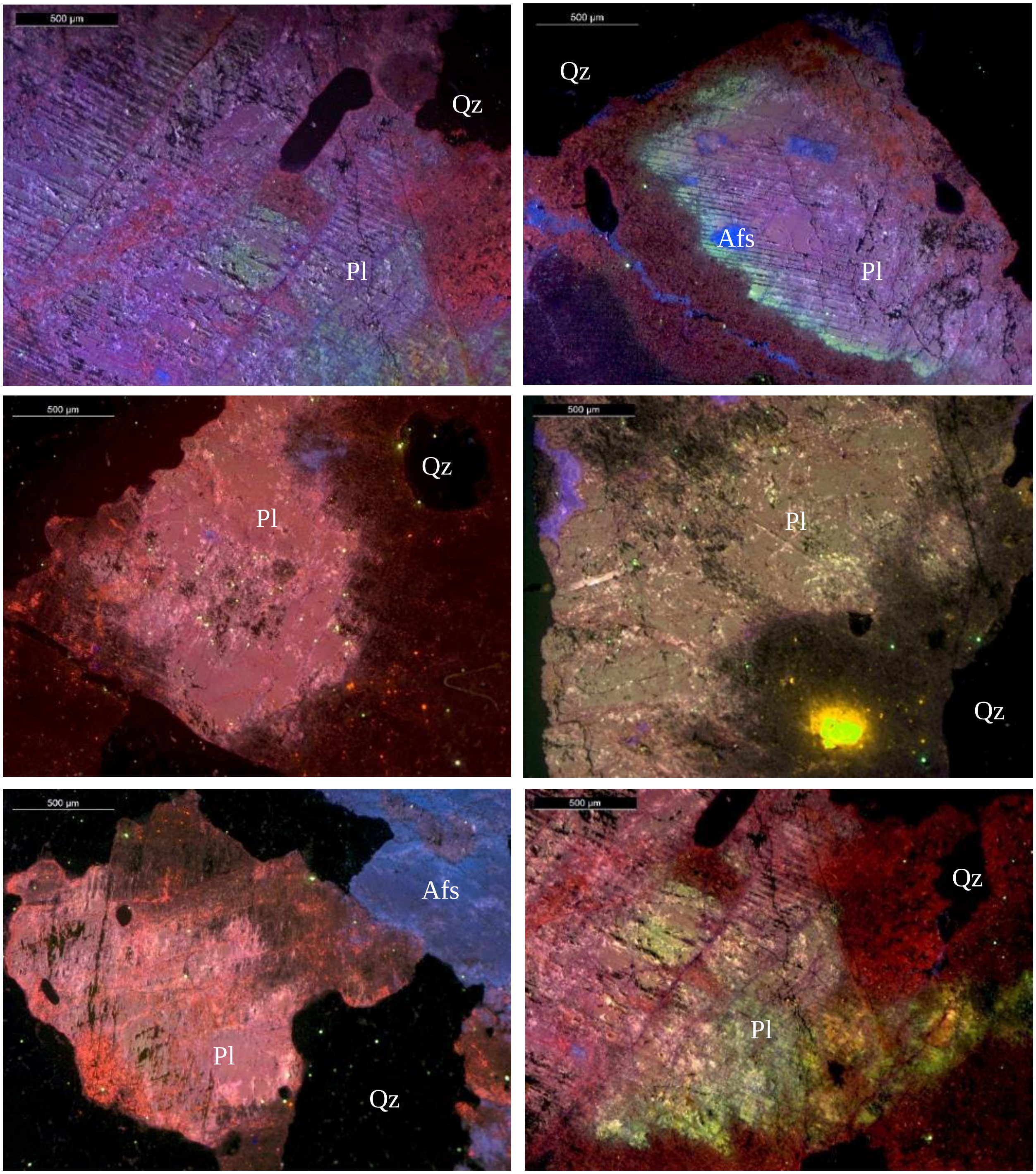

Mineral abbreviations taken from (Whitney and Evans, 2010). Moderate to bright blue alkali feldspar. Brown, bright green, pink, and red plagioclase.

COMMENTS AND INTERPRETATION:

Based on the QAP ratio of 49.62:7.18:43.19 of the likely primary magmatic minerals, this rock is best classified as Biotite Granodiorite with secondary alteration to muscovite/sericite and chlorite. The fact that the alkali-feldspar and plagioclase from separate phenocrysts implies that the granodiorite is subsolvus.

The magmatic paragenetic sequence is likely (Plagioclase) > (Biotite + opaques) > (microcline + quartz) then hydrothermal alteration to muscovite/sericite + chlorite.

Following the crystallization of the igneous minerals there are a series of subsolidus changes to the minerals. Post-crystallization deformation likely generated the quartz deformations features and allowed excess to aqueous fluids associated with alteration.

Granodiorite classification, and myrmekitic texture suggest this sample is likely sourced by the Idaho Batholith.

SAMPLE: SMC 13-31

Last update: 2/26/20

Petrographer: Kyle Tollefson

LOCATION: 44°09.051N, 115°00.801W
COLLECTOR: Barbara Dutrow

DATE COLLECTED: July 10th 2013

AGE DATE:

ROCK TYPE: Biotite-bearing Syeno-Granite

MEGASCOPIC DESCRIPTION: Leucocratic, white, coarse-grained granitoid chiefly composed of microcline megacrysts in a matrix of plagioclase and quartz with minor biotite.
===
MINERAL ASSEMBLAGES: (Point counted modes)

Plagioclase (13%) [0.1-2 mm] Anhedral to subhedral grains exhibiting albite twinning and moderate seritization.

Microcline (56.3%) [1-15 mm] Anhedral to subhedral grains exhibiting pervasive perthite and minor seritization.

Quartz (30%) [0.1-2 mm] Anhedral grains exhibiting major sweeping extinction and checkerboard extinction. Recrystallized quartz.

Biotite (0.7%) [<1 mm] Subhedral laths exhibiting brown to green pleochroism, birds eye extinction, and major chloritization.

Chlorite (tr%) [0.2 mm] Subhedral green laths replacing biotite.
===

TEXTURES: Hypidiomorphic coarse-grained to porphyritic texture dominated by microcline, plagioclase, quartz, and biotite, respectively. Microcline exhibits perthitic texture. Recrystallization in the quartz indicates post-crystallization deformation.

ALTERATION: Moderate metasomatic/hydrothermal alteration from biotite to chlorite and plagioclase to sericite/muscovite.

OPTICAL CATHODOLUMINESCENCE

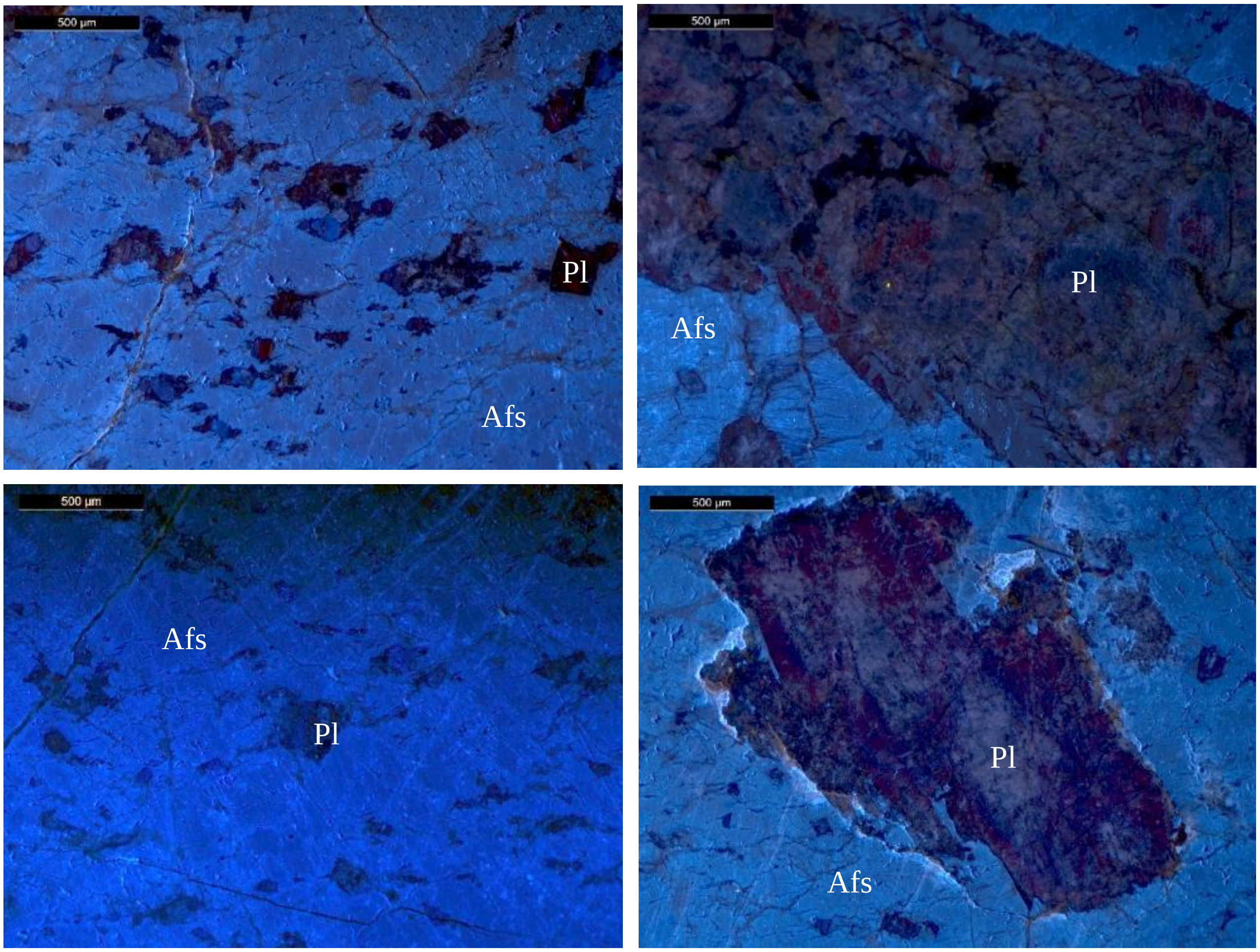

Mineral abbreviations taken from (Whitney and Evans, 2010). Bright to moderate blue alkali feldspar with brown plagioclase.

COMMENTS AND INTERPRETATION:

Based on the QAP ratio of 30.21:56.70:13.09 of the likely primary magmatic minerals, this rock is best classified as Biotite-bearing Syeno-Granite with secondary alteration to muscovite/sericite and chlorite. The fact that the alkali-feldspar and plagioclase from separate phenocrysts implies that the granite is a subsolvus granite.

The magmatic paragenetic sequence is likely (microcline + plagioclase) > (biotite + quartz) and then hydrothermal alteration to muscovite/sericite + chlorite.

Following the crystallization of the igneous minerals there are a series of subsolidus changes to the minerals. Post-crystallization deformation likely generated the quartz deformations features and allowed excess to aqueous fluids associated with alteration.

Syeno-Granite classification and pervasive perthitic microcline suggest this sample is likely sourced by the Sawtooth Batholith.

SAMPLE: SMC 13-132

Last update: 2/26/20

Petrographer: Kyle Tollefson

LOCATION: 44°08.513N, 115°00.438W
COLLECTOR:

DATE COLLECTED: July 17th 2013

AGE DATE:

ROCK TYPE: Biotite-bearing Monzo-Granite

MEGASCOPIC DESCRIPTION: Leucocratic, white, coarse-grained phaneritic granitoid chiefly composed of microcline, plagioclase, and quartz with minor biotite.
==

MINERAL ASSEMBLAGES: (Point counted modes)

Plagioclase (32.3%) [0.1-9 mm] Subhedral grains exhibiting faint albite twinning and moderate seritization.

Microcline (26.3%) [0.1-10 mm] Anhedral to subhedral grains exhibiting tartan twining, minor perthite, and minor seritization. Pervasive myrmekites of plagioclase-quartz develop at margins with plagioclase.

Quartz (39%) [0.01-10 mm] Anhedral grains exhibiting moderate sweeping extinction and checkerboard extinction. Recrystallized quartz.

Biotite (1.3%) [0.1-5 mm] Subhedral to euhedral laths exhibiting reddish-brown to green pleochroism, birds eye extinction, and minor chloritization.

Sericite (1%) [0.1-0.4 mm] Subhedral colorless laths exhibiting high birefringence.

Clinozoisite (tr%) [0.05 mm] Anhedral colorless grains with moderate relief and lst order birefringence.

Chlorite (tr%) [0.1 mm] Subhedral green laths replacing biotite.

Zircon (tr%) [<0.15 mm] Euhedral colorless grains with high relief and high birefringence.
==

TEXTURES: Hypidiomorphic coarse-grained texture dominated by microcline, plagioclase, quartz, and biotite, respectively. Microcline exhibits perthitic texture. Microcline, plagioclase, and quartz exhibit myrmekitic texture. Recrystallization in the quartz indicates post-crystallization deformation.

ALTERATION: Minor metasomatic/hydrothermal alteration from biotite to chlorite and plagioclase to sericite/muscovite.

OPTICAL CATHODOLUMINESCENCE

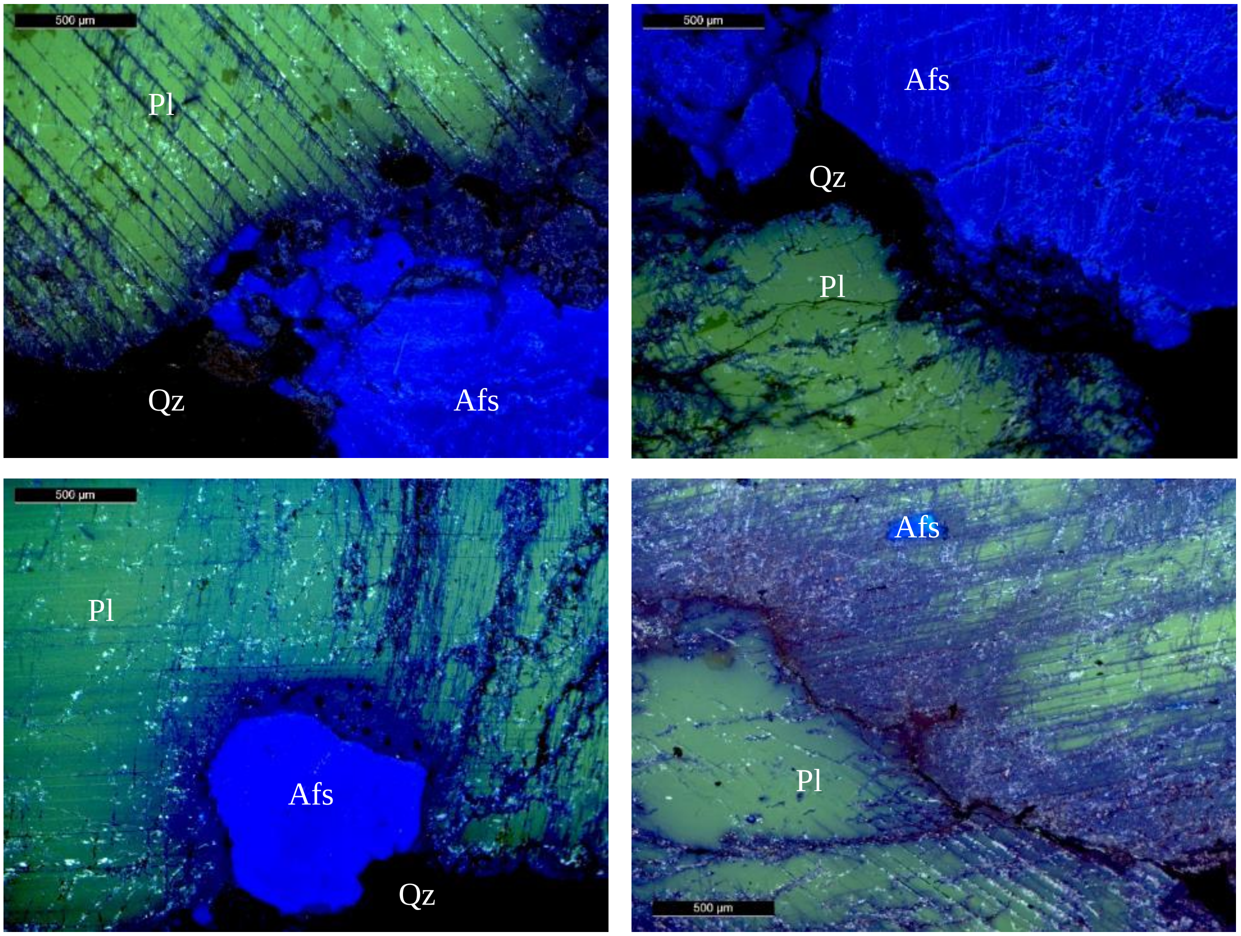

Mineral abbreviations taken from (Whitney and Evans, 2010). Moderate blue alkali feldspar with moderate green plagioclase. Extensive blue alteration (REE fluids) on albite twinning planes present and myrmekitic texture observed.

COMMENTS AND INTERPRETATION:

Based on the QAP ratio of 39.96:26.95:33.09 of the likely primary magmatic minerals, this rock is best classified as Biotite-bearing Monzo-Granite with secondary alteration to muscovite/sericite and chlorite. The fact that the alkali-feldspar and plagioclase from separate phenocrysts implies that the granite is a subsolvus granite.

The magmatic paragenetic sequence is likely (Plagioclase) > (Microcline + quartz) > (Biotite) and then hydrothermal alteration to muscovite/sericite + chlorite.

Following the crystallization of the igneous minerals there are a series of subsolidus changes to the minerals. Post-crystallization deformation likely generated the quartz deformations features and allowed excess to aqueous fluids associated with alteration.

An age date of 87.41 ± 0.44 Ma and moderate green plagioclase CL responses suggest this sample is likely sourced by the Idaho Batholith.

SAMPLE: SMC 14-09

Last update: 3/12/2020

Petrographer: Kyle Tollefson

LOCATION: 44°08.842N, 114°59.757W
COLLECTOR: Barbara Dutrow

DATE COLLECTED: July 7th 2014

AGE DATE:

ROCK TYPE: Biotite Granodiorite

MEGASCOPIC DESCRIPTION: Leucocratic, white, coarse-grained phaneritic granitoid chiefly composed of microcline, plagioclase, and quartz with minor biotite.
===
MINERAL ASSEMBLAGES: (Point counted modes)

Plagioclase (40%) [0.1-7 mm] Subhedral grains exhibiting albite twinning and moderate seritization.

Microcline (20%) [0.1-4 mm] Anhedral to subhedral grains exhibiting tartan twining, minor perthite, and minor seritization. Moderate myrmekites of plagioclase-quartz develop at margins with plagioclase.

Quartz (33.7%) [0.01-5 mm] Anhedral grains exhibiting moderate sweeping extinction.

Biotite (5.7%) [0.1-2.5 mm] Subhedral to euhedral laths exhibiting reddish-brown to green pleochroism, birds eye extinction, and moderate chloritization.

Sericite (tr%) [0.1-0.75 mm] Subhedral colorless laths exhibiting high birefringence.

Apatite (tr%) [<0.1-0.25 mm] Subhedral colorless grains with moderate relief and 1st order birefringence.

Allanite (tr%) [0.2 mm] Subhedral to euhedral equant grains with brown to reddish brown pleochroism, high relief, and high birefringence.

Chlorite (tr%) [0.1-2 mm] Subhedral green laths replacing biotite.

Magnetite (tr%) [<0.2 mm] Subhedral to euhedral opaque grains exhibiting brownish-grey, isotropic, and a pitted nature in reflective light.

Zircon (tr%) [<0.2 mm] Euhedral colorless grains with high relief and high birefringence.
===

TEXTURES: Hypidiomorphic coarse-grained texture dominated by microcline, plagioclase, quartz, and biotite, respectively. Microcline exhibits minor perthitic texture. Microcline, plagioclase, and quartz exhibit myrmekitic texture.

ALTERATION: Moderate metasomatic/hydrothermal alteration from biotite to chlorite and plagioclase to sericite/muscovite.

OPTICAL CATHODOLUMINESCENCE

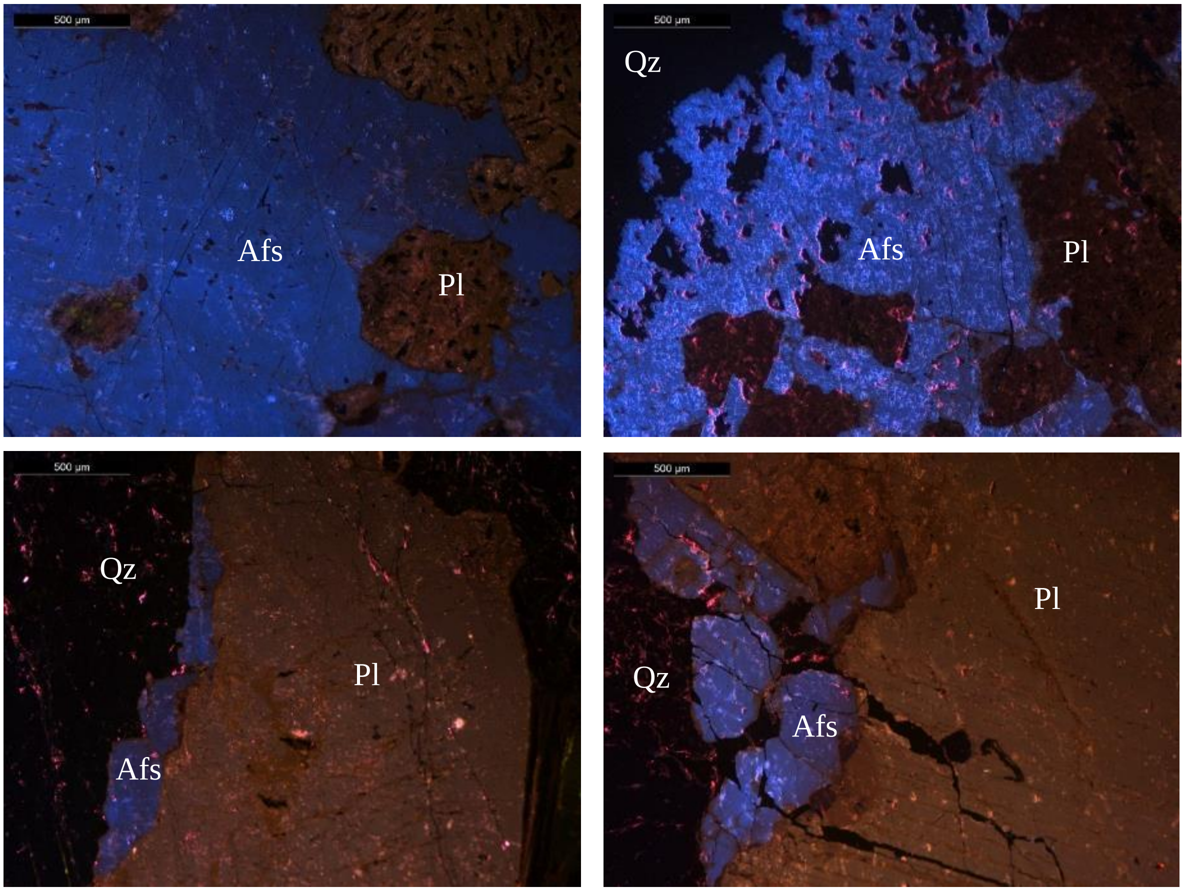

Mineral abbreviations taken from (Whitney and Evans, 2010). Moderate blue alkali feldspar with brown plagioclase. Myrmekitic texture observed.

COMMENTS AND INTERPRETATION:

Based on the QAP ratio of 35.97:21.34:42.69of the likely primary magmatic minerals, this rock is best classified as Biotite Granodiorite with secondary alteration to muscovite/sericite and chlorite. The fact that the alkali-feldspar and plagioclase from separate phenocrysts implies that the granite is a subsolvus granite.

The magmatic paragenetic sequence is likely (Plagioclase + microcline) > (Magnetite + Biotite) > (quartz) and then hydrothermal alteration to muscovite/sericite + chlorite.

Granodiorite classification and an age date of 93.94 ± 0.46 Ma suggest the likely sourced of this sample is the Idaho batholith.

SAMPLE: SMC 14-11

Last update: 2/26/20

Petrographer: Kyle Tollefson

LOCATION: 44°10.262N, 115°01.018W

COLLECTOR: Barbara Dutrow

DATE COLLECTED:

AGE DATE: 80.6 ± 0.7 Ma

ROCK TYPE: Biotite-bearing monzo-granite

MEGASCOPIC DESCRIPTION: Leucocratic, white, coarse-grained granitoid chiefly composed of microcline, plagioclase, and quartz with minor biotite.

==

MINERAL ASSEMBLAGES: (Point counted modes)

Plagioclase (28.3%) [0.1-8 mm] Anhedral to subhedral grains exhibiting albite twinning and moderate seritization.

Microcline (33.3%) [1-10 mm] Anhedral to subhedral grains exhibiting pervasive perthite and minor seritization.

Quartz (38%) [0.1-2 mm] Anhedral grains exhibiting major sweeping extinction and checkerboard extinction. Recrystallized quartz.

Biotite (0.3%) [<1-1.5 mm] Subhedral laths exhibiting brown to green pleochroism, birds eye extinction, and major chloritization.

Chlorite (tr%) [0.2 mm] Subhedral green laths replacing biotite.

Zircon (tr%) [<0.1 mm] Euhedral colorless grains with hi relief and hi birefringence.

==

TEXTURES: Hypidiomorphic coarse-grained texture dominated by microcline, plagioclase, quartz, and biotite, respectively. Microcline exhibits perthitic texture. Recrystallization in the quartz indicates post-crystallization deformation.

ALTERATION: Moderate metasomatic/hydrothermal alteration from biotite to chlorite and plagioclase to sericite/muscovite.

OPTICAL CATHODOLUMINESCENCE

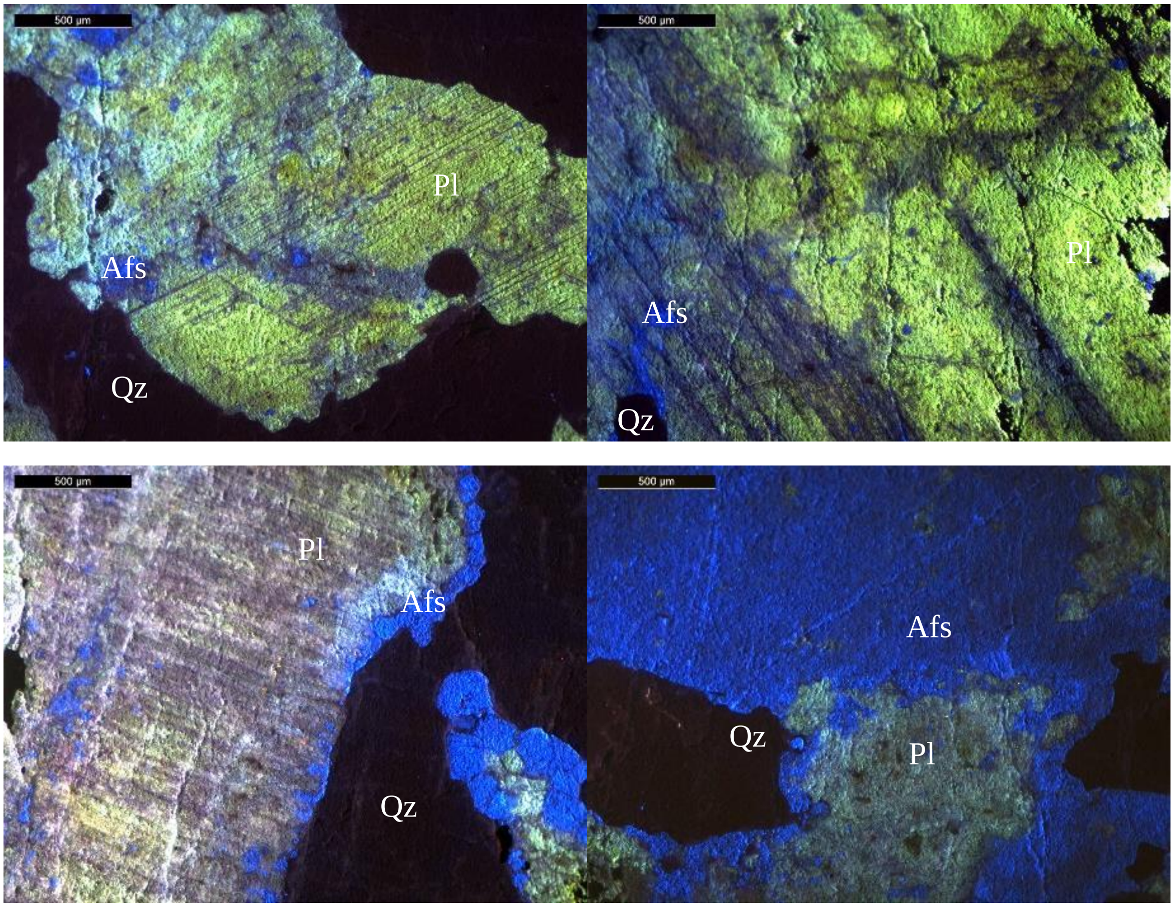

Mineral abbreviations taken from (Whitney and Evans, 2010). Moderate blue alkali feldspar with green plagioclase.

COMMENTS AND INTERPRETATION:

Based on the QAP ratio of 38.15, 33.43, 28.41 of the likely primary magmatic minerals, this rock is best classified as biotite-bearing monzo-granite with secondary alteration to muscovite/sericite and chlorite. The fact that the alkali-feldspar and plagioclase from separate phenocrysts implies that the granite is a subsolvus granite.

The magmatic paragenetic sequence is likely (microcline + plagioclase) > (biotite + quartz) and then hydrothermal alteration to muscovite/sericite + chlorite.

Following the crystallization of the igneous minerals there are a series of subsolidus changes to the minerals. Post-crystallization deformation likely generated the quartz deformations features and allowed excess to aqueous fluids associated with alteration.

Green plagioclase OM-CL responses and an age date of 80.6 ± 0.7 Ma suggest this sample is likely sourced by the Idaho batholith.

SAMPLE: SMC 14-26

Last update: 2/26/20

Petrographer: Kyle Tollefson

LOCATION: 44°09.994N, 115°01.019W
COLLECTOR: Barbara Dutrow

DATE COLLECTED: July 25th 2014

AGE DATE:

ROCK TYPE: Biotite-bearing Monzo-Granite

MEGASCOPIC DESCRIPTION: Leucocratic, white, coarse-grained phaneritic granitoid chiefly composed of microcline, plagioclase, and quartz with minor biotite.
==

MINERAL ASSEMBLAGES: (Point counted modes)

Plagioclase (29%) [0.2-6 mm] Anhedral to subhedral grains exhibiting albite twinning and major seritization.

Microcline (36.7%) [0.2-8 mm] Anhedral to subhedral grains exhibiting minor perthite, and minor seritization. Moderate myrmekite and graphic texture of plagioclase-quartz develop at margins with plagioclase.

Quartz (33.3%) [0.02-1 mm] Anhedral grains exhibiting moderate sweeping extinction. Recrystallized quartz.

Hematite (tr%) [<0.1 mm] Anhedral to subhedral opaque grains with red rims.

Biotite (0.7%) [0.2-4 mm] Subhedral laths exhibiting brown to green pleochroism, birds eye extinction, and major chloritization.

Magnetite (tr%) [<0.25 mm] Subhedral to euhedral opaque grains exhibiting brownish-grey, isotropic, and a pitted nature in reflective light.

Sericite (0.3%) [<2 mm] Subhedral colorless laths exhibiting high birefringence.

Chlorite (tr%) [0.2 mm] Subhedral green laths replacing biotite.

Zircon (tr%) [<0.1 mm] Euhedral colorless grains with high relief and high birefringence.
==

TEXTURES: Allotriomorphic coarse-grained texture dominated by microcline, plagioclase, quartz, and biotite, respectively. Microcline exhibits perthite texture. Microcline, plagioclase, and quartz exhibit myrmekitic texture. Recrystallization in the quartz indicates post-crystallization deformation.

ALTERATION: Pervasive metasomatic/hydrothermal alteration from plagioclase to sericite/muscovite.

OPTICAL CATHODOLUMINESCENCE

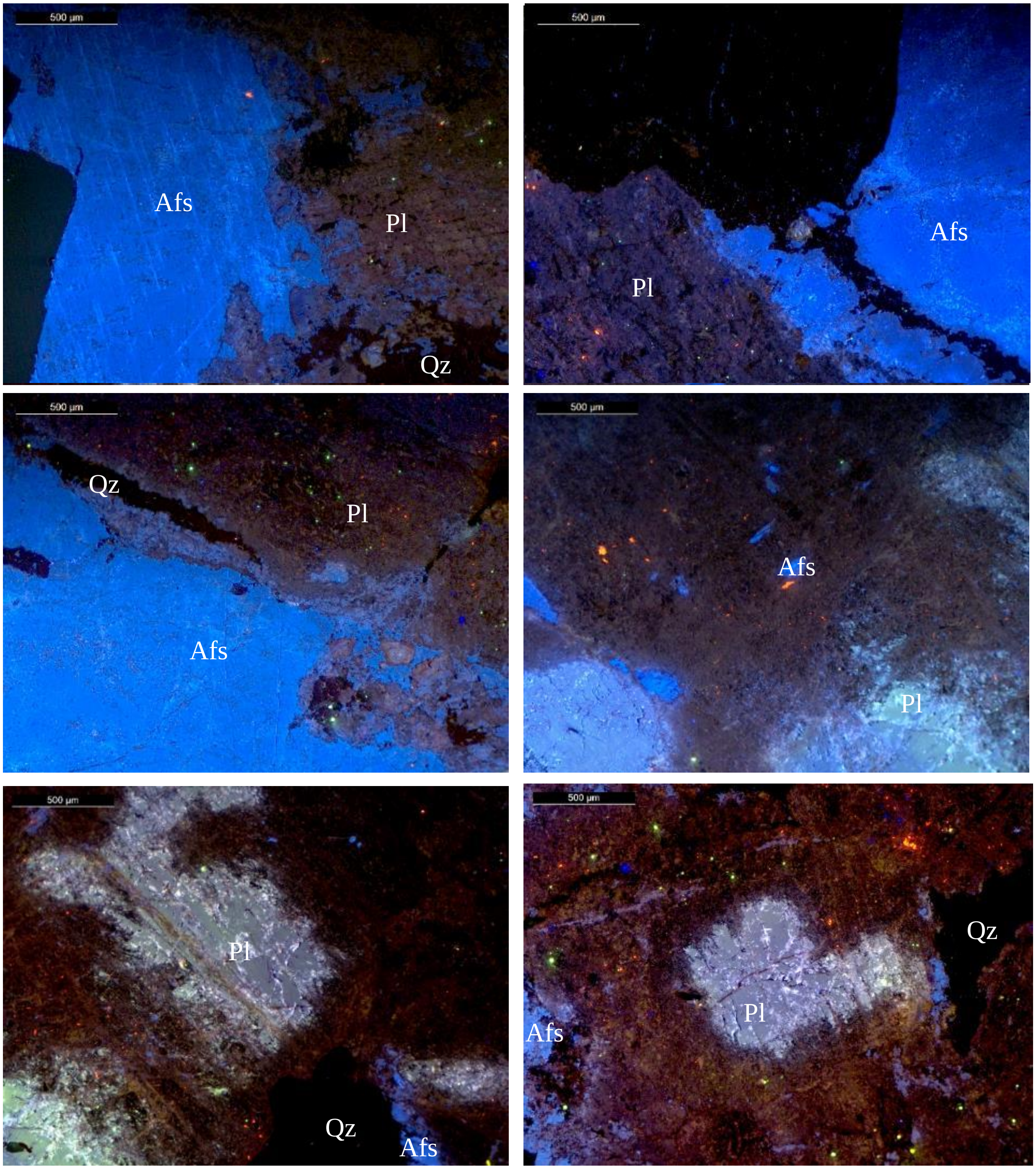

Mineral abbreviations taken from (Whitney and Evans, 2010). Bright blue alkali feldspar with brown and blue plagioclase. Orange carbonates observed.

COMMENTS AND INTERPRETATION:

Based on the QAP ratio of 33.64:37.07:29.29 of the likely primary magmatic minerals, this rock is best classified as Biotite-bearing Monzo-Granite with secondary alteration to muscovite/sericite and chlorite. The fact that the alkali-feldspar and plagioclase from separate phenocrysts implies that the granite is a subsolvus granite.

The magmatic paragenetic sequence is likely (Plagioclase + microcline) > (opaques) > (quartz) and then hydrothermal alteration to muscovite/sericite + chlorite.

Following the crystallization of the igneous minerals there are a series of subsolidus changes to the minerals. Post-crystallization deformation likely generated the quartz deformations features and allowed excess to aqueous fluids associated with alteration.

Blue plagioclase and no other distinct characteristics suggests the likely source of this sample is anatectic melts.

SAMPLE: SMC 14-40

Last update: 2/26/20

Petrographer: Kyle Tollefson

LOCATION: 44°09.048N, 115°01.005W
COLLECTOR: Barbara Dutrow

DATE COLLECTED: July 16th 2014

AGE DATE:

ROCK TYPE: Monzo-Granite

MEGASCOPIC DESCRIPTION: Leucocratic, white, medium-grained phaneritic granitoid chiefly composed of microcline, plagioclase, and quartz with no visible mafics.
==
MINERAL ASSEMBLAGES: (Point counted modes)

Plagioclase (23.7%) [0.2-2 mm] Anhedral grains exhibiting albite twinning and moderate seritization.

Microcline (24.3%) [0.2-5 mm] Anhedral to subhedral grains exhibiting tartan twinning, Moderate perthite, and minor seritization. Minor myrmekites of plagioclase-quartz develop at margins with plagioclase.

Quartz (52%) [0.01-2 mm] Anhedral grains exhibiting major sweeping extinction. Recrystallized quartz.

Hematite (tr%) [<0.01 mm] Anhedral opaque grains with red rims.
==

TEXTURES: Allotriomorphic medium-grained texture dominated by microcline, plagioclase, and quartz, respectively. Microcline exhibits perthite texture. Microcline, plagioclase, and quartz exhibit myrmekitic texture. Recrystallization in the quartz indicates post-crystallization deformation.

ALTERATION: Minor metasomatic/hydrothermal alteration from plagioclase to sericite/muscovite.

OPTICAL CATHODOLUMINESCENCE

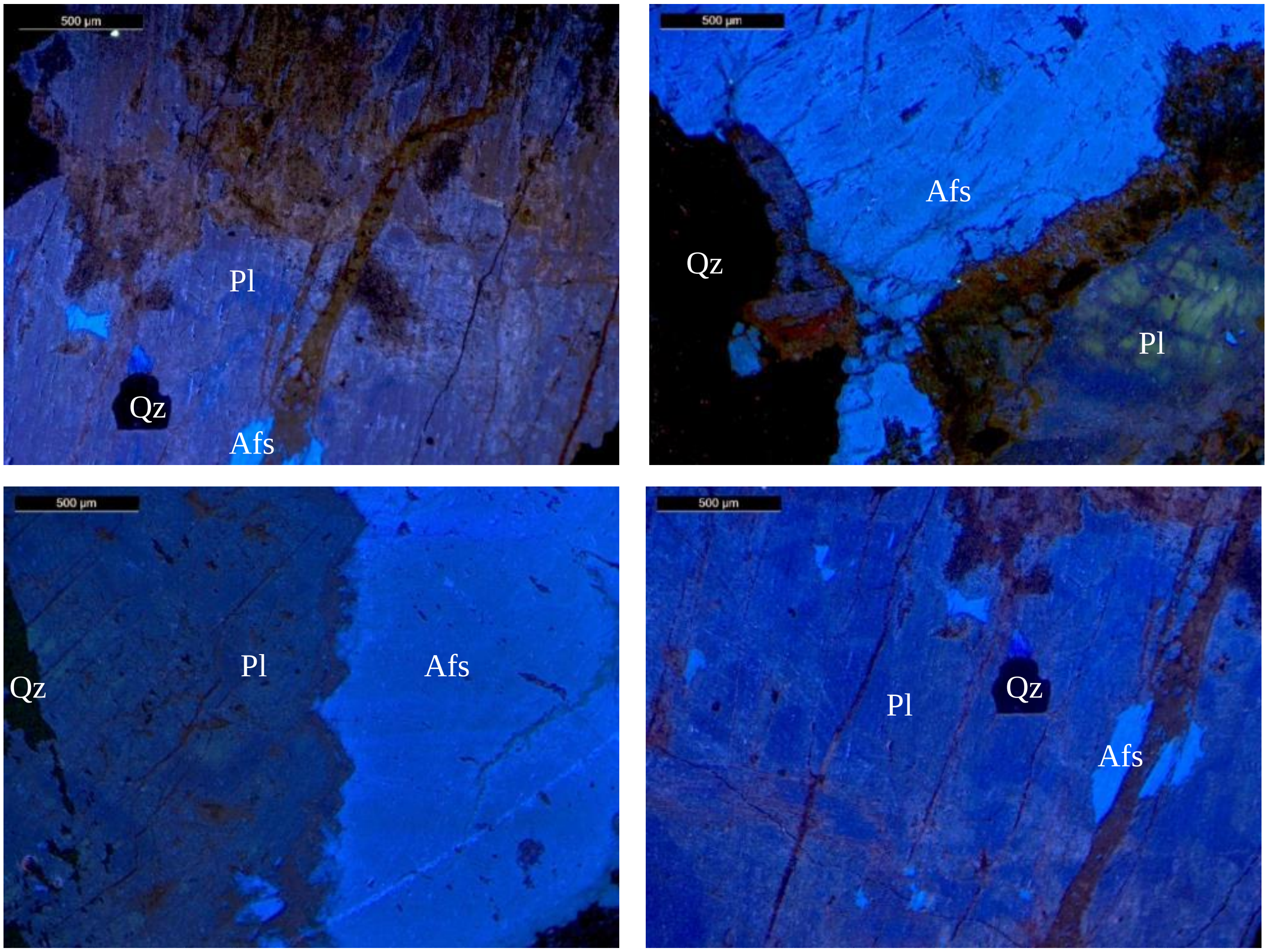

Mineral abbreviations taken from (Whitney and Evans, 2010). Bright blue alkali feldspar with moderate green and moderate blue plagioclase.

COMMENTS AND INTERPRETATION:

Based on the QAP ratio of 52.00:24.30:23.70 of the likely primary magmatic minerals, this rock is best classified as Monzo-Granite with secondary alteration to muscovite/sericite and chlorite. The fact that the alkali-feldspar and plagioclase from separate phenocrysts implies that the granite is a subsolvus granite.

The magmatic paragenetic sequence is likely (Plagioclase) > (microcline + quartz) and then hydrothermal alteration to muscovite/sericite + chlorite.

Following the crystallization of the igneous minerals there are a series of subsolidus changes to the minerals. Post-crystallization deformation likely generated the quartz deformations features and allowed excess to aqueous fluids associated with alteration.

Blue plagioclase and no other distinct characteristics suggest this sample is likely sourced by anatectic melts.

SAMPLE: SMC 14-43

Last update: 2/26/20

Petrographer: Kyle Tollefson

LOCATION: 44°09.765N, 115°02.176W
COLLECTOR: Barbara Dutrow

DATE COLLECTED: July 20th 2014

AGE DATE:

ROCK TYPE: Monzo-Granite

MEGASCOPIC DESCRIPTION: Leucocratic, white, fine-grained phaneritic equigranular granitoid chiefly composed of microcline, plagioclase, and quartz with no visible mafics.
===
MINERAL ASSEMBLAGES: (Point counted modes)

Plagioclase (26.3%) [0.2-2.5 mm**]** Anhedral to subhedral grains exhibiting deformed albite twinning (kink structure) and moderate seritization.

Microcline (36%) [0.2-4 mm] Anhedral to subhedral grains exhibiting moderate perthite and minor seritization.

Quartz (37.3%) [0.02-1 mm] Anhedral grains exhibiting moderate sweeping extinction. Recrystallized quartz.

Sericite (0.3%) [<0.5 mm] Subhedral colorless laths exhibiting high birefringence.

Hematite (tr%) [<0.1 mm] Anhedral to subhedral opaque grains with red rims.

Magnetite (tr%) [<0.25 mm] Subhedral to euhedral opaque grains exhibiting brownish-grey, isotropic, and a pitted nature in reflective light.
===

TEXTURES: Allotriomorphic fine-grained texture dominated by microcline, plagioclase, and quartz, respectively. Microcline exhibits perthite texture. Recrystallization in the quartz indicates post-crystallization deformation.

ALTERATION: Minor metasomatic/hydrothermal alteration from biotite to chlorite and plagioclase to sericite/muscovite.

OPTICAL CATHODOLUMINESCENCE

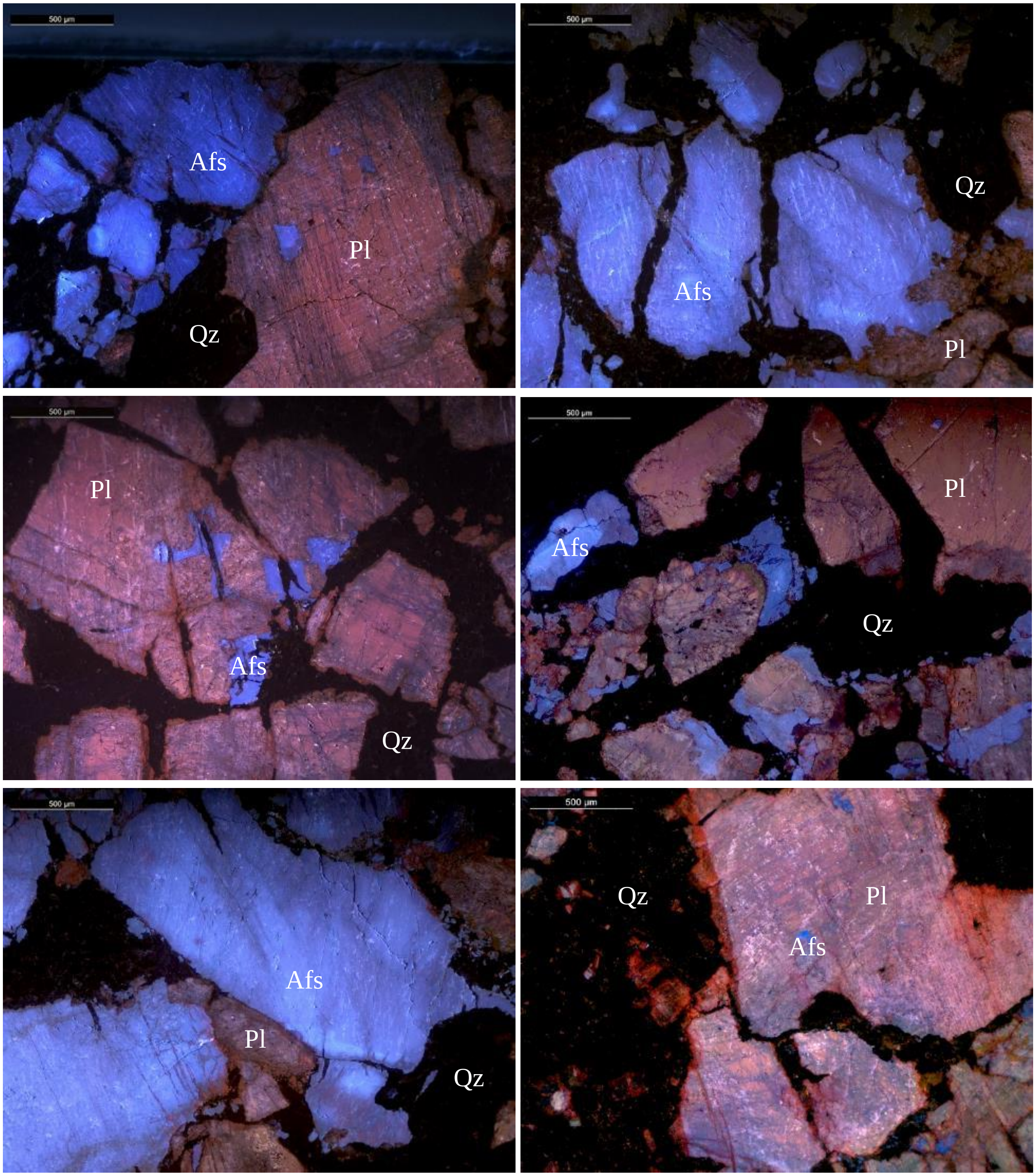

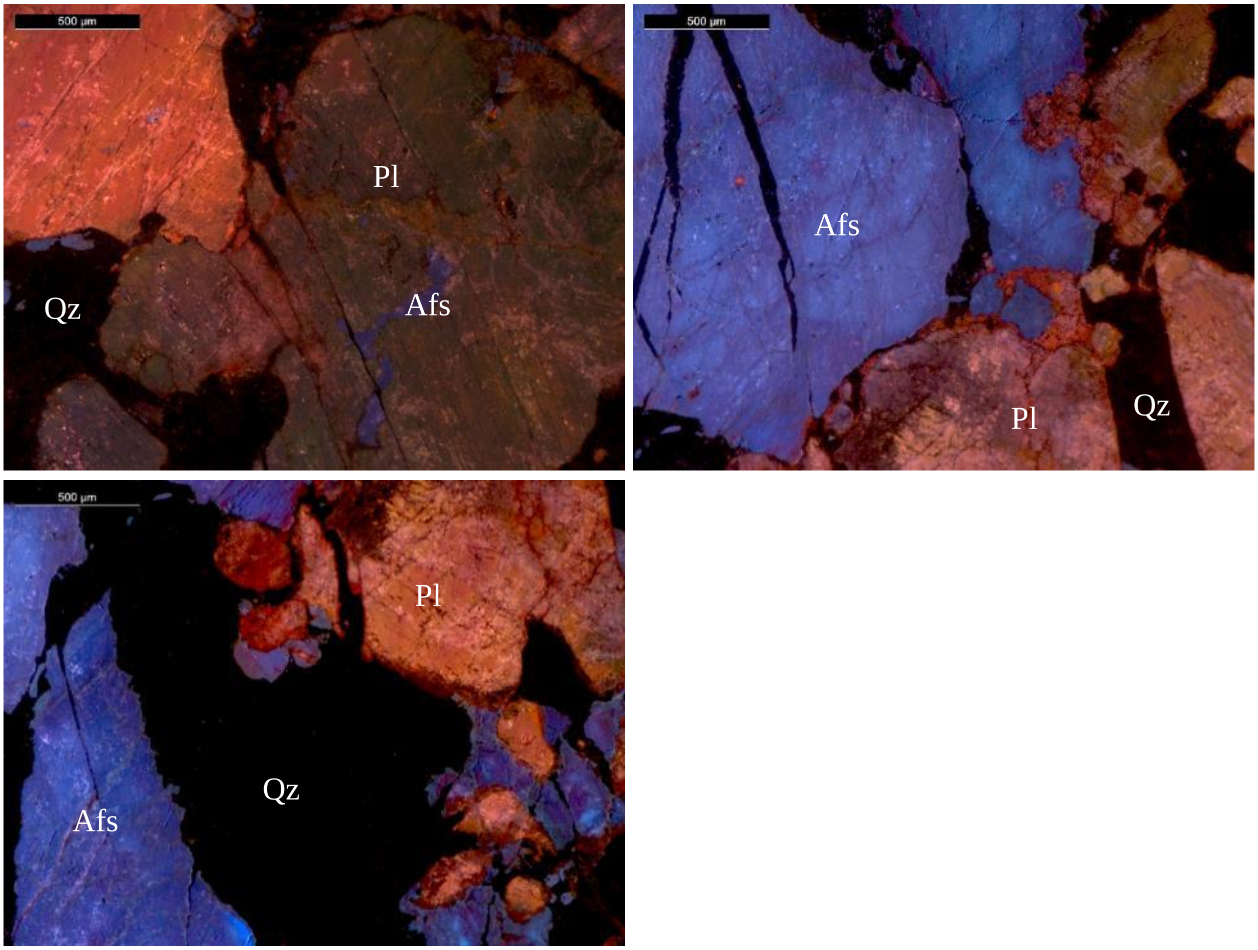

Mineral abbreviations taken from (Whitney and Evans, 2010). Bright to moderate blue alkali feldspar with brown and red plagioclase.

COMMENTS AND INTERPRETATION:
Based on the QAP ratio of 37.45:36.14:26.41 of the likely primary magmatic minerals, this rock is best classified as Monzo-Granite with secondary alteration to muscovite/sericite and chlorite. The fact that the alkali-feldspar and plagioclase from separate phenocrysts implies that the granite is a subsolvus granite.

The magmatic paragenetic sequence is (Plagioclase + microcline) > (opaques) > (quartz**)** and then hydrothermal alteration to muscovite/sericite + chlorite.

Following the crystallization of the igneous minerals there are a series of subsolidus changes to the minerals. Post-crystallization deformation likely generated the quartz deformations features and allowed excess to aqueous fluids associated with alteration.

An age date of 75.46 ± 0.63 Ma an no other distinct characteristics suggests this sample was likely sourced by the Idaho batholith.

SAMPLE: SMC 14-44

Last update: 2/26/20

Petrographer: Kyle Tollefson

LOCATION: 44°10.258N, 115°02.313W
COLLECTOR: Barbara Dutrow

DATE COLLECTED: July 20th 2014

AGE DATE:

ROCK TYPE: Hornblende Biotite-bearing Monzo-Granite

MEGASCOPIC DESCRIPTION: Leucocratic, white, fine-grained phaneritic granitoid chiefly composed of microcline, plagioclase, and quartz with minor biotite.
==
MINERAL ASSEMBLAGES: (Point counted modes)

Plagioclase (18%) [0.25-3 mm] Anhedral grains exhibiting faint albite twinning and major seritization.

Microcline (33%) [0.1-5 mm] Anhedral grains exhibiting moderate perthite, and major seritization.

Quartz (48%) [0.05-2 mm] Anhedral grains exhibiting minor sweeping extinction. Recrystallized quartz.

Biotite (tr%) [0.1-0.75 mm] Anhedral laths exhibiting brown to green pleochroism, birds eye extinction, and major chloritization.

Magnetite (tr%) [<0.1 mm] Subhedral opaque grains exhibiting brownish-grey, isotropic, and a pitted nature in reflective light.

Apatite (tr%) [<0.25 mm] Anhedral to subhedral colorless grains with moderate relief and 1st order birefringence.

Hornblende (tr%) [0.1-0.25 mm] Subhedral grains exhibiting reddish brown to tan pleochroism.

Clinozoisite (tr%) [<0.2 mm] Anhedral to subhedral colorless grains with moderate relief and lst order birefringence.

Chlorite (tr%) [0.05-0.1 mm] Subhedral green laths replacing biotite.

Zircon (tr%) [<0.1 mm] Euhedral colorless grains with high relief and high birefringence.
==

TEXTURES: Allotriomorphic fine-grained texture dominated by microcline, plagioclase, quartz, and biotite, respectively. Microcline exhibits perthite texture. Recrystallization in the quartz indicates post-crystallization deformation.

ALTERATION: Pervasive metasomatic/hydrothermal alteration from biotite to chlorite and plagioclase to sericite/muscovite.

OPTICAL CATHODOLUMINESCENCE

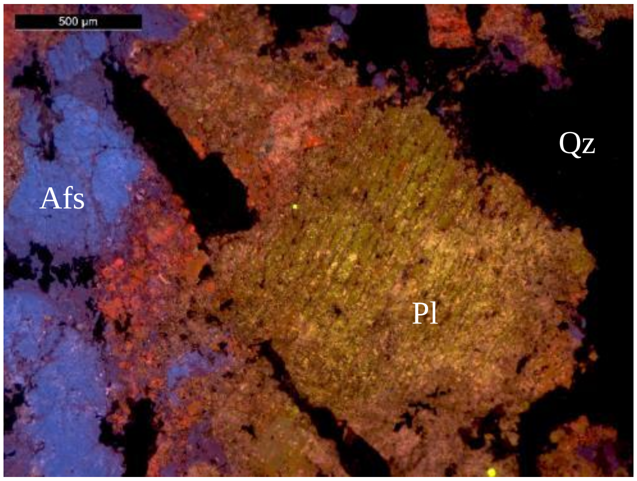

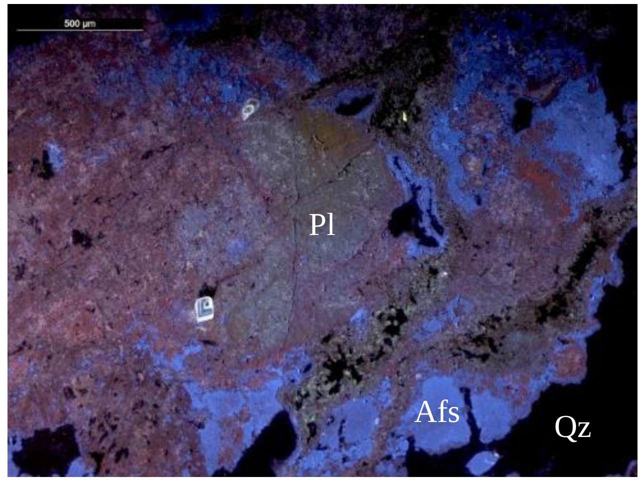

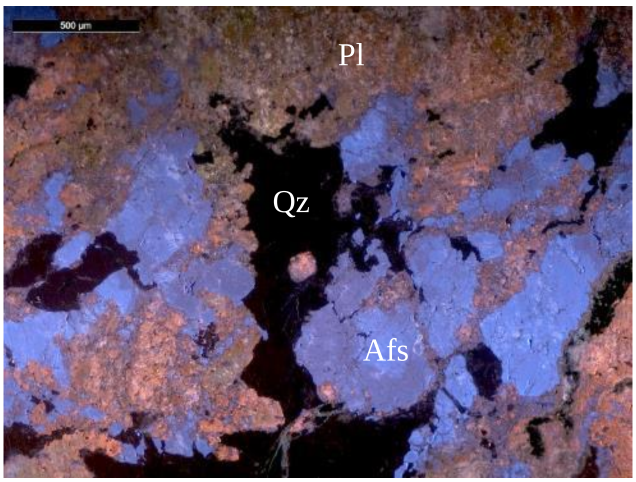

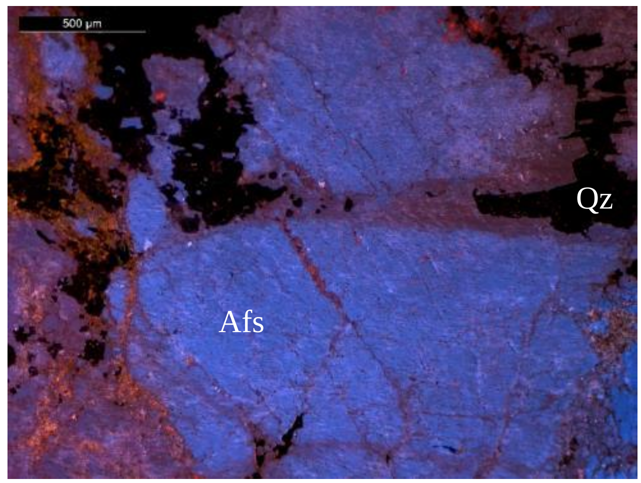

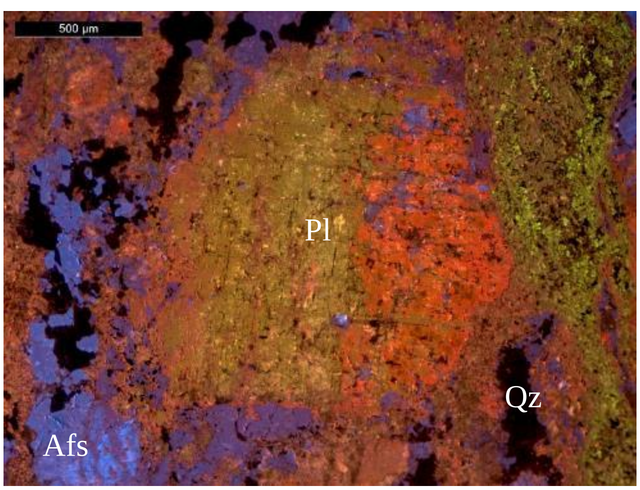

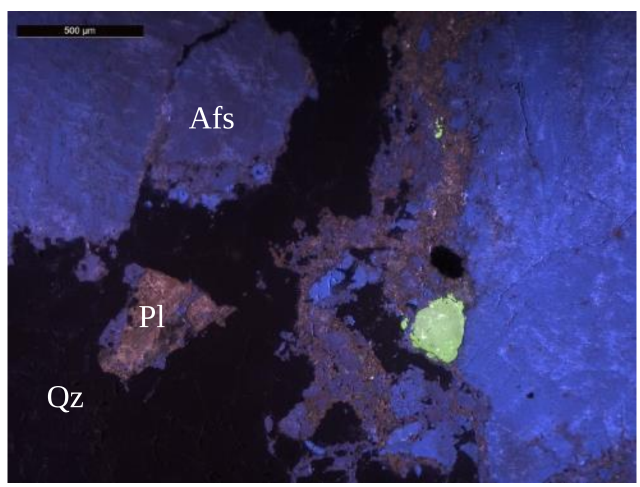

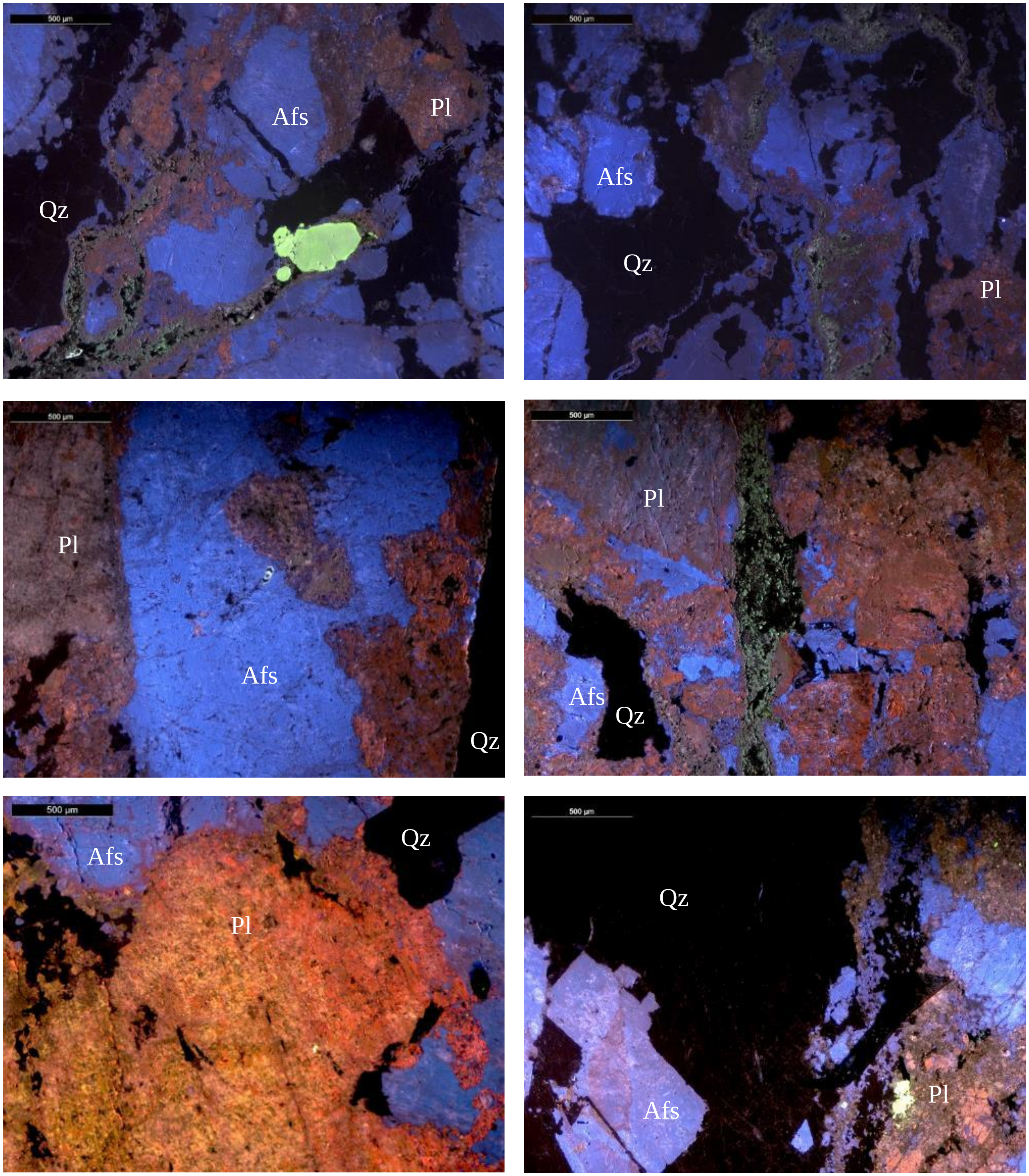

Mineral abbreviations taken from (Whitney and Evans, 2010). Moderate blue and red alkali feldspar with brown and red plagioclase.

COMMENTS AND INTERPRETATION:

Based on the QAP ratio of 48.48:33.33:18.18 of the likely primary magmatic minerals, this rock is best classified as Hornblende Biotite-bearing Monzo-Granite with secondary alteration to muscovite/sericite and chlorite. The fact that the alkali-feldspar and plagioclase from separate phenocrysts implies that the granite is a subsolvus granite.

The magmatic paragenetic sequence is likely (Plagioclase + microcline) > (Biotite + opaques) > (quartz) and then hydrothermal alteration to muscovite/sericite + chlorite.

Following the crystallization of the igneous minerals there are a series of subsolidus changes to the minerals. Post-crystallization deformation likely generated the quartz deformations features and allowed excess to aqueous fluids associated with alteration.

Red zonation of alkali feldspar suggests this sample was sourced by the Idaho batholith.

SAMPLE: SMC 14-47

Last update: 2/26/20

Petrographer: Kyle Tollefson

LOCATION: 44°10.964N, 115°03.458W
COLLECTOR: Barbara Dutrow

DATE COLLECTED: July 22nd 2014

AGE DATE:

ROCK TYPE: Monzo-Granite

MEGASCOPIC DESCRIPTION: Leucocratic, white, fine-grained phaneritic granitoid chiefly composed of microcline, plagioclase, and quartz.
===
MINERAL ASSEMBLAGES: (Point counted modes)

Plagioclase (19%) [0.1-0.5 mm] Anhedral grains exhibiting albite twinning and minor seritization.

Microcline (34%) [0.2-1 mm] Anhedral grains exhibiting pervasive perthite, and moderate seritization.

Quartz (47%) [0.01-3 mm] Anhedral grains exhibiting minor sweeping extinction.

Magnetite (tr%) [<0.25 mm**]** Subhedral to euhedral opaque grains exhibiting brownish-grey, isotropic, and a pitted nature in reflective light.

Zircon (tr%) [<0.1 mm] Euhedral colorless grains with high relief and high birefringence.
===

TEXTURES: Allotriomorphic fine-grained texture dominated by microcline, plagioclase, and quartz, respectively. Microcline exhibits perthite texture.

ALTERATION: Minor metasomatic/hydrothermal alteration from biotite to chlorite and plagioclase to sericite/muscovite.

OPTICAL CATHODOLUMINESCENCE

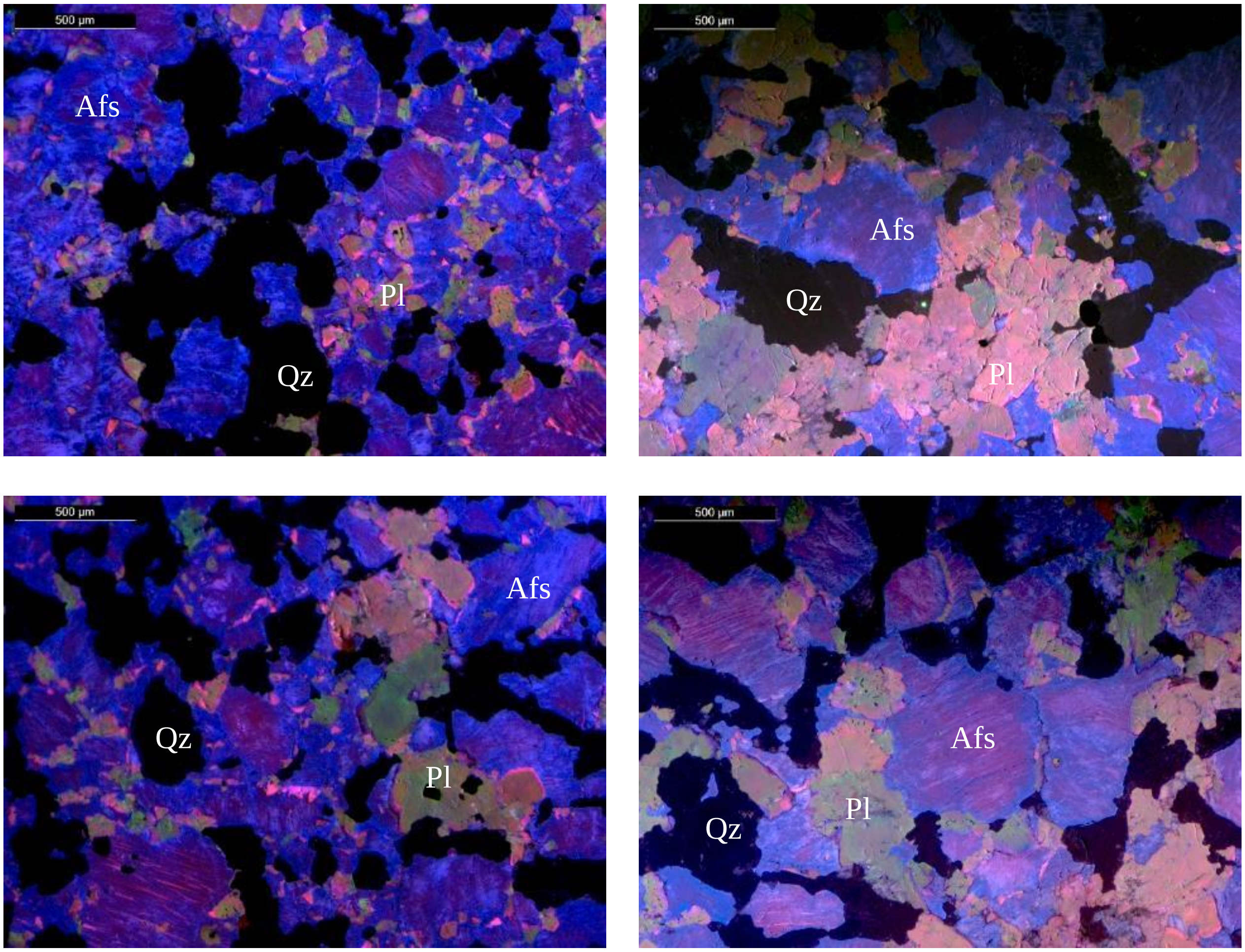

Mineral abbreviations taken from (Whitney and Evans, 2010). Dark to moderate blue and red alkali feldspar with pink to red albite exsolution (perthite). Moderate green to light orange plagioclase. Myrmekitic texture observed.

COMMENTS AND INTERPRETATION:

Based on the QAP ratio of 47.00:34.00:19.00of the likely primary magmatic minerals, this rock is best classified as Monzo-Granite with secondary alteration to muscovite/sericite and chlorite. The fact that the alkali-feldspar and plagioclase from separate phenocrysts implies that the granite is a subsolvus granite.

The magmatic paragenetic sequence is likely (Plagioclase + microcline) > (Magnetite + quartz) and then hydrothermal alteration to muscovite/sericite + chlorite.

Following the crystallization of the igneous minerals there are a series of subsolidus changes to the minerals. Post-crystallization deformation likely generated the quartz deformations features and allowed excess to aqueous fluids associated with alteration.

Perthitic microcline and orange plagioclase CL responses suggest this sample was likely sourced by the Sawtooth Batholith.

SAMPLE: SMC 14-61

Last update: 2/26/20

Petrographer: Kyle Tollefson

LOCATION: 44°10.829N, 115°04.397W
COLLECTOR: Barbara Dutrow

DATE COLLECTED: July 28th 2014

AGE DATE:

ROCK TYPE: Biotite Granodiorite

MEGASCOPIC DESCRIPTION: Leucocratic, white, medium-grained phaneritic granitoid chiefly composed of microcline, plagioclase, and quartz with minor biotite.
===
MINERAL ASSEMBLAGES: (Point counted modes)

<u>Plagioclase</u> (35%) [0.2-3 mm] Anhedral to subhedral grains exhibiting albite twinning and major seritization.

<u>Microcline</u> (17%) [0.2-2.5 mm] Anhedral to subhedral grains exhibiting tartan twinning, minor perthite, and minor seritization. Minor myrmekites of plagioclase-quartz develop at margins with plagioclase.

<u>Quartz</u> (42.7%) [0.01-1.75 mm**]** Anhedral grains exhibiting moderate sweeping extinction. Recrystallized quartz.

<u>Biotite</u> (5%) [0.1-2 mm] Anhedral to subhedral laths exhibiting brown to green pleochroism, birds eye extinction, and moderate chloritization.

<u>Magnetite</u> (tr%) [<0.25 mm] Anhedral to subhedral opaque grains exhibiting brownish-grey, isotropic, and a pitted nature in reflective light.

<u>Allanite</u> (tr%) [<0.1 mm] Subhedral light brown grains exhibiting high relief and 1st order birefringence.

<u>Chlorite</u> (tr%) [0.1 mm] Subhedral green laths replacing biotite.

<u>Zircon</u> (tr%) [<0.1 mm] Euhedral colorless grains with high relief and high birefringence.
===

TEXTURES: Allotriomorphic medium-grained texture dominated by microcline, plagioclase, quartz, and biotite, respectively. Microcline exhibits perthite texture. Microcline, plagioclase, and quartz exhibit myrmekitic texture. Recrystallization in the quartz indicates post-crystallization deformation.

ALTERATION: Moderate metasomatic/hydrothermal alteration from biotite to chlorite and plagioclase to sericite/muscovite.

OPTICAL CATHODOLUMINESCENCE

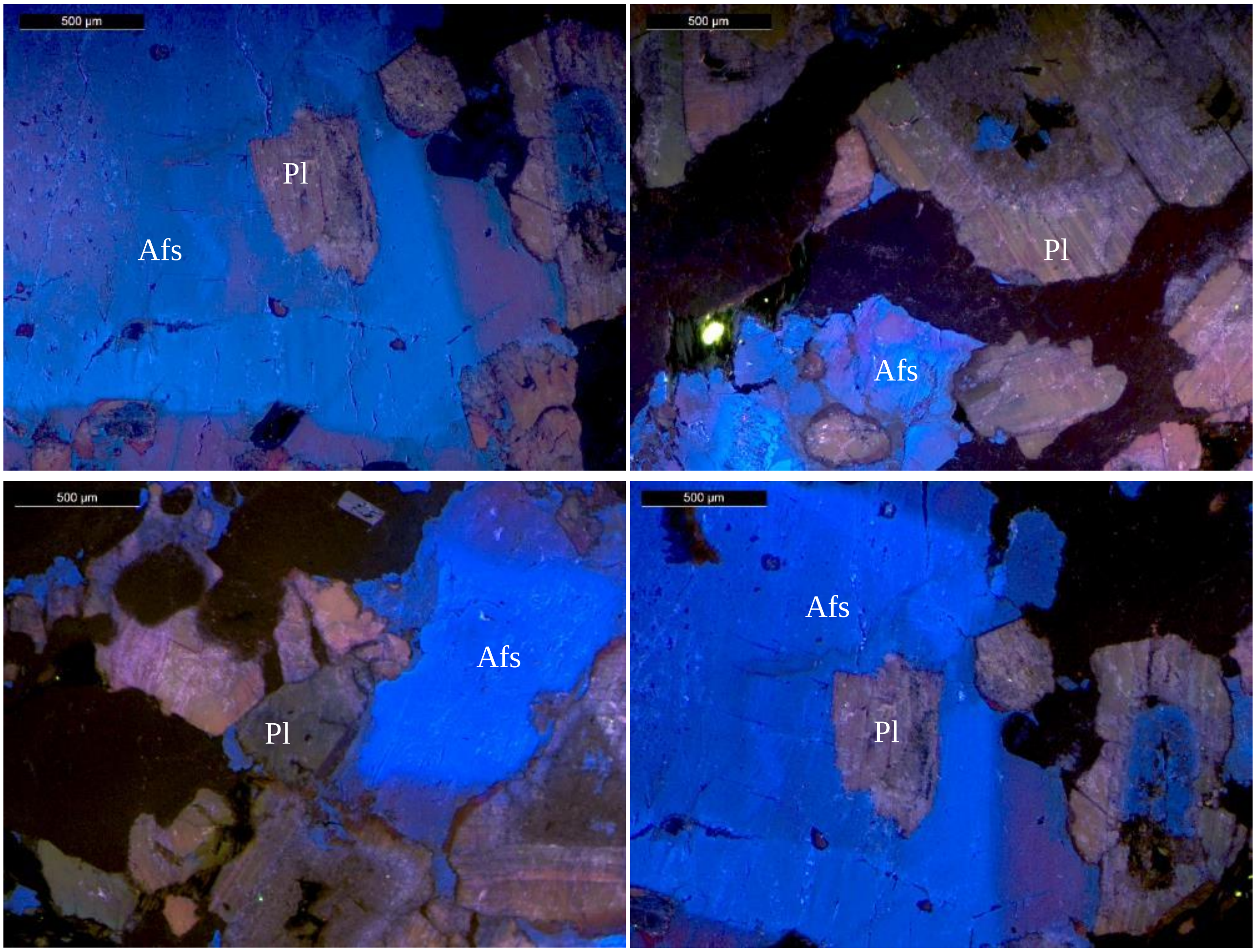

Mineral abbreviations taken from (Whitney and Evans, 2010). Bright to moderate blue and red oscillatory zoned alkali feldspar. Brown and green plagioclase with highly altered cores.

COMMENTS AND INTERPRETATION:

Based on the QAP ratio of 45.09:17.95:36.96of the likely primary magmatic minerals, this rock is best classified as Biotite Granodiorite with secondary alteration to muscovite/sericite and chlorite. The fact that the alkali-feldspar and plagioclase from separate phenocrysts implies that the granite is a subsolvus granite.

The magmatic paragenetic sequence is likely (Plagioclase + microcline) > (Magnetite + Biotite) > (quartz) and then hydrothermal alteration to muscovite/sericite + chlorite.

Following the crystallization of the igneous minerals there are a series of subsolidus changes to the minerals. Post-crystallization deformation likely generated the quartz deformations features and allowed excess to aqueous fluids associated with alteration.

Granodiorite classification, minor myrmekitic texture, green plagioclase CL responses, and red zoned alkali feldspar suggests this sample was likely sourced by the Idaho batholith.

SAMPLE: SMC 14-62

Last update: 2/26/20

Petrographer: Kyle Tollefson

LOCATION: 44°10.769N, 115°04.147W
COLLECTOR: Barbara Dutrow

DATE COLLECTED: July 28th 2014

AGE DATE:

ROCK TYPE: Biotite-bearing Granodiorite

MEGASCOPIC DESCRIPTION: Leucocratic, white, medium-grained phaneritic granitoid chiefly composed of microcline, plagioclase, and quartz with minor biotite.
===
MINERAL ASSEMBLAGES: (Point counted modes)

Plagioclase (35.3%) [0.2-3 mm] Anhedral to subhedral grains exhibiting albite twinning and major seritization of cores.

Microcline (14.7%) [0.2-2.5 mm] Anhedral to subhedral grains exhibiting tartan twinning, minor perthite, and minor seritization.

Quartz (48%) [0.01-1.75 mm] Anhedral grains exhibiting moderate sweeping extinction. Recrystallized quartz.

Biotite (2%) [0.1-2 mm] Anhedral to subhedral laths exhibiting brown to green pleochroism, birds eye extinction, and moderate chloritization.

Magnetite (tr%) [<0.25 mm] Anhedral to subhedral opaque grains exhibiting brownish-grey, isotropic, and a pitted nature in reflective light.

Chlorite (tr%) [0.1-0.2 mm] Subhedral green laths replacing biotite.

Zircon (tr%) [<0.1 mm] Euhedral colorless grains with high relief and high birefringence.
===

TEXTURES: Allotriomorphic medium-grained texture dominated by microcline, plagioclase, quartz, and biotite, respectively. Microcline exhibits perthite texture. Recrystallization in the quartz indicates post-crystallization deformation.

ALTERATION: Moderate metasomatic/hydrothermal alteration from biotite to chlorite and plagioclase to sericite/muscovite.

OPTICAL CATHODOLUMINESCENCE

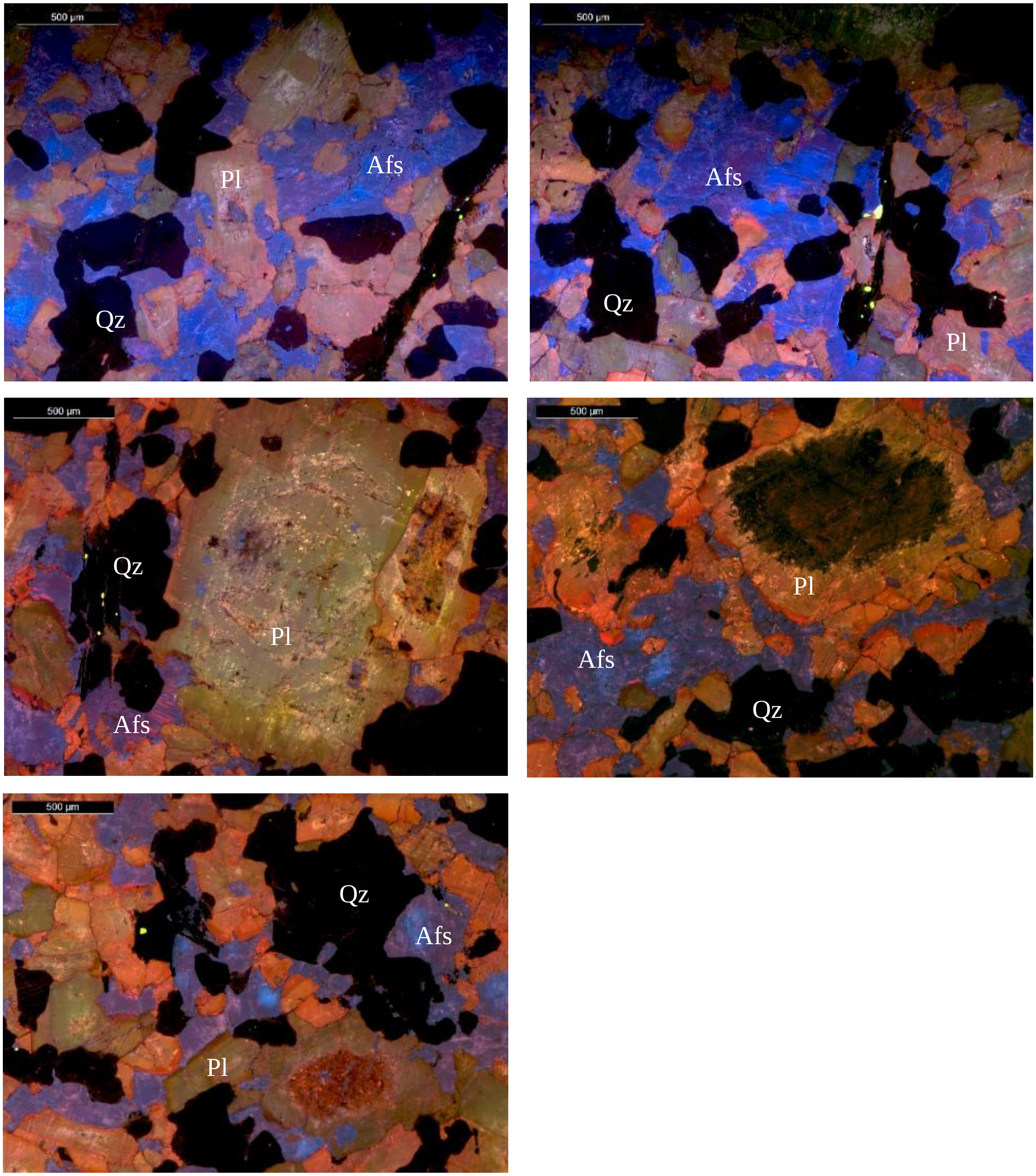

Mineral abbreviations taken from (Whitney and Evans, 2010). Moderate blue and red zoned alkali feldspar with pink to red albite exsolution (perhite). Brown and moderate green to orange plagioclase with some highly altered cores.

COMMENTS AND INTERPRETATION:

Based on the QAP ratio of 48.98:15.00:36.02 of the likely primary magmatic minerals, this rock is best classified as Biotite-bearing Granodiorite with secondary alteration to muscovite/sericite and chlorite. The fact that the alkali-feldspar and plagioclase from separate phenocrysts implies that the granite is a subsolvus granite.

The magmatic paragenetic sequence is likely (Plagioclase + microcline) > (Magnetite + Biotite) > (quartz) and then hydrothermal alteration to muscovite/sericite + chlorite.

Following the crystallization of the igneous minerals there are a series of subsolidus changes to the minerals. Post-crystallization deformation likely generated the quartz deformations features and allowed excess to aqueous fluids associated with alteration.

Granodiorite classification, moderate green plagioclase CL, and red zoned alkali feldspar suggests this sample was sourced by the Idaho batholith.

SAMPLE: SMC 14-112

Last update: 2/26/20

Petrographer: Kyle Tollefson

LOCATION: 44°08.294N, 115°00.355W
COLLECTOR:

DATE COLLECTED: July 26th 2014

AGE DATE:

ROCK TYPE: Biotite-bearing Syeno-Granite

MEGASCOPIC DESCRIPTION: Leucocratic, white, coarse-grained granitoid chiefly composed of microcline megacrysts in a plagioclase, and quartz mstrix.
==
MINERAL ASSEMBLAGES: (Point counted modes)

Plagioclase (9%) [0.1-5 mm] Anhedral to subhedral grains exhibiting albite twinning and minor seritization.

Microcline (48%) [0.25-15 mm] Anhedral to subhedral grains exhibiting tartan twinning, pervasive perthite, and minor seritization. Minor myrmekites of plagioclase-quartz develop at margins with plagioclase.

Quartz (40.7%) [0.01-5 mm] Anhedral to subhedral grains exhibiting moderate sweeping extinction.

Biotite (1.3%) [0.1-1.75 mm] Anhedral to subhedral laths exhibiting tan to light green pleochroism, birds eye extinction, and minor chloritization.

Sericite (1%) [0.2-2.25 mm] Subhedral to euhedral colorless laths exhibiting high birefringence.

Magnetite (tr%) [<0.3 mm] Anhedral to subhedral opaque grains exhibiting brownish-grey, isotropic, and a pitted nature in reflective light.

Clinozoisite (tr%) [<0.2 mm] Anhedral to subhedral colorless grains with moderate relief and lst order birefringence.

Chlorite (tr%) [0.05-0.75 mm] Subhedral green laths replacing biotite.
==

TEXTURES: Allotriomorphic dominated by microcline, plagioclase, quartz, and biotite, respectively. Microcline exhibits perthite texture. Microcline, plagioclase, and quartz exhibit myrmekitic texture.

ALTERATION: Minor metasomatic/hydrothermal alteration from biotite to chlorite and plagioclase to sericite/muscovite.

OPTICAL CATHODOLUMINESCENCE

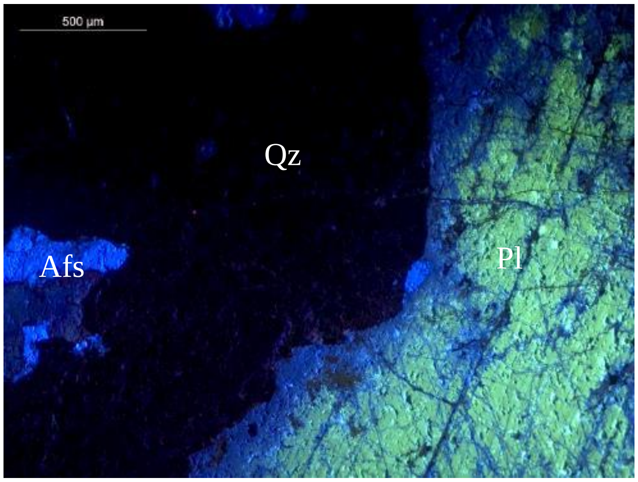

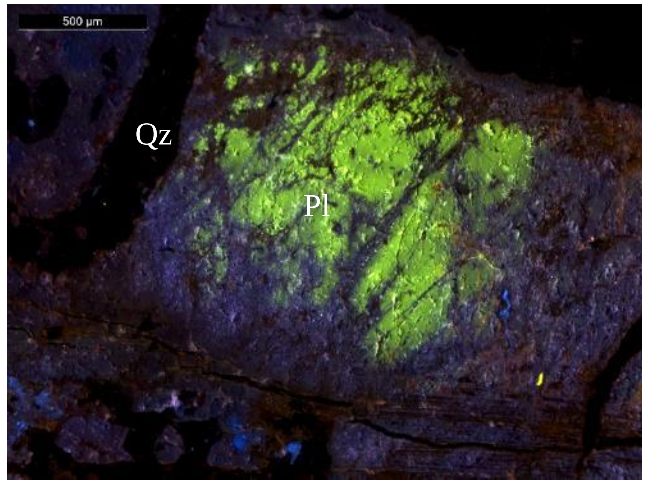

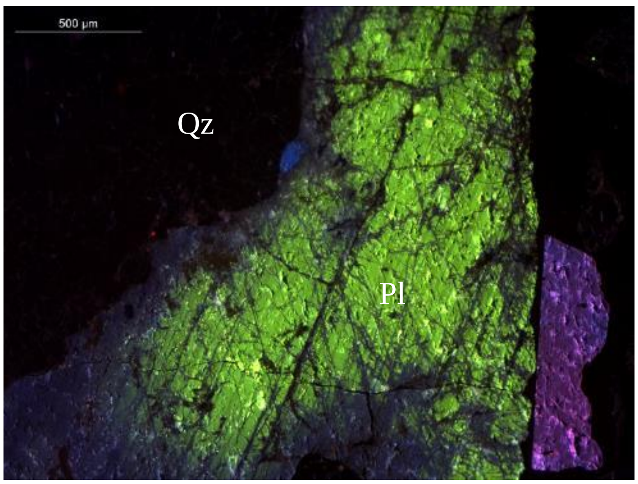

Mineral abbreviations taken from (Whitney and Evans, 2010). Bright blue alkali feldspar with moderate green plagioclase.

COMMENTS AND INTERPRETATION:

Based on the QAP ratio of 41.66:49.13:9.21 of the likely primary magmatic minerals, this rock is best classified as Biotite-bearing Syeno-Granite with secondary alteration to muscovite/sericite and chlorite. The fact that the alkali-feldspar and plagioclase from separate phenocrysts implies that the granite is a subsolvus granite.

The magmatic paragenetic sequence is (Microcline megacrysts) > (Plagioclase + Biotite) and then hydrothermal alteration to muscovite/sericite + chlorite.

Following the crystallization of the igneous minerals there are a series of subsolidus changes to the minerals. Post-crystallization deformation likely generated the quartz deformations features and allowed excess to aqueous fluids associated with alteration.

Syeno-Granite classification and pervasive perthitic microcline suggest this sample is likely sourced by the Sawtooth batholith.

SAMPLE: SMC 15-03

Last update: 2/26/20

Petrographer: Kyle Tollefson

LOCATION: 44°10.523N, 115°02.504W
COLLECTOR: Barbara Dutrow

DATE COLLECTED: July 2nd 2015

AGE DATE:

ROCK TYPE: Biotite-bearing Syeno-granite

MEGASCOPIC DESCRIPTION: Leucocratic, white, coarse-grained phaneritic granitoid chiefly composed of microcline, plagioclase, and quartz with minor biotite and muscovite.
===
MINERAL ASSEMBLAGES: (Point counted modes)

Plagioclase (9%) [0.2-4 mm] Anhedral grains exhibiting faint albite twinning and major seritization.

Microcline (59.7%) [0.2-13 mm] Anhedral grains exhibiting pervasive perthite and major seritization.

Quartz (31.3%) [0.05-3 mm] Anhedral grains exhibiting minor sweeping extinction. Recrystallized quartz.

Magnetite (tr%) [<0.1 mm] Anhedral to subhedral opaque grains exhibiting brownish-grey, isotropic, and a pitted nature in reflective light.

Biotite (tr%) [<0.05 mm] Subhedral laths exhibiting brown to green pleochroism, birds eye extinction, and major chloritization.

Chlorite (tr%) [0.01-0.05 mm] Subhedral green laths replacing biotite.

Zircon (tr%) [<0.1 mm] Euhedral colorless grains with high relief and high birefringence.
===

TEXTURES: Allotriomorphic coarse-grained texture dominated by microcline, plagioclase, quartz, and biotite, respectively. Microcline exhibits perthite texture. Recrystallization in the quartz indicates post-crystallization deformation.

ALTERATION: Pervasive metasomatic/hydrothermal alteration from biotite to chlorite and plagioclase to sericite/muscovite.

OPTICAL CATHODOLUMINESCENCE

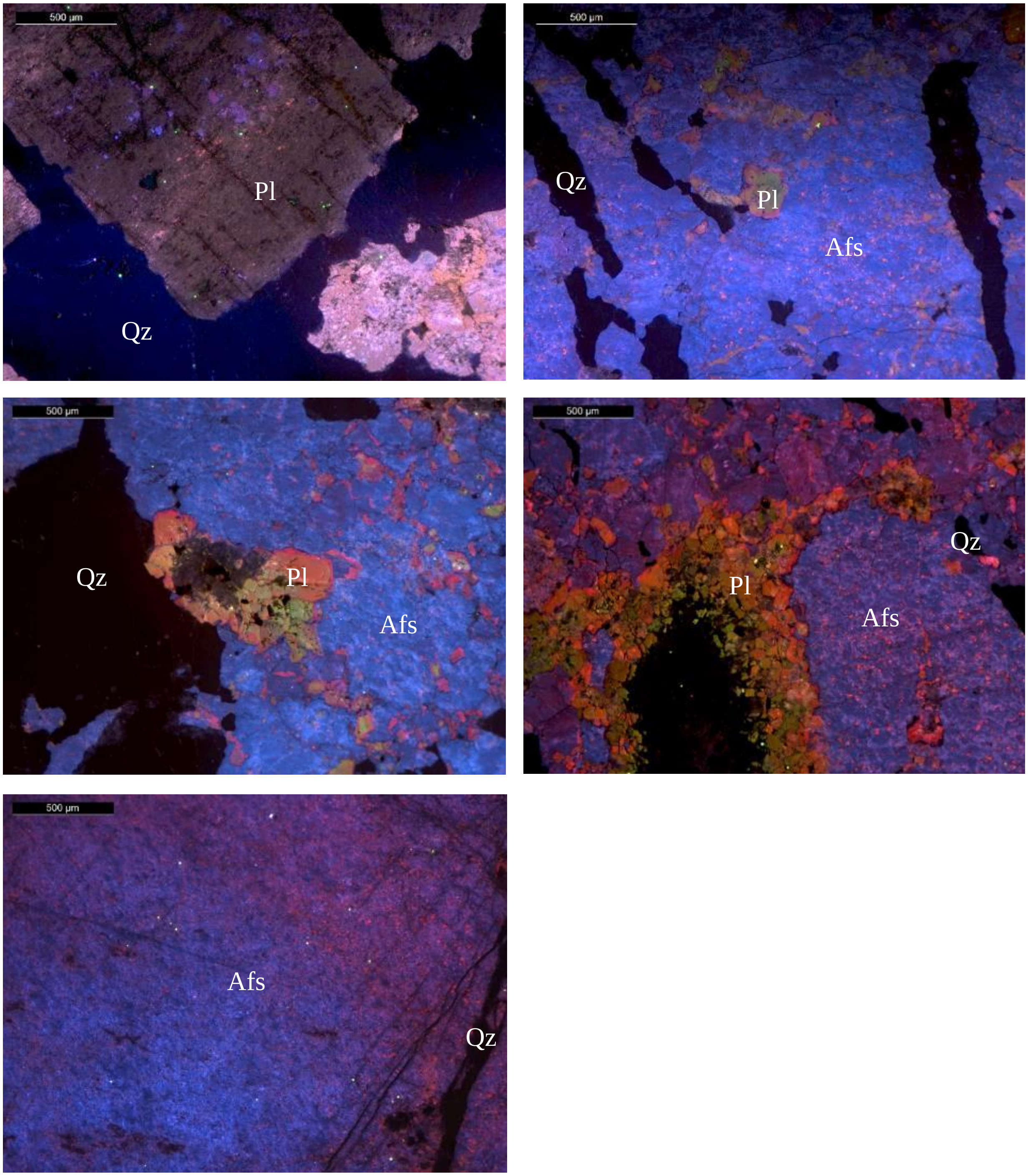

Mineral abbreviations taken from (Whitney and Evans, 2010). Bright to moderate blue alkali feldspar with pink albite exsolution (perthite). Brown, green, and orange plagioclase with highly altered cores.

COMMENTS AND INTERPRETATION:

Based on the the QAP ratio of 31.30:59.70:9.00 of the likely primary magmatic minerals, this rock is best classified as Biotite-bearing Syeno-granite with secondary alteration to muscovite/sericite and chlorite. The fact that the alkali-feldspar and plagioclase from separate phenocrysts implies that the granite is a subsolvus granite.

Following the crystallization of the igneous minerals there are a series of subsolidus changes to the minerals. Post-crystallization deformation likely generated the quartz deformations features and allowed excess to aqueous fluids associated with alteration.

Syeno-Granite classification, perthitic microcline, and orange plagioclase CL responses suggests this sample is likely sourced by the Sawtooth Batholith.

SAMPLE: SMC 15-05

Last update: 2/26/20

Petrographer: Kyle Tollefson

LOCATION: 44°10.323N, 115°14.715W
COLLECTOR: Barbara Dutrow

DATE COLLECTED: July 3rd 2015

AGE DATE:

ROCK TYPE: Biotite-bearing Granodiorite

MEGASCOPIC DESCRIPTION: Leucocratic, white, medium-grained phaneritic equigranular granitoid chiefly composed of microcline, plagioclase, and quartz with minor biotite.
==

MINERAL ASSEMBLAGES: (Point counted modes)

Plagioclase (40%) [0.1-4 mm] Anhedral to subhedral grains exhibiting albite twinning and moderate seritization.

Microcline (20%) [0.02-2 mm] Anhedral to subhedral grains exhibiting tartan twinning, minor perthite, and minor seritization. Minor myrmekites of plagioclase-quartz develop at margins with plagioclase.

Quartz (37.7%) [0.05-4.5 mm] Anhedral grains exhibiting minor sweeping extinction. Recrystallized quartz.

Biotite (1%) [0.1-1.5 mm] Anhedral to subhedral laths exhibiting brown to green pleochroism, birds eye extinction, and moderate chloritization.

Sericite (0.3%) [<0.3 mm] Anhedral to subhedral colorless laths exhibiting high birefringence.

Apatite (tr%) [<0.1 mm] Subhedral colorless grains with moderate relief and 1st order birefringence.

Magnetite (tr%) [<0.25 mm] Anhedral to subhedral opaque grains exhibiting brownish-grey, isotropic, and a pitted nature in reflective light.

Epidote (tr%) [<0.1 mm] Subhedral light green grains exhibiting moderate relief and high birefringence.

Clinozoisite (tr%) [<0.25 mm] Anhedral to subhedral colorless grains with moderate relief and lst order birefringence.

Allanite (tr%) [<0.2 mm] Euhedral light brown grains exhibiting high relief and 1st order birefringence.

Chlorite (tr%) [0.1 mm] Subhedral green laths replacing biotite.

Zircon (tr%) [<0.2 mm] Euhedral colorless grains with high relief and high birefringence.
==

TEXTURES: Allotriomorphic medium-grained texture dominated by microcline, plagioclase, quartz, and biotite, respectively. Microcline exhibits perthite texture. Microcline, plagioclase, and quartz exhibit myrmekitic texture. Recrystallization in the quartz indicates post-crystallization deformation.

ALTERATION: Moderate metasomatic/hydrothermal alteration from biotite to chlorite and plagioclase to sericite/muscovite.

OPTICAL CATHODOLUMINESCENCE

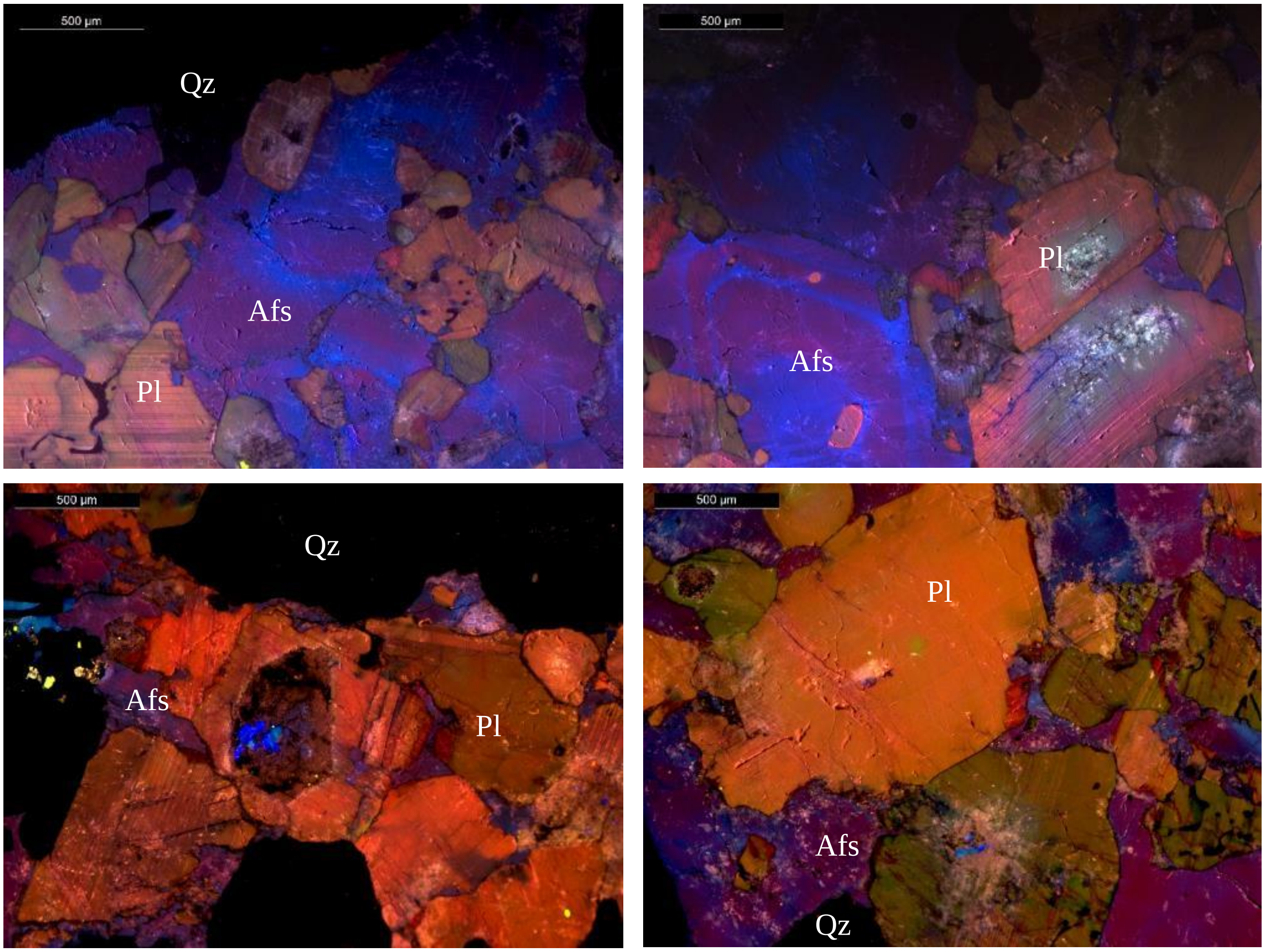

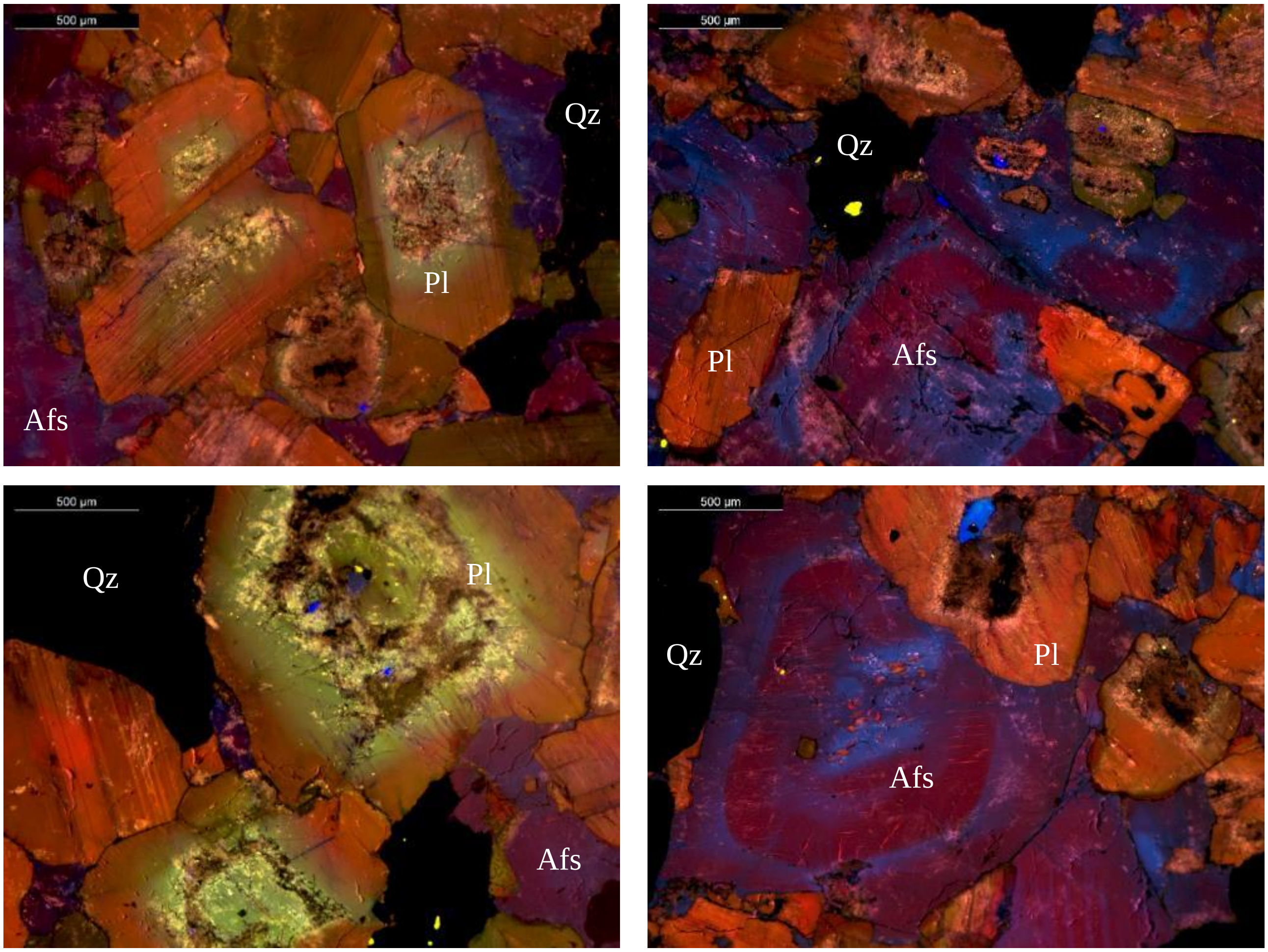

Mineral abbreviations taken from (Whitney and Evans, 2010). Bright to moderate blue alkali feldspar with red oscillatory zoning. Plagioclase is moderate green to orange. Myrmekitic texture observed.

COMMENTS AND INTERPRETATION:

Based on the QAP ratio of 38.59:20.47:40.9421 of the likely primary magmatic minerals, this rock is best classified as Biotite-bearing Granodiorite secondary alteration to muscovite/sericite and chlorite. The fact that the alkali-feldspar and plagioclase from separate phenocrysts implies that the granite is a subsolvus granite.

The magmatic paragenetic sequence is likely (Plagioclase) > (Microcline + Biotite) > (Quartz) and then hydrothermal alteration to muscovite/sericite + chlorite.

Following the crystallization of the igneous minerals there are a series of subsolidus changes to the minerals. Post-crystallization deformation likely generated the quartz deformations features and allowed excess to aqueous fluids associated with alteration.

Granodiorite classification, myrmekitic texture, moderate green plagioclase CL responses, and an age of 79.16 ± 1.18 Ma suggests this sample was most likely sourced by the Idaho batholith.

SAMPLE: SMC 16-09

Last update: 2/26/20

Petrographer: Kyle Tollefson

LOCATION: 44°08.927N, 114°59.599W

COLLECTOR: Barbara Dutrow

DATE COLLECTED:

AGE DATE: 86.5 ± 0.5 Ma

ROCK TYPE: Biotite-bearing monzo-granite

MEGASCOPIC DESCRIPTION: Leucocratic, white, coarse-grained granitoid chiefly composed of microcline megacrysts in a matrix of plagioclase and quartz with minor biotite.

==

MINERAL ASSEMBLAGES: (Point counted modes)

Plagioclase (24.3%) [0.1-2 mm] Anhedral to subhedral grains exhibiting albite twinning and moderate seritization.

Microcline (40.3%) [1-10 mm] Anhedral to subhedral grains exhibiting pervasive perthite and minor seritization.

Quartz (35%) [0.1-2 mm] Anhedral grains exhibiting major sweeping extinction and checkerboard extinction. Recrystallized quartz.

Biotite (tr%) [<1 mm] Subhedral laths exhibiting brown to green pleochroism, birds eye extinction, and major chloritization.

Chlorite (tr%) [0.2 mm] Subhedral green laths replacing biotite.

==

TEXTURES: Hypidiomorphic coarse-grained texture dominated by microcline, plagioclase, quartz, and biotite, respectively. Microcline exhibits perthitic texture. Recrystallization in the quartz indicates post-crystallization deformation.

ALTERATION: Moderate metasomatic/hydrothermal alteration from biotite to chlorite and plagioclase to sericite/muscovite.

OPTICAL CATHODOLUMINESCENCE

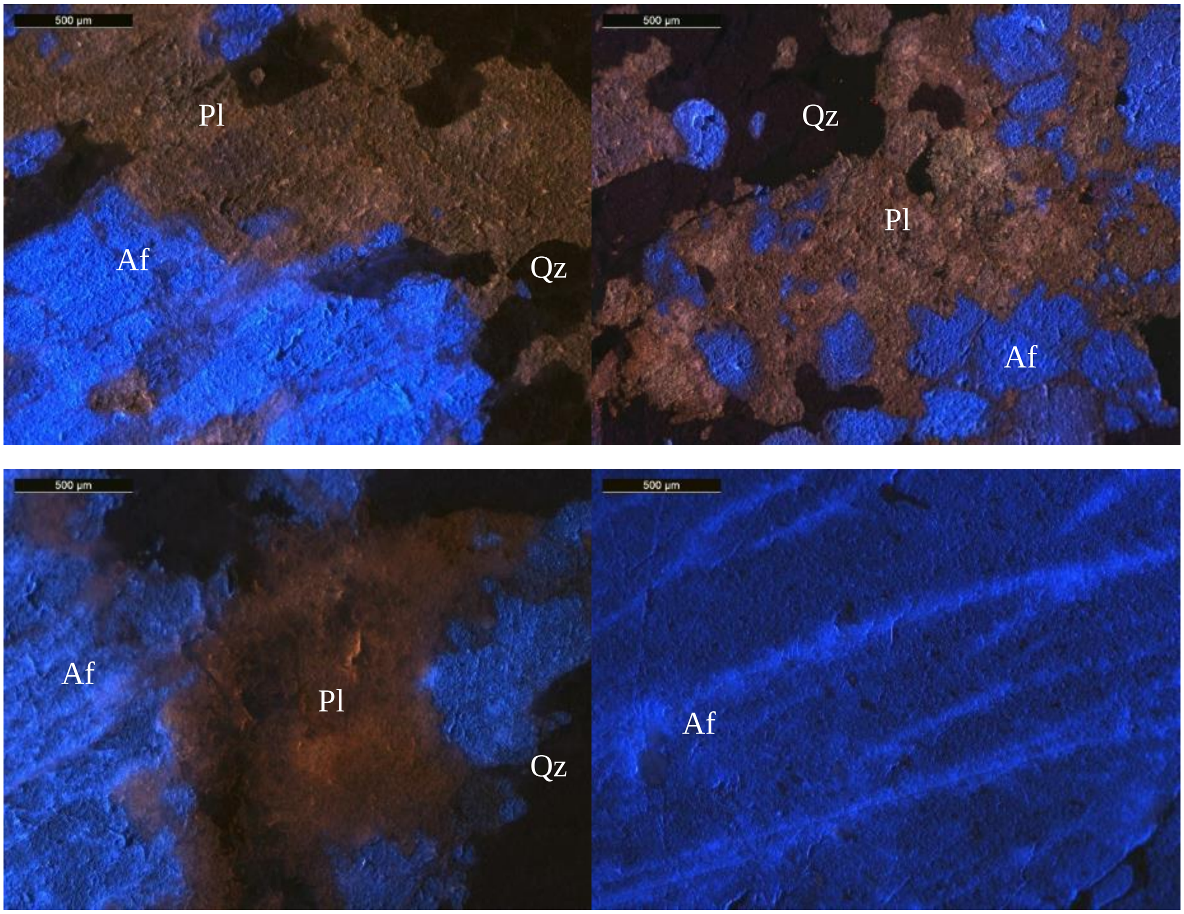

Mineral abbreviations taken from (Whitney and Evans, 2010). Bright to moderate blue alkali feldspar with brown plagioclase.

COMMENTS AND INTERPRETATION:

Based on the QAP ratio of 35.14, 40.46, 24.40 of the likely primary magmatic minerals, this rock is best classified as Biotite-bearing Monzo-granite with secondary alteration to muscovite/sericite and chlorite. The fact that the alkali-feldspar and plagioclase from separate phenocrysts implies that the granite is a subsolvus granite.

The magmatic paragenetic sequence is likely (microcline + plagioclase) > (biotite + quartz) and then hydrothermal alteration to muscovite/sericite + chlorite.

Following the crystallization of the igneous minerals there are a series of subsolidus changes to the minerals. Post-crystallization deformation likely generated the quartz deformations features and allowed excess to aqueous fluids associated with alteration.

An age date of 86.5 ± 0.5 Ma suggests this sample is likely sourced by the Idaho batholith.

SAMPLE: SMC 16-22

Last update: 2/26/20

Petrographer: Kyle Tollefson

LOCATION: 44°10.790N, 115°03.140W
COLLECTOR: Barbara Dutrow

DATE COLLECTED: July 8th 2016

AGE DATE:

ROCK TYPE: Granodiorite

MEGASCOPIC DESCRIPTION: Leucocratic, white, coarse-grained phaneritic granitoid chiefly composed of microcline, plagioclase, and quartz with minor hornblende.
==
MINERAL ASSEMBLAGES: (Point counted modes)

Plagioclase (45.3%) [0.2-7.5 mm] Anhedral to subhedral grains exhibiting albite twinning and moderate seritization.

Microcline (11.3%) [0.2-4 mm] Anhedral to subhedral grains exhibiting minor perthite and moderate seritization.

Quartz (38.7%) [0.05-4 mm] Anhedral grains exhibiting major sweeping extinction. Recrystallized quartz.

Sericite (0.7%) [0.1-1 mm] Subhedral colorless laths exhibiting high birefringence.

Hornblende (4%) [0.1-4 mm] Subhedral light green grains exhibiting high relief, moderate birefringence.

Apatite (tr%) [<0.1 mm] Subhedral to euhedral colorless grains with moderate relief and 1st order birefringence.

Allanite (tr%) [<0.1 mm] Subhedral to euhedral light brown grains exhibiting high relief and 1st order birefringence.

Magnetite (tr%) [<0.05 mm] Anhedral to subhedral opaque grains exhibiting brownish-grey, isotropic, and a pitted nature in reflective light.

Zircon (tr%) [<0.15 mm] Euhedral colorless grains with high relief and high birefringence.
==

TEXTURES: Allotriomorphic coarse-grained texture dominated by microcline, plagioclase, and quartz, respectively. Microcline exhibits minor perthite texture. Recrystallization in the quartz indicates post-crystallization deformation.

ALTERATION: Moderate metasomatic/hydrothermal alteration from plagioclase to sericite/muscovite.

OPTICAL CATHODOLUMINESCENCE

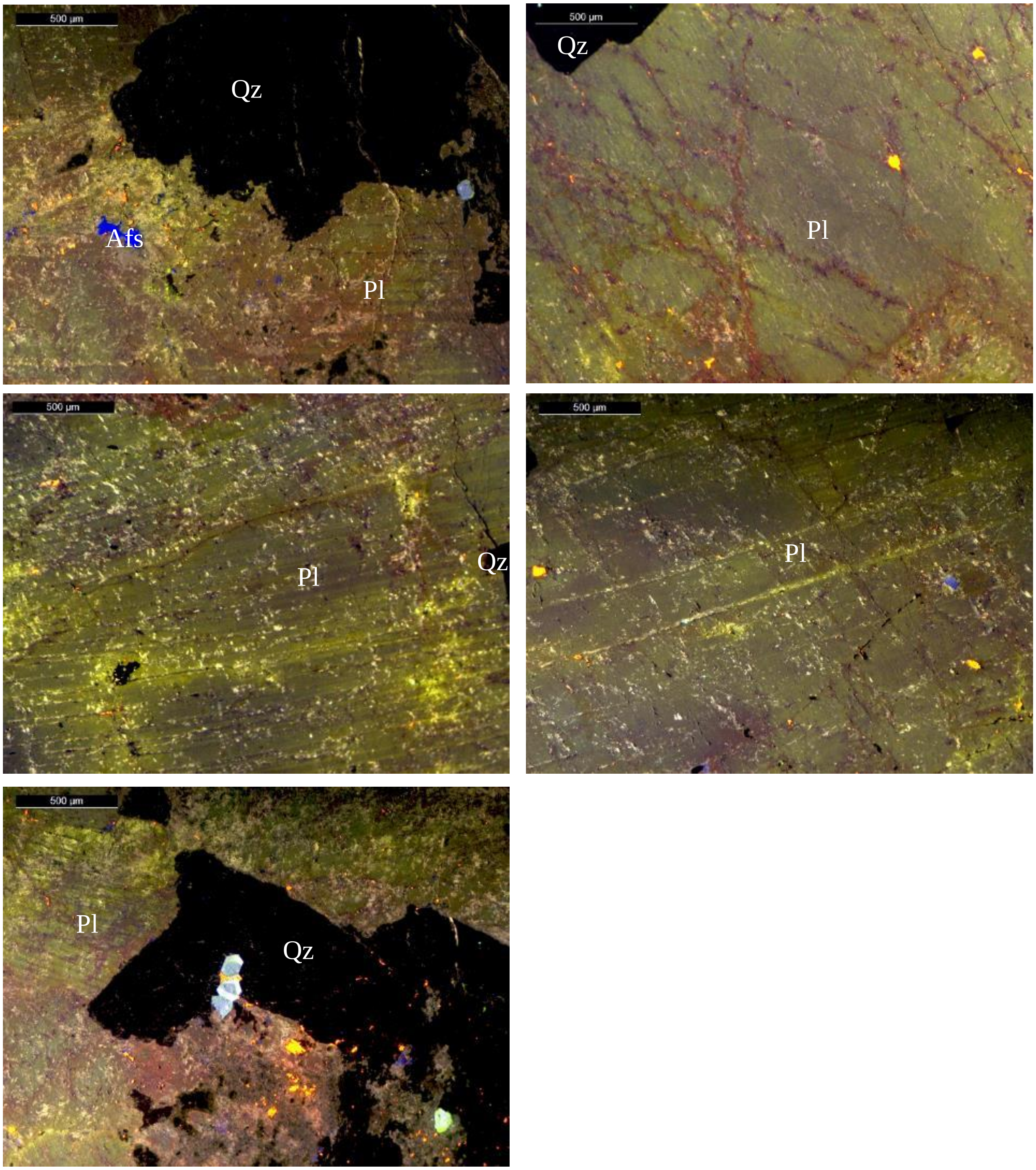

Mineral abbreviations taken from (Whitney and Evans, 2010). Dark blue alkali feldspar. Yellow plagioclase. Orange carbonates observed.

COMMENTS AND INTERPRETATION:

Based on the QAP ratio of 40.61:11.86:47.53 of the likely primary magmatic minerals, this rock is best classified as Granodiorite with secondary alteration to muscovite/sericite. The fact that the alkali-feldspar and plagioclase from separate phenocrysts implies that the granite is a subsolvus granite.

The magmatic paragenetic sequence is likely (Plagioclase) > (Microcline + quartz) > (Biotite + hornblende + opaques) and then hydrothermal alteration to muscovite/sericite + chlorite.

Following the crystallization of the igneous minerals there are a series of subsolidus changes to the minerals. Post-crystallization deformation likely generated the quartz deformations features and allowed excess to aqueous fluids associated with alteration.

Granodiorite classification and with an age date of 80.27 ± 0.64 Ma suggests this sample is likely sourced by the Idaho batholith.

SAMPLE: SMC 16-34

Last update: 2/26/20

Petrographer: Kyle Tollefson

LOCATION: 44°08.863N, 115°00.845W
COLLECTOR: Barbara Dutrow

DATE COLLECTED: July 14th 2016

AGE DATE:

ROCK TYPE: Biotite-bearing Granodiorite

MEGASCOPIC DESCRIPTION: Leucocratic, white, medium-grained phaneritic granitoid chiefly composed of microcline, plagioclase, and quartz with minor biotite.
===
MINERAL ASSEMBLAGES: (Point counted modes)

Plagioclase (34.7%) [0.5-4 mm] Anhedral to subhedral grains exhibiting albite twinning and major seritization of cores.

Microcline (12.7%) [0.1-0.5 mm] Anhedral to subhedral grains exhibiting tartan twinning, minor perthite, and minor seritization. Minor myrmekites of plagioclase-quartz develop at margins with plagioclase.

Quartz (52%) [0.01-5 mm] Anhedral grains exhibiting major sweeping extinction and checkerboard extinction. Recrystallized quartz.

Biotite (0.7%) [0.25-1 mm] Anhedral to subhedral laths exhibiting brown to green pleochroism, birds eye extinction, and major chloritization.

Apatite (tr%) [<0.1 mm] Subhedral to euhedral colorless grains with moderate relief and 1st order birefringence.

Magnetite (tr%) [0.1-1.25 mm] Subhedral opaque grains exhibiting brownish-grey, isotropic, and a pitted nature in reflective light.

Hematite (tr%) [< 0.3 mm] Anhedral opaque grains with red rims.

Chlorite (tr%) [0.01-1 mm] Subhedral green laths replacing biotite.

Zircon (tr%) [<0.2 mm] Euhedral colorless grains with high relief and high birefringence.
===

TEXTURES: Allotriomorphic medium-grained texture dominated by microcline, plagioclase, quartz, and biotite, respectively. Microcline, plagioclase, and quartz exhibit myrmekitic texture. Recrystallization in the quartz indicates post-crystallization deformation.

ALTERATION: Pervasive metasomatic/hydrothermal alteration from biotite to chlorite and plagioclase to sericite/muscovite.

OPTICAL CATHODOLUMINESCENCE

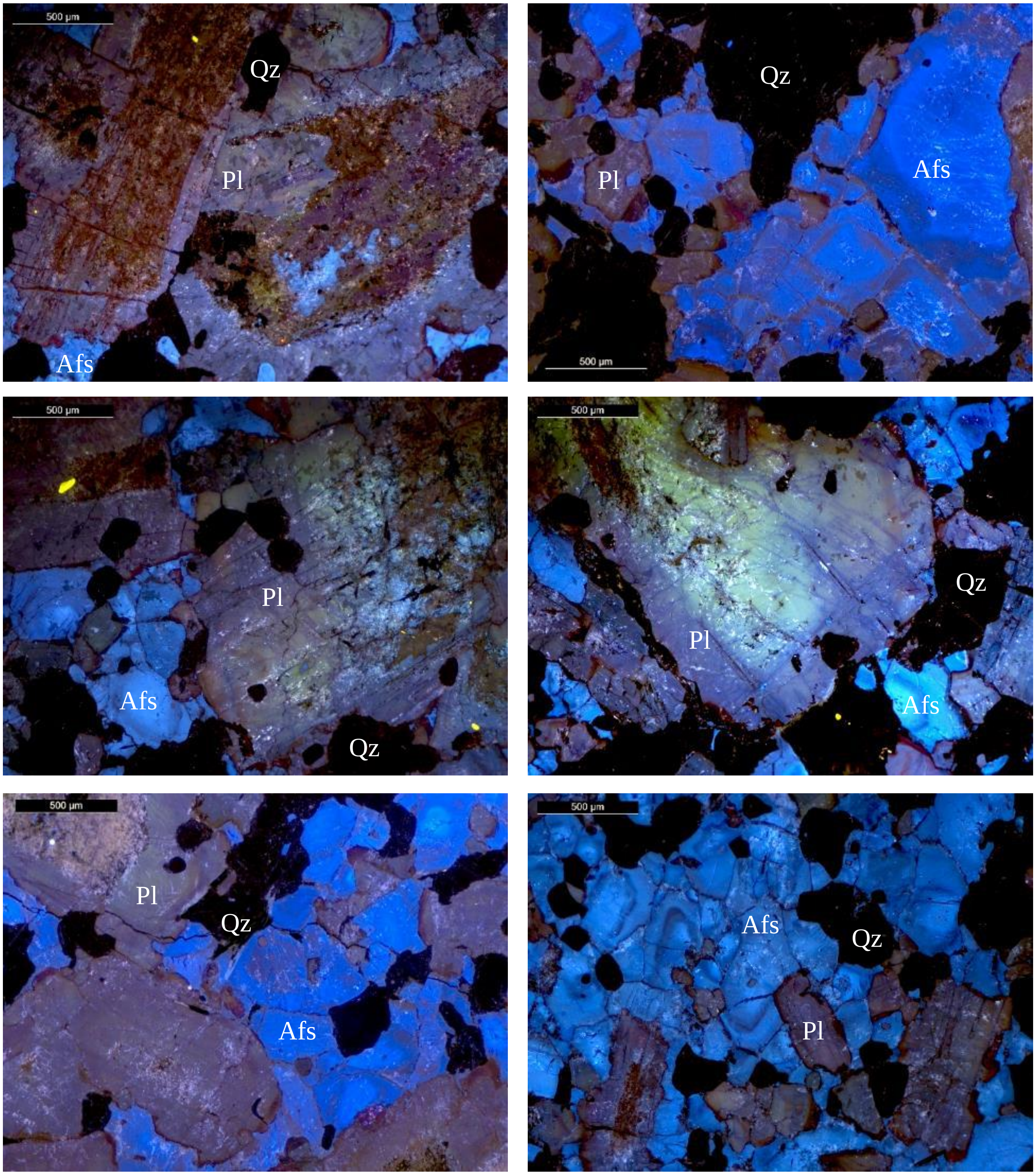

Mineral abbreviations taken from (Whitney and Evans, 2010). Dark to moderate blue alkali feldspar with oscillatory zoning indicated by red bands. Brown and moderate green plagioclase.

COMMENTS AND INTERPRETATION:

Based on the QAP ratio of 52.31:12.78:34.91 of the likely primary magmatic minerals, this rock is best classified as Biotite-bearing Granodiorite with secondary alteration to muscovite/sericite and chlorite. The fact that the alkali-feldspar and plagioclase from separate phenocrysts implies that the granite is a subsolvus granite.

The magmatic paragenetic sequence is likely (Plagioclase + Microcline) > (Biotite + quartz) and then hydrothermal alteration to muscovite/sericite + chlorite.

Following the crystallization of the igneous minerals there are a series of subsolidus changes to the minerals. Post-crystallization deformation likely generated the quartz deformations features and allowed excess to aqueous fluids associated with alteration.

Granodiorite classification, moderate green plagioclase CL, and red zoned alkali feldspar CL suggest this sample was likely sourced by the Idaho Batholith.

APPENDIX B. BSE IMAGES WITH EMPA ANALYSIS POINTS

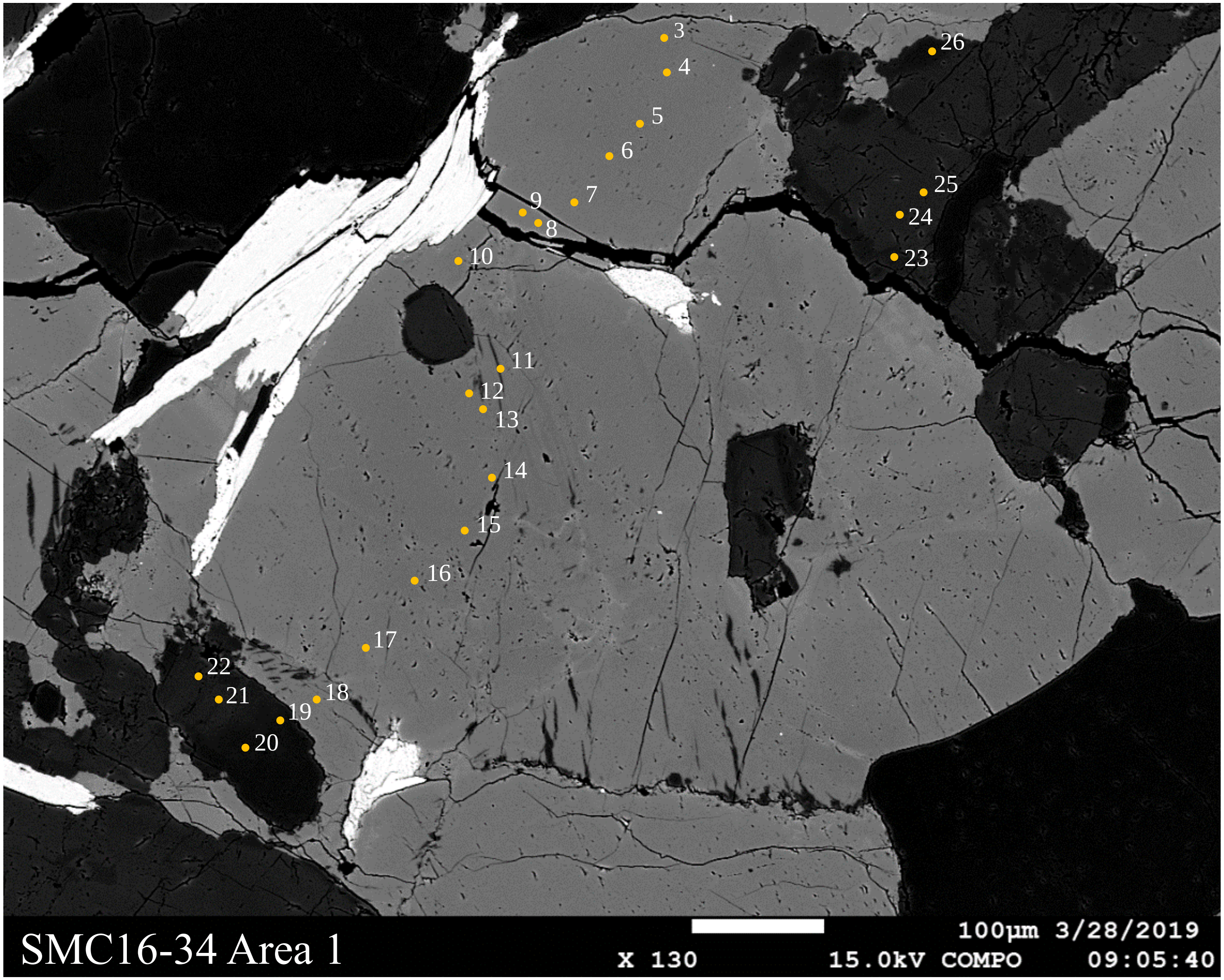

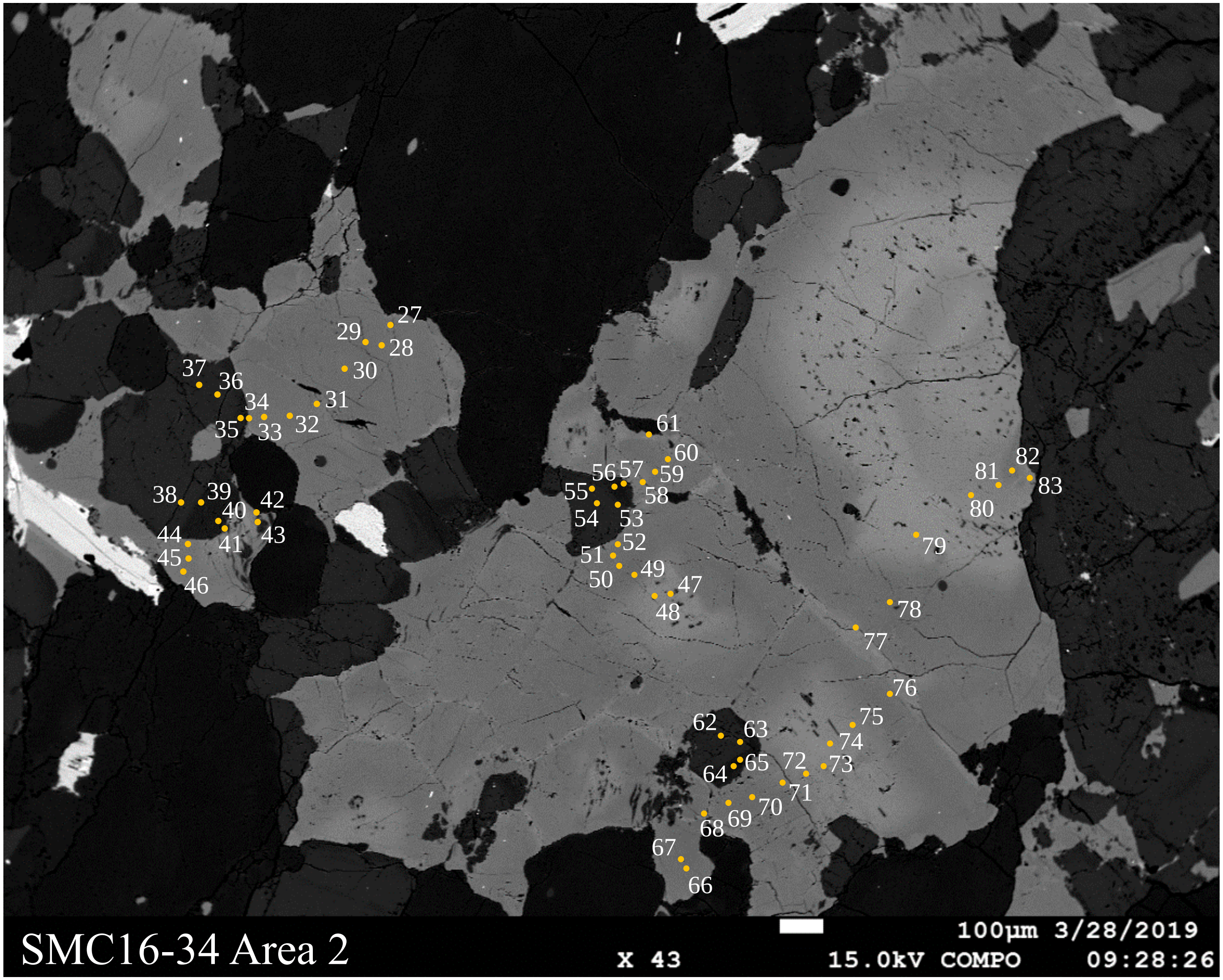
27
29
28
30
37
36
34
31
35
33
32
61
60
56
57
59
55
58
81
82
83
38
39
42
40
54
53
80
44
41
43
52
79
51
45
49
46
50
47
48
78
77
76
75
62
63
74
65
72
73
64
71
70
69
68
67
66
SMC16-34 Area 2
X 43
100µm 3/28/2019
15.0kV COMPO
09:28:26

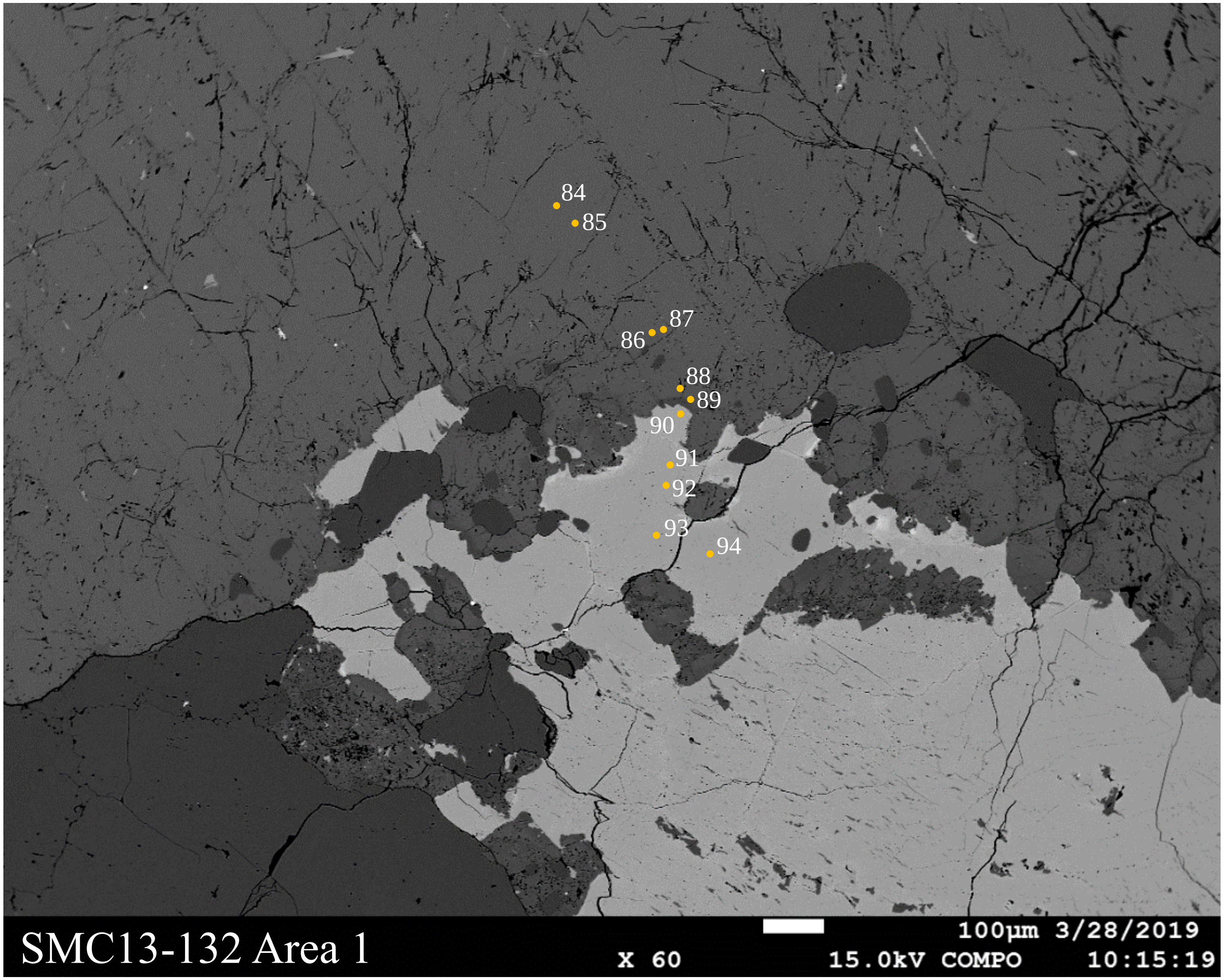
84
85
86
87
88
89
90
91
92
93
94
SMC13-132 Area 1
X 60
100µm 3/28/2019
15.0kV COMPO
10:15:19

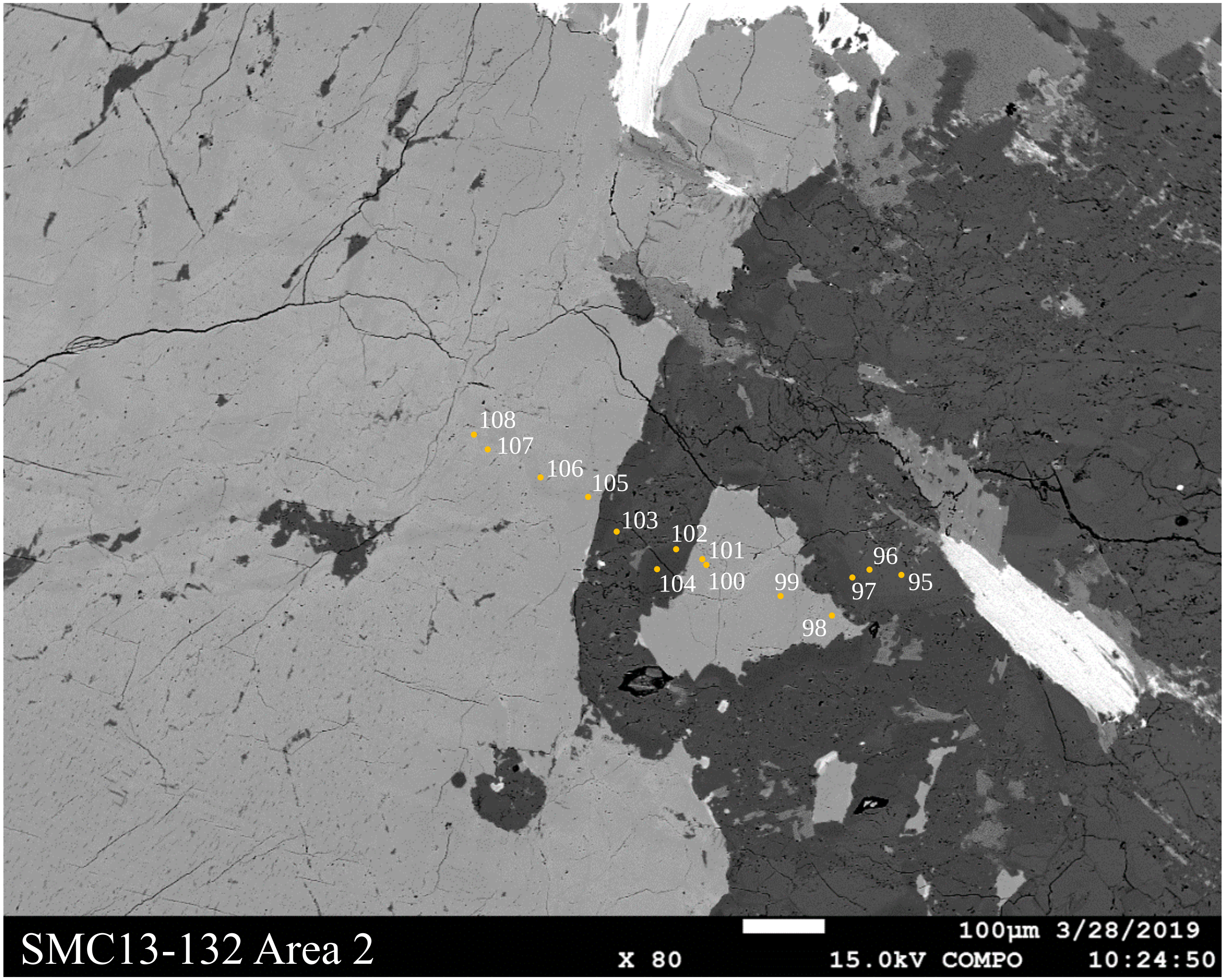
108
107
106
105
103
102
101
104
100
99
96
97
95
98
SMC13-132 Area 2
X 80
100µm 3/28/2019
15.0kV COMPO
10:24:50

APPENDIX C. EMPA DATA AND STOICHIOMETRIC CALCULATIONS

SMC16-34 Analysis pt. #	3	4	5	6	7	8
Comment	Kspar_001	Kspar_002	Kspar_003	Kspar_004	Kspar_005	Kspar_006
SiO2	64.73	65.076	64.858	65.178	65.078	65.039
Al2O3	18.53	18.503	18.447	18.507	18.587	18.72
Fe2O3						
FeO	0.007	0.004	0.03	0.026	0.054	0.097
MnO						
MgO						
CaO				0.004	0.011	0.002
BaO	0.527	0.502	0.524	0.57	0.747	0.776
SrO						
Na2O	0.831	0.861	0.877	0.885	0.967	0.891
K2O	16.049	16.006	15.895	15.893	15.861	15.738
Total	100.67	100.95	100.63	101.06	101.31	101.26
All Fe as FeO	0.01	0.00	0.03	0.03	0.05	0.10
All Fe as Fe2O3	0.01	0.00	0.03	0.03	0.06	0.11
Assumed FeO						
Assumed Fe2O3						
Si	2.155	2.166	2.159	2.170	2.166	2.165
Al	0.545	0.544	0.543	0.545	0.547	0.551
Fe3+						
Fe2+	0.000	0.000	0.000	0.000	0.001	0.001
Mn2+						
Mg						
Ca				0.000	0.000	0.000
Ba	0.003	0.003	0.003	0.004	0.005	0.005
Sr						
Na	0.013	0.014	0.014	0.014	0.016	0.014
K	0.170	0.170	0.169	0.169	0.168	0.167
Total	2.887	2.898	2.888	2.901	2.903	2.904
Factor (8 O2-)	2.771	2.761	2.770	2.757	2.756	2.755
Si	2.985	2.990	2.990	2.991	2.985	2.982
Al	1.007	1.002	1.002	1.001	1.005	1.012
Fe3+						
Fe2+	0.000	0.000	0.001	0.001	0.002	0.004
Mn						

Mg						
Ca				0.000	0.001	0.000
Ba	0.010	0.009	0.009	0.010	0.013	0.014
Sr						
Na	0.074	0.077	0.078	0.079	0.086	0.079
K	0.944	0.938	0.935	0.930	0.928	0.921

Analysis pt. #	3	4	5	6	7	8
Comment	Kspar_001	Kspar_002	Kspar_003	Kspar_004	Kspar_005	Kspar_006
SiO_2	64.73	65.08	64.86	65.18	65.08	65.04
Al_2O_3	18.53	18.50	18.45	18.51	18.59	18.72
Fe2O3						
FeO	0.01	0.00	0.03	0.03	0.05	0.10
MnO						
MgO						
CaO				0.00	0.01	0.00
BaO	0.53	0.50	0.52	0.57	0.75	0.78
SrO						
Na_2O	0.83	0.86	0.88	0.89	0.97	0.89
K_2O	16.05	16.01	15.90	15.89	15.86	15.74
Total	100.67	100.95	100.63	101.06	101.31	101.26

Structural formula based on 8 oxygens

T (iv) site: Si	2.985	2.990	2.990	2.991	2.985	2.982
Al	1.007	1.002	1.002	1.001	1.005	1.012
Fe^{3+}						
T site total	3.992	3.992	3.992	3.992	3.990	3.994

Fe3+						
Fe2+	0.000	0.000	0.001	0.001	0.002	0.004
Mn						
Mg						
Ca				0.000	0.001	0.000
Ba	0.010	0.009	0.009	0.010	0.013	0.014
Sr						
Na	0.074	0.077	0.078	0.079	0.086	0.079
K	0.944	0.938	0.935	0.930	0.928	0.921
M-site total	1.028	1.024	1.023	1.020	1.028	1.014

Main feldspar components	Kspar_001	Kspar_002	Kspar_003	Kspar_004	Kspar_005	Kspar_006
albite (mol%)	7.23	7.49	7.67	7.72	8.36	7.81
anorthite (mol%)				0.02	0.05	0.01
orthoclase (mol%)	91.85	91.63	91.41	91.25	90.28	90.80
celsian (mol%)	0.93	0.88	0.93	1.01	1.31	1.38
Barian species						

SMC16-34 Analysis pt. #	9	10	11	12	13	14
Comment	Kspar_007	Kspar_008	Kspar_009	Kspar_010	Kspar_011	Kspar_012
SiO2	64.671	65.343	64.98	65.191	65.12	65.311
Al2O3	18.127	18.661	18.67	18.674	18.523	18.514
Fe2O3						
FeO	0.196	0.213	0.037	0.032	0.023	
MnO						
MgO						
CaO			0.016	0.017		
BaO	0.768	0.712	0.665	0.554	0.546	0.427
SrO						
Na2O	0.899	0.791	0.85	1.137	1.045	0.944
K2O	15.978	15.993	16.021	15.559	15.673	15.775
Total	100.64	101.71	101.24	101.16	100.93	100.97
All Fe as FeO	0.20	0.21	0.04	0.03	0.02	
All Fe as Fe2O3	0.22	0.24	0.04	0.04	0.03	
Assumed FeO						
Assumed Fe2O3						

Si	2.153	2.175	2.163	2.170	2.168	2.174
Al	0.533	0.549	0.549	0.549	0.545	0.545
Fe3+						
Fe2+	0.003	0.003	0.001	0.000	0.000	
Mn2+						
Mg						
Ca			0.000	0.000		
Ba	0.005	0.005	0.004	0.004	0.004	0.003
Sr						
Na	0.015	0.013	0.014	0.018	0.017	0.015
K	0.170	0.170	0.170	0.165	0.166	0.167
Total	2.878	2.914	2.901	2.907	2.900	2.904
Factor (8 O2-)	2.780	2.745	2.757	2.752	2.759	2.755

Si	2.992	2.985	2.982	2.986	2.990	2.994

Al	0.988	1.005	1.010	1.008	1.002	1.000
Fe3+						
Fe2+	0.008	0.008	0.001	0.001	0.001	
Mn						
Mg						
Ca			0.001	0.001		
Ba	0.014	0.013	0.012	0.010	0.010	0.008
Sr						
Na	0.081	0.070	0.076	0.101	0.093	0.084
K	0.943	0.932	0.938	0.909	0.918	0.923

Comment	Kspar_007	Kspar_008	Kspar_009	Kspar_010	Kspar_011	Kspar_012
SiO_2	64.67	**65.34**	64.98	65.19	65.12	**65.31**
Al_2O_3	18.13	**18.66**	18.67	18.67	18.52	**18.51**
Fe2O3						
FeO	0.20	**0.21**	0.04	0.03	0.02	
MnO						
MgO						
CaO			0.02	0.02		
BaO	0.77	**0.71**	0.67	0.55	0.55	**0.43**
SrO						
Na_2O	0.90	**0.79**	0.85	1.14	1.05	**0.94**
K_2O	15.98	**15.99**	16.02	15.56	15.67	**15.78**
Total	100.64	**101.71**	101.24	101.16	100.93	**100.97**
T (iv) site: Si	2.992	**2.985**	2.982	2.986	2.990	**2.994**
Al	0.988	**1.005**	1.010	1.008	1.002	**1.000**
Fe^{3+}						
T site total	3.980	**3.990**	3.992	3.993	3.992	**3.995**
Fe3+						
Fe2+	0.008	**0.008**	0.001	0.001	0.001	
Mn						
Mg						
Ca			0.001	0.001		
Ba	0.014	**0.013**	0.012	0.010	0.010	**0.008**
Sr						
Na	0.081	**0.070**	0.076	0.101	0.093	**0.084**
K	0.943	**0.932**	0.938	0.909	0.918	**0.923**
M-site total	1.038	**1.015**	1.026	1.021	1.021	**1.014**

Main feldspar components	Kspar_007	Kspar_008	Kspar_009	Kspar_010	Kspar_011	Kspar_012
albite (mol%)	7.77	**6.90**	7.37	9.89	9.11	**8.27**
anorthite (mol%)			0.08	0.08		
orthoclase (mol%)	90.89	**91.84**	91.39	89.05	89.93	**90.97**
celsian (mol%)	1.34	**1.26**	1.17	0.97	0.96	**0.76**

Barian species

SMC16-34 Analysis pt. #	14	15	16	17	18	19
Comment	Kspar_012	Kspar_013	Kspar_014	Kspar_015	Kspar_016	Plag_001
SiO2	65.311	65.67	65.284	64.733	65.058	67.663
Al2O3	18.514	18.499	18.512	18.524	18.65	20.508
Fe2O3						
FeO		0.024	0.008	0.015	0.011	0.022
MnO						
MgO						
CaO			0.004	0.005		1.159
BaO	0.427	0.331	0.56	0.66	0.758	0.019
SrO						
Na2O	0.944	0.901	1.03	1.071	0.897	11.041
K2O	15.775	15.979	15.63	15.566	15.823	0.175
Total	100.97	101.40	101.03	100.57	101.20	100.59
All Fe as FeO		0.02	0.01	0.02	0.01	0.02
All Fe as Fe2O3		0.03	0.01	0.02	0.01	0.02
Assumed FeO						
Assumed Fe2O3						

Si	2.174	2.186	2.173	2.155	2.166	2.252
Al	0.545	0.544	0.545	0.545	0.549	0.603
Fe3+						
Fe2+		0.000	0.000	0.000	0.000	0.000
Mn2+						
Mg						
Ca			0.000	0.000		0.021
Ba	0.003	0.002	0.004	0.004	0.005	0.000
Sr						
Na	0.015	0.015	0.017	0.017	0.014	0.178
K	0.167	0.170	0.166	0.165	0.168	0.002
Total	2.904	2.917	2.904	2.887	2.902	3.057
Factor (8 O2-)	2.755	2.743	2.755	2.771	2.757	2.617

Si	2.994	2.998	2.993	2.986	2.985	2.947

Al	1.000	0.995	1.000	1.007	1.009	1.053
Fe3+						
Fe2+		0.001	0.000	0.001	0.000	0.001
Mn						
Mg						
Ca			0.000	0.000		0.054
Ba	0.008	0.006	0.010	0.012	0.014	0.000
Sr						
Na	0.084	0.080	0.092	0.096	0.080	0.932
K	0.923	0.930	0.914	0.916	0.926	0.010

Comment	Kspar_012	Kspar_013	Kspar_014	Kspar_015	Kspar_016	Plag_001
SiO_2	**65.31**	65.67	65.28	64.73	**65.06**	67.66
Al_2O_3	**18.51**	18.50	18.51	18.52	**18.65**	20.51
Fe2O3						
FeO		0.02	0.01	0.02	**0.01**	0.02
MnO						
MgO						
CaO			0.00	0.01		1.16
BaO	**0.43**	0.33	0.56	0.66	**0.76**	0.02
SrO						
Na_2O	**0.94**	0.90	1.03	1.07	**0.90**	11.04
K_2O	**15.78**	15.98	15.63	15.57	**15.82**	0.18
Total	**100.97**	101.40	101.03	100.57	**101.20**	100.59

T (iv) site: Si	**2.994**	2.998	2.993	2.986	**2.985**	2.947
Al	**1.000**	0.995	1.000	1.007	**1.009**	1.053
Fe^{3+}						
T site total	**3.995**	3.993	3.993	3.992	**3.994**	4.000

Fe3+						
Fe2+		0.001	0.000	0.001	**0.000**	0.001
Mn						
Mg						
Ca			0.000	0.000		0.054
Ba	**0.008**	0.006	0.010	0.012	**0.014**	0.000
Sr						
Na	**0.084**	0.080	0.092	0.096	**0.080**	0.932
K	**0.923**	0.930	0.914	0.916	**0.926**	0.010
M-site total	**1.014**	1.016	1.016	1.024	**1.020**	0.997

Main feldspar components	Kspar_012	Kspar_013	Kspar_014	Kspar_015	Kspar_016	Plag_001
albite (mol%)	**8.27**	7.85	9.01	9.35	**7.83**	93.56
anorthite (mol%)			0.02	0.02		5.43
orthoclase (mol%)	**90.97**	91.57	89.98	89.46	**90.84**	0.98
celsian (mol%)	**0.76**	0.58	0.99	1.17	**1.34**	0.03

Barian species

SMC16-34 Analysis pt. #	20	21	22	23	24	25
Comment	Plag_002	Plag_003	Plag_004	Plag_005	Plag_006	Plag_007
SiO2	67.889	66.043	66.049	65.62	65.545	65.478
Al2O3	20.241	21.651	21.617	21.785	22.012	22.083
Fe2O3						
FeO	0.03	0.043			0.008	0.007
MnO						
MgO						
CaO	0.918	2.475	2.485	2.773	2.89	2.826
BaO	0.025	0.026	0.018	0.037	0.012	0.003
SrO						
Na2O	11.203	10.363	10.345	10.108	10.109	10.169
K2O	0.142	0.144	0.159	0.166	0.134	0.145
Total	100.45	100.75	100.67	100.49	100.71	100.71
All Fe as FeO	0.03	0.04			0.01	0.01
All Fe as Fe2O3	0.03	0.05			0.01	0.01
Assumed FeO						
Assumed Fe2O3						

Si	2.260	2.198	2.199	2.184	2.182	2.180
Al	0.596	0.637	0.636	0.641	0.648	0.650
Fe3+						
Fe2+	0.000	0.001			0.000	0.000
Mn2+						
Mg						
Ca	0.016	0.044	0.044	0.049	0.052	0.050
Ba	0.000	0.000	0.000	0.000	0.000	0.000
Sr						
Na	0.181	0.167	0.167	0.163	0.163	0.164
K	0.002	0.002	0.002	0.002	0.001	0.002
Total	3.055	3.049	3.048	3.040	3.046	3.045
Factor (8 O2-)	2.619	2.624	2.625	2.632	2.627	2.627

Si	2.959	2.884	2.886	2.874	2.865	2.863

Al	1.040	1.114	1.113	1.125	1.134	1.138
Fe3+						
Fe2+	0.001	0.002			0.000	0.000
Mn						
Mg						
Ca	0.043	0.116	0.116	0.130	0.135	0.132
Ba	0.000	0.000	0.000	0.001	0.000	0.000
Sr						
Na	0.947	0.877	0.876	0.858	0.857	0.862
K	0.008	0.008	0.009	0.009	0.007	0.008

Comment	Plag_002	Plag_003	Plag_004	Plag_005	Plag_006	Plag_007
SiO_2	67.89	66.04	**66.05**	65.62	65.55	65.48
Al_2O_3	20.24	21.65	**21.62**	21.79	22.01	22.08
Fe2O3						
FeO	0.03	0.04			0.01	0.01
MnO						
MgO						
CaO	0.92	2.48	**2.49**	2.77	2.89	2.83
BaO	0.03	0.03	**0.02**	0.04	0.01	0.00
SrO						
Na_2O	11.20	10.36	**10.35**	10.11	10.11	10.17
K_2O	0.14	0.14	**0.16**	0.17	0.13	0.15
Total	100.45	100.75	**100.67**	100.49	100.71	100.71

T (iv) site: Si	2.959	2.884	**2.886**	2.874	2.865	2.863
Al	1.040	1.114	**1.113**	1.125	1.134	1.138
Fe^{3+}						
T site total	3.999	3.998	**3.999**	3.999	4.000	4.001

Fe3+						
Fe2+	0.001	0.002			0.000	0.000
Mn						
Mg						
Ca	0.043	0.116	**0.116**	0.130	0.135	0.132
Ba	0.000	0.000	**0.000**	0.001	0.000	0.000
Sr						
Na	0.947	0.877	**0.876**	0.858	0.857	0.862
K	0.008	0.008	**0.009**	0.009	0.007	0.008
M-site total	0.998	1.002	**1.002**	0.998	1.000	1.003

Main feldspar components	Plag_002	Plag_003	Plag_004	Plag_005	Plag_006	Plag_007
albite (mol%)	94.87	87.59	**87.47**	85.97	85.69	85.98
anorthite (mol%)	4.30	11.56	**11.61**	13.03	13.54	13.20
orthoclase (mol%)	0.79	0.80	**0.88**	0.93	0.75	0.81
celsian (mol%)	0.04	0.04	**0.03**	0.06	0.02	0.01

Barian species

SMC16-34 Analysis pt. #	26	27	28	29	30	31
Comment	Plag_008	Kspar_001	Kspar_002	Kspar_003	Kspar_004	Kspar_005
SiO2	68.35	63.155	63.101	63.14	63.014	63.11
Al2O3	20.073	18.52	18.548	18.638	18.718	18.739
Fe2O3						
FeO	0.023			0.009	0.013	0.025
MnO						
MgO						
CaO	0.705	0.006		0.029	0.021	
BaO	0.022	0.736	0.611	0.648	0.573	0.765
SrO						
Na2O	11.489	0.764	0.684	0.815	0.807	0.763
K2O	0.201	15.351	15.574	15.425	15.27	15.373
Total	100.86	98.53	98.52	98.70	98.42	98.78
All Fe as FeO	0.02			0.01	0.01	0.03
All Fe as Fe2O3	0.03			0.01	0.01	0.03
Assumed FeO						
Assumed Fe2O3						

Si	2.275	2.102	2.100	2.102	2.098	2.101
Al	0.591	0.545	0.546	0.548	0.551	0.551
Fe3+						
Fe2+	0.000			0.000	0.000	0.000
Mn2+						
Mg						
Ca	0.013	0.000		0.001	0.000	
Ba	0.000	0.005	0.004	0.004	0.004	0.005
Sr						
Na	0.185	0.012	0.011	0.013	0.013	0.012
K	0.002	0.163	0.165	0.164	0.162	0.163
Total	3.066	2.827	2.827	2.832	2.828	2.833
Factor (8 O2-)	2.609	2.829	2.830	2.825	2.829	2.824

Si	2.968	2.974	2.972	2.969	2.967	2.966

Al	1.027	1.028	1.030	1.033	1.039	1.038
Fe3+						
Fe2+	0.001			0.000	0.001	0.001
Mn						
Mg						
Ca	0.033	0.000		0.001	0.001	
Ba	0.000	0.014	0.011	0.012	0.011	0.014
Sr						
Na	0.967	0.070	0.062	0.074	0.074	0.070
K	0.011	0.922	0.936	0.925	0.917	0.922

Comment	Plag_008	Kspar_001	Kspar_002	Kspar_003	Kspar_004	Kspar_005
SiO_2	**68.35**	63.16	63.10	63.14	63.01	**63.11**
Al_2O_3	**20.07**	18.52	18.55	18.64	18.72	**18.74**
Fe2O3						
FeO	**0.02**			0.01	0.01	**0.03**
MnO						
MgO						
CaO	**0.71**	0.01		0.03	0.02	
BaO	**0.02**	0.74	0.61	0.65	0.57	**0.77**
SrO						
Na_2O	**11.49**	0.76	0.68	0.82	0.81	**0.76**
K_2O	**0.20**	15.35	15.57	15.43	15.27	**15.37**
Total	**100.86**	98.53	98.52	98.70	98.42	**98.78**

T (iv) site: Si	**2.968**	2.974	2.972	2.969	2.967	**2.966**
Al	**1.027**	1.028	1.030	1.033	1.039	**1.038**
Fe^{3+}						
T site total	**3.995**	4.002	4.002	4.001	4.006	**4.004**

Fe3+						
Fe2+	**0.001**			0.000	0.001	**0.001**
Mn						
Mg						
Ca	**0.033**	0.000		0.001	0.001	
Ba	**0.000**	0.014	0.011	0.012	0.011	**0.014**
Sr						
Na	**0.967**	0.070	0.062	0.074	0.074	**0.070**
K	**0.011**	0.922	0.936	0.925	0.917	**0.922**
M-site total	**1.012**	1.006	1.010	1.013	1.003	**1.005**

Main feldspar components	Plag_008	Kspar_001	Kspar_002	Kspar_003	Kspar_004	Kspar_005
albite (mol%)	**95.62**	6.93	6.19	7.33	7.35	**6.92**
anorthite (mol%)	**3.24**	0.03		0.14	0.11	
orthoclase (mol%)	**1.10**	91.68	92.70	91.34	91.49	**91.68**
celsian (mol%)	**0.04**	1.35	1.12	1.18	1.05	**1.40**

Barian species

SMC16-34 Analysis pt. #	32	33	34	35	36	37
Comment	Kspar_006	Kspar_007	Plag_001	Plag_002	Plag_003	Plag_004
SiO2	63.294	63.254	63.929	63.843	65.923	65.811
Al2O3	18.814	18.816	22.013	22.113	21.752	22.036
Fe2O3						
FeO	0.025	0.019	0.026	0.013	0.009	0.007
MnO						
MgO						
CaO			2.786	2.861	2.611	2.739
BaO	0.738	0.784		0.021		0.037
SrO						
Na2O	0.845	0.764	10.058	10.147	10.069	10.231
K2O	15.32	15.323	0.119	0.116	0.182	0.125
Total	99.04	98.96	98.93	99.11	100.55	100.99
All Fe as FeO	0.03	0.02	0.03	0.01	0.01	0.01
All Fe as Fe2O3	0.03	0.02	0.03	0.01	0.01	0.01
Assumed FeO						
Assumed Fe2O3						

Si	2.107	2.106	2.128	2.125	2.194	2.191
Al	0.554	0.554	0.648	0.651	0.640	0.648
Fe3+						
Fe2+	0.000	0.000	0.000	0.000	0.000	0.000
Mn2+						
Mg						
Ca			0.050	0.051	0.047	0.049
Ba	0.005	0.005		0.000		0.000
Sr						
Na	0.014	0.012	0.162	0.164	0.162	0.165
K	0.163	0.163	0.001	0.001	0.002	0.001
Total	2.842	2.840	2.989	2.992	3.045	3.055
Factor (8 O2-)	2.815	2.817	2.676	2.674	2.627	2.619

Si	2.965	2.966	2.848	2.841	2.882	2.869

Al	1.039	1.040	1.156	1.160	1.121	1.132
Fe3+						
Fe2+	0.001	0.001	0.001	0.000	0.000	0.000
Mn						
Mg						
Ca			0.133	0.136	0.122	0.128
Ba	0.014	0.014		0.000		0.001
Sr						
Na	0.077	0.069	0.869	0.875	0.854	0.865
K	0.916	0.917	0.007	0.007	0.010	0.007

Comment	Kspar_006	Kspar_007	Plag_001	Plag_002	Plag_003	Plag_004
SiO_2	63.29	63.25	63.93	63.84	65.92	65.81
Al_2O_3	18.81	18.82	22.01	22.11	21.75	22.04
Fe2O3						
FeO	0.03	0.02	0.03	0.01	0.01	0.01
MnO						
MgO						
CaO			2.79	2.86	2.61	2.74
BaO	0.74	0.78		0.02		0.04
SrO						
Na_2O	0.85	0.76	10.06	10.15	10.07	10.23
K_2O	15.32	15.32	0.12	0.12	0.18	0.13
Total	99.04	98.96	98.93	99.11	100.55	100.99

T (iv) site: Si	2.965	2.966	2.848	2.841	2.882	2.869
Al	1.039	1.040	1.156	1.160	1.121	1.132
Fe^{3+}						
T site total	4.004	4.006	4.003	4.001	4.003	4.001

Fe3+						
Fe2+	0.001	0.001	0.001	0.000	0.000	0.000
Mn						
Mg						
Ca			0.133	0.136	0.122	0.128
Ba	0.014	0.014		0.000		0.001
Sr						
Na	0.077	0.069	0.869	0.875	0.854	0.865
K	0.916	0.917	0.007	0.007	0.010	0.007
M-site total	1.006	1.000	1.008	1.019	0.986	1.000

Main feldspar components	Kspar_006	Kspar_007	Plag_001	Plag_002	Plag_003	Plag_004
albite (mol%)	7.63	6.94	86.14	85.93	86.57	86.45
anorthite (mol%)			13.19	13.39	12.40	12.79
orthoclase (mol%)	91.02	91.62	0.67	0.65	1.03	0.69
celsian (mol%)	1.35	1.44		0.04		0.06

Barian species

SMC16-34 Analysis pt. #	38	39	40	41	42	43
Comment	Plag_005	Plag_006	Plag_007	Plag_008	Kspar_008	Kspar_009
SiO2	65.845	66.114	66.218	67.21	62.46	62.342
Al2O3	22.16	22.013	20.409	20.705	18.991	19.101
Fe2O3						
FeO	0.007	0.01	0.007		0.029	
MnO						
MgO						
CaO	2.831	2.727	0.838	0.863	0.013	0.011
BaO	0.02	0.007			1.51	1.739
SrO						
Na2O	10.117	10.243	11.467	11.035	0.948	0.891
K2O	0.155	0.17	0.193	0.201	14.712	14.729
Total	101.14	101.28	99.13	100.01	98.66	98.81
All Fe as FeO	0.01	0.01	0.01		0.03	
All Fe as Fe2O3	0.01	0.01	0.01		0.03	
Assumed FeO						
Assumed Fe2O3						

Si	2.192	2.201	2.204	2.237	2.079	2.075
Al	0.652	0.648	0.600	0.609	0.559	0.562
Fe3+						
Fe2+	0.000	0.000	0.000		0.000	
Mn2+						
Mg						
Ca	0.050	0.049	0.015	0.015	0.000	0.000
Ba	0.000	0.000			0.010	0.011
Sr						
Na	0.163	0.165	0.185	0.178	0.015	0.014
K	0.002	0.002	0.002	0.002	0.156	0.156
Total	3.059	3.064	3.007	3.042	2.820	2.819
Factor (8 O2-)	2.615	2.611	2.661	2.630	2.837	2.837

Si	2.866	2.873	2.932	2.942	2.949	2.944

Al	1.137	1.127	1.065	1.068	1.057	1.063
Fe3+						
Fe2+	0.000	0.000	0.000		0.001	
Mn						
Mg						
Ca	0.132	0.127	0.040	0.040	0.001	0.001
Ba	0.000	0.000			0.028	0.032
Sr						
Na	0.854	0.863	0.985	0.936	0.087	0.082
K	0.009	0.009	0.011	0.011	0.886	0.887

Comment	Plag_005	Plag_006	Plag_007	Plag_008	Kspar_008	Kspar_009
SiO_2	**65.85**	**66.11**	**66.22**	**67.21**	**62.46**	**62.34**
Al_2O_3	**22.16**	**22.01**	**20.41**	**20.71**	**18.99**	**19.10**
Fe2O3						
FeO	**0.01**	**0.01**	**0.01**		**0.03**	
MnO						
MgO						
CaO	**2.83**	**2.73**	**0.84**	**0.86**	**0.01**	**0.01**
BaO	**0.02**	**0.01**			**1.51**	**1.74**
SrO						
Na_2O	**10.12**	**10.24**	**11.47**	**11.04**	**0.95**	**0.89**
K_2O	**0.16**	**0.17**	**0.19**	**0.20**	**14.71**	**14.73**
Total	**101.14**	**101.28**	**99.13**	**100.01**	**98.66**	**98.81**

T (iv) site: Si	**2.866**	**2.873**	**2.932**	**2.942**	**2.949**	**2.944**
Al	**1.137**	**1.127**	**1.065**	**1.068**	**1.057**	**1.063**
Fe^{3+}						
T site total	**4.002**	**4.000**	**3.997**	**4.010**	**4.006**	**4.007**

Fe3+						
Fe2+	**0.000**	**0.000**	**0.000**		**0.001**	
Mn						
Mg						
Ca	**0.132**	**0.127**	**0.040**	**0.040**	**0.001**	**0.001**
Ba	**0.000**	**0.000**			**0.028**	**0.032**
Sr						
Na	**0.854**	**0.863**	**0.985**	**0.936**	**0.087**	**0.082**
K	**0.009**	**0.009**	**0.011**	**0.011**	**0.886**	**0.887**
M-site total	**0.995**	**0.999**	**1.035**	**0.988**	**1.002**	**1.002**

Main feldspar components	Plag_005	Plag_006	Plag_007	Plag_008	Kspar_008	Kspar_009
albite (mol%)	85.83	86.34	95.11	94.77	8.67	8.14
anorthite (mol%)	13.27	12.70	3.84	4.10	0.07	0.06
orthoclase (mol%)	0.87	0.94	1.05	1.14	88.48	88.59
celsian (mol%)	0.03	0.01			2.79	3.21

Barian species

SMC16-34 Analysis pt. #	44	45	46	47	48	49
Comment	Kspar_010	Kspar_011	Kspar_012	Kspar_001	Kspar_002	Kspar_003
SiO2	63.561	63.128	63.346	62.012	62.799	63.501
Al2O3	18.958	18.786	18.875	19.15	19.058	18.686
Fe2O3						
FeO	0.036	0.036	0.004	0.01	0.01	0.003
MnO						
MgO						
CaO	0.003	0.009	0.009	0.024	0.022	
BaO	0.65	0.68	0.757	1.816	1.329	0.508
SrO						
Na2O	0.995	0.976	0.95	0.776	0.836	0.92
K2O	15.084	15.146	14.985	14.856	14.903	15.36
Total	99.29	98.76	98.93	98.64	98.96	98.98
All Fe as FeO	0.04	0.04	0.00	0.01	0.01	0.00
All Fe as Fe2O3	0.04	0.04	0.00	0.01	0.01	0.00
Assumed FeO						
Assumed Fe2O3						

Si	2.116	2.101	2.109	2.064	2.090	2.114
Al	0.558	0.553	0.555	0.563	0.561	0.550
Fe3+						
Fe2+	0.001	0.001	0.000	0.000	0.000	0.000
Mn2+						
Mg						
Ca	0.000	0.000	0.000	0.000	0.000	
Ba	0.004	0.004	0.005	0.012	0.009	0.003
Sr						
Na	0.016	0.016	0.015	0.013	0.013	0.015
K	0.160	0.161	0.159	0.158	0.158	0.163
Total	2.855	2.836	2.844	2.810	2.832	2.845
Factor (8 O2-)	2.803	2.821	2.813	2.847	2.825	2.812

Si	2.965	2.964	2.966	2.938	2.952	2.972

Al	1.042	1.040	1.042	1.069	1.056	1.031
Fe3+						
Fe2+	0.001	0.001	0.000	0.000	0.000	0.000
Mn						
Mg						
Ca	0.000	0.000	0.000	0.001	0.001	
Ba	0.012	0.013	0.014	0.034	0.024	0.009
Sr						
Na	0.090	0.089	0.086	0.071	0.076	0.083
K	0.898	0.907	0.895	0.898	0.894	0.917

Comment	Kspar_010	Kspar_011	Kspar_012	Kspar_001	Kspar_002	Kspar_003
SiO_2	**63.56**	**63.13**	**63.35**	**62.01**	**62.80**	**63.50**
Al_2O_3	**18.96**	**18.79**	**18.88**	**19.15**	**19.06**	**18.69**
Fe2O3						
FeO	**0.04**	**0.04**	**0.00**	**0.01**	**0.01**	**0.00**
MnO						
MgO						
CaO	**0.00**	**0.01**	**0.01**	**0.02**	**0.02**	
BaO	**0.65**	**0.68**	**0.76**	**1.82**	**1.33**	**0.51**
SrO						
Na_2O	**1.00**	**0.98**	**0.95**	**0.78**	**0.84**	**0.92**
K_2O	**15.08**	**15.15**	**14.99**	**14.86**	**14.90**	**15.36**
Total	**99.29**	**98.76**	**98.93**	**98.64**	**98.96**	**98.98**

T (iv) site: Si	**2.965**	**2.964**	**2.966**	**2.938**	**2.952**	**2.972**
Al	**1.042**	**1.040**	**1.042**	**1.069**	**1.056**	**1.031**
Fe^{3+}						
T site total	**4.007**	**4.004**	**4.008**	**4.007**	**4.008**	**4.003**

Fe3+						
Fe2+	**0.001**	**0.001**	**0.000**	**0.000**	**0.000**	**0.000**
Mn						
Mg						
Ca	**0.000**	**0.000**	**0.000**	**0.001**	**0.001**	
Ba	**0.012**	**0.013**	**0.014**	**0.034**	**0.024**	**0.009**
Sr						
Na	**0.090**	**0.089**	**0.086**	**0.071**	**0.076**	**0.083**
K	**0.898**	**0.907**	**0.895**	**0.898**	**0.894**	**0.917**
M-site total	**1.000**	**1.009**	**0.996**	**1.004**	**0.996**	**1.010**

Main feldspar components	Kspar_010	Kspar_011	Kspar_012	Kspar_001	Kspar_002	Kspar_003
albite (mol%)	**9.00**	**8.81**	**8.66**	**7.10**	**7.65**	**8.27**
anorthite (mol%)	**0.01**	**0.04**	**0.05**	**0.12**	**0.11**	
orthoclase (mol%)	**89.79**	**89.91**	**89.90**	**89.42**	**89.78**	**90.81**
celsian (mol%)	**1.19**	**1.24**	**1.39**	**3.36**	**2.46**	**0.92**

Barian species

SMC16-34 Analysis pt. #	50	51	52	53	54	55
Comment	Kspar_004	Kspar_005	Kspar_006	Plag_001	Plag_002	Plag_003
SiO2	63.327	63.528	63.29	63.627	63.543	66.275
Al2O3	18.858	18.847	18.915	22.147	22.15	20.41
Fe2O3						
FeO		0.027			0.039	
MnO						
MgO						
CaO	0.001		0.01	2.941	2.78	0.841
BaO	0.759	0.758	0.85	0.014	0.008	0.003
SrO						
Na2O	0.913	0.869	0.755	9.919	10.023	11.312
K2O	15.206	15.215	15.347	0.183	0.237	0.105
Total	99.06	99.24	99.17	98.83	98.78	98.95
All Fe as FeO		0.03			0.04	
All Fe as Fe2O3		0.03			0.04	
Assumed FeO						
Assumed Fe2O3						

Si	2.108	2.115	2.107	2.118	2.115	2.206
Al	0.555	0.555	0.557	0.652	0.652	0.601
Fe3+						
Fe2+		0.000			0.001	
Mn2+						
Mg						
Ca	0.000		0.000	0.052	0.050	0.015
Ba	0.005	0.005	0.006	0.000	0.000	0.000
Sr						
Na	0.015	0.014	0.012	0.160	0.162	0.183
K	0.161	0.162	0.163	0.002	0.003	0.001
Total	2.844	2.850	2.844	2.984	2.981	3.005
Factor (8 O2-)	2.813	2.807	2.813	2.681	2.683	2.662

Si	2.965	2.968	2.963	2.839	2.838	2.936

Al	1.041	1.038	1.044	1.165	1.166	1.066
Fe3+						
Fe2+		0.001			0.001	
Mn						
Mg						
Ca	0.000		0.001	0.141	0.133	0.040
Ba	0.014	0.014	0.016	0.000	0.000	0.000
Sr						
Na	0.083	0.079	0.069	0.858	0.868	0.972
K	0.908	0.907	0.917	0.010	0.014	0.006

Comment	Kspar_004	Kspar_005	Kspar_006	Plag_001	Plag_002	Plag_003
SiO_2	**63.33**	**63.53**	**63.29**	**63.63**	**63.54**	**66.28**
Al_2O_3	**18.86**	**18.85**	**18.92**	**22.15**	**22.15**	**20.41**
Fe2O3						
FeO		**0.03**			**0.04**	
MnO						
MgO						
CaO	**0.00**		**0.01**	**2.94**	**2.78**	**0.84**
BaO	**0.76**	**0.76**	**0.85**	**0.01**	**0.01**	**0.00**
SrO						
Na_2O	**0.91**	**0.87**	**0.76**	**9.92**	**10.02**	**11.31**
K_2O	**15.21**	**15.22**	**15.35**	**0.18**	**0.24**	**0.11**
Total	**99.06**	**99.24**	**99.17**	**98.83**	**98.78**	**98.95**

T (iv) site: Si	**2.965**	**2.968**	**2.963**	**2.839**	**2.838**	**2.936**
Al	**1.041**	**1.038**	**1.044**	**1.165**	**1.166**	**1.066**
Fe^{3+}						
T site total	**4.005**	**4.006**	**4.007**	**4.004**	**4.004**	**4.002**

Fe3+						
Fe2+		**0.001**			**0.001**	
Mn						
Mg						
Ca	**0.000**		**0.001**	**0.141**	**0.133**	**0.040**
Ba	**0.014**	**0.014**	**0.016**	**0.000**	**0.000**	**0.000**
Sr						
Na	**0.083**	**0.079**	**0.069**	**0.858**	**0.868**	**0.972**
K	**0.908**	**0.907**	**0.917**	**0.010**	**0.014**	**0.006**
M-site total	**1.005**	**0.999**	**1.001**	**1.009**	**1.015**	**1.018**

Main feldspar components	Kspar_004	Kspar_005	Kspar_006	Plag_001	Plag_002	Plag_003
albite (mol%)	**8.25**	**7.88**	**6.84**	**85.01**	**85.54**	**95.49**
anorthite (mol%)	**0.00**		**0.05**	**13.93**	**13.11**	**3.92**
orthoclase (mol%)	**90.36**	**90.74**	**91.55**	**1.03**	**1.33**	**0.58**
celsian (mol%)	**1.39**	**1.39**	**1.56**	**0.02**	**0.01**	**0.01**

Barian species

SMC16-34 Analysis pt. #	56	57	58	59	60	61
Comment	Plag_004	Plag_005	Kspar_007	Kspar_008	Kspar_009	Kspar_010
SiO2	65.889	64.849	63.071	63.347	63.53	62.954
Al2O3	20.801	21.26	18.901	18.767	18.932	18.909
Fe2O3						
FeO	0.029		0.011	0.011	0.008	0.025
MnO						
MgO						
CaO	1.141	1.964		0.005		0.018
BaO	0.008	0.03	0.981	0.854	0.729	1.37
SrO						
Na2O	11.144	10.687	0.765	0.76	0.774	0.876
K2O	0.146	0.125	15.292	15.317	15.422	14.961
Total	99.16	98.92	99.02	99.06	99.40	99.11
All Fe as FeO	0.03		0.01	0.01	0.01	0.03
All Fe as Fe2O3	0.03		0.01	0.01	0.01	0.03
Assumed FeO						
Assumed Fe2O3						

Si	2.193	2.159	2.099	2.109	2.115	2.096
Al	0.612	0.626	0.556	0.552	0.557	0.556
Fe3+						
Fe2+	0.000		0.000	0.000	0.000	0.000
Mn2+						
Mg						
Ca	0.020	0.035		0.000		0.000
Ba	0.000	0.000	0.006	0.006	0.005	0.009
Sr						
Na	0.180	0.172	0.012	0.012	0.012	0.014
K	0.002	0.001	0.162	0.163	0.164	0.159
Total	3.007	2.993	2.837	2.842	2.853	2.834
Factor (8 O2-)	2.660	2.673	2.820	2.815	2.804	2.822

Si	2.917	2.885	2.960	2.968	2.965	2.957

Al	1.085	1.115	1.046	1.036	1.041	1.047
Fe3+						
Fe2+	0.001		0.000	0.000	0.000	0.001
Mn						
Mg						
Ca	0.054	0.094		0.000		0.001
Ba	0.000	0.001	0.018	0.016	0.013	0.025
Sr						
Na	0.957	0.922	0.070	0.069	0.070	0.080
K	0.008	0.007	0.916	0.916	0.918	0.897

Comment	Plag_004	Plag_005	Kspar_007	Kspar_008	Kspar_009	Kspar_010
SiO_2	**65.89**	**64.85**	**63.07**	**63.35**	**63.53**	**62.95**
Al_2O_3	**20.80**	**21.26**	**18.90**	**18.77**	**18.93**	**18.91**
Fe2O3						
FeO	**0.03**		**0.01**	**0.01**	**0.01**	**0.03**
MnO						
MgO						
CaO	**1.14**	**1.96**		**0.01**		**0.02**
BaO	**0.01**	**0.03**	**0.98**	**0.85**	**0.73**	**1.37**
SrO						
Na_2O	**11.14**	**10.69**	**0.77**	**0.76**	**0.77**	**0.88**
K_2O	**0.15**	**0.13**	**15.29**	**15.32**	**15.42**	**14.96**
Total	**99.16**	**98.92**	**99.02**	**99.06**	**99.40**	**99.11**

T (iv) site: Si	**2.917**	**2.885**	**2.960**	**2.968**	**2.965**	**2.957**
Al	**1.085**	**1.115**	**1.046**	**1.036**	**1.041**	**1.047**
Fe^{3+}						
T site total	**4.002**	**3.999**	**4.006**	**4.005**	**4.006**	**4.004**

Fe3+						
Fe2+	**0.001**		**0.000**	**0.000**	**0.000**	**0.001**
Mn						
Mg						
Ca	**0.054**	**0.094**		**0.000**		**0.001**
Ba	**0.000**	**0.001**	**0.018**	**0.016**	**0.013**	**0.025**
Sr						
Na	**0.957**	**0.922**	**0.070**	**0.069**	**0.070**	**0.080**
K	**0.008**	**0.007**	**0.916**	**0.916**	**0.918**	**0.897**
M-site total	**1.019**	**1.023**	**1.003**	**1.001**	**1.002**	**1.002**

Main feldspar components	Plag_004	Plag_005	Kspar_007	Kspar_008	Kspar_009	Kspar_010
albite (mol%)	**93.87**	**90.10**	**6.94**	**6.90**	**6.99**	**7.96**
anorthite (mol%)	**5.31**	**9.15**		**0.03**		**0.09**
orthoclase (mol%)	**0.81**	**0.69**	**91.26**	**91.51**	**91.68**	**89.44**
celsian (mol%)	**0.01**	**0.05**	**1.80**	**1.57**	**1.33**	**2.52**

Barian species

SMC16-34 Analysis pt. #	62	63	64	65	66	67
Comment	Plag_001	Plag_002	Plag_003	Plag_004	Kspar_001	Kspar_002
SiO2	63.929	63.96	66.486	64.348	63.432	63.043
Al2O3	22.071	22.185	20.578	21.616	18.92	18.835
Fe2O3						
FeO		0.005	0.007		0.027	
MnO						
MgO						
CaO	2.511	2.752	0.876	2.24		
BaO	0.004				0.842	0.712
SrO						
Na2O	10.297	10.24	11.316	10.536	0.973	0.832
K2O	0.219	0.171	0.136	0.151	15.108	15.3
Total	99.03	99.31	99.40	98.89	99.30	98.72
All Fe as FeO		0.01	0.01		0.03	
All Fe as Fe2O3		0.01	0.01		0.03	
Assumed FeO						
Assumed Fe2O3						

Si	2.128	2.129	2.213	2.142	2.111	2.099
Al	0.649	0.653	0.605	0.636	0.557	0.554
Fe3+						
Fe2+		0.000	0.000		0.000	
Mn2+						
Mg						
Ca	0.045	0.049	0.016	0.040		
Ba	0.000				0.005	0.005
Sr						
Na	0.166	0.165	0.183	0.170	0.016	0.013
K	0.002	0.002	0.001	0.002	0.160	0.162
Total	2.991	2.998	3.018	2.990	2.850	2.833
Factor (8 O2-)	2.675	2.668	2.650	2.676	2.807	2.824

Si	2.846	2.841	2.933	2.866	2.963	2.963

Al	1.158	1.161	1.070	1.135	1.042	1.043
Fe3+						
Fe2+		0.000	0.000		0.001	
Mn						
Mg						
Ca	0.120	0.131	0.041	0.107		
Ba	0.000				0.015	0.013
Sr						
Na	0.889	0.882	0.968	0.910	0.088	0.076
K	0.012	0.010	0.008	0.009	0.900	0.917

Comment	Plag_001	Plag_002	Plag_003	Plag_004	Kspar_001	Kspar_002
SiO_2	**63.93**	**63.96**	**66.49**	**64.35**	**63.43**	**63.04**
Al_2O_3	**22.07**	**22.19**	**20.58**	**21.62**	**18.92**	**18.84**
Fe2O3						
FeO		**0.01**	**0.01**		**0.03**	
MnO						
MgO						
CaO	**2.51**	**2.75**	**0.88**	**2.24**		
BaO	**0.00**				**0.84**	**0.71**
SrO						
Na_2O	**10.30**	**10.24**	**11.32**	**10.54**	**0.97**	**0.83**
K_2O	**0.22**	**0.17**	**0.14**	**0.15**	**15.11**	**15.30**
Total	**99.03**	**99.31**	**99.40**	**98.89**	**99.30**	**98.72**

T (iv) site: Si	**2.846**	**2.841**	**2.933**	**2.866**	**2.963**	**2.963**
Al	**1.158**	**1.161**	**1.070**	**1.135**	**1.042**	**1.043**
Fe^{3+}						
T site total	**4.004**	**4.002**	**4.003**	**4.001**	**4.005**	**4.006**

Fe3+						
Fe2+		**0.000**	**0.000**		**0.001**	
Mn						
Mg						
Ca	**0.120**	**0.131**	**0.041**	**0.107**		
Ba	**0.000**				**0.015**	**0.013**
Sr						
Na	**0.889**	**0.882**	**0.968**	**0.910**	**0.088**	**0.076**
K	**0.012**	**0.010**	**0.008**	**0.009**	**0.900**	**0.917**
M-site total	**1.021**	**1.022**	**1.017**	**1.025**	**1.004**	**1.006**

Main feldspar components	Plag_001	Plag_002	Plag_003	Plag_004	Kspar_001	Kspar_002
albite (mol%)	**87.04**	**86.24**	**95.18**	**88.74**	**8.78**	**7.53**
anorthite (mol%)	**11.73**	**12.81**	**4.07**	**10.43**		
orthoclase (mol%)	**1.22**	**0.95**	**0.75**	**0.84**	**89.69**	**91.16**
celsian (mol%)	**0.01**				**1.54**	**1.30**

Barian species

SMC16-34 Analysis pt. #	68	69	70	71	72	73
Comment	Kspar_003	Kspar_004	Kspar_005	Kspar_006	Kspar_007	Kspar_008
SiO2	63.625	63.414	63.37	63.227	64.341	64.3
Al2O3	18.807	18.773	18.623	18.749	19.03	19.048
Fe2O3						
FeO	0.008		0.006	0.033		0.002
MnO						
MgO						
CaO		0.003			0.023	0.02
BaO	0.334	0.75	0.576	0.749	1.536	1.822
SrO						
Na2O	0.854	0.906	0.899	0.899	0.869	0.685
K2O	15.411	15.235	15.286	15.262	15.538	15.593
Total	99.04	99.08	98.76	98.92	101.34	101.47
All Fe as FeO	0.01		0.01	0.03		0.00
All Fe as Fe2O3	0.01		0.01	0.04		0.00
Assumed FeO						
Assumed Fe2O3						

Si	2.118	2.111	2.109	2.105	2.142	2.140
Al	0.553	0.552	0.548	0.552	0.560	0.560
Fe3+						
Fe2+	0.000		0.000	0.000		0.000
Mn2+						
Mg						
Ca		0.000			0.000	0.000
Ba	0.002	0.005	0.004	0.005	0.010	0.012
Sr						
Na	0.014	0.015	0.015	0.015	0.014	0.011
K	0.164	0.162	0.162	0.162	0.165	0.166
Total	2.851	2.845	2.838	2.838	2.891	2.890
Factor (8 O2-)	2.806	2.812	2.819	2.819	2.767	2.768

Si	2.972	2.968	2.973	2.966	2.963	2.963
Al	1.035	1.036	1.030	1.037	1.033	1.034
Fe3+						

Fe2+	0.000		0.000	0.001		0.000
Mn						
Mg						
Ca		0.000			0.001	0.001
Ba	0.006	0.014	0.011	0.014	0.028	0.033
Sr						
Na	0.077	0.082	0.082	0.082	0.078	0.061
K	0.918	0.910	0.915	0.913	0.913	0.917

Comment	Kspar_003	Kspar_004	Kspar_005	Kspar_006	Kspar_007	Kspar_008
SiO_2	**63.63**	**63.41**	**63.37**	**63.23**	**64.34**	**64.30**
Al_2O_3	**18.81**	**18.77**	**18.62**	**18.75**	**19.03**	**19.05**
Fe2O3						
FeO	**0.01**		**0.01**	**0.03**		**0.00**
MnO						
MgO						
CaO		**0.00**			**0.02**	**0.02**
BaO	**0.33**	**0.75**	**0.58**	**0.75**	**1.54**	**1.82**
SrO						
Na_2O	**0.85**	**0.91**	**0.90**	**0.90**	**0.87**	**0.69**
K_2O	**15.41**	**15.24**	**15.29**	**15.26**	**15.54**	**15.59**
Total	**99.04**	**99.08**	**98.76**	**98.92**	**101.34**	**101.47**

T (iv) site: Si	**2.972**	**2.968**	**2.973**	**2.966**	**2.963**	**2.963**
Al	**1.035**	**1.036**	**1.030**	**1.037**	**1.033**	**1.034**
Fe^{3+}						
T site total	**4.007**	**4.004**	**4.003**	**4.003**	**3.996**	**3.997**

Fe3+						
Fe2+	**0.000**		**0.000**	**0.001**		**0.000**
Mn						
Mg						
Ca		**0.000**			**0.001**	**0.001**
Ba	**0.006**	**0.014**	**0.011**	**0.014**	**0.028**	**0.033**
Sr						
Na	**0.077**	**0.082**	**0.082**	**0.082**	**0.078**	**0.061**
K	**0.918**	**0.910**	**0.915**	**0.913**	**0.913**	**0.917**
M-site total	**1.002**	**1.006**	**1.007**	**1.009**	**1.019**	**1.012**

Main feldspar components	Kspar_003	Kspar_004	Kspar_005	Kspar_006	Kspar_007	Kspar_008

albite (mol%)	**7.72**	**8.17**	**8.12**	**8.10**	**7.61**	**6.05**
anorthite (mol%)		**0.01**			**0.11**	**0.10**
orthoclase (mol%)	**91.67**	**90.44**	**90.83**	**90.53**	**89.56**	**90.60**
celsian (mol%)	**0.61**	**1.37**	**1.05**	**1.36**	**2.72**	**3.25**

Barian species

SMC16-34 Analysis pt. #	74	75	76	77	78	79
Comment	Kspar_009	Kspar_010	Kspar_011	Kspar_012	Kspar_013	Kspar_014
SiO2	61.883	62.11	63.288	62.387	63.215	61.501
Al2O3	19.253	19.092	18.715	19.103	18.793	19.204
Fe2O3						
FeO	0.019	0.016	0.016	0.002		
MnO						
MgO						
CaO	0.036	0.013		0.007		0.037
BaO	2.07	1.759	0.555	1.768	0.623	2.406
SrO						
Na2O	0.806	0.817	0.745	0.859	0.85	0.729
K2O	14.79	14.898	15.448	14.907	15.241	14.585
Total	98.86	98.71	98.77	99.03	98.72	98.46
All Fe as FeO	0.02	0.02	0.02	0.00		
All Fe as Fe2O3	0.02	0.02	0.02	0.00		
Assumed FeO						
Assumed Fe2O3						

Si	2.060	2.067	2.107	2.077	2.104	2.047
Al	0.566	0.562	0.551	0.562	0.553	0.565
Fe3+						
Fe2+	0.000	0.000	0.000	0.000		
Mn2+						
Mg						
Ca	0.001	0.000		0.000		0.001
Ba	0.014	0.011	0.004	0.012	0.004	0.016
Sr						
Na	0.013	0.013	0.012	0.014	0.014	0.012
K	0.157	0.158	0.164	0.158	0.162	0.155
Total	2.811	2.812	2.837	2.823	2.837	2.795
Factor (8 O2-)	2.846	2.844	2.820	2.834	2.820	2.862

Si	2.931	2.940	2.970	2.943	2.967	2.930
Al	1.075	1.065	1.035	1.062	1.040	1.078
Fe3+						

Fe2+	0.001	0.001	0.001	0.000		
Mn						
Mg						
Ca	0.002	0.001		0.000		0.002
Ba	0.038	0.033	0.010	0.033	0.011	0.045
Sr						
Na	0.074	0.075	0.068	0.079	0.077	0.067
K	0.894	0.900	0.925	0.897	0.913	0.886

Comment	Kspar_009	Kspar_010	Kspar_011	Kspar_012	Kspar_013	Kspar_014
SiO_2	**61.88**	**62.11**	**63.29**	**62.39**	**63.22**	**61.50**
Al_2O_3	**19.25**	**19.09**	**18.72**	**19.10**	**18.79**	**19.20**
Fe2O3						
FeO	**0.02**	**0.02**	**0.02**	**0.00**		
MnO						
MgO						
CaO	**0.04**	**0.01**		**0.01**		**0.04**
BaO	**2.07**	**1.76**	**0.56**	**1.77**	**0.62**	**2.41**
SrO						
Na_2O	**0.81**	**0.82**	**0.75**	**0.86**	**0.85**	**0.73**
K_2O	**14.79**	**14.90**	**15.45**	**14.91**	**15.24**	**14.59**
Total	**98.86**	**98.71**	**98.77**	**99.03**	**98.72**	**98.46**

T (iv) site: Si	**2.931**	**2.940**	**2.970**	**2.943**	**2.967**	**2.930**
Al	**1.075**	**1.065**	**1.035**	**1.062**	**1.040**	**1.078**
Fe^{3+}						
T site total	**4.006**	**4.006**	**4.005**	**4.005**	**4.007**	**4.008**

Fe3+						
Fe2+	**0.001**	**0.001**	**0.001**	**0.000**		
Mn						
Mg						
Ca	**0.002**	**0.001**		**0.000**		**0.002**
Ba	**0.038**	**0.033**	**0.010**	**0.033**	**0.011**	**0.045**
Sr						
Na	**0.074**	**0.075**	**0.068**	**0.079**	**0.077**	**0.067**
K	**0.894**	**0.900**	**0.925**	**0.897**	**0.913**	**0.886**
M-site total	**1.008**	**1.008**	**1.003**	**1.009**	**1.001**	**1.000**

Main feldspar components	Kspar_009	Kspar_010	Kspar_011	Kspar_012	Kspar_013	Kspar_014

albite (mol%)	**7.34**	**7.44**	**6.76**	**7.79**	**7.72**	**6.73**
anorthite (mol%)	**0.18**	**0.07**		**0.04**		**0.19**
orthoclase (mol%)	**88.66**	**89.26**	**92.22**	**88.94**	**91.13**	**88.59**
celsian (mol%)	**3.81**	**3.24**	**1.02**	**3.24**	**1.14**	**4.49**

Barian species

SMC16-34 Analysis pt. #	80	81	82	83
Comment	Kspar_001	Kspar_002	Kspar_003	Kspar_004
SiO2	62.003	62.315	62.736	62.478
Al2O3	19.109	19.185	18.956	18.98
Fe2O3				
FeO		0.02	0.02	0.005
MnO				
MgO				
CaO	0.008	0.023		
BaO	1.964	1.675	0.858	1.494
SrO				
Na2O	0.694	0.757	0.794	0.762
K2O	14.825	14.948	15.369	15.139
Total	98.60	98.92	98.73	98.86
All Fe as FeO		0.02	0.02	0.01
All Fe as Fe2O3		0.02	0.02	0.01
Assumed FeO				
Assumed Fe2O3				

Si	2.064	2.074	2.088	2.080
Al	0.562	0.564	0.558	0.558
Fe3+				
Fe2+		0.000	0.000	0.000
Mn2+				
Mg				
Ca	0.000	0.000		
Ba	0.013	0.011	0.006	0.010
Sr				
Na	0.011	0.012	0.013	0.012
K	0.157	0.159	0.163	0.161
Total	2.808	2.821	2.828	2.821
Factor (8 O2-)	2.849	2.836	2.829	2.836

Si	2.940	2.941	2.954	2.949
Al	1.068	1.067	1.052	1.056
Fe3+				

Fe2+		0.001	0.001	0.000
Mn				
Mg				
Ca	0.000	0.001		
Ba	0.036	0.031	0.016	0.028
Sr				
Na	0.064	0.069	0.072	0.070
K	0.897	0.900	0.923	0.912

Comment	Kspar_001	Kspar_002	Kspar_003	Kspar_004
SiO_2	**62.00**	**62.32**	**62.74**	**62.48**
Al_2O_3	**19.11**	**19.19**	**18.96**	**18.98**
Fe2O3				
FeO		**0.02**	**0.02**	**0.01**
MnO				
MgO				
CaO	**0.01**	**0.02**		
BaO	**1.96**	**1.68**	**0.86**	**1.49**
SrO				
Na_2O	**0.69**	**0.76**	**0.79**	**0.76**
K_2O	**14.83**	**14.95**	**15.37**	**15.14**
Total	**98.60**	**98.92**	**98.73**	**98.86**

T (iv) site: Si	**2.940**	**2.941**	**2.954**	**2.949**
Al	**1.068**	**1.067**	**1.052**	**1.056**
Fe^{3+}				
T site total	**4.008**	**4.008**	**4.006**	**4.005**

Fe3+				
Fe2+		**0.001**	**0.001**	**0.000**
Mn				
Mg				
Ca	**0.000**	**0.001**		
Ba	**0.036**	**0.031**	**0.016**	**0.028**
Sr				
Na	**0.064**	**0.069**	**0.072**	**0.070**
K	**0.897**	**0.900**	**0.923**	**0.912**
M-site total	**0.998**	**1.001**	**1.011**	**1.009**

Main feldspar components	Kspar_001	Kspar_002	Kspar_003	Kspar_004

albite (mol%)	**6.40**	**6.92**	**7.17**	**6.91**
anorthite (mol%)	**0.04**	**0.12**		
orthoclase (mol%)	**89.90**	**89.87**	**91.27**	**90.35**
celsian (mol%)	**3.66**	**3.09**	**1.57**	**2.74**

Barian species

SMC13-132 Analysis pt. #	84	85	86	87	88	89
Comment	Plag_001	Plag_002	Plag_003	Plag_004	Plag_005	Plag_006
SiO2	62.315	62.425	63.403	63.246	63.598	68.303
Al2O3	24.044	24.084	23.443	23.749	23.488	20.415
Fe2O3						
FeO		0.012	0.029	0.008		
MnO						
MgO						
CaO	5.092	4.873	4.496	4.748	4.373	0.884
BaO	0.027	0.029	0.039	0.039	0.003	0.007
SrO						
Na2O	8.603	8.515	9.055	8.874	9.155	11.214
K2O	0.403	0.361	0.163	0.222	0.167	0.158
Total	100.48	100.30	100.63	100.89	100.78	100.98
All Fe as FeO		0.01	0.03	0.01		
All Fe as Fe2O3		0.01	0.03	0.01		
Assumed FeO						
Assumed Fe2O3						

Si	2.074	2.078	2.111	2.105	2.117	2.274
Al	0.707	0.709	0.690	0.699	0.691	0.601
Fe3+						
Fe2+		0.000	0.000	0.000		
Mn2+						
Mg						
Ca	0.091	0.087	0.080	0.085	0.078	0.016
Ba	0.000	0.000	0.000	0.000	0.000	0.000
Sr						
Na	0.139	0.137	0.146	0.143	0.148	0.181
K	0.004	0.004	0.002	0.002	0.002	0.002
Total	3.016	3.015	3.029	3.035	3.036	3.073
Factor (8 O2-)	2.653	2.653	2.641	2.636	2.635	2.604

Si	2.751	2.757	2.787	2.775	2.790	2.960
Al	1.251	1.253	1.215	1.228	1.214	1.043
Fe3+						

Fe2+		0.000	0.001	0.000		
Mn						
Mg						
Ca	0.241	0.231	0.212	0.223	0.206	0.041
Ba	0.000	0.001	0.001	0.001	0.000	0.000
Sr						
Na	0.736	0.729	0.772	0.755	0.779	0.942
K	0.023	0.020	0.009	0.012	0.009	0.009

Comment	Plag_001	Plag_002	Plag_003	Plag_004	Plag_005	Plag_006
SiO_2	62.32	62.43	63.40	63.25	63.60	68.30
Al_2O_3	24.04	24.08	23.44	23.75	23.49	20.42
Fe2O3						
FeO		0.01	0.03	0.01		
MnO						
MgO						
CaO	5.09	4.87	4.50	4.75	4.37	0.88
BaO	0.03	0.03	0.04	0.04	0.00	0.01
SrO						
Na_2O	8.60	8.52	9.06	8.87	9.16	11.21
K_2O	0.40	0.36	0.16	0.22	0.17	0.16
Total	100.48	100.30	100.63	100.89	100.78	100.98
	Structural formula based on 8 oxygens					
T (iv) site: Si	2.751	2.757	2.787	2.775	2.790	2.960
Al	1.251	1.253	1.215	1.228	1.214	1.043
Fe^{3+}						
T site total	4.002	4.010	4.002	4.003	4.004	4.002
Fe3+						
Fe2+		0.000	0.001	0.000		
Mn						
Mg						
Ca	0.241	0.231	0.212	0.223	0.206	0.041
Ba	0.000	0.001	0.001	0.001	0.000	0.000
Sr						
Na	0.736	0.729	0.772	0.755	0.779	0.942
K	0.023	0.020	0.009	0.012	0.009	0.009
M-site total	1.000	0.980	0.993	0.991	0.993	0.992

Main feldspar components	Plag_001	Plag_002	Plag_003	Plag_004	Plag_005	Plag_006
albite (mol%)	73.61	74.36	77.69	76.16	78.37	94.97
anorthite (mol%)	24.08	23.52	21.32	22.52	20.69	4.14
orthoclase (mol%)	2.27	2.07	0.92	1.25	0.94	0.88
celsian (mol%)	0.05	0.05	0.07	0.07	0.01	0.01

Barian species

SMC13-132 Analysis pt. #	90	91	92	93	94	95
Comment	Kspar_001	Kspar_002	Kspar_003	Kspar_004	Kspar_005	Plag_001
SiO2	62.718	62.92	62.666	62.437	62.821	64.374
Al2O3	18.901	18.831	18.958	18.829	18.995	22.997
Fe2O3						
FeO	0.017			0.001	0.007	0.03
MnO						
MgO						
CaO	0.004		0.018	0.003	0.008	3.928
BaO	1.215	1.123	1.107	1.093	1.045	0.017
SrO						
Na2O	0.926	0.924	0.973	0.912	0.804	9.435
K2O	14.776	15.031	14.854	15.064	15.147	0.129
Total	98.56	98.83	98.58	98.34	98.83	100.91
All Fe as FeO	0.02			0.00	0.01	0.03
All Fe as Fe2O3	0.02			0.00	0.01	0.03
Assumed FeO						
Assumed Fe2O3						

Si	2.088	2.094	2.086	2.078	2.091	2.143
Al	0.556	0.554	0.558	0.554	0.559	0.677
Fe3+						
Fe2+	0.000			0.000	0.000	0.000
Mn2+						
Mg						
Ca	0.000		0.000	0.000	0.000	0.070
Ba	0.008	0.007	0.007	0.007	0.007	0.000
Sr						
Na	0.015	0.015	0.016	0.015	0.013	0.152
K	0.157	0.160	0.158	0.160	0.161	0.001
Total	2.824	2.830	2.825	2.814	2.831	3.044
Factor (8 O2-)	2.833	2.827	2.832	2.843	2.826	2.628

Si	2.957	2.960	2.954	2.954	2.955	2.816

Al	1.050	1.044	1.053	1.050	1.053	1.186
Fe3+						
Fe2+	0.001			0.000	0.000	0.001
Mn						
Mg						
Ca	0.000		0.001	0.000	0.000	0.184
Ba	0.022	0.021	0.020	0.020	0.019	0.000
Sr						
Na	0.085	0.084	0.089	0.084	0.073	0.800
K	0.889	0.902	0.893	0.909	0.909	0.007

Comment	Kspar_001	Kspar_002	Kspar_003	Kspar_004	Kspar_005	Plag_001
SiO_2	62.72	**62.92**	62.67	62.44	62.82	**64.37**
Al_2O_3	18.90	**18.83**	18.96	18.83	19.00	**23.00**
Fe2O3						
FeO	0.02			0.00	0.01	**0.03**
MnO						
MgO						
CaO	0.00		0.02	0.00	0.01	**3.93**
BaO	1.22	**1.12**	1.11	1.09	1.05	**0.02**
SrO						
Na_2O	0.93	**0.92**	0.97	0.91	0.80	**9.44**
K_2O	14.78	**15.03**	14.85	15.06	15.15	**0.13**
Total	98.56	**98.83**	98.58	98.34	98.83	**100.91**

T (iv) site: Si	2.957	**2.960**	2.954	2.954	2.955	**2.816**
Al	1.050	**1.044**	1.053	1.050	1.053	**1.186**
Fe^{3+}						
T site total	4.008	**4.004**	4.007	4.004	4.008	**4.002**

Fe3+						
Fe2+	0.001			0.000	0.000	**0.001**
Mn						
Mg						
Ca	0.000		0.001	0.000	0.000	**0.184**
Ba	0.022	**0.021**	0.020	0.020	0.019	**0.000**
Sr						
Na	0.085	**0.084**	0.089	0.084	0.073	**0.800**
K	0.889	**0.902**	0.893	0.909	0.909	**0.007**
M-site total	0.996	**1.007**	1.003	1.013	1.002	**0.992**

Main feldspar components	Kspar_001	Kspar_002	Kspar_003	Kspar_004	Kspar_005	Plag_001
albite (mol%)	8.50	**8.37**	8.86	8.26	7.32	**80.68**
anorthite (mol%)	0.02		0.09	0.02	0.04	**18.56**
orthoclase (mol%)	89.23	**89.58**	89.01	89.73	90.72	**0.73**
celsian (mol%)	2.25	**2.06**	2.04	2.00	1.92	**0.03**

Barian species

SMC13-132 Analysis pt. #	96	97	98	99	100	101
Comment	Plag_002	Plag_003	Kspar_001	Kspar_002	Kspar_003	Kspar_004
SiO2	65.074	65.603	62.73	62.574	62.613	62.737
Al2O3	22.433	20.669	18.859	19.006	18.766	18.898
Fe2O3						
FeO	0.019	0.013	0.001	0.007		
MnO						
MgO						
CaO	3.207	1.205	0.011	0.012		
BaO	0.029	0.012	1.01	0.908	1.109	1.122
SrO						
Na2O	9.957	11.082	0.885	0.763	0.94	0.94
K2O	0.114	0.093	15.114	15.395	14.977	15.037
Total	100.83	98.68	98.61	98.67	98.41	98.73
All Fe as FeO	0.02	0.01	0.00	0.01		
All Fe as Fe2O3	0.02	0.01	0.00	0.01		
Assumed FeO						
Assumed Fe2O3						

Si	2.166	2.184	2.088	2.083	2.084	2.088
Al	0.660	0.608	0.555	0.559	0.552	0.556
Fe3+						
Fe2+	0.000	0.000	0.000	0.000		
Mn2+						
Mg						
Ca	0.057	0.021	0.000	0.000		
Ba	0.000	0.000	0.007	0.006	0.007	0.007
Sr						
Na	0.161	0.179	0.014	0.012	0.015	0.015
K	0.001	0.001	0.160	0.163	0.159	0.160
Total	3.046	2.993	2.825	2.824	2.818	2.827
Factor (8 O2-)	2.627	2.673	2.832	2.833	2.839	2.830

Si	2.845	2.918	2.957	2.950	2.959	2.955

Al	1.156	1.084	1.048	1.056	1.045	1.049
Fe3+						
Fe2+	0.001	0.000	0.000	0.000		
Mn						
Mg						
Ca	0.150	0.057	0.001	0.001		
Ba	0.000	0.000	0.019	0.017	0.021	0.021
Sr						
Na	0.844	0.956	0.081	0.070	0.086	0.086
K	0.006	0.005	0.909	0.926	0.903	0.904

Comment	Plag_002	Plag_003	Kspar_001	Kspar_002	Kspar_003	Kspar_004
SiO_2	65.07	65.60	62.73	**62.57**	62.61	62.74
Al_2O_3	22.43	20.67	18.86	**19.01**	18.77	18.90
Fe2O3						
FeO	0.02	0.01	0.00	**0.01**		
MnO						
MgO						
CaO	3.21	1.21	0.01	**0.01**		
BaO	0.03	0.01	1.01	**0.91**	1.11	1.12
SrO						
Na_2O	9.96	11.08	0.89	**0.76**	0.94	0.94
K_2O	0.11	0.09	15.11	**15.40**	14.98	15.04
Total	100.83	98.68	98.61	**98.67**	98.41	98.73

T (iv) site: Si	2.845	2.918	2.957	**2.950**	2.959	2.955
Al	1.156	1.084	1.048	**1.056**	1.045	1.049
Fe^{3+}						
T site total	4.001	4.002	4.005	**4.006**	4.004	4.005

Fe3+						
Fe2+	0.001	0.000	0.000	**0.000**		
Mn						
Mg						
Ca	0.150	0.057	0.001	**0.001**		
Ba	0.000	0.000	0.019	**0.017**	0.021	0.021
Sr						
Na	0.844	0.956	0.081	**0.070**	0.086	0.086
K	0.006	0.005	0.909	**0.926**	0.903	0.904
M-site total	1.001	1.019	1.009	**1.013**	1.009	1.010

Main feldspar components	Plag_002	Plag_003	Kspar_001	Kspar_002	Kspar_003	Kspar_004
albite (mol%)	84.31	93.82	8.02	**6.88**	8.53	8.50
anorthite (mol%)	15.01	5.64	0.06	**0.06**		
orthoclase (mol%)	0.64	0.52	90.08	**91.40**	89.43	89.45
celsian (mol%)	0.05	0.02	1.85	**1.66**	2.03	2.05

Barian species

SMC13-132 Analysis pt. #	102	103	104	105	106	107	108
Comment	Plag_004	Plag_006	Plag_005	Kspar_005	Kspar_006	Kspar_007	Kspar_008
SiO2	66.307	68.641	68.369	62.518	62.363	62.661	62.992
Al2O3	20.181	20.003	20.276	18.908	18.876	18.986	18.978
Fe2O3							
FeO	0.016	0.011	0.022		0.024	0.016	
MnO							
MgO							
CaO	0.867	0.456	0.713		0.05	0.019	
BaO	0.011	0.021	0.01	1.179	1.215	1.301	1.142
SrO							
Na2O	11.312	11.573	11.392	0.77	0.714	0.829	0.756
K2O	0.11	0.133	0.068	15.277	15.189	14.982	15.246
Total	98.80	100.84	100.85	98.65	98.43	98.79	99.11
All Fe as FeO	0.02	0.01	0.02		0.02	0.02	
All Fe as Fe2O3	0.02	0.01	0.02		0.03	0.02	
Assumed FeO							
Assumed Fe2O3							

Si	2.207	2.285	2.276	2.081	2.076	2.086	2.097
Al	0.594	0.589	0.597	0.556	0.555	0.559	0.558
Fe3+							
Fe2+	0.000	0.000	0.000		0.000	0.000	
Mn2+							
Mg							
Ca	0.015	0.008	0.013		0.001	0.000	
Ba	0.000	0.000	0.000	0.008	0.008	0.008	0.007
Sr							
Na	0.183	0.187	0.184	0.012	0.012	0.013	0.012
K	0.001	0.001	0.001	0.162	0.161	0.159	0.162
Total	3.000	3.070	3.070	2.820	2.813	2.826	2.837
Factor (8 O2-)	2.666	2.606	2.606	2.837	2.844	2.831	2.820

Si	2.943	2.977	2.965	2.952	2.952	2.952	2.957

Al	1.055	1.022	1.036	1.052	1.053	1.054	1.050
Fe3+							
Fe2+	0.001	0.000	0.001		0.001	0.001	
Mn							
Mg							
Ca	0.041	0.021	0.033		0.003	0.001	
Ba	0.000	0.000	0.000	0.022	0.023	0.024	0.021
Sr							
Na	0.973	0.973	0.958	0.070	0.066	0.076	0.069
K	0.006	0.007	0.004	0.920	0.917	0.901	0.913

Comment	Plag_004	Plag_006	Plag_005	Kspar_005	Kspar_006	Kspar_007	Kspar_008
SiO_2	66.31	**68.64**	68.37	62.52	62.36	**62.66**	62.99
Al_2O_3	20.18	**20.00**	20.28	18.91	18.88	**18.99**	18.98
Fe2O3							
FeO	0.02	**0.01**	0.02		0.02	**0.02**	
MnO							
MgO							
CaO	0.87	**0.46**	0.71		0.05	**0.02**	
BaO	0.01	**0.02**	0.01	1.18	1.22	**1.30**	1.14
SrO							
Na_2O	11.31	**11.57**	11.39	0.77	0.71	**0.83**	0.76
K_2O	0.11	**0.13**	0.07	15.28	15.19	**14.98**	15.25
Total	98.80	**100.84**	100.85	98.65	98.43	**98.79**	99.11
T (iv) site: Si	2.943	**2.977**	2.965	2.952	2.952	**2.952**	2.957
Al	1.055	**1.022**	1.036	1.052	1.053	**1.054**	1.050
Fe^{3+}							
T site total	3.998	**4.000**	4.002	4.004	4.005	**4.007**	4.007
Fe3+							
Fe2+	0.001	**0.000**	0.001		0.001	**0.001**	
Mn							
Mg							
Ca	0.041	**0.021**	0.033		0.003	**0.001**	
Ba	0.000	**0.000**	0.000	0.022	0.023	**0.024**	0.021
Sr							
Na	0.973	**0.973**	0.958	0.070	0.066	**0.076**	0.069
K	0.006	**0.007**	0.004	0.920	0.917	**0.901**	0.913
M-site total	1.021	**1.002**	0.995	1.013	1.008	**1.001**	1.003

Main feldspar components	Plag_004	Plag_006	Plag_005	Kspar_005	Kspar_006	Kspar_007	Kspar_008
albite (mol%)	95.33	**97.12**	96.27	6.96	6.50	**7.56**	6.86
anorthite (mol%)	4.04	**2.11**	3.33		0.25	**0.10**	
orthoclase (mol%)	0.61	**0.73**	0.38	90.88	91.01	**89.94**	91.04
celsian (mol%)	0.02	**0.04**	0.02	2.15	2.24	**2.40**	2.09

Barian species

APPENDIX D. SEM IMAGES FOR ZIRCON LA-ICP-MS ANALYSES

SMC13-132

BSE **CL**

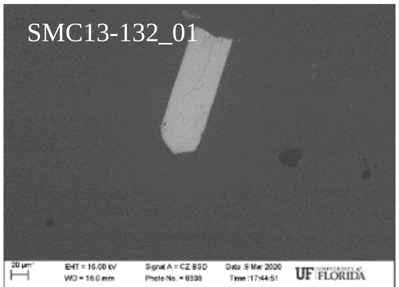

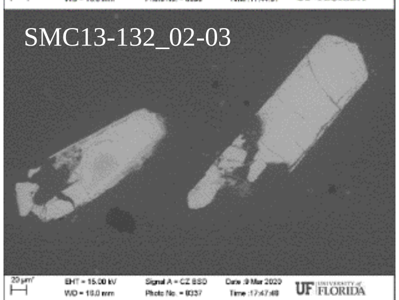

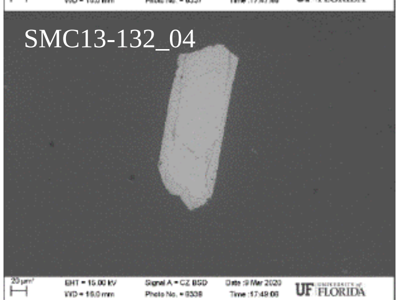

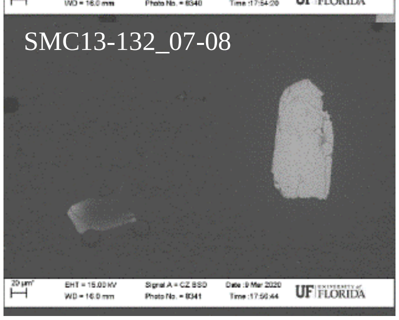

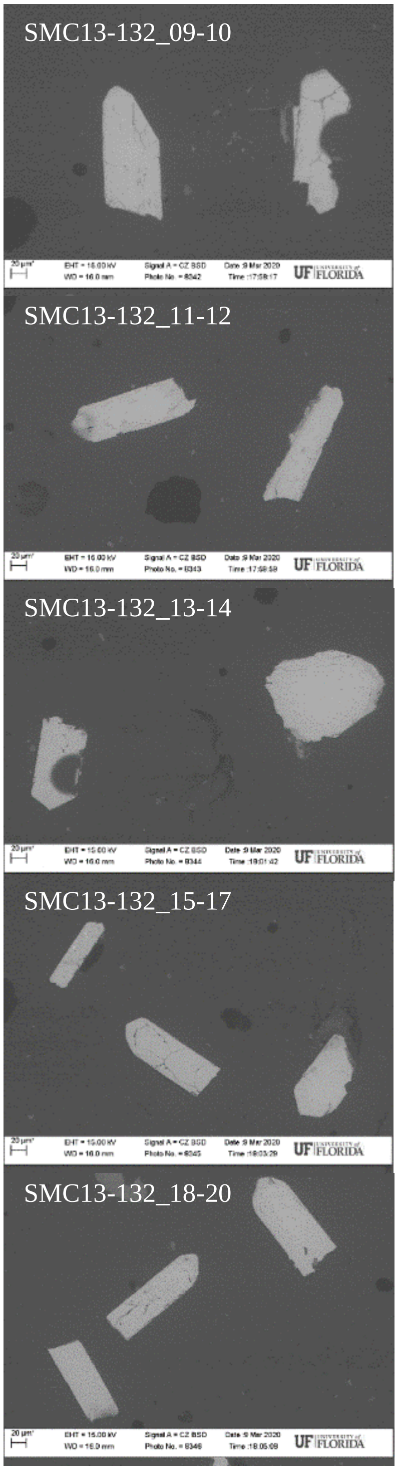
SMC13-132_09-10
SMC13-132_11-12
SMC13-132_13-14
SMC13-132_15-17
SMC13-132_18-20

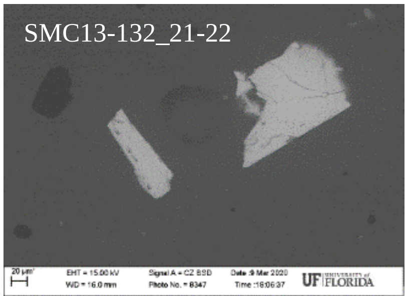
SMC13-132_21-22

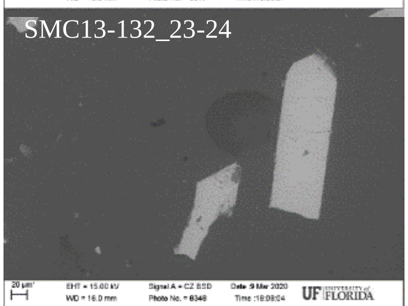
SMC13-132_23-24

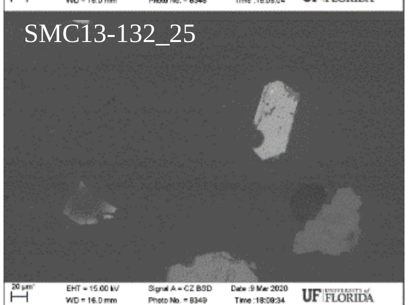
SMC13-132_25

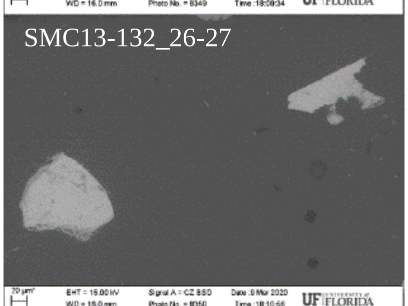
SMC13-132_26-27

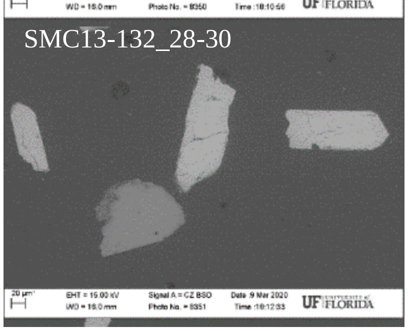
SMC13-132_28-30

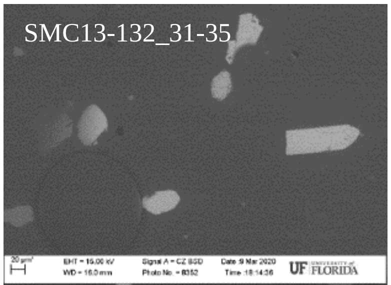
SMC13-132_31-35

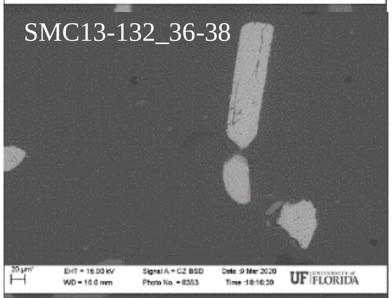
SMC13-132_36-38

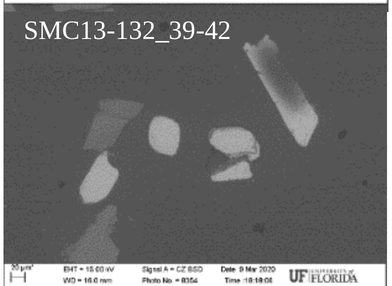
SMC13-132_39-42


SMC13-132_42-45

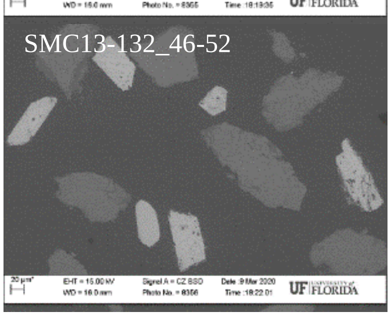
SMC13-132_46-52

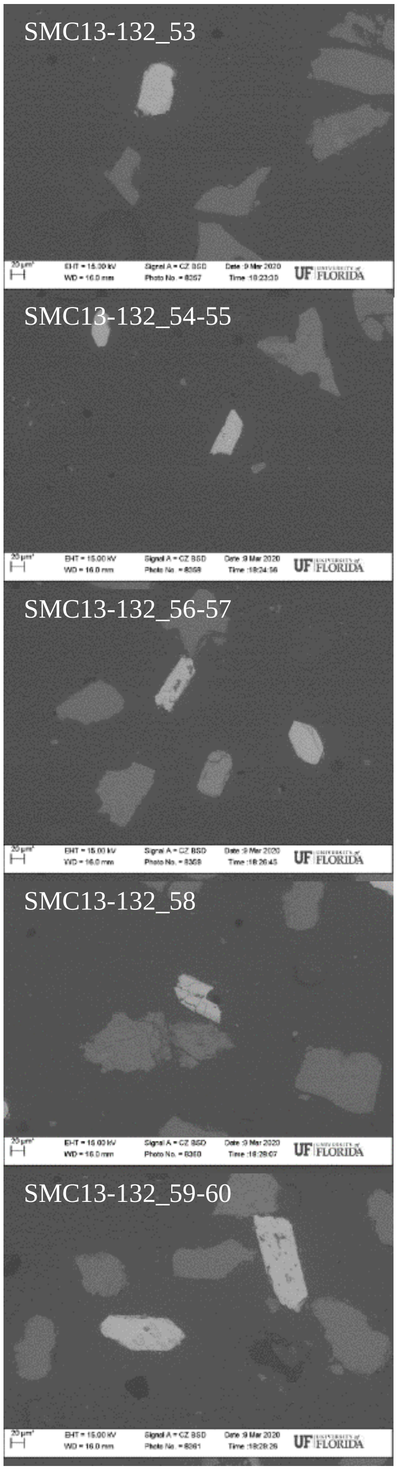
SMC13-132_53
SMC13-132_54-55
SMC13-132_56-57
SMC13-132_58
SMC13-132_59-60

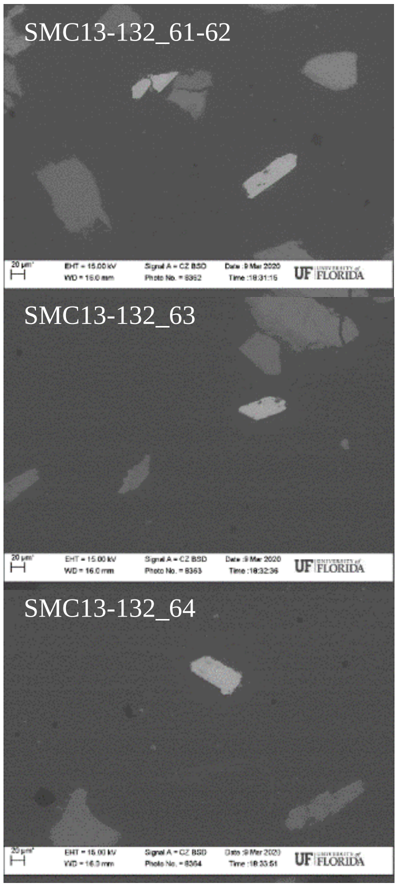
SMC13-132_61-62
SMC13-132_63
SMC13-132_64

SMC14-09

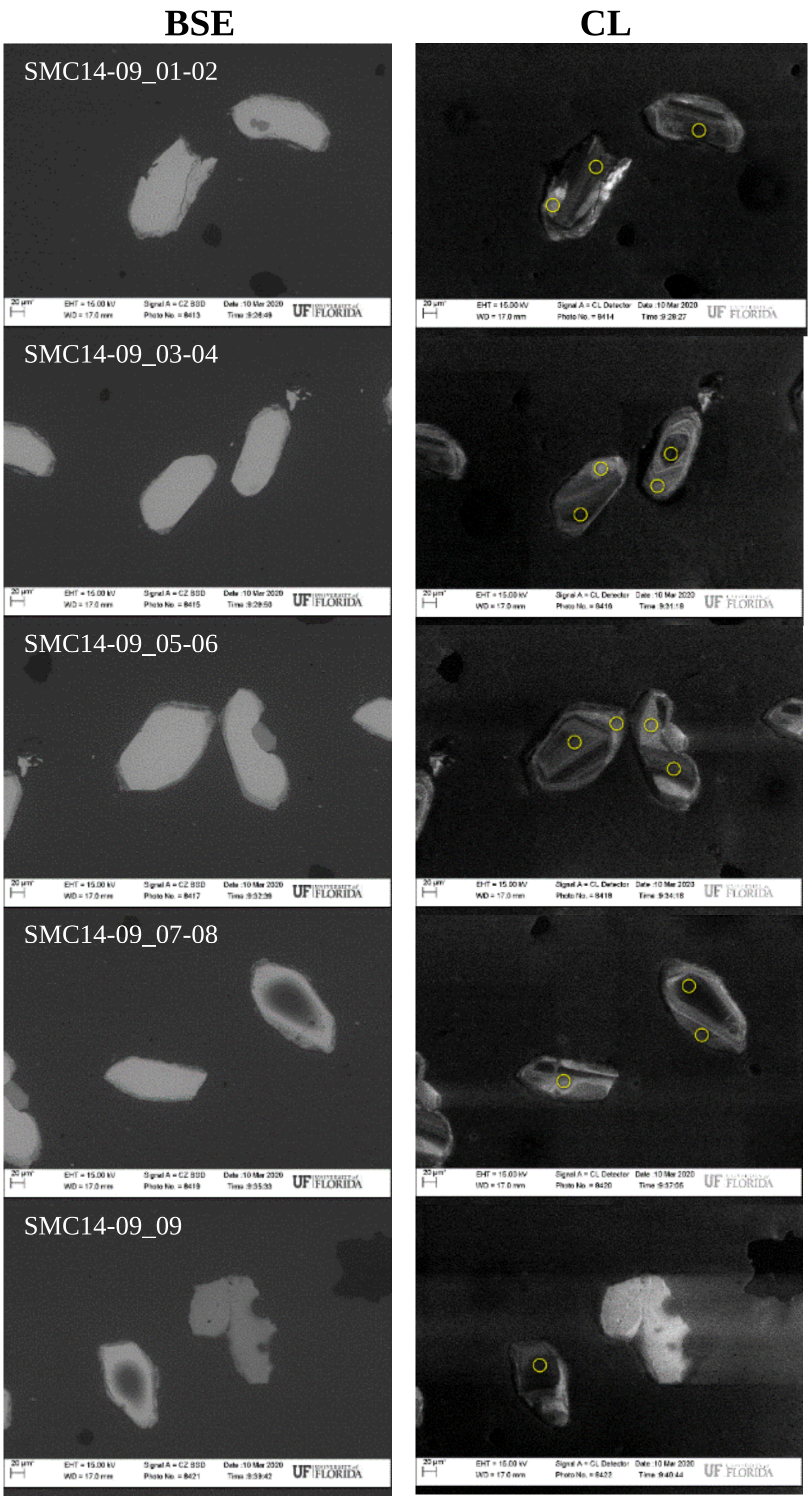
BSE
CL
SMC14-09_01-02
SMC14-09_03-04
SMC14-09_05-06
SMC14-09_07-08
SMC14-09_09

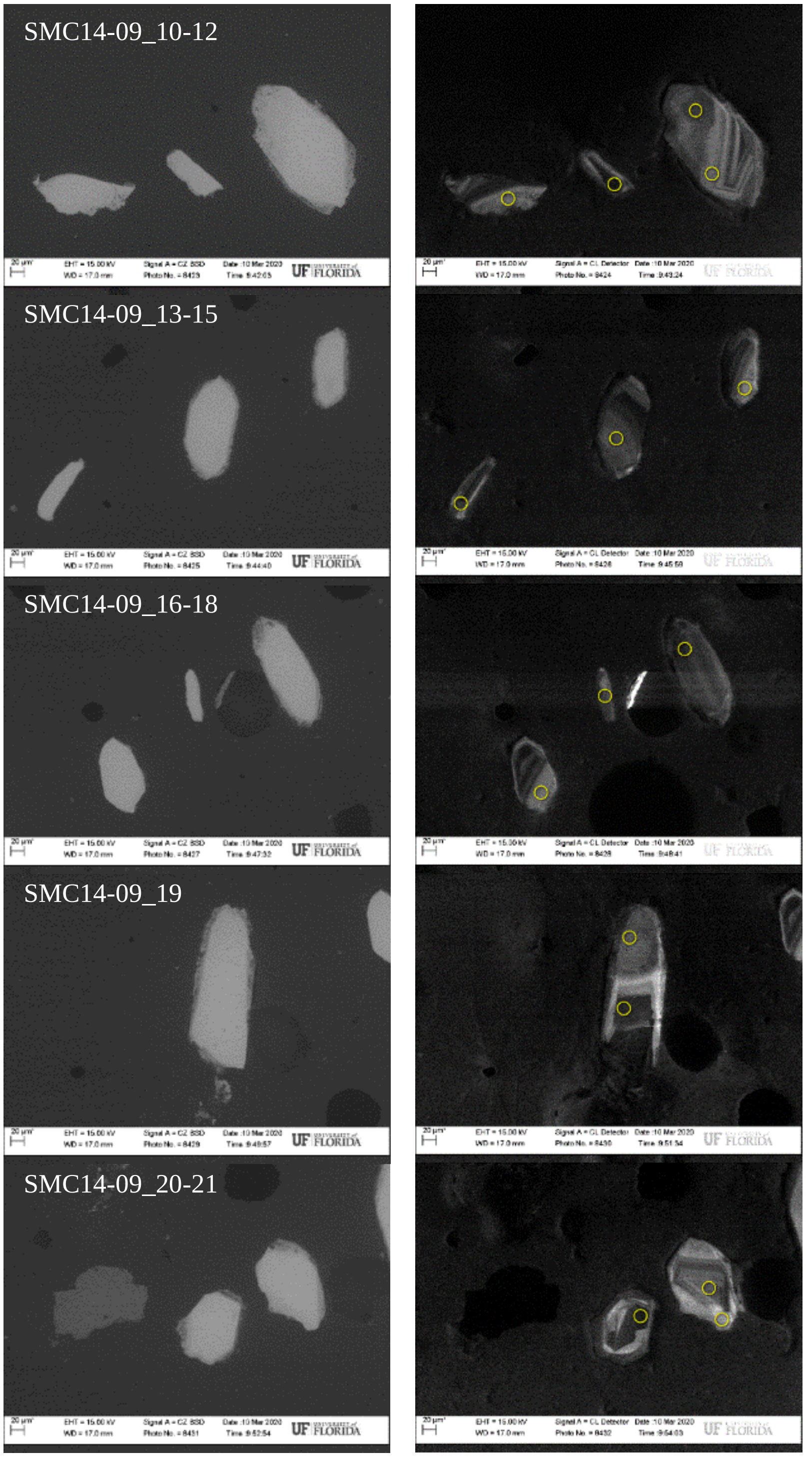
SMC14-09_10-12
SMC14-09_13-15
SMC14-09_16-18
SMC14-09_19
SMC14-09_20-21

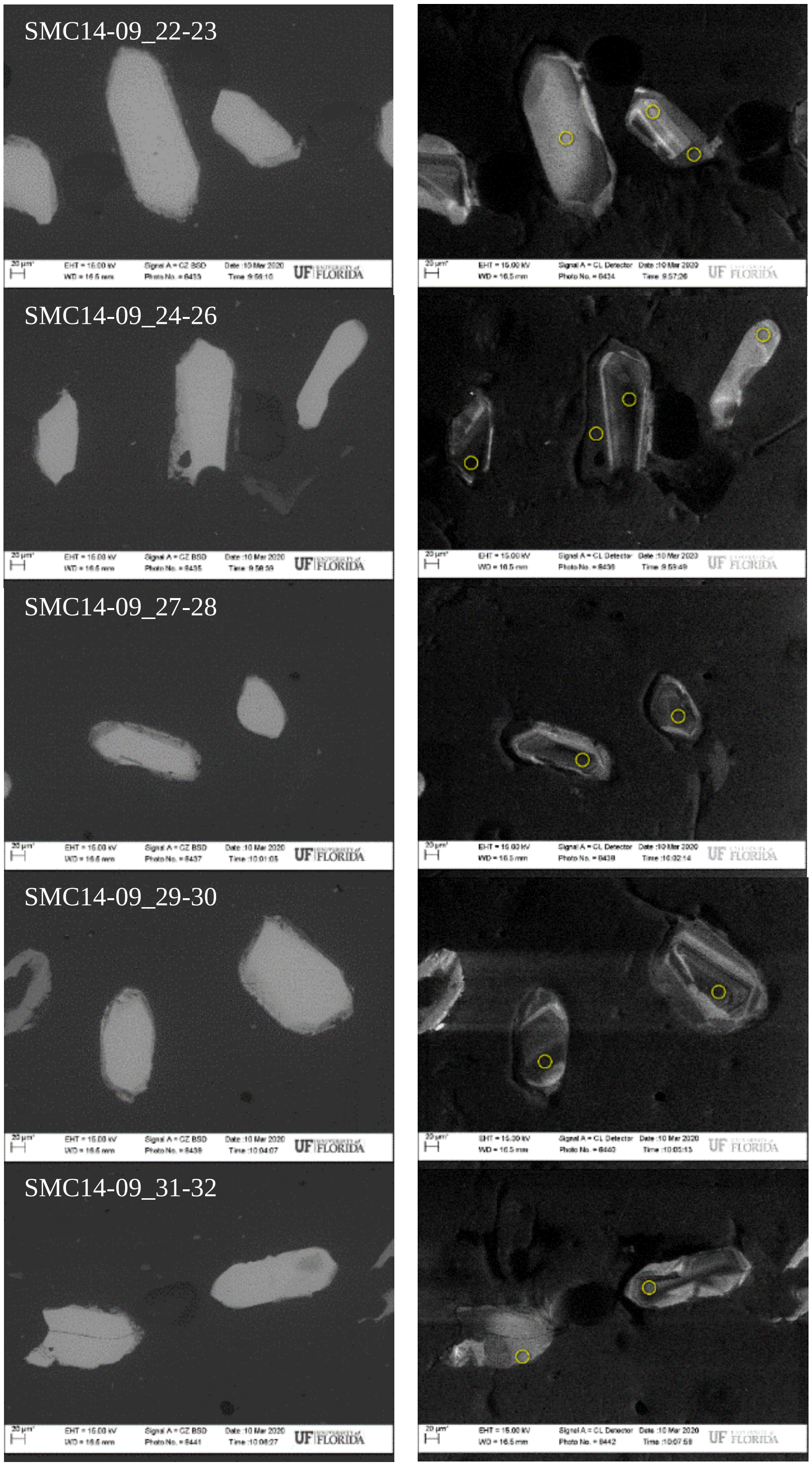
SMC14-09_22-23
SMC14-09_24-26
SMC14-09_27-28
SMC14-09_29-30
SMC14-09_31-32

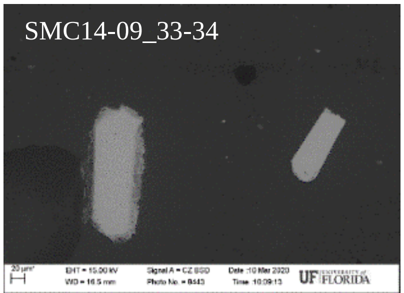
SMC14-09_33-34
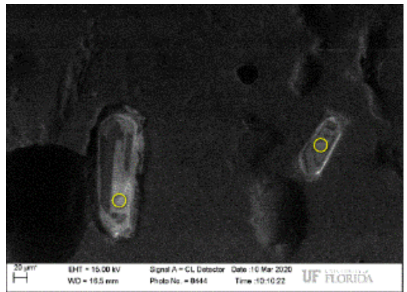
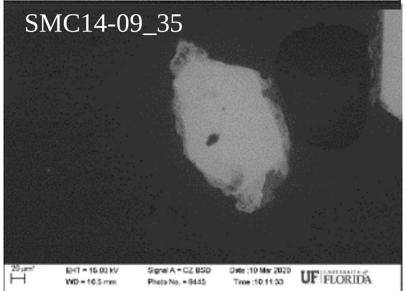
SMC14-09_35
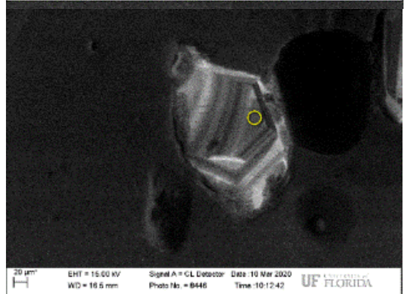
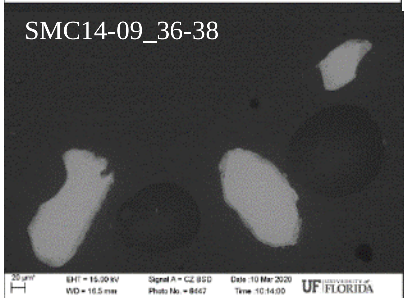
SMC14-09_36-38
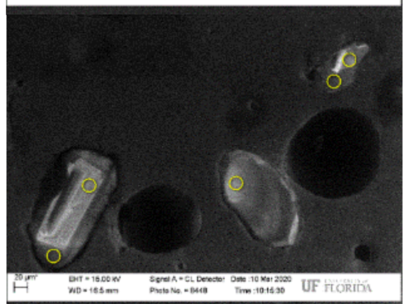
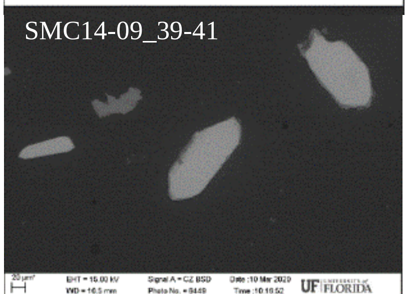
SMC14-09_39-41
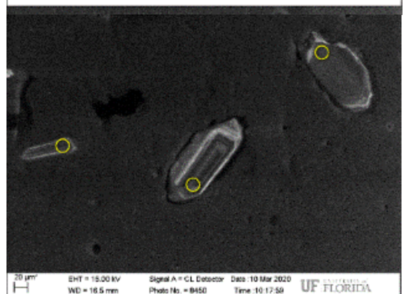
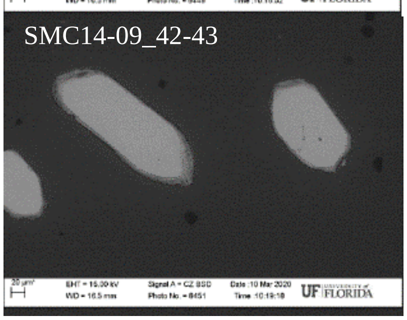
SMC14-09_42-43


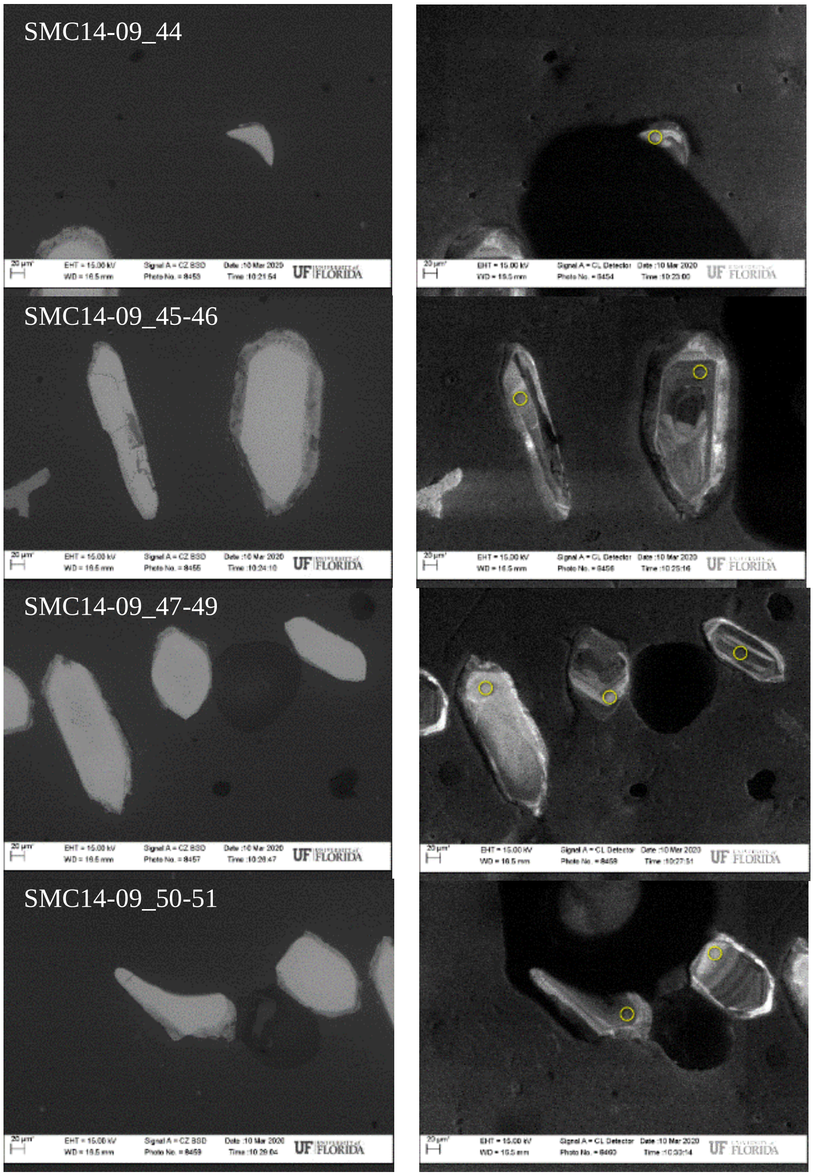
SMC14-09_44
SMC14-09_45-46
SMC14-09_47-49
SMC14-09_50-51

SMC14-11

BSE **CL**

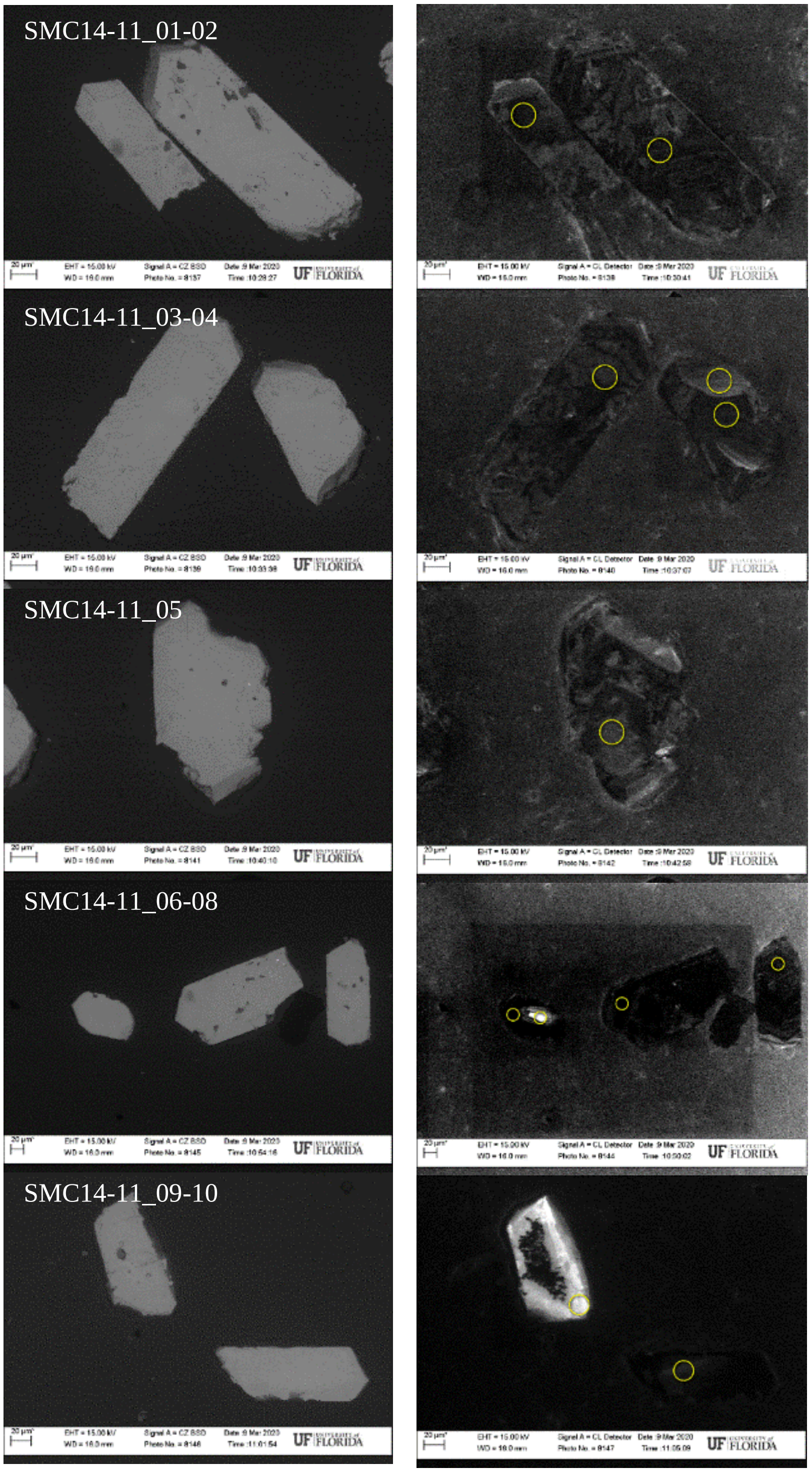

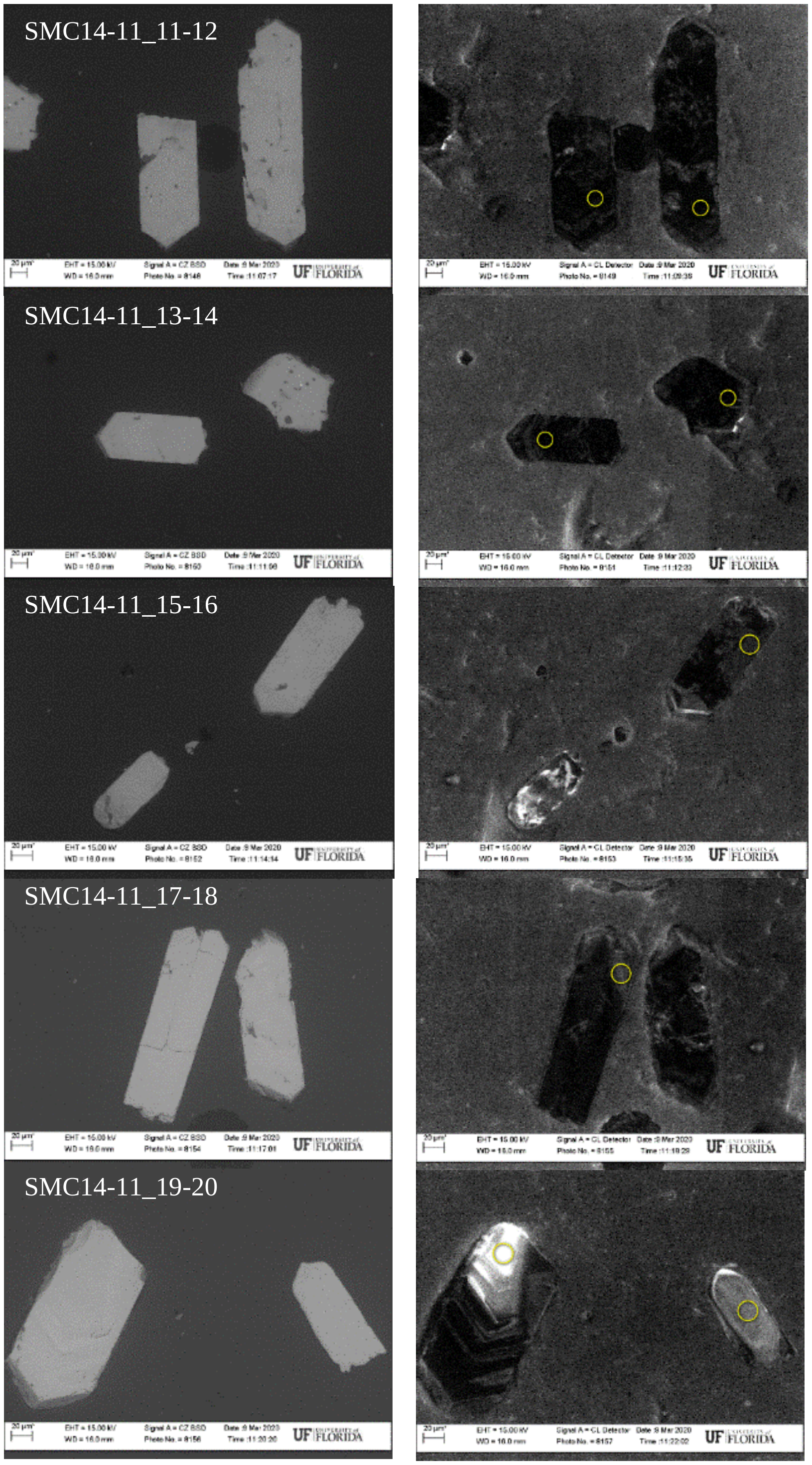
SMC14-11_11-12
SMC14-11_13-14
SMC14-11_15-16
SMC14-11_17-18
SMC14-11_19-20

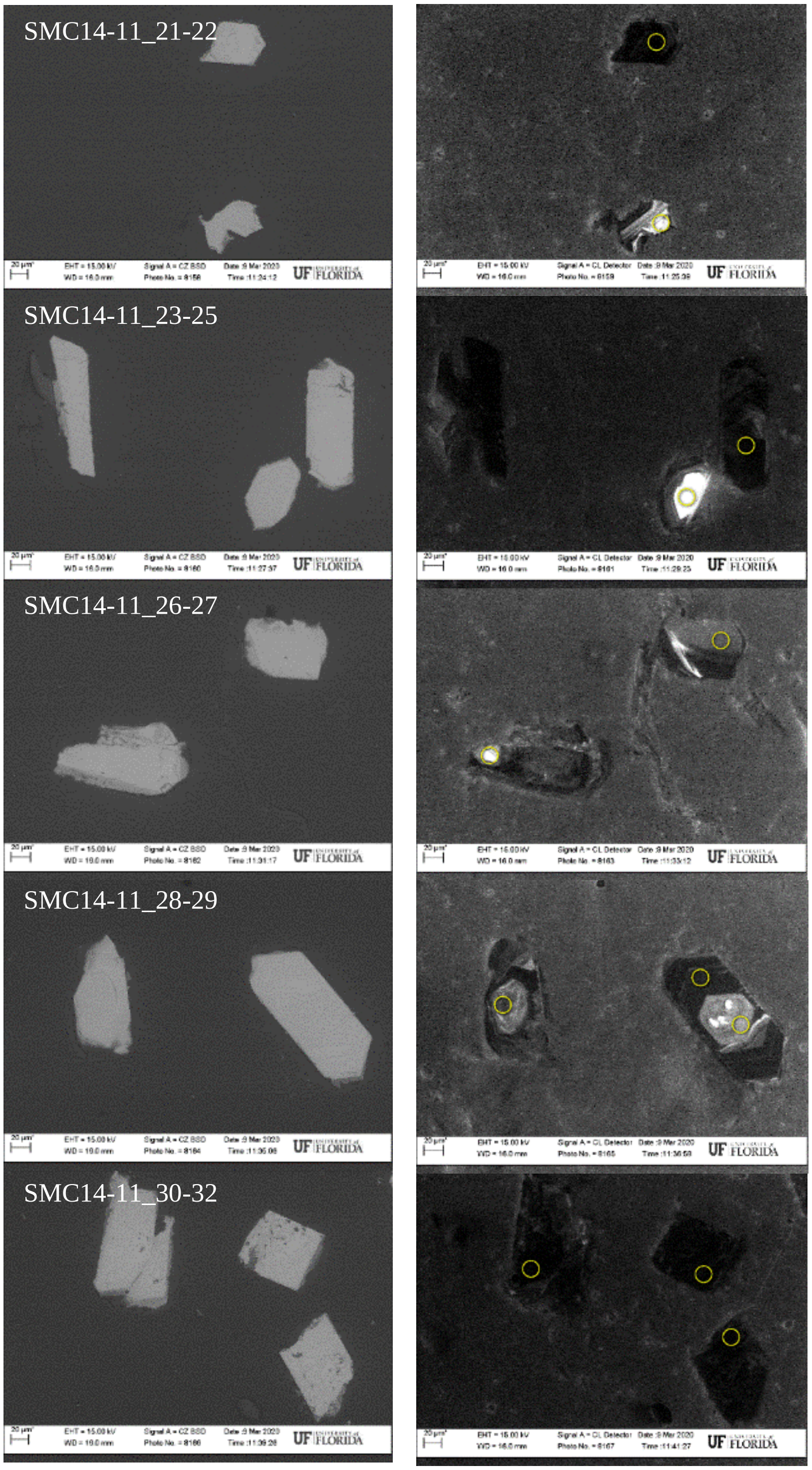
SMC14-11_21-22
SMC14-11_23-25
SMC14-11_26-27
SMC14-11_28-29
SMC14-11_30-32

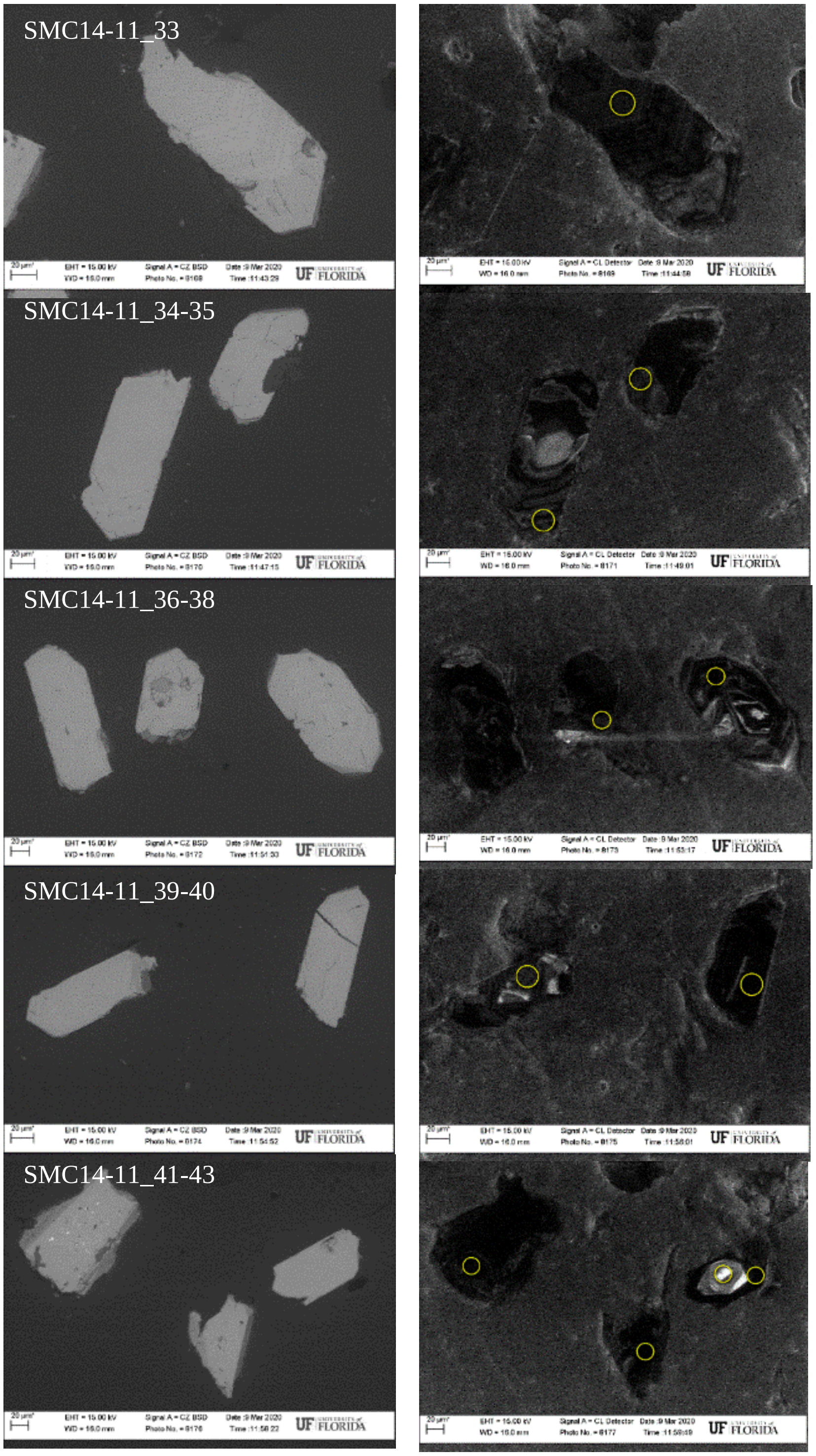
SMC14-11_33
SMC14-11_34-35
SMC14-11_36-38
SMC14-11_39-40
SMC14-11_41-43

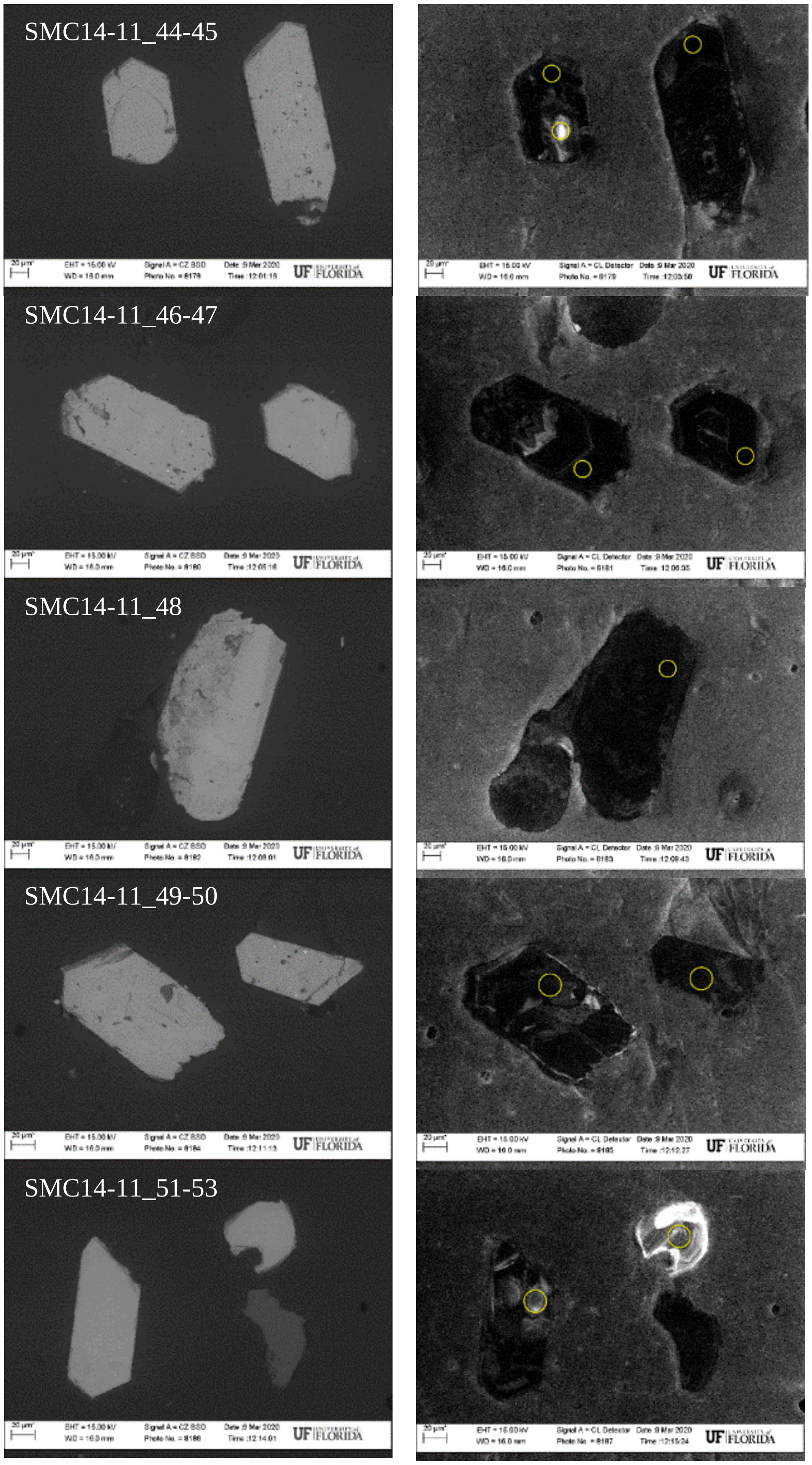
SMC14-11_44-45
SMC14-11_46-47
SMC14-11_48
SMC14-11_49-50
SMC14-11_51-53

SMC14-43

BSE **CL**

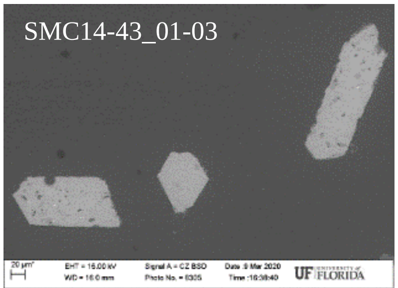

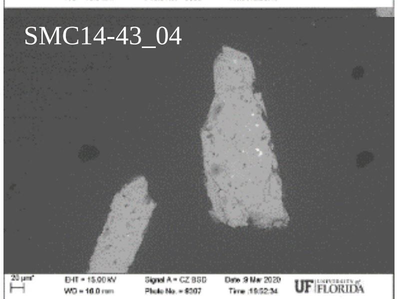

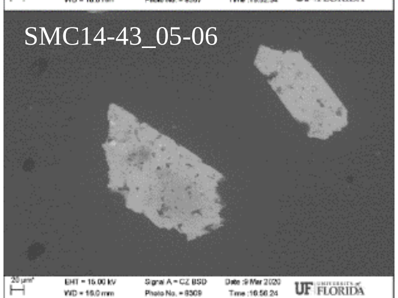

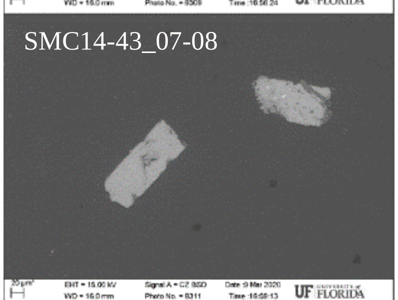

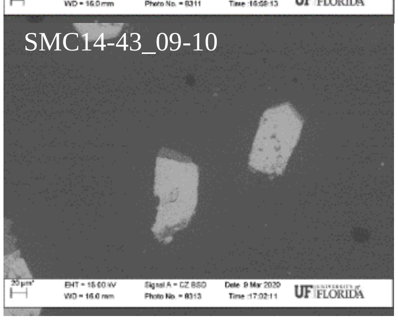

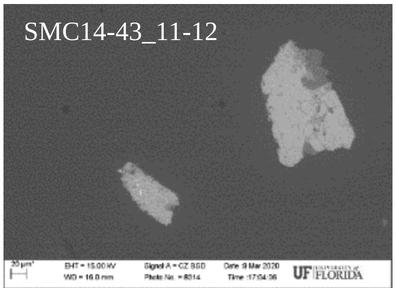
SMC14-43_11-12
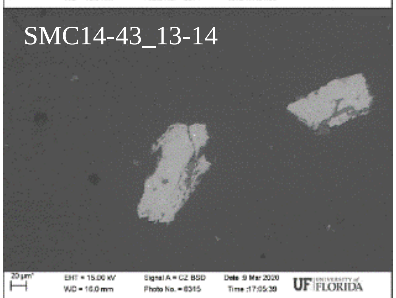
SMC14-43_13-14
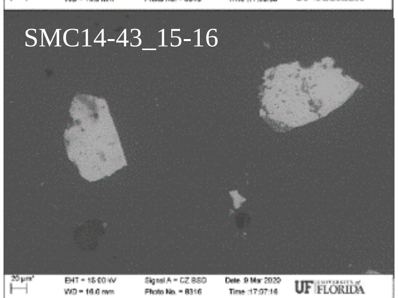
SMC14-43_15-16
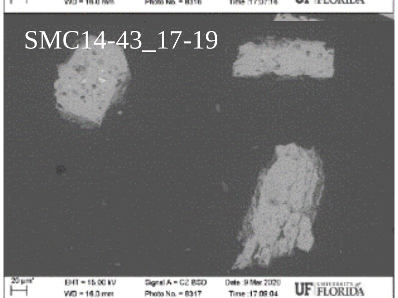
SMC14-43_17-19
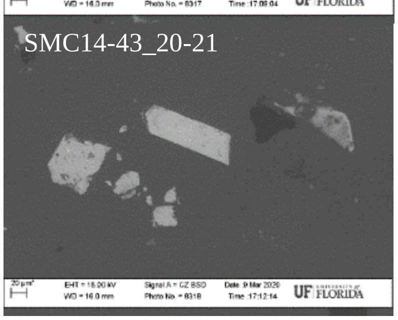
SMC14-43_20-21

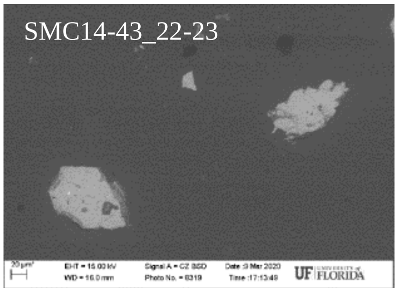
SMC14-43_22-23

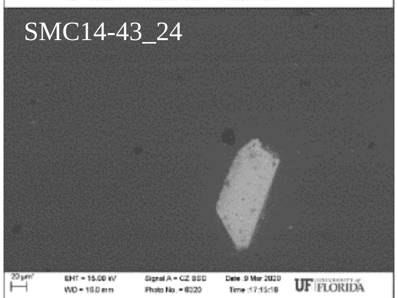
SMC14-43_24


SMC14-43_25-26


SMC14-43_27

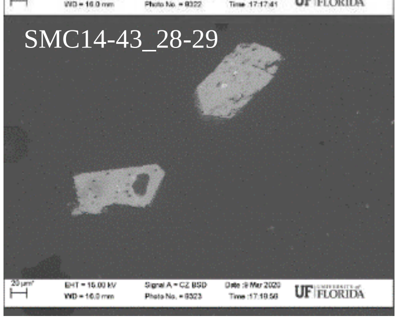
SMC14-43_28-29

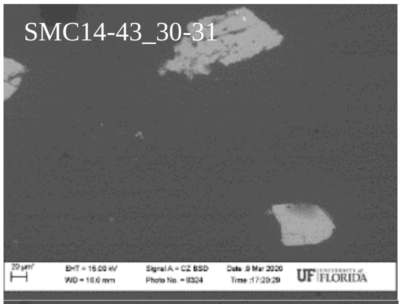
SMC14-43_30-31

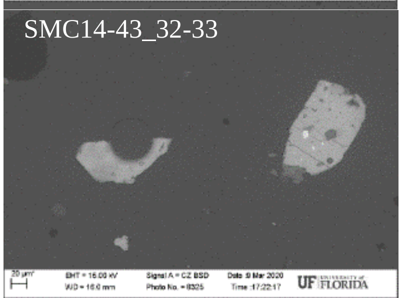
SMC14-43_32-33

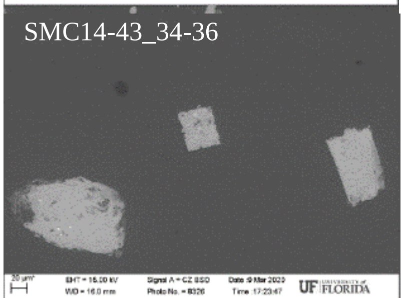
SMC14-43_34-36

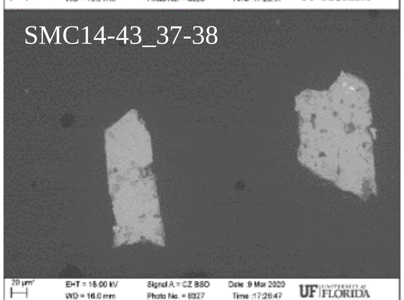
SMC14-43_37-38

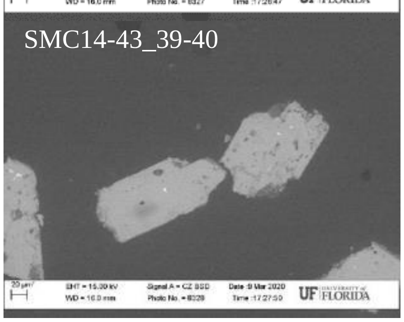
SMC14-43_39-40

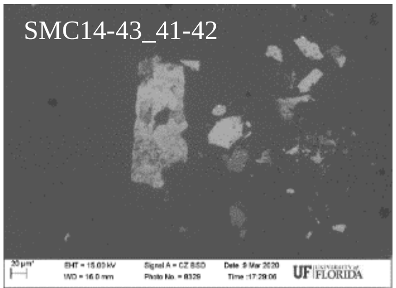
SMC14-43_41-42

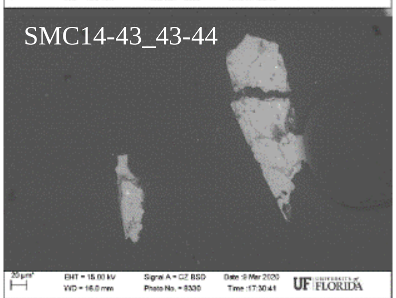
SMC14-43_43-44

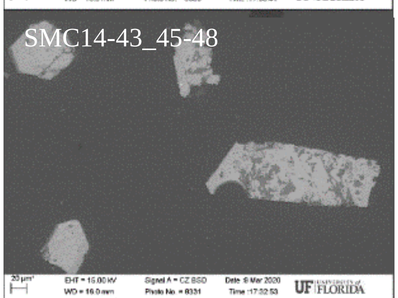
SMC14-43_45-48

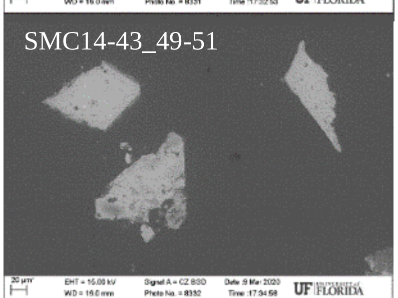
SMC14-43_49-51

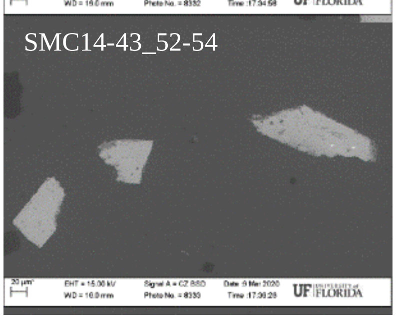
SMC14-43_52-54

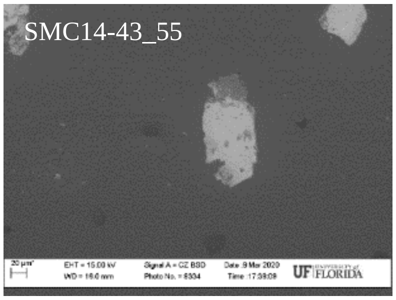
SMC14-43_55
20 µm
EHT = 15.00 kV
WD = 16.0 mm
Signal A = CZ BSD
Photo No. = 8334
Date :9 Mar 2020
Time :17:39:09
UF FLORIDA

SMC15-05

BSE **CL**

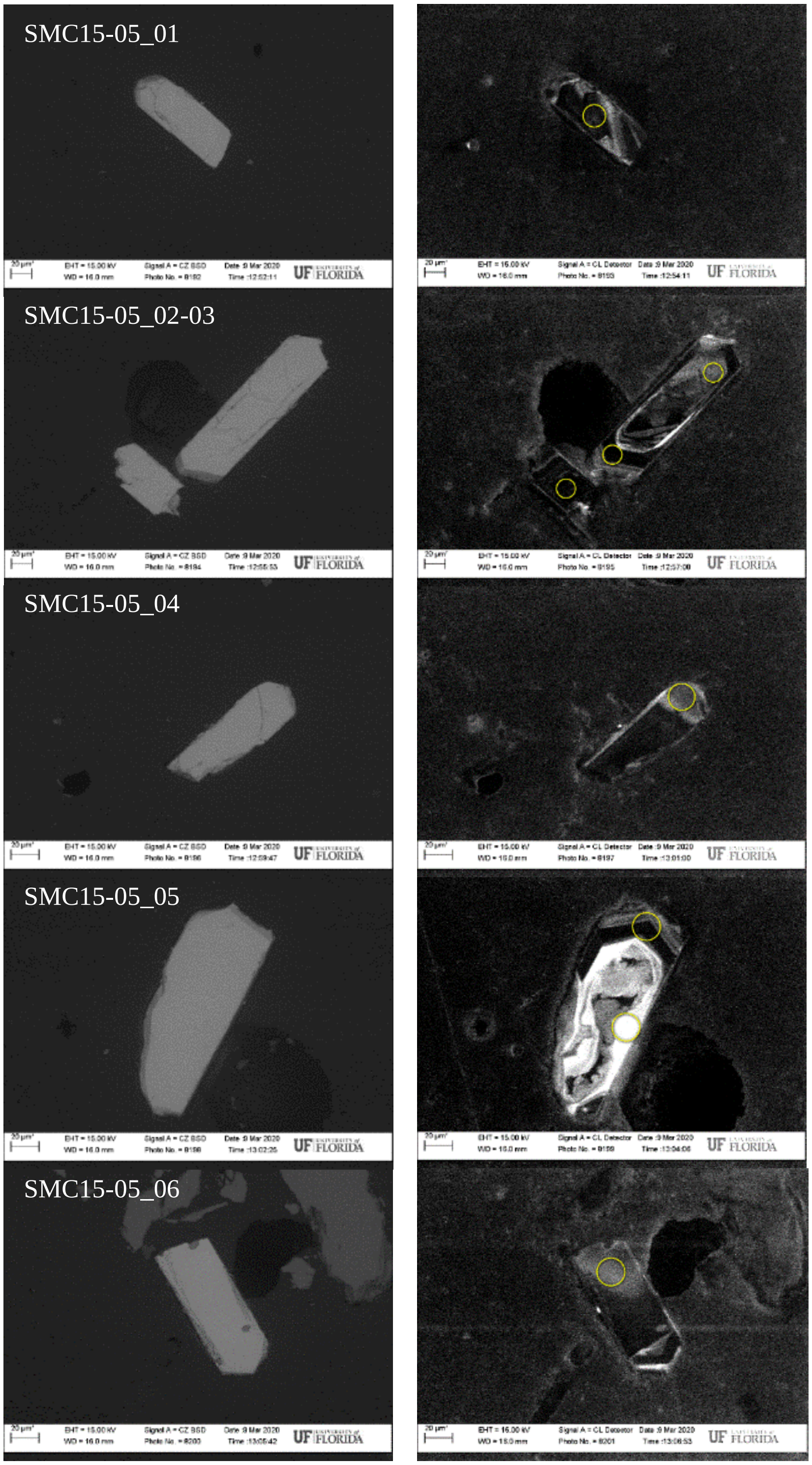

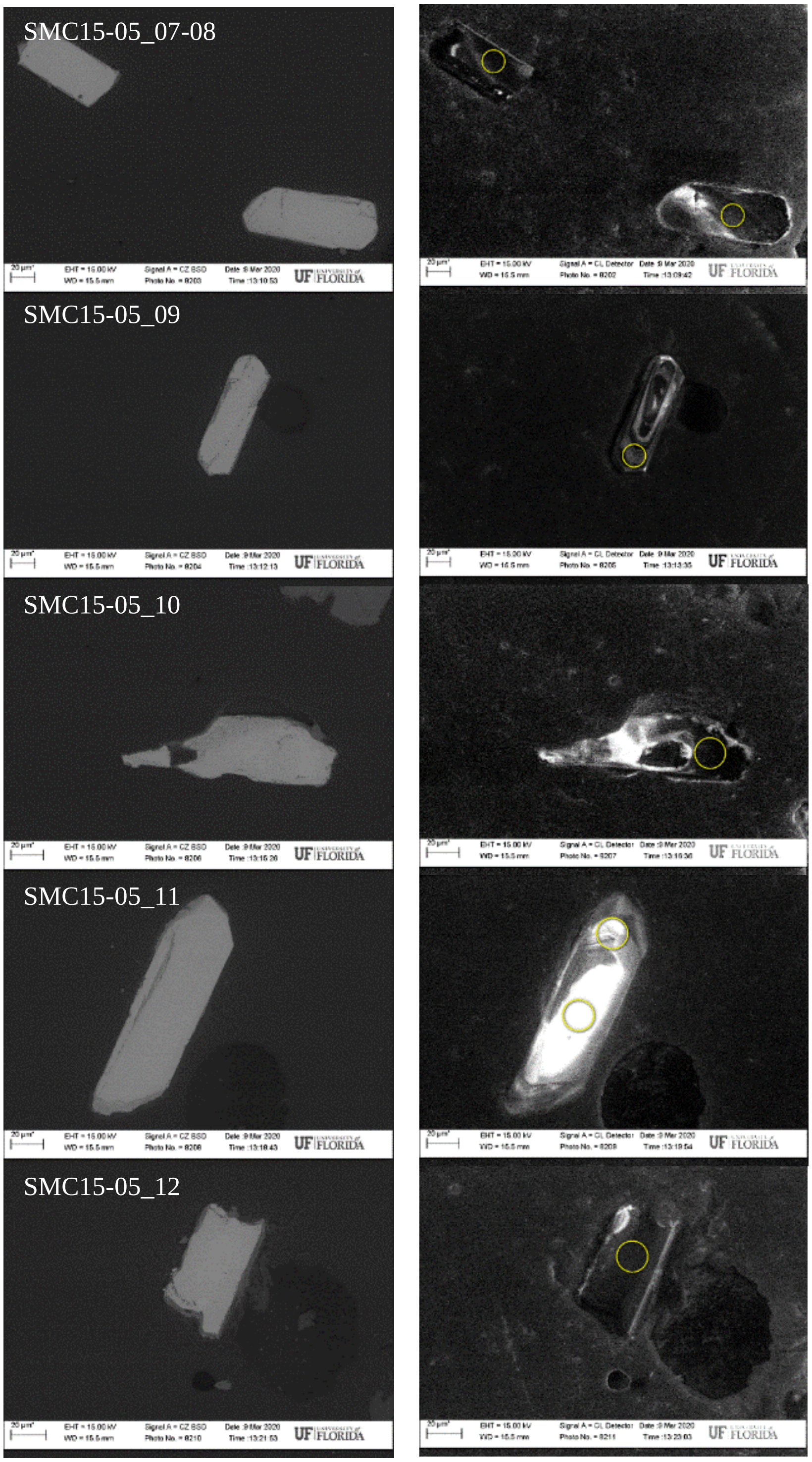
SMC15-05_07-08
SMC15-05_09
SMC15-05_10
SMC15-05_11
SMC15-05_12

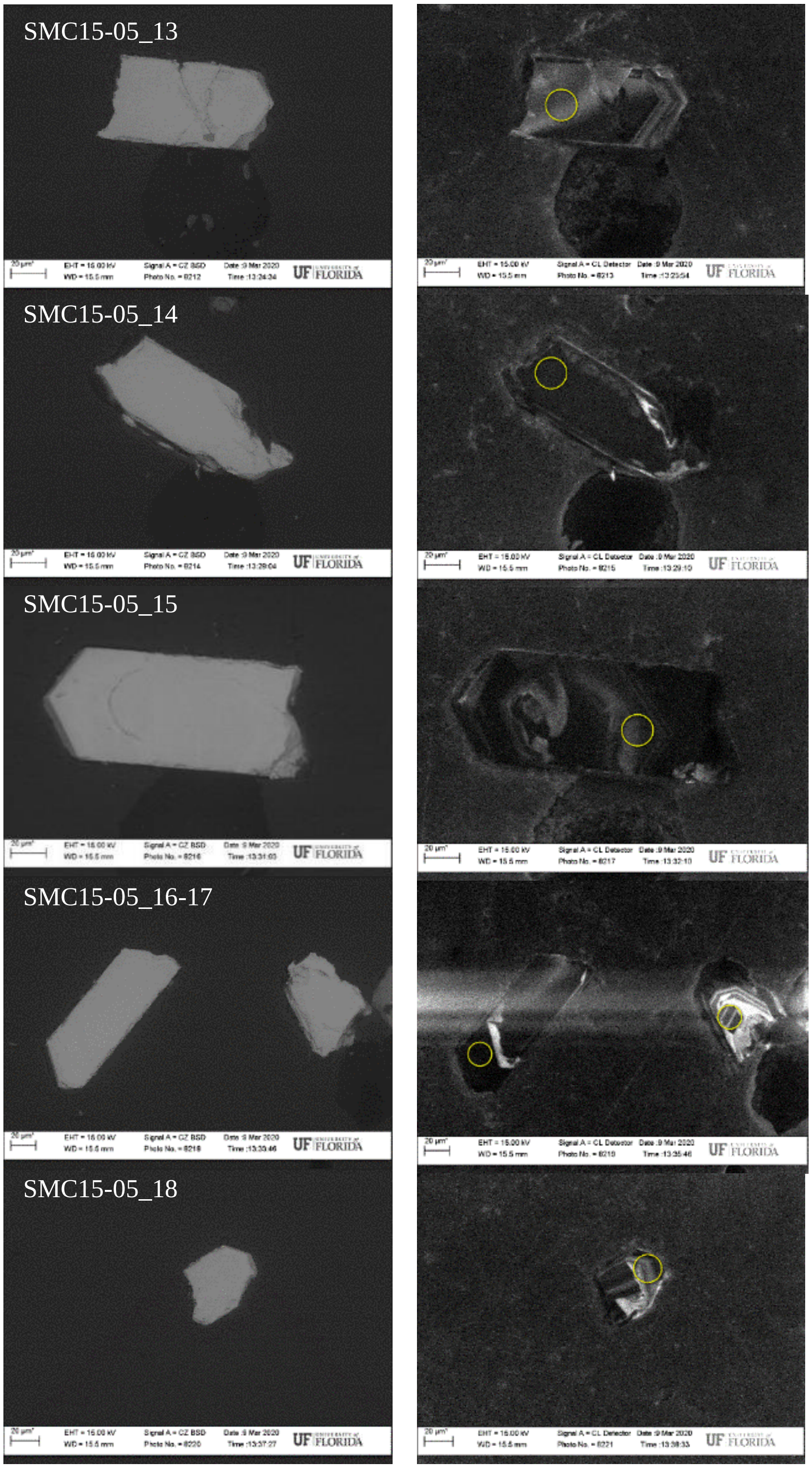
SMC15-05_13
SMC15-05_14
SMC15-05_15
SMC15-05_16-17
SMC15-05_18

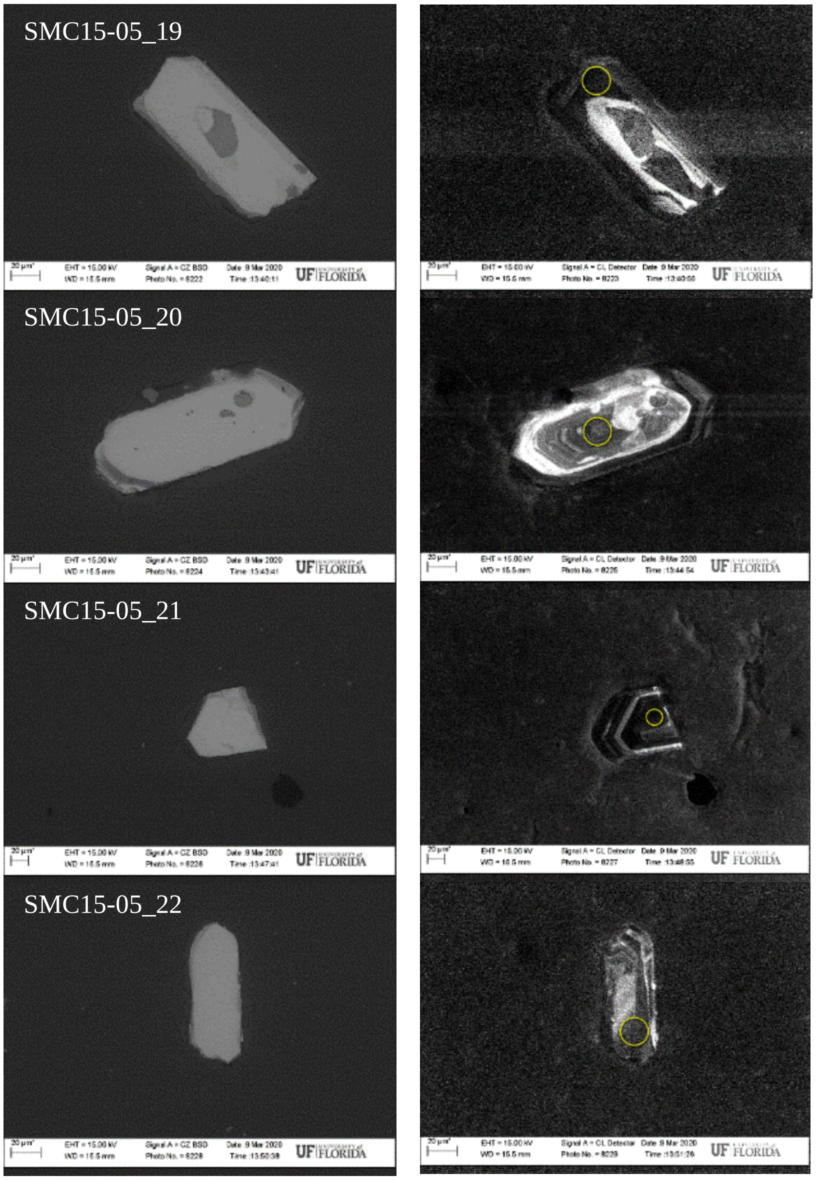
SMC15-05_19
SMC15-05_20
SMC15-05_21
SMC15-05_22

SMC16-09

BSE **CL**

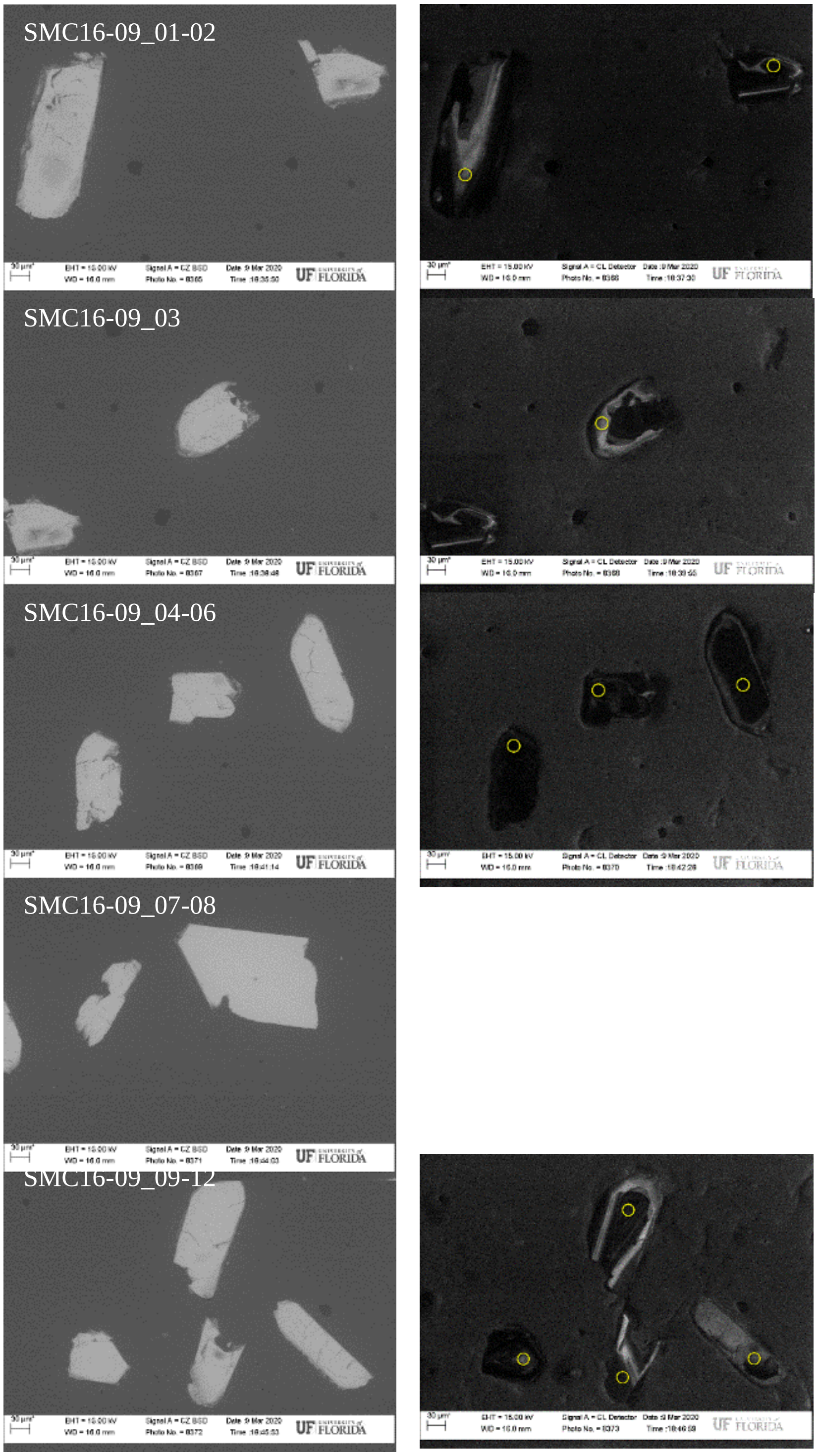

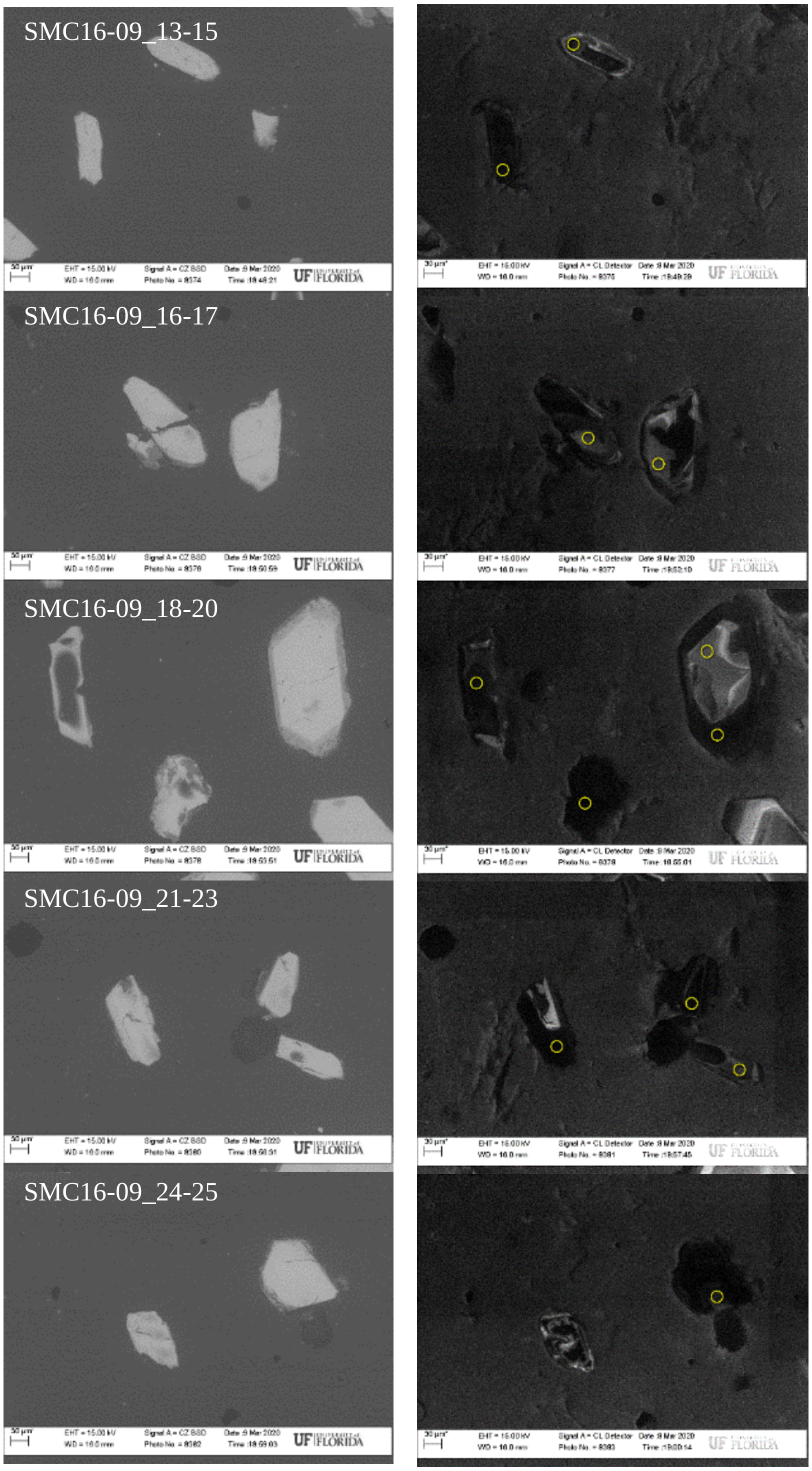
SMC16-09_13-15
SMC16-09_16-17
SMC16-09_18-20
SMC16-09_21-23
SMC16-09_24-25

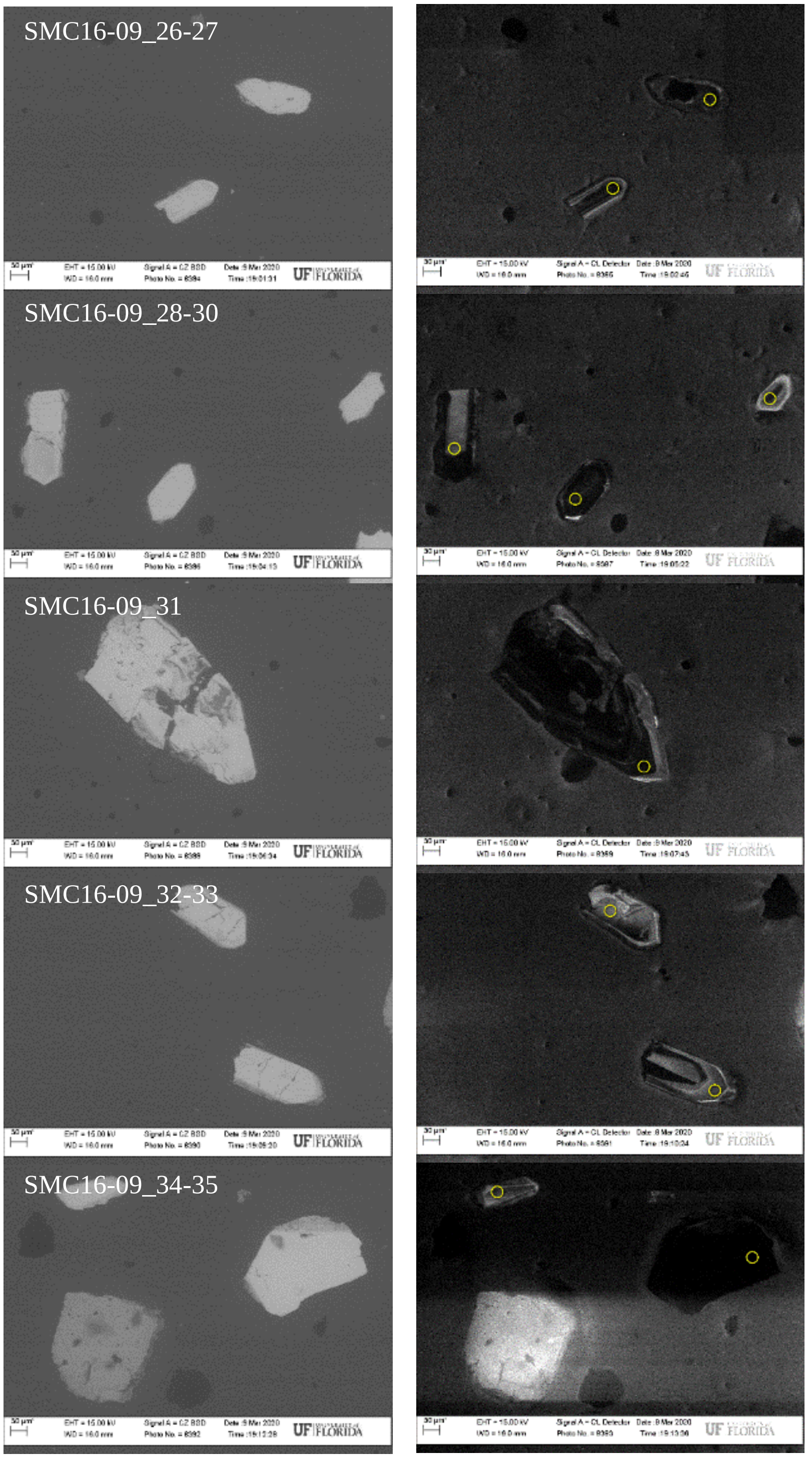
SMC16-09_26-27
SMC16-09_28-30
SMC16-09_31
SMC16-09_32-33
SMC16-09_34-35

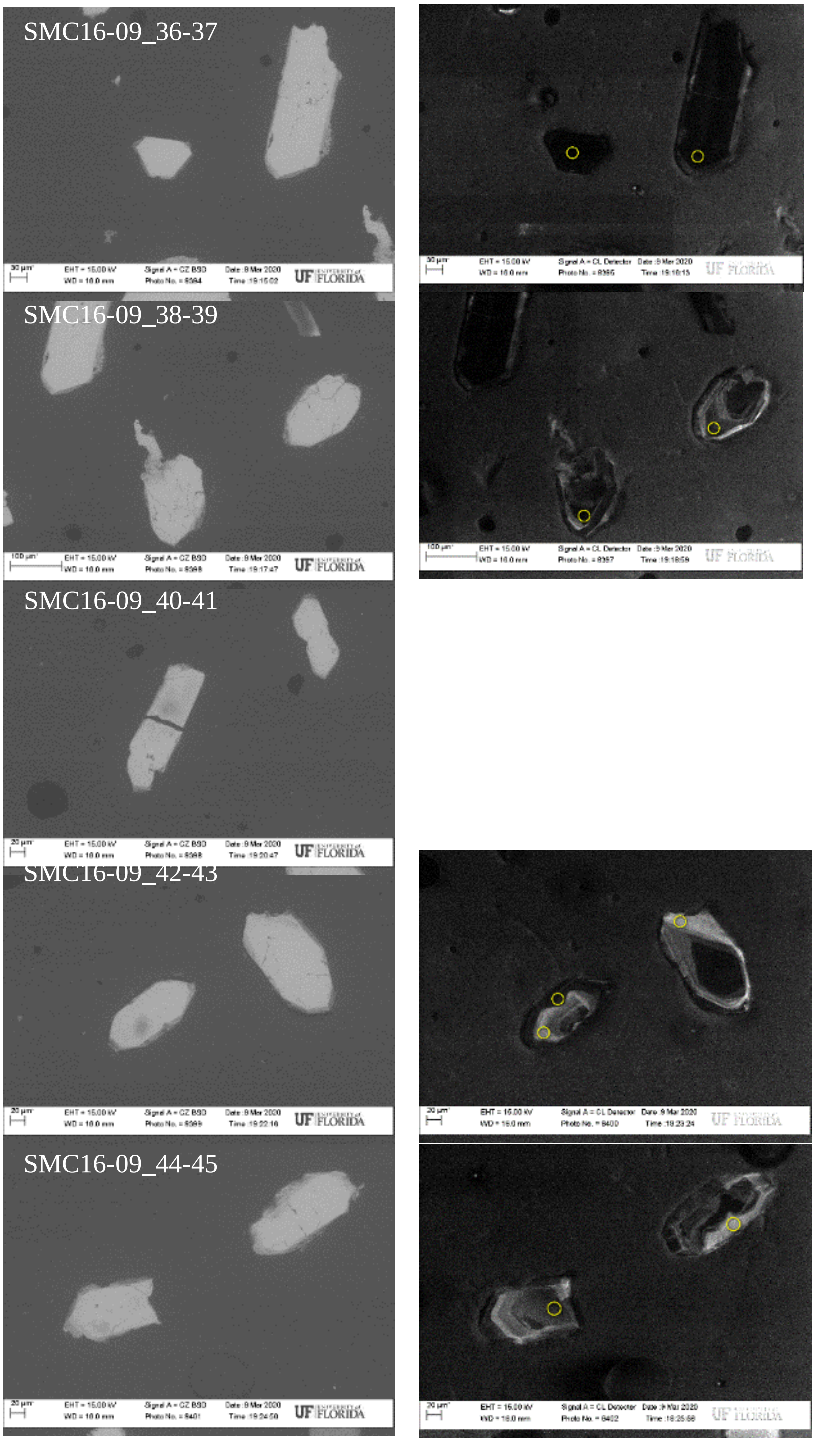
SMC16-09_36-37
SMC16-09_38-39
SMC16-09_40-41
SMC16-09_42-43
SMC16-09_44-45

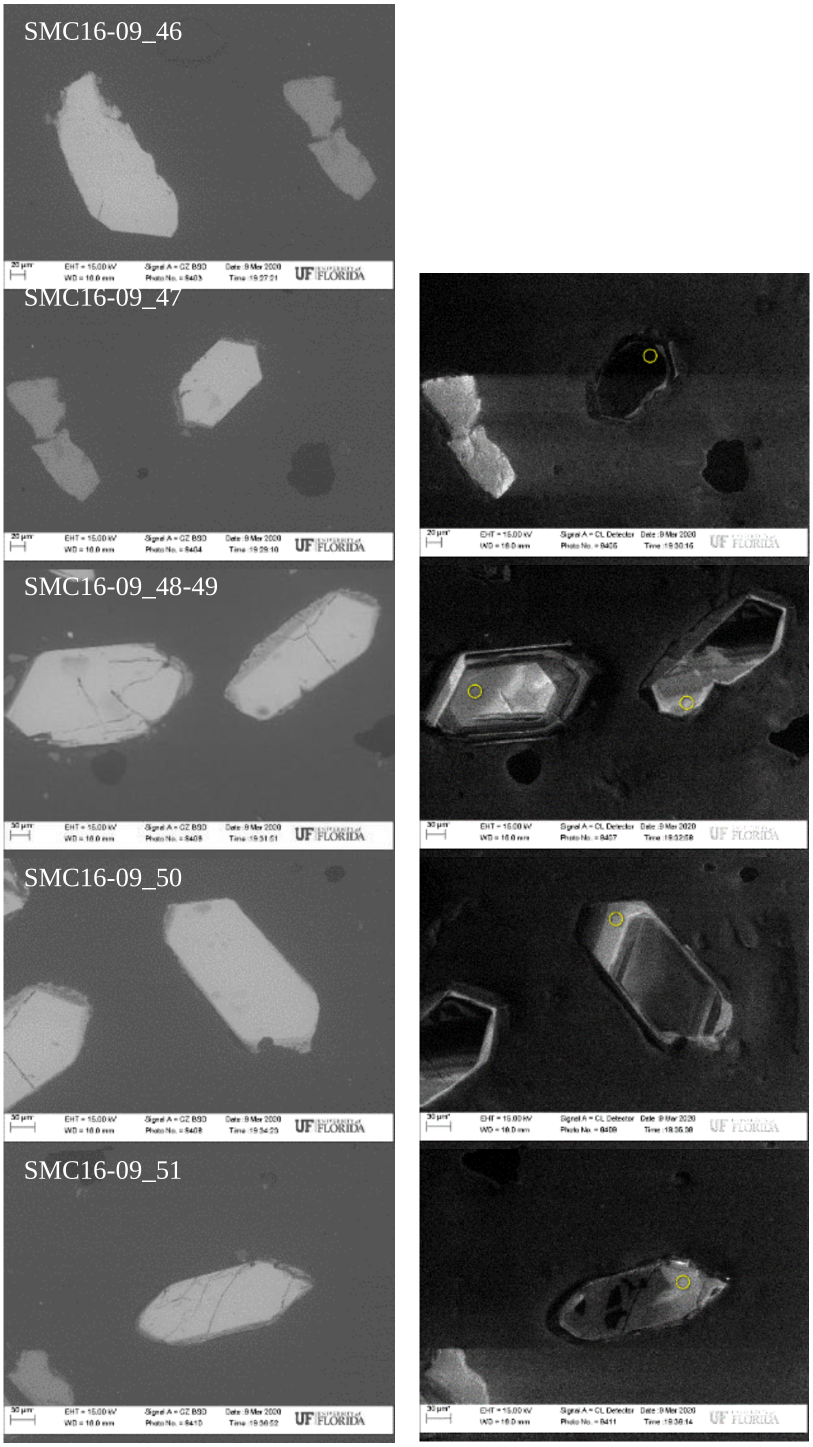
SMC16-09_46
SMC16-09_47
SMC16-09_48-49
SMC16-09_50
SMC16-09_51

SMC16-22

BSE **CL**

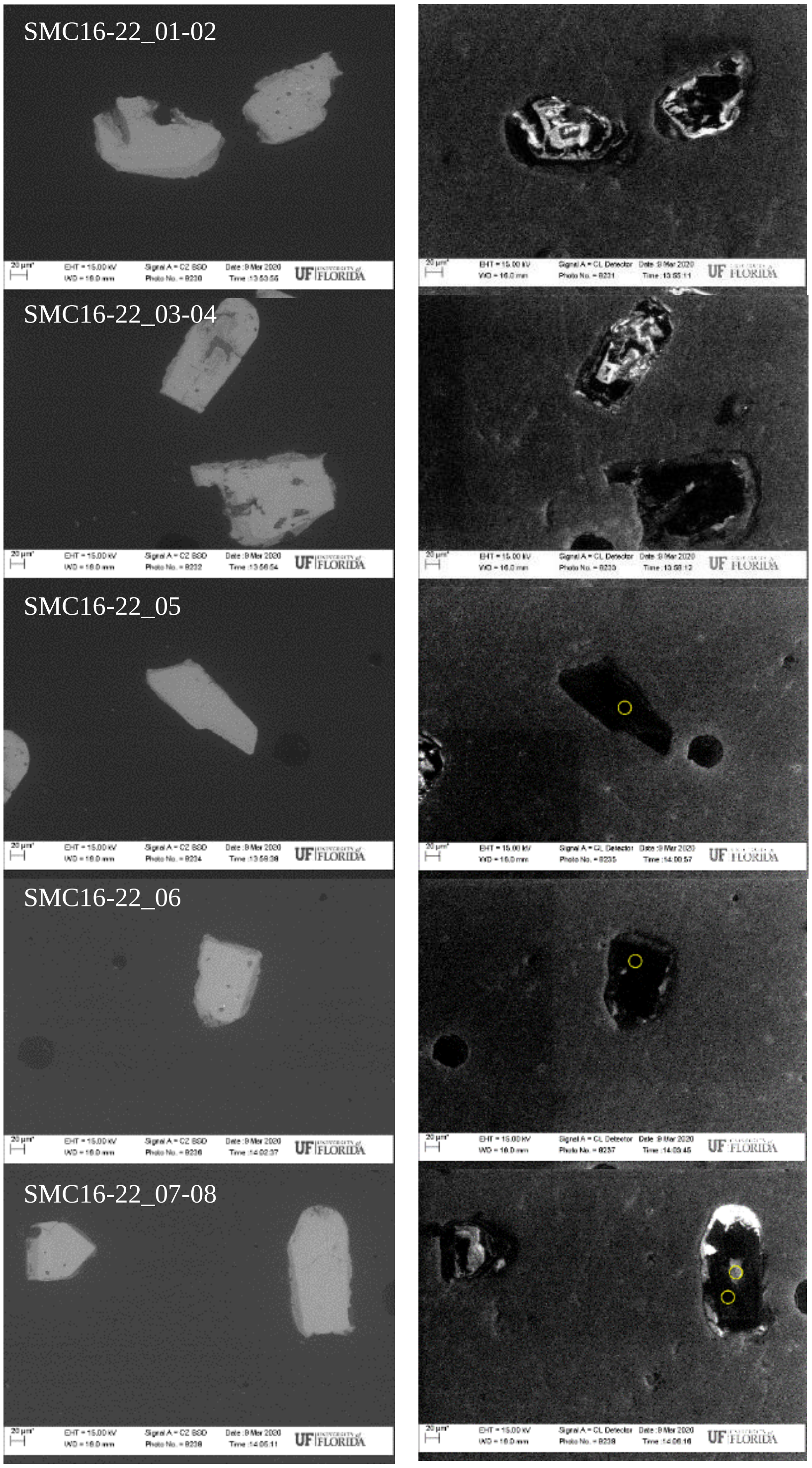

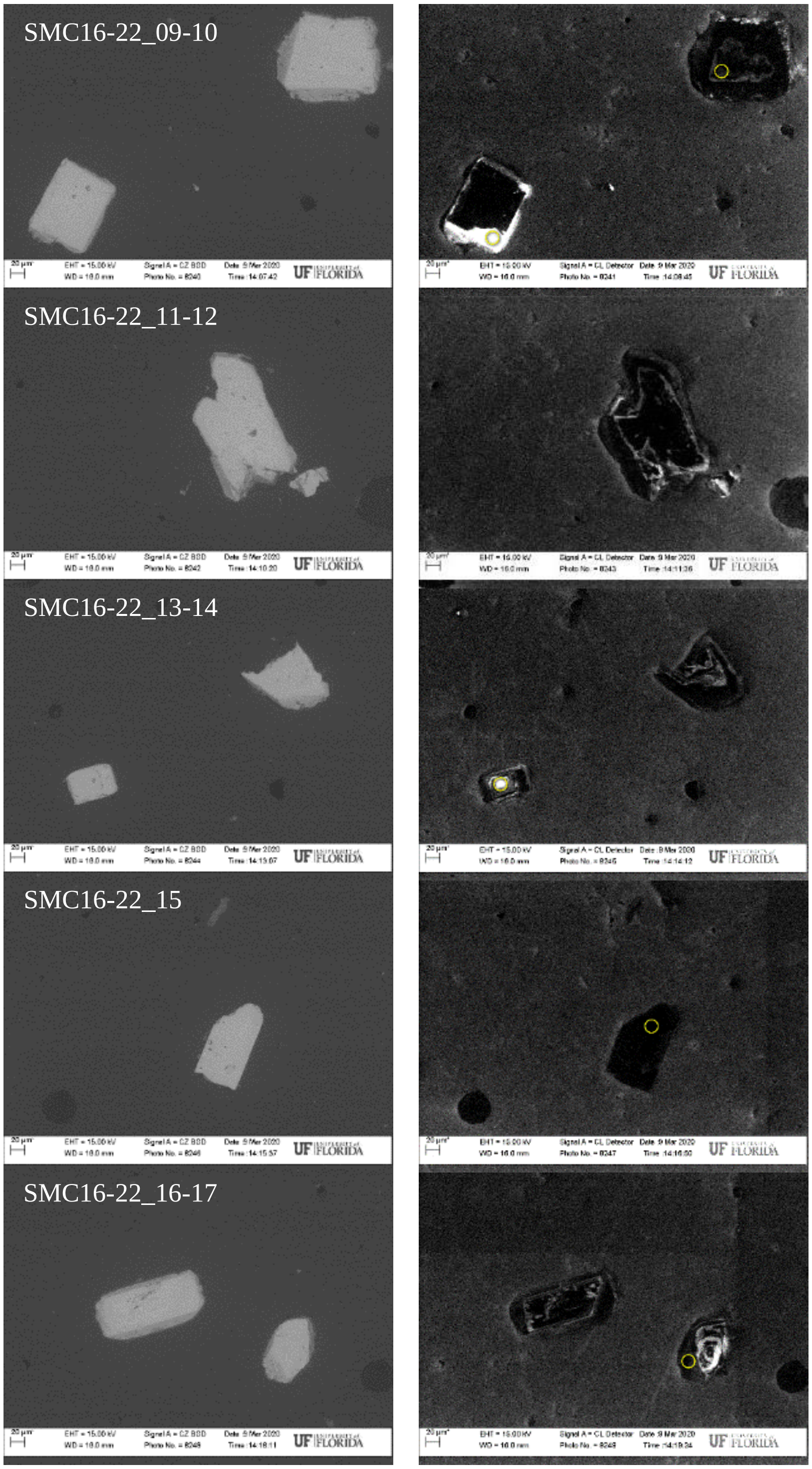
SMC16-22_09-10
SMC16-22_11-12
SMC16-22_13-14
SMC16-22_15
SMC16-22_16-17

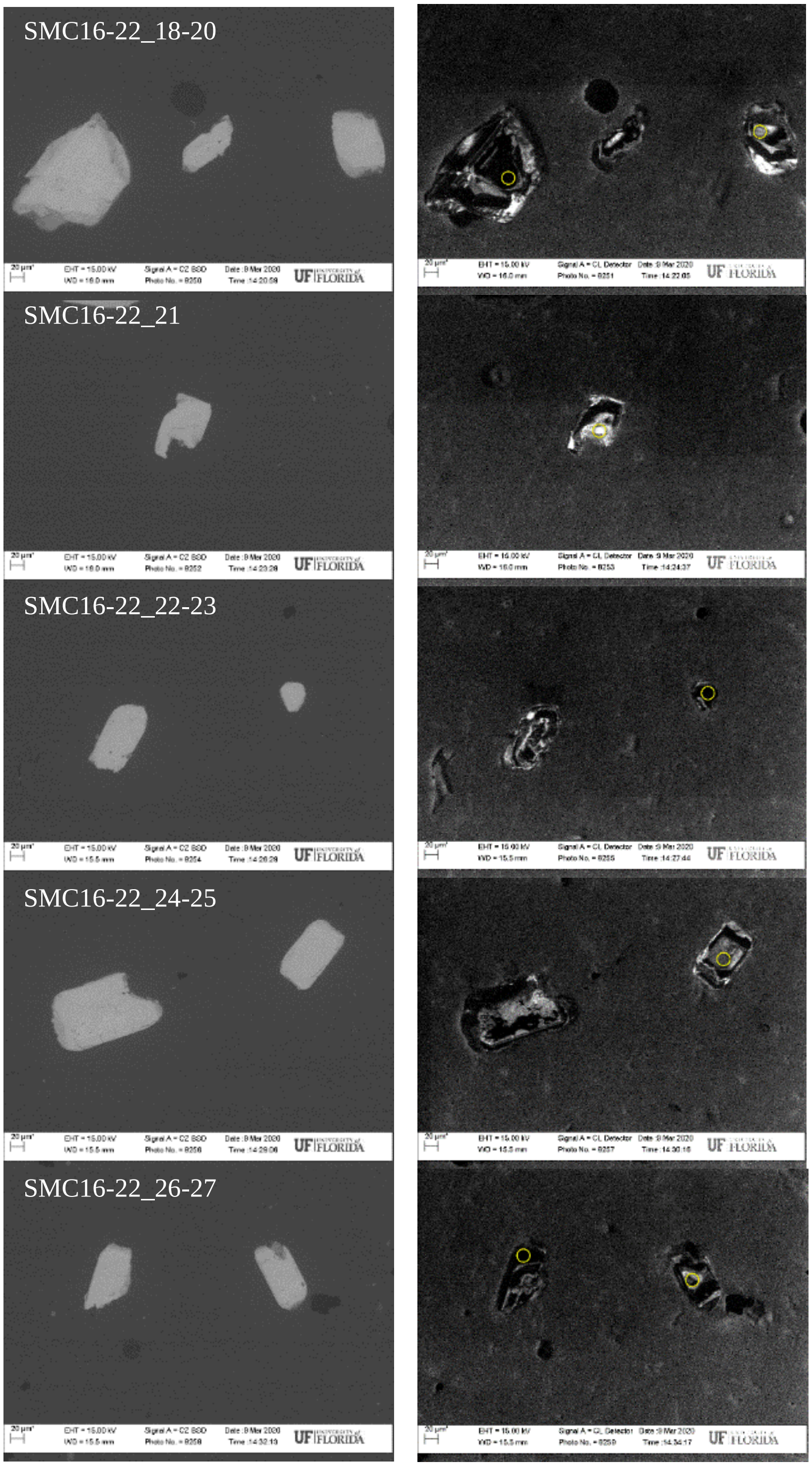
SMC16-22_18-20
SMC16-22_21
SMC16-22_22-23
SMC16-22_24-25
SMC16-22_26-27

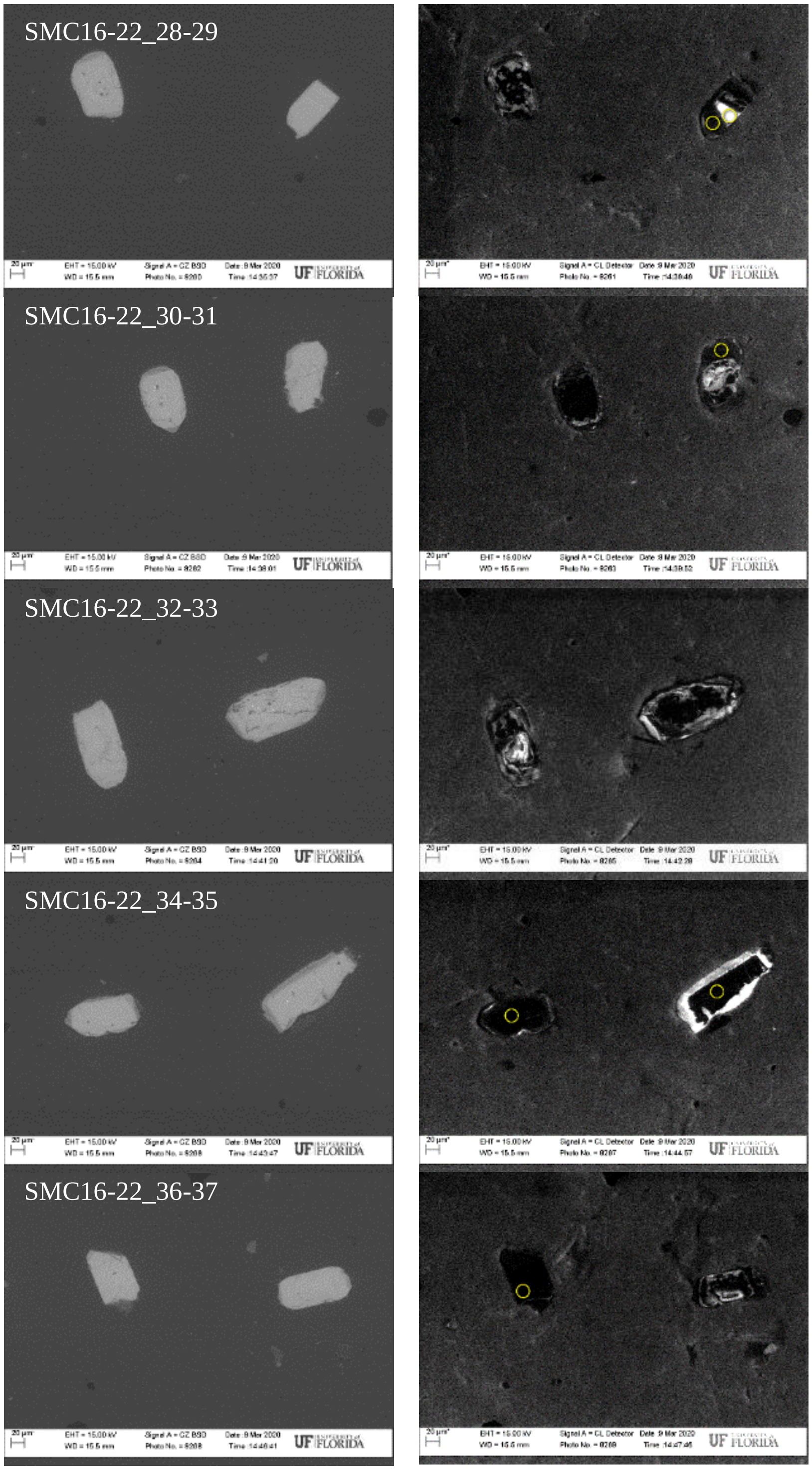
SMC16-22_28-29
SMC16-22_30-31
SMC16-22_32-33
SMC16-22_34-35
SMC16-22_36-37

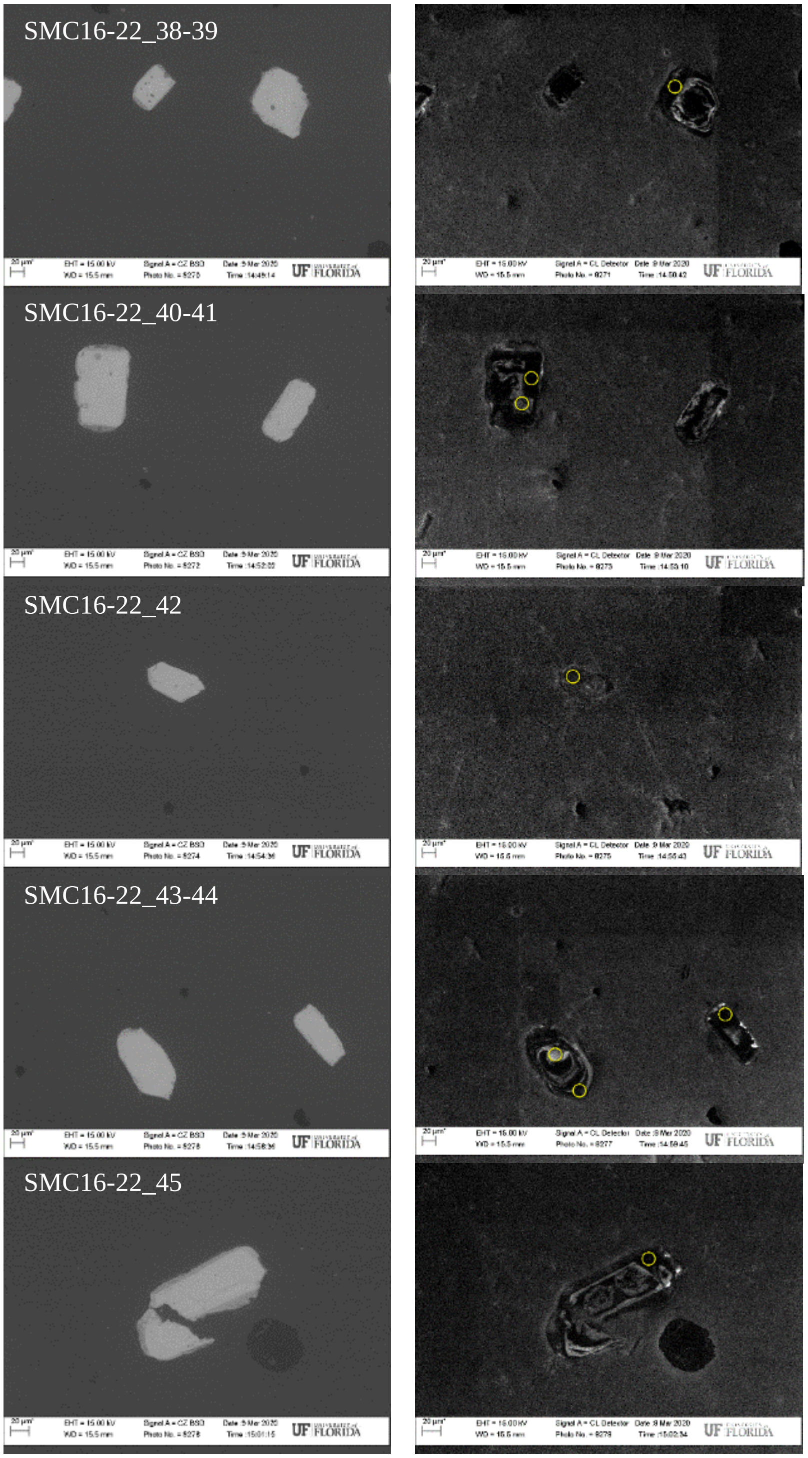
SMC16-22_38-39
SMC16-22_40-41
SMC16-22_42
SMC16-22_43-44
SMC16-22_45

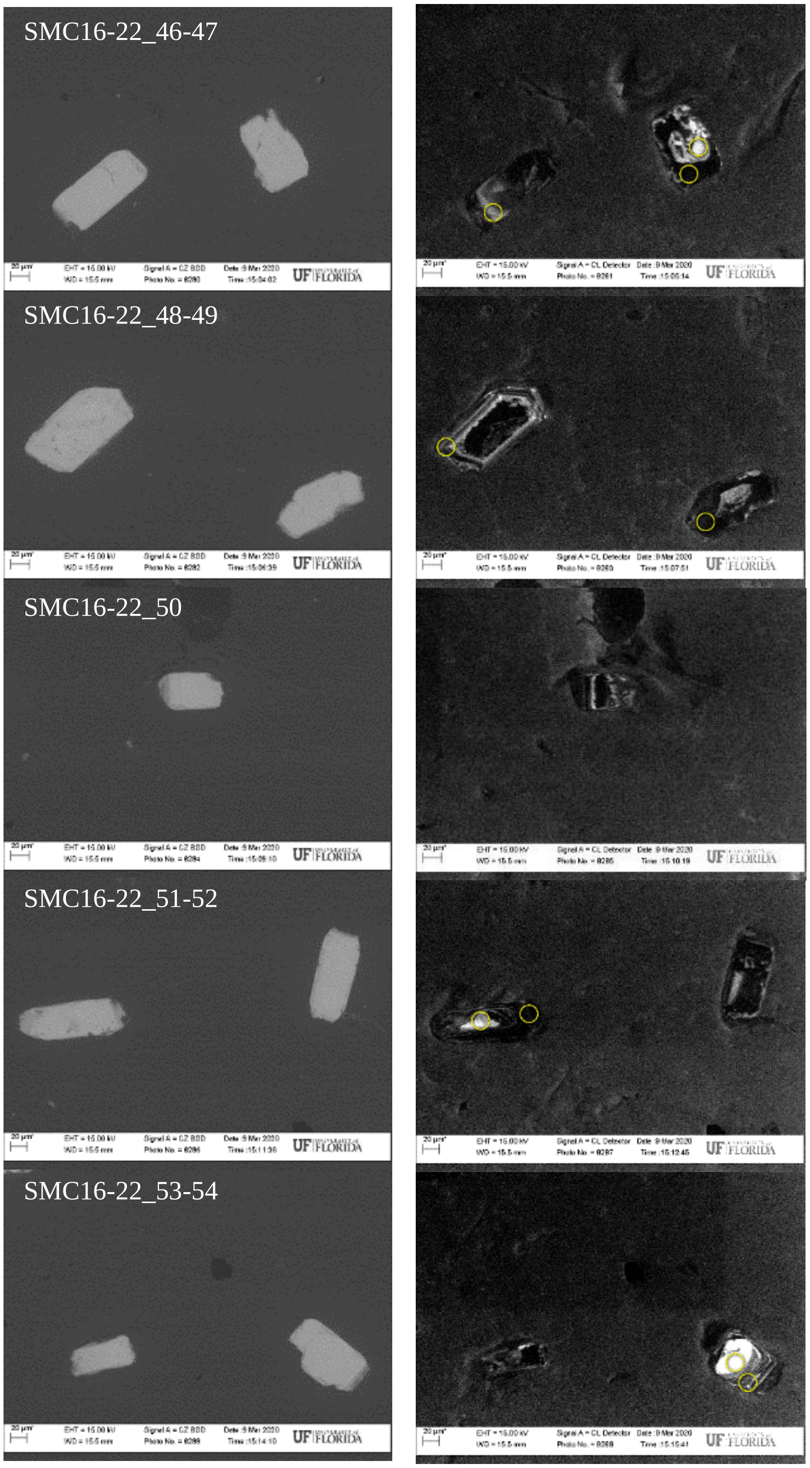
SMC16-22_46-47
SMC16-22_48-49
SMC16-22_50
SMC16-22_51-52
SMC16-22_53-54

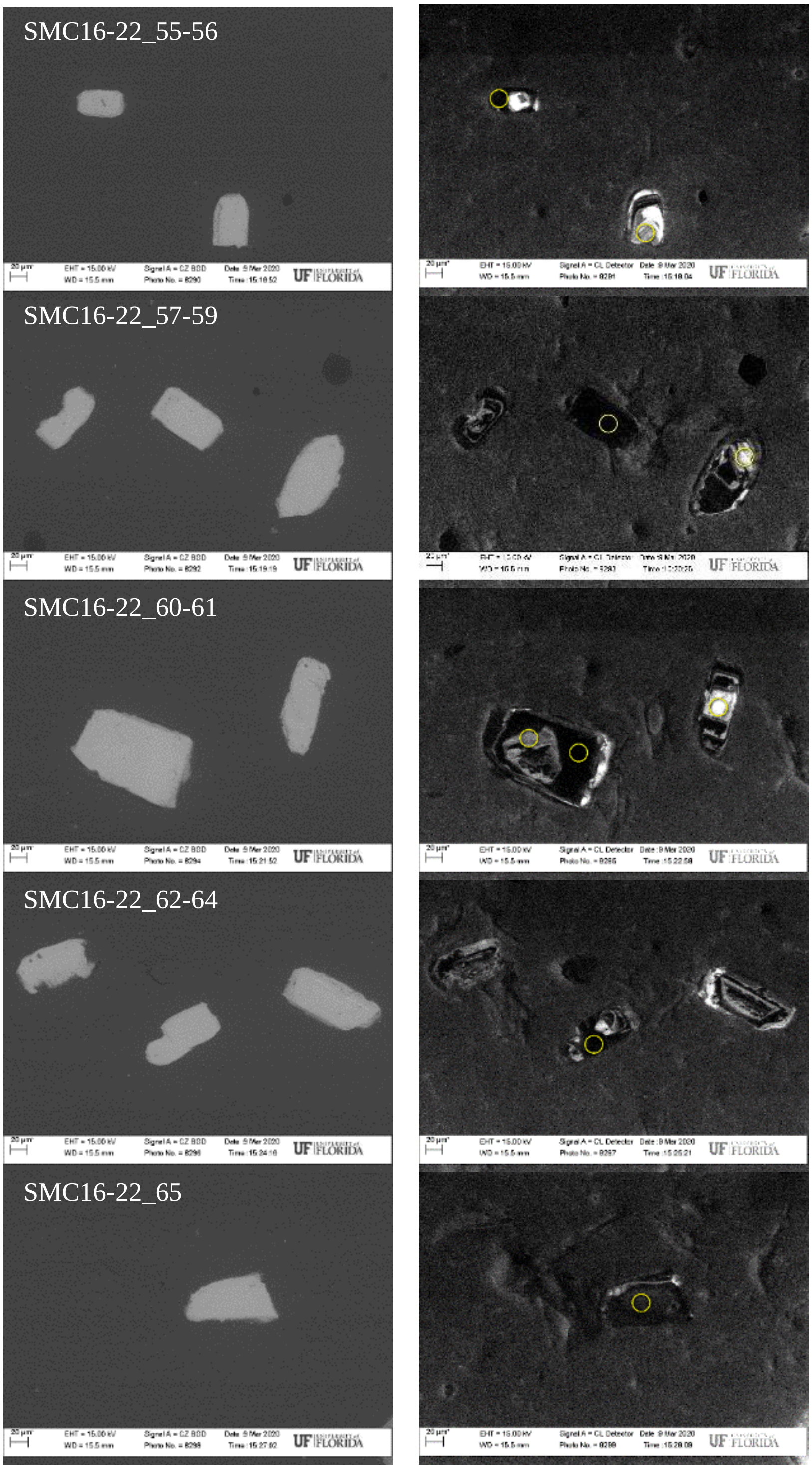
SMC16-22_55-56
SMC16-22_57-59
SMC16-22_60-61
SMC16-22_62-64
SMC16-22_65

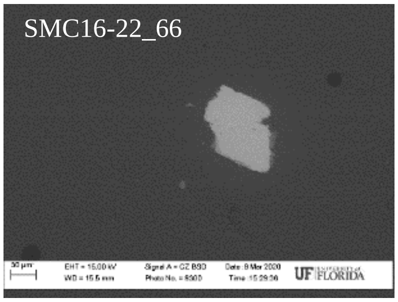
SMC16-22_66
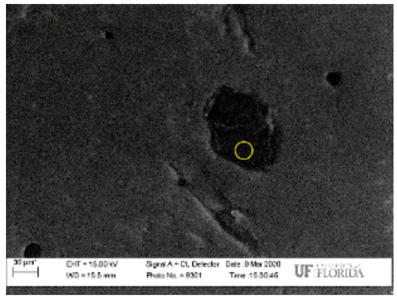

APPENDIX E. REDUCED U-PB ISOTOPE GEOCHRONOLOGY DATA

							Apparent Ages (Ma)						Percent	Percent	
Spot Name	207Pb / 235U Ratio	207Pb / 235U 2 SE	206Pb / 238U Ratio	206Pb / 238U 2 SE	207Pb / 206Pb Ratio	207Pb / 206Pb 2 SE	207Pb / 235U Ma	207Pb / 235U 2 SE	206Pb / 238U Ma	206Pb / 238U 2 SE	207Pb / 206Pb Ma	207Pb / 206Pb 2 SE	Discordance 207Pb/235U vs 206Pb/238U	Discordance 207Pb/206Pb vs 206Pb/238U	Th/U Ratio
SMC13-132															
13132-01A	0.0989	0.0037	0.0150	0.0002	0.0482	0.0017	95.7	3.3	96.1	1.5	94.0	65.0	-0.42%	-47.85%	0.08
13132-01A-b	0.7560	0.0460	0.0201	0.0006	0.2740	0.0120	570.0	26.0	128.0	3.9	3318.0	70.0	77.54%	-82.86%	0.10
13132-01B	0.0924	0.0011	0.0140	0.0002	0.0479	0.0008	89.8	1.0	89.9	1.1	92.0	38.0	-0.11%	-136.45%	0.21
13132-02A	0.0904	0.0019	0.0138	0.0002	0.0477	0.0011	87.8	1.8	88.2	1.5	84.0	51.0	-0.46%	-72.94%	0.06
13132-02B	0.0931	0.0014	0.0141	0.0002	0.0481	0.0009	90.3	1.3	90.5	1.3	100.0	40.0	-0.22%	-126.25%	0.14
13132-03A	0.0877	0.0026	0.0131	0.0002	0.0484	0.0013	85.3	2.4	84.0	1.5	112.0	58.0	1.52%	-44.83%	0.06
13132-03B	0.0940	0.0014	0.0143	0.0002	0.0476	0.0009	91.2	1.3	91.7	1.2	78.0	42.0	-0.55%	-118.33%	0.18
13132-04A	0.0948	0.0019	0.0144	0.0002	0.0476	0.0011	91.9	1.8	91.8	1.3	78.0	50.0	0.11%	-83.60%	0.08
13132-04B	0.1093	0.0022	0.0163	0.0003	0.0484	0.0009	105.3	2.0	104.4	2.0	115.0	43.0	0.85%	-142.79%	0.27
13132-05A	0.1080	0.0019	0.0163	0.0002	0.0478	0.0011	104.1	1.7	104.4	1.4	85.0	50.0	-0.29%	-108.80%	0.09
13132-05B	0.1100	0.0017	0.0165	0.0002	0.0484	0.0008	105.9	1.5	105.3	1.3	114.0	39.0	0.57%	-170.00%	0.23
13132-06A	0.1079	0.0019	0.0164	0.0003	0.0482	0.0008	104.0	1.7	104.9	1.6	107.0	37.0	-0.87%	-183.51%	0.09
13132-06B	0.1081	0.0023	0.0163	0.0003	0.0478	0.0009	104.2	2.1	104.3	1.9	88.0	43.0	-0.10%	-142.56%	0.13
13132-07A	0.1068	0.0025	0.0164	0.0004	0.0475	0.0012	103.0	2.3	104.6	2.4	72.0	54.0	-1.55%	-93.70%	0.17
13132-07B	0.0943	0.0019	0.0134	0.0002	0.0511	0.0009	91.4	1.8	85.8	1.5	240.0	41.0	6.13%	-109.27%	0.23
13132-09A	0.0948	0.0017	0.0143	0.0002	0.0481	0.0010	92.0	1.6	91.7	1.4	107.0	45.0	0.33%	-103.78%	0.08
13132-09B	0.1093	0.0044	0.0136	0.0002	0.0587	0.0024	105.2	4.0	87.1	1.1	512.0	79.0	17.21%	-10.24%	0.14
13132-09B-b	0.1197	0.0094	0.0138	0.0003	0.0628	0.0041	114.4	8.4	88.5	1.8	640.0	130.0	22.64%	31.92%	0.07
13132-10A	0.0928	0.0029	0.0138	0.0003	0.0481	0.0015	90.0	2.7	88.3	1.6	109.0	72.0	1.89%	-22.64%	0.07
13132-10B	0.1077	0.0060	0.0137	0.0002	0.0574	0.0032	103.6	5.4	87.9	1.5	460.0	110.0	15.15%	20.09%	0.14
13132-11A	0.0890	0.0012	0.0135	0.0002	0.0480	0.0008	86.5	1.1	86.4	1.1	95.0	36.0	0.12%	-140.00%	0.11
13132-11B	0.0891	0.0014	0.0137	0.0002	0.0474	0.0008	86.8	1.3	87.4	1.2	69.0	37.0	-0.67%	-136.16%	0.10

Spot Name	207Pb/235U Ratio	207Pb/235U 2 SE	206Pb/238U Ratio	206Pb/238U 2 SE	207Pb/206Pb Ratio	207Pb/206Pb 2 SE	Apparent Ages (Ma) 207Pb/235U Ma	207Pb/235U 2 SE	206Pb/238U Ma	206Pb/238U 2 SE	207Pb/206Pb Ma	207Pb/206Pb 2 SE	Percent Discordance 207Pb/235U vs 206Pb/238U	Percent Discordance 207Pb/206Pb vs 206Pb/238U	Th/U Ratio
SMC13-132															
13132-12	0.0910	0.0011	0.0138	0.0002	0.0480	0.0008	88.4	1.0	88.1	1.2	97.0	39.0	0.33%	-125.97%	0.14
13132-13A	0.1034	0.0022	0.0157	0.0003	0.0481	0.0011	99.8	2.0	100.4	1.7	109.0	53.0	-0.60%	-89.43%	0.14
13132-13B	0.0903	0.0038	0.0138	0.0003	0.0473	0.0019	87.8	3.5	88.5	1.6	81.0	89.0	-0.80%	0.56%	0.13
13132-14	0.0908	0.0020	0.0138	0.0002	0.0480	0.0011	88.2	1.9	88.3	1.3	97.0	51.0	-0.11%	-73.14%	0.07
13132-16A	0.0897	0.0015	0.0137	0.0003	0.0473	0.0011	87.2	1.4	87.4	1.7	64.0	52.0	-0.23%	-68.08%	0.07
13132-16B	0.1101	0.0027	0.0145	0.0002	0.0553	0.0016	106.0	2.5	92.8	1.4	408.0	66.0	12.45%	-40.61%	0.09
13132-17	0.0974	0.0016	0.0145	0.0002	0.0483	0.0008	94.3	1.4	92.7	1.2	112.0	40.0	1.70%	-131.75%	0.09
13132-18	0.0910	0.0019	0.0137	0.0002	0.0482	0.0011	88.4	1.8	87.8	1.6	104.0	52.0	0.68%	-68.85%	0.06
13132-19	0.1319	0.0055	0.0151	0.0002	0.0637	0.0027	125.6	4.9	96.8	1.3	677.0	93.0	22.91%	-4.11%	0.19
13132-20	0.0967	0.0023	0.0144	0.0003	0.0485	0.0011	93.7	2.1	92.4	1.6	126.0	52.0	1.39%	-77.69%	0.10
13132-22A	0.0912	0.0012	0.0138	0.0002	0.0478	0.0008	88.6	1.1	88.5	1.3	85.0	39.0	0.09%	-126.97%	0.08
13132-22B	0.0906	0.0018	0.0136	0.0002	0.0488	0.0010	88.1	1.7	87.0	1.4	136.0	48.0	1.25%	-81.25%	0.09
13132-23	0.0888	0.0016	0.0135	0.0002	0.0484	0.0010	86.4	1.5	86.5	1.4	112.0	45.0	-0.12%	-92.22%	0.09
13132-24A	0.0899	0.0019	0.0136	0.0002	0.0475	0.0010	87.4	1.8	87.3	1.4	73.0	48.0	0.11%	-81.88%	0.09
13132-24B	0.0868	0.0015	0.0132	0.0002	0.0476	0.0009	84.5	1.4	84.2	1.2	78.0	42.0	0.37%	-100.45%	0.11
13132-25	0.0972	0.0011	0.0147	0.0002	0.0478	0.0007	94.3	1.0	94.1	1.2	89.0	34.0	0.20%	-176.76%	0.13
13132-27A	0.0976	0.0018	0.0151	0.0002	0.0476	0.0010	94.6	1.6	96.6	1.5	76.0	48.0	-2.11%	-101.25%	0.25
13132-27B	0.1080	0.0078	0.0161	0.0006	0.0470	0.0032	103.8	7.2	102.8	3.7	60.0	130.0	0.96%	20.92%	0.22
13132-28	0.0997	0.0024	0.0139	0.0002	0.0518	0.0011	96.4	2.2	89.1	1.4	265.0	50.0	7.57%	-78.20%	0.10
13132-29	0.0888	0.0019	0.0135	0.0003	0.0475	0.0012	86.4	1.7	86.7	1.8	73.0	56.0	-0.35%	-54.82%	0.09
13132-30	0.1488	0.0092	0.0132	0.0003	0.0818	0.0047	140.1	8.0	84.3	2.2	1180.0	110.0	39.83%	23.36%	0.18

Spot Name	207Pb / 235U Ratio	207Pb / 235U 2 SE	206Pb / 238U Ratio	206Pb / 238U 2 SE	207Pb / 206Pb Ratio	207Pb / 206Pb 2 SE	Apparent Ages (Ma) 207Pb / 235U Ma	207Pb / 235U 2 SE	206Pb / 238U Ma	206Pb / 238U 2 SE	207Pb / 206Pb Ma	207Pb / 206Pb 2 SE	Percent Discordance 207Pb/235U vs 206Pb/238U	Percent Discordance 207Pb/206Pb vs 206Pb/238U	Th/U Ratio
SMC14-09															
1409-01A	0.0981	0.0037	0.0147	0.0003	0.0492	0.0018	95.0	3.4	94.3	2.0	161.0	85.0	0.74%	-10.94%	0.11
1409-01B	0.0971	0.0026	0.0147	0.0002	0.0473	0.0013	94.1	2.5	94.2	1.5	69.0	62.0	-0.11%	-51.94%	0.15
1409-02	0.0950	0.0029	0.0148	0.0003	0.0468	0.0013	92.1	2.6	94.6	1.6	39.0	60.0	-2.71%	-57.67%	0.09
1409-03A	0.0959	0.0028	0.0148	0.0003	0.0469	0.0014	93.0	2.6	94.4	1.6	52.0	66.0	-1.51%	-43.03%	0.08
1409-03B	0.0981	0.0029	0.0149	0.0003	0.0482	0.0015	94.9	2.6	95.0	1.7	99.0	69.0	-0.11%	-37.68%	0.11
1409-04A	0.0988	0.0025	0.0146	0.0002	0.0487	0.0013	95.6	2.3	93.4	1.5	132.0	58.0	2.30%	-61.03%	0.11
1409-04B	0.1070	0.0120	0.0148	0.0003	0.0520	0.0046	102.3	9.8	94.8	2.1	160.0	130.0	7.33%	27.08%	0.10
1409-05A	0.0983	0.0030	0.0148	0.0002	0.0476	0.0013	95.2	2.8	94.8	1.4	95.0	62.0	0.42%	-52.90%	0.09
1409-05B	0.0957	0.0031	0.0145	0.0002	0.0482	0.0016	92.7	2.9	92.9	1.5	108.0	73.0	-0.22%	-27.26%	0.09
1409-06A	0.0618	0.0019	0.0095	0.0002	0.0474	0.0015	60.9	1.8	60.7	1.1	74.0	68.0	0.36%	10.76%	0.10
1409-06B	0.0944	0.0025	0.0147	0.0002	0.0474	0.0013	91.6	2.3	93.7	1.3	69.0	60.0	-2.31%	-56.20%	0.08
1409-07	0.0954	0.0024	0.0146	0.0002	0.0477	0.0014	92.5	2.2	93.6	1.5	80.0	61.0	-1.19%	-53.44%	0.10
1409-07A	0.1072	0.0039	0.0162	0.0003	0.0483	0.0017	103.3	3.6	103.4	2.2	110.0	77.0	-0.10%	-34.29%	0.10
1409-07A-b	0.0957	0.0025	0.0147	0.0002	0.0475	0.0015	92.8	2.4	94.3	1.4	70.0	69.0	-1.62%	-36.67%	0.11
1409-07B	0.0935	0.0026	0.0145	0.0002	0.0471	0.0014	90.7	2.4	92.8	1.5	58.0	65.0	-2.32%	-42.77%	0.09
1409-08A	0.0969	0.0028	0.0147	0.0003	0.0481	0.0014	94.4	2.6	93.8	1.7	118.0	60.0	0.64%	-56.33%	0.08
1409-08B	0.0971	0.0037	0.0149	0.0003	0.0476	0.0018	94.0	3.4	95.2	1.6	70.0	81.0	-1.28%	-17.53%	0.10
1409-09A	0.0941	0.0028	0.0146	0.0003	0.0469	0.0015	91.5	2.6	93.7	1.6	61.0	69.0	-2.40%	-35.80%	0.08
1409-09B	0.0971	0.0037	0.0148	0.0003	0.0469	0.0019	93.9	3.5	94.6	1.8	56.0	88.0	-0.75%	-7.50%	0.09
1409-11	0.0958	0.0026	0.0148	0.0003	0.0475	0.0014	92.9	2.4	94.7	1.8	82.0	68.0	-1.94%	-39.26%	0.13
1409-13	0.0974	0.0028	0.0147	0.0003	0.0480	0.0014	94.3	2.6	94.0	1.6	99.0	62.0	0.32%	-51.61%	0.08

Spot Name	207Pb / 235U Ratio	207Pb / 235U 2 SE	206Pb / 238U Ratio	206Pb / 238U 2 SE	207Pb / 206Pb Ratio	207Pb / 206Pb 2 SE	Apparent Ages (Ma) 207Pb / 235U Ma	207Pb / 235U 2 SE	206Pb / 238U Ma	206Pb / 238U 2 SE	207Pb / 206Pb Ma	207Pb / 206Pb 2 SE	Percent Discordance 207Pb/235U vs 206Pb/238U	Percent Discordance 207Pb/206Pb vs 206Pb/238U	Th/U Ratio
SMC14-09															
1409-14A	0.0978	0.0029	0.0148	0.0002	0.0487	0.0015	94.6	2.7	94.9	1.5	128.0	63.0	-0.32%	-50.63%	0.07
1409-14B	0.0979	0.0035	0.0148	0.0002	0.0478	0.0017	94.8	3.2	94.9	1.4	98.0	79.0	-0.11%	-20.13%	0.09
1409-15	0.0952	0.0027	0.0148	0.0003	0.0469	0.0014	92.3	2.5	94.9	1.6	41.0	63.0	-2.82%	-50.63%	0.10
1409-16A	0.0948	0.0030	0.0146	0.0003	0.0473	0.0014	91.9	2.7	93.1	1.7	60.0	65.0	-1.31%	-43.23%	0.08
1409-16B	0.0973	0.0029	0.0147	0.0002	0.0488	0.0016	94.2	2.7	93.8	1.5	148.0	74.0	0.42%	-26.76%	0.10
1409-17A	0.0966	0.0027	0.0147	0.0002	0.0480	0.0014	93.6	2.5	93.7	1.5	93.0	63.0	-0.11%	-48.73%	0.09
1409-17B	0.0989	0.0034	0.0147	0.0002	0.0487	0.0016	95.7	3.1	93.9	1.5	123.0	72.0	1.88%	-30.42%	0.08
1409-19A	0.0997	0.0027	0.0147	0.0003	0.0491	0.0015	96.4	2.5	94.2	1.6	160.0	69.0	2.28%	-36.52%	0.10
1409-19B	0.0936	0.0061	0.0147	0.0004	0.0477	0.0036	90.6	5.7	94.3	2.4	110.0	140.0	-4.08%	32.64%	0.08
1409-19B-b	0.1241	0.0057	0.0186	0.0004	0.0483	0.0023	118.7	5.2	119.0	2.8	120.0	100.0	-0.25%	-19.00%	0.11
1409-20	0.0955	0.0034	0.0147	0.0003	0.0472	0.0017	92.6	3.2	94.1	2.0	75.0	76.0	-1.62%	-23.82%	0.10
1409-21A	0.0958	0.0030	0.0149	0.0003	0.0474	0.0015	92.9	2.8	95.1	1.8	68.0	68.0	-2.37%	-39.85%	0.10
1409-21B	0.0979	0.0032	0.0147	0.0002	0.0484	0.0017	94.7	3.0	93.9	1.5	109.0	76.0	0.84%	-23.55%	0.08
1409-22A	0.1018	0.0034	0.0151	0.0003	0.0493	0.0017	98.4	3.1	96.5	1.6	163.0	75.0	1.93%	-28.67%	0.08
1409-22B	0.0950	0.0030	0.0148	0.0002	0.0476	0.0016	92.4	2.8	94.5	1.5	70.0	72.0	-2.27%	-31.25%	0.08
1409-23A	0.0939	0.0039	0.0147	0.0003	0.0479	0.0020	91.0	3.7	94.1	1.6	93.0	87.0	-3.41%	-8.16%	0.08
1409-23B	0.0988	0.0044	0.0150	0.0003	0.0479	0.0022	95.9	4.0	95.8	1.8	106.0	96.0	0.10%	0.21%	0.09
1409-25A	0.0938	0.0027	0.0146	0.0003	0.0468	0.0014	91.0	2.5	93.7	1.6	48.0	66.0	-2.97%	-41.97%	0.10
1409-25B	0.0934	0.0038	0.0145	0.0003	0.0476	0.0020	90.6	3.5	92.8	2.0	81.0	88.0	-2.43%	-5.45%	0.08
1409-26	0.0950	0.0038	0.0146	0.0003	0.0473	0.0019	92.0	3.5	93.5	1.7	68.0	87.0	-1.63%	-7.47%	0.09
1409-27	0.0980	0.0025	0.0148	0.0002	0.0479	0.0012	94.9	2.4	94.8	1.4	96.0	55.0	0.11%	-72.36%	0.09

Spot Name	207Pb / 235U Ratio	207Pb / 235U 2 SE	206Pb / 238U Ratio	206Pb / 238U 2 SE	207Pb / 206Pb Ratio	207Pb / 206Pb 2 SE	**Apparent Ages (Ma)** 207Pb / 235U Ma	207Pb / 235U 2 SE	206Pb / 238U Ma	206Pb / 238U 2 SE	207Pb / 206Pb Ma	207Pb / 206Pb 2 SE	Percent Discordance 207Pb/235U vs 206Pb/238U	Percent Discordance 207Pb/206Pb vs 206Pb/238U	Th/U Ratio
SMC14-09															
1409-28	0.0986	0.0029	0.0148	0.0002	0.0483	0.0015	95.7	2.6	94.8	1.5	134.0	67.0	0.94%	-41.49%	0.08
1409-29A	0.1040	0.0031	0.0161	0.0003	0.0478	0.0015	100.4	2.9	103.0	2.1	82.0	66.0	-2.59%	-56.06%	0.13
1409-29B	0.0929	0.0033	0.0148	0.0003	0.0466	0.0017	90.1	3.1	94.4	1.6	36.0	76.0	-4.77%	-24.21%	0.08
1409-30	0.0970	0.0035	0.0149	0.0003	0.0475	0.0018	93.9	3.3	95.0	1.6	68.0	79.0	-1.17%	-20.25%	0.08
1409-31	0.0990	0.0027	0.0150	0.0002	0.0484	0.0014	95.8	2.5	96.1	1.4	109.0	62.0	-0.31%	-55.00%	0.09
1409-32	0.0953	0.0029	0.0148	0.0003	0.0471	0.0015	93.0	2.7	94.9	1.7	55.0	69.0	-2.04%	-37.54%	0.08
1409-35A	0.0969	0.0032	0.0147	0.0002	0.0479	0.0016	93.9	2.9	94.2	1.4	106.0	69.0	-0.32%	-36.52%	0.08
1409-35B	0.0991	0.0039	0.0148	0.0003	0.0487	0.0019	95.8	3.6	94.4	1.6	136.0	82.0	1.46%	-15.12%	0.11

Spot Name	207Pb / 235U Ratio	207Pb / 235U 2 SE	206Pb / 238U Ratio	206Pb / 238U 2 SE	207Pb / 206Pb Ratio	207Pb / 206Pb 2 SE	Apparent Ages (Ma) 207Pb / 235U Ma	207Pb / 235U 2 SE	206Pb / 238U Ma	206Pb / 238U 2 SE	207Pb / 206Pb Ma	207Pb / 206Pb 2 SE	Percent Discordance 207Pb/235U vs 206Pb/238U	Percent Discordance 207Pb/206Pb vs 206Pb/238U	Th/U Ratio
SMC14-11															
1411-01	0.1050	0.0018	0.0152	0.0003	0.0500	0.0010	101.4	1.6	97.1	1.7	194.0	45.0	4.24%	-115.78%	0.14
1411-02	0.1061	0.0020	0.0154	0.0003	0.0499	0.0010	102.3	1.8	98.4	2.1	186.0	45.0	3.81%	-118.67%	0.07
1411-03	0.1003	0.0040	0.0131	0.0002	0.0558	0.0022	97.4	3.8	84.0	1.3	410.0	81.0	13.76%	-3.70%	0.06
1411-04A	0.0839	0.0019	0.0129	0.0002	0.0469	0.0012	81.8	1.8	82.7	1.3	55.0	58.0	-1.10%	-42.59%	0.07
1411-04B	0.0989	0.0026	0.0148	0.0003	0.0484	0.0012	95.7	2.4	94.5	1.8	117.0	56.0	1.25%	-68.75%	0.04
1411-05A	0.0835	0.0017	0.0126	0.0002	0.0478	0.0011	81.4	1.6	81.0	1.1	86.0	52.0	0.52%	-55.73%	0.18
1411-05B	0.0865	0.0014	0.0131	0.0002	0.0479	0.0009	84.3	1.2	84.1	1.1	94.0	41.0	0.26%	-105.07%	0.06
1411-06A	0.1178	0.0098	0.0168	0.0008	0.0507	0.0023	112.9	8.9	107.3	5.1	220.0	100.0	4.96%	-7.30%	0.04
1411-06A-b	2.8120	0.0710	0.2334	0.0053	0.0880	0.0028	1358.0	19.0	1352.0	28.0	1386.0	56.0	0.44%	-2314.29%	0.65
1411-06B	0.0988	0.0014	0.0150	0.0002	0.0475	0.0008	95.7	1.3	95.9	1.4	80.0	40.0	-0.21%	-139.75%	0.10
1411-07	0.0949	0.0018	0.0134	0.0002	0.0514	0.0011	92.0	1.6	85.7	1.4	250.0	50.0	6.85%	-71.40%	0.09
1411-08	0.0817	0.0024	0.0126	0.0003	0.0472	0.0013	79.7	2.2	80.4	1.6	65.0	60.0	-0.88%	-34.00%	0.16
1411-09	0.1420	0.0220	0.0149	0.0007	0.0672	0.0094	133.0	19.0	95.3	4.3	670.0	280.0	28.35%	65.96%	0.11
1411-10	0.0828	0.0019	0.0126	0.0002	0.0475	0.0012	80.7	1.8	80.5	1.4	76.0	57.0	0.25%	-41.23%	0.06
1411-11	0.0859	0.0013	0.0131	0.0002	0.0474	0.0008	83.7	1.2	83.9	1.1	69.0	38.0	-0.26%	-120.84%	0.09
1411-12A	0.1041	0.0087	0.0127	0.0002	0.0595	0.0043	97.7	6.2	81.5	1.5	470.0	110.0	16.58%	25.91%	0.09
1411-12B	0.0983	0.0023	0.0130	0.0003	0.0540	0.0014	95.2	2.2	83.0	1.7	358.0	60.0	12.82%	-38.33%	0.06
1411-13	0.1118	0.0026	0.0153	0.0003	0.0530	0.0011	107.6	2.3	97.6	2.0	320.0	49.0	9.29%	-99.18%	0.03
1411-13-b	0.0910	0.0030	0.0135	0.0003	0.0490	0.0017	88.4	2.8	86.6	1.6	137.0	76.0	2.04%	-13.95%	0.09
1411-14	0.0973	0.0020	0.0139	0.0002	0.0508	0.0013	94.2	1.9	88.7	1.3	229.0	58.0	5.84%	-52.93%	0.08
1411-15	0.0881	0.0017	0.0133	0.0002	0.0478	0.0009	85.7	1.6	84.9	1.4	88.0	40.0	0.93%	-112.25%	0.09

Spot Name	207Pb / 235U Ratio	207Pb / 235U 2 SE	206Pb / 238U Ratio	206Pb / 238U 2 SE	207Pb / 206Pb Ratio	207Pb / 206Pb 2 SE	Apparent Ages (Ma) 207Pb / 235U Ma	207Pb / 235U 2 SE	206Pb / 238U Ma	206Pb / 238U 2 SE	207Pb / 206Pb Ma	207Pb / 206Pb 2 SE	Percent Discordance 207Pb/235U vs 206Pb/238U	Percent Discordance 207Pb/206Pb vs 206Pb/238U	Th/U Ratio
SMC14-11															
1411-18A	0.0875	0.0013	0.0132	0.0002	0.0483	0.0009	85.1	1.2	84.7	1.1	112.0	41.0	0.51%	-106.51%	0.17
1411-18B	0.0901	0.0019	0.0135	0.0002	0.0483	0.0012	87.6	1.8	86.3	1.3	116.0	57.0	1.51%	-51.37%	0.07
1411-19	0.1055	0.0033	0.0157	0.0003	0.0490	0.0015	101.8	3.0	100.3	1.9	146.0	68.0	1.47%	-47.50%	0.03
1411-20A	0.0700	0.0100	0.0116	0.0003	0.0422	0.0067	67.8	9.7	74.2	2.1	-180.0	250.0	-9.44%	70.32%	0.78
1411-20B	0.0872	0.0011	0.0133	0.0002	0.0476	0.0008	84.9	1.1	85.1	1.1	76.0	37.0	-0.27%	-130.08%	0.13
1411-21	0.0969	0.0016	0.0147	0.0002	0.0476	0.0009	93.9	1.5	94.0	1.6	77.0	43.0	-0.11%	-118.60%	0.07
1411-22	0.0819	0.0027	0.0122	0.0002	0.0479	0.0015	79.8	2.5	78.2	1.5	95.0	67.0	2.01%	-16.72%	0.18
1411-24	4.5000	0.0890	0.2998	0.0062	0.1088	0.0022	1729.0	16.0	1689.0	31.0	1788.0	36.0	2.31%	-4591.67%	0.31
1411-25A	0.0961	0.0023	0.0146	0.0002	0.0478	0.0013	93.1	2.2	93.2	1.5	91.0	55.0	-0.11%	-69.45%	0.06
1411-25B	0.1223	0.0090	0.0155	0.0004	0.0575	0.0035	116.5	7.9	98.9	2.3	450.0	120.0	15.11%	17.58%	0.11
1411-26	0.8420	0.0700	0.0608	0.0046	0.1004	0.0021	624.0	38.0	380.0	28.0	1628.0	40.0	39.10%	-850.00%	0.18
1411-26-b	1.6380	0.0470	0.1134	0.0024	0.1065	0.0023	984.0	18.0	692.0	14.0	1737.0	40.0	29.67%	-1630.00%	0.34
1411-26-c	4.7900	0.1200	0.3121	0.0078	0.1105	0.0034	1782.0	22.0	1751.0	38.0	1803.0	55.0	1.74%	-3083.64%	1.11
1411-27	0.0955	0.0022	0.0137	0.0002	0.0507	0.0012	92.6	2.0	87.7	1.6	224.0	58.0	5.29%	-51.21%	0.26
1411-27-b	0.1025	0.0039	0.0148	0.0003	0.0496	0.0019	99.0	3.6	95.0	1.9	192.0	92.0	4.04%	-3.26%	0.15
1411-28	0.1670	0.0150	0.0214	0.0016	0.0564	0.0040	157.0	13.0	136.0	10.0	460.0	160.0	13.38%	15.00%	0.02
1411-28-b	2.6720	0.0470	0.2258	0.0039	0.0856	0.0019	1320.0	13.0	1312.0	21.0	1322.0	42.0	0.61%	-3023.81%	0.51
1411-29A	0.1093	0.0050	0.0162	0.0004	0.0491	0.0022	105.3	4.6	103.3	2.4	149.0	100.0	1.90%	-3.30%	0.01
1411-29A-b	4.1400	0.1600	0.2794	0.0075	0.1064	0.0030	1660.0	32.0	1588.0	38.0	1749.0	59.0	4.34%	-2591.53%	0.82
1411-29B	0.0862	0.0015	0.0130	0.0002	0.0483	0.0009	83.9	1.4	83.3	1.1	111.0	43.0	0.68%	-93.79%	0.14
1411-30	0.0851	0.0015	0.0126	0.0002	0.0484	0.0009	82.9	1.4	80.9	1.2	120.0	44.0	2.44%	-83.82%	0.06

Spot Name	207Pb / 235U Ratio	207Pb / 235U 2 SE	206Pb / 238U Ratio	206Pb / 238U 2 SE	207Pb / 206Pb Ratio	207Pb / 206Pb 2 SE	Apparent Ages (Ma) 207Pb / 235U Ma	207Pb / 235U 2 SE	206Pb / 238U Ma	206Pb / 238U 2 SE	207Pb / 206Pb Ma	207Pb / 206Pb 2 SE	Percent Discordance 207Pb/235U vs 206Pb/238U	Percent Discordance 207Pb/206Pb vs 206Pb/238U	Th/U Ratio
SMC14-11															
1411-31	0.0902	0.0014	0.0134	0.0002	0.0491	0.0011	87.6	1.3	85.5	1.1	149.0	50.0	2.41%	-70.98%	0.07
1411-32	0.1429	0.0061	0.0121	0.0005	0.0856	0.0023	135.4	5.4	77.4	3.1	1336.0	48.0	42.84%	-61.25%	0.09
1411-33A	0.0882	0.0015	0.0134	0.0002	0.0478	0.0009	85.8	1.4	86.0	1.1	85.0	42.0	-0.20%	-104.69%	0.10
1411-33B	0.1375	0.0096	0.0131	0.0003	0.0768	0.0058	130.3	8.5	84.1	1.7	1050.0	150.0	35.46%	43.93%	0.04
1411-34	0.0815	0.0011	0.0124	0.0002	0.0481	0.0008	79.6	1.0	79.4	1.2	96.0	39.0	0.18%	-103.69%	0.12
1411-35A	0.0952	0.0033	0.0141	0.0003	0.0483	0.0020	92.3	3.0	90.4	2.0	120.0	90.0	2.06%	-0.44%	0.01
1411-35A-b	1.1700	0.2200	0.1201	0.0054	0.0700	0.0140	770.0	100.0	731.0	31.0	940.0	370.0	5.06%	-97.57%	0.22
1411-35B	0.0967	0.0029	0.0146	0.0003	0.0479	0.0015	93.7	2.7	93.6	1.8	89.0	66.0	0.11%	-41.82%	0.03
1411-36	0.0845	0.0018	0.0127	0.0002	0.0477	0.0012	82.3	1.7	81.5	1.5	84.0	55.0	0.97%	-48.18%	0.02
1411-37	0.1030	0.0023	0.0148	0.0003	0.0504	0.0011	99.5	2.1	94.8	1.9	204.0	51.0	4.72%	-85.88%	0.12
1411-39A	0.0929	0.0014	0.0139	0.0002	0.0486	0.0009	90.4	1.3	88.8	1.2	129.0	44.0	1.80%	-101.75%	0.17
1411-39B	0.0980	0.0019	0.0147	0.0003	0.0485	0.0009	94.9	1.8	93.7	1.7	123.0	42.0	1.26%	-123.10%	0.09
1411-40	0.1025	0.0053	0.0158	0.0003	0.0465	0.0020	99.0	4.8	100.9	1.9	28.0	91.0	-1.92%	-10.88%	0.02
1411-40-b	3.6900	0.3000	0.2460	0.0140	0.1075	0.0039	1564.0	65.0	1415.0	73.0	1754.0	66.0	9.53%	-2043.94%	0.44
1411-41A	4.0000	0.1300	0.2747	0.0088	0.1025	0.0024	1618.0	34.0	1561.0	46.0	1672.0	42.0	3.52%	-3616.67%	0.22
1411-41B	0.1002	0.0018	0.0151	0.0002	0.0482	0.0010	96.9	1.7	96.8	1.4	104.0	45.0	0.10%	-115.11%	0.08
1411-42	1.5400	0.2800	0.0253	0.0023	0.3840	0.0420	880.0	110.0	161.0	14.0	3630.0	210.0	81.70%	23.33%	0.11
1411-43	0.0935	0.0019	0.0142	0.0002	0.0483	0.0009	90.8	1.7	90.8	1.5	111.0	40.0	0.00%	-127.00%	0.09
1411-44A	3.0640	0.0610	0.2437	0.0045	0.0917	0.0019	1422.0	15.0	1405.0	23.0	1454.0	39.0	1.20%	-3502.56%	0.40
1411-44B	0.0910	0.0011	0.0139	0.0002	0.0475	0.0009	88.4	1.0	89.1	1.2	72.0	40.0	-0.83%	-122.85%	0.10
1411-45	0.0895	0.0020	0.0136	0.0003	0.0480	0.0009	87.1	1.9	87.2	1.9	91.0	44.0	-0.11%	-98.18%	0.08

Spot Name	207Pb / 235U Ratio	207Pb / 235U 2 SE	206Pb / 238U Ratio	206Pb / 238U 2 SE	207Pb / 206Pb Ratio	207Pb / 206Pb 2 SE	Apparent Ages (Ma) 207Pb / 235U Ma	207Pb / 235U 2 SE	206Pb / 238U Ma	206Pb / 238U 2 SE	207Pb / 206Pb Ma	207Pb / 206Pb 2 SE	Percent Discordance 207Pb/235U vs 206Pb/238U	Percent Discordance 207Pb/206Pb vs 206Pb/238U	Th/U Ratio
SMC14-11															
1411-46A	0.0871	0.0072	0.0129	0.0009	0.0475	0.0010	84.6	6.6	82.7	6.0	73.0	49.0	2.25%	-68.78%	0.07
1411-46B	0.2590	0.0390	0.0145	0.0006	0.1260	0.0160	225.0	29.0	93.0	3.6	1780.0	190.0	58.67%	51.05%	0.16
1411-47A	0.1440	0.0150	0.0140	0.0002	0.0746	0.0078	135.0	13.0	89.9	1.3	870.0	200.0	33.41%	55.05%	0.11
1411-47B	0.0915	0.0013	0.0136	0.0002	0.0489	0.0009	88.9	1.2	87.2	1.2	139.0	40.0	1.95%	-117.93%	0.07
1411-48	0.0863	0.0012	0.0130	0.0002	0.0482	0.0008	84.0	1.1	83.2	1.1	104.0	36.0	0.96%	-131.08%	0.10
1411-49	0.3190	0.0800	0.0146	0.0007	0.1250	0.0170	234.0	40.0	93.5	4.7	1790.0	180.0	60.04%	48.06%	0.09
1411-50	0.2370	0.0160	0.0144	0.0003	0.1214	0.0066	214.0	13.0	92.1	2.0	1926.0	89.0	56.96%	-3.48%	0.07
1411-51	0.0891	0.0029	0.0136	0.0002	0.0473	0.0016	86.6	2.7	87.2	1.4	77.0	72.0	-0.69%	-21.11%	0.04
1411-52	0.0987	0.0025	0.0149	0.0002	0.0481	0.0013	95.5	2.3	95.6	1.5	102.0	60.0	-0.10%	-59.33%	0.12

Spot Name	207Pb / 235U Ratio	207Pb / 235U 2 SE	206Pb / 238U Ratio	206Pb / 238U 2 SE	207Pb / 206Pb Ratio	207Pb / 206Pb 2 SE	Apparent Ages (Ma) 207Pb / 235U Ma	207Pb / 235U 2 SE	206Pb / 238U Ma	206Pb / 238U 2 SE	207Pb / 206Pb Ma	207Pb / 206Pb 2 SE	Percent Discordance 207Pb/235U vs 206Pb/238U	Percent Discordance 207Pb/206Pb vs 206Pb/238U	Th/U Ratio
SMC14-43															
1443-01	0.1330	0.0140	0.0141	0.0005	0.0659	0.0054	125.0	12.0	90.3	2.9	680.0	140.0	27.76%	35.50%	0.09
1443-02	0.0951	0.0033	0.0128	0.0003	0.0531	0.0016	92.2	3.1	82.3	2.0	315.0	65.0	10.74%	-26.62%	0.19
1443-03	0.2040	0.0310	0.0136	0.0004	0.1000	0.0130	182.0	25.0	87.0	2.5	1360.0	240.0	52.20%	63.75%	0.74
1443-04A	2.5600	0.3900	0.0324	0.0036	0.5230	0.0300	1140.0	120.0	205.0	22.0	4238.0	100.0	82.02%	-105.00%	0.64
1443-04B	0.1580	0.0120	0.0124	0.0003	0.0900	0.0056	147.0	10.0	79.7	1.7	1320.0	120.0	45.78%	33.58%	0.27
1443-05	0.4880	0.0810	0.0176	0.0015	0.1800	0.0220	372.0	53.0	112.5	9.6	2390.0	220.0	69.76%	48.86%	0.25
1443-06	0.0845	0.0037	0.0114	0.0003	0.0524	0.0015	82.2	3.4	73.1	1.6	290.0	64.0	11.07%	-14.22%	0.10
1443-08	0.0771	0.0026	0.0118	0.0003	0.0475	0.0013	75.4	2.4	75.4	2.1	69.0	59.0	0.00%	-27.80%	0.03
1443-09	0.1590	0.0130	0.0143	0.0004	0.0768	0.0052	149.0	11.0	91.7	2.3	1060.0	140.0	38.46%	34.50%	0.08
1443-10	0.0820	0.0020	0.0120	0.0002	0.0494	0.0012	80.3	1.8	76.6	1.3	157.0	52.0	4.61%	-47.31%	0.06
1443-11	0.0797	0.0023	0.0113	0.0002	0.0505	0.0014	77.8	2.1	72.8	1.3	214.0	62.0	6.43%	-17.42%	0.12
1443-15	0.0854	0.0027	0.0113	0.0002	0.0550	0.0020	83.1	2.5	72.4	1.2	378.0	77.0	12.90%	6.00%	0.05
1443-16	0.0858	0.0058	0.0113	0.0002	0.0544	0.0032	83.4	5.3	72.5	1.5	340.0	110.0	13.07%	34.09%	0.11
1443-17	0.0768	0.0023	0.0118	0.0003	0.0480	0.0012	75.1	2.1	75.5	1.6	97.0	57.0	-0.53%	-32.46%	0.04
1443-18	0.1970	0.0430	0.0130	0.0005	0.0970	0.0150	164.0	28.0	83.0	3.2	1250.0	210.0	49.39%	60.48%	0.07
1443-20	0.2100	0.0360	0.0126	0.0003	0.1260	0.0200	190.0	29.0	80.7	1.9	1580.0	280.0	57.53%	71.18%	0.35
1443-22	0.0838	0.0037	0.0126	0.0005	0.0480	0.0009	81.6	3.4	80.4	2.9	101.0	41.0	1.47%	-96.10%	0.12
1443-23	0.0777	0.0019	0.0116	0.0003	0.0478	0.0011	76.0	1.8	74.1	1.9	88.0	53.0	2.50%	-39.81%	0.03
1443-23-b	0.0877	0.0025	0.0132	0.0003	0.0478	0.0013	85.4	2.3	84.4	2.0	88.0	61.0	1.17%	-38.36%	0.04
1443-26	0.0817	0.0026	0.0116	0.0002	0.0515	0.0015	79.7	2.4	74.2	1.3	253.0	65.0	6.90%	-14.15%	0.04
1443-27A	0.8600	0.2500	0.0202	0.0026	0.2310	0.0310	498.0	95.0	128.0	16.0	2850.0	200.0	74.30%	36.00%	0.53

Spot Name	207Pb / 235U Ratio	207Pb / 235U 2 SE	206Pb / 238U Ratio	206Pb / 238U 2 SE	207Pb / 206Pb Ratio	207Pb / 206Pb 2 SE	Apparent Ages (Ma) 207Pb / 235U Ma	207Pb / 235U 2 SE	206Pb / 238U Ma	206Pb / 238U 2 SE	207Pb / 206Pb Ma	207Pb / 206Pb 2 SE	Percent Discordance 207Pb/235U vs 206Pb/238U	Percent Discordance 207Pb/206Pb vs 206Pb/238U	Th/U Ratio
SMC14-43															
1443-27B	0.0803	0.0029	0.0124	0.0003	0.0474	0.0018	78.4	2.7	79.1	1.7	69.0	82.0	-0.89%	3.54%	0.02
1443-27B-b	0.0761	0.0026	0.0113	0.0002	0.0491	0.0016	74.9	2.6	72.3	1.4	161.0	78.0	3.47%	7.31%	0.06
1443-28	0.0871	0.0019	0.0133	0.0003	0.0476	0.0011	84.8	1.7	85.0	1.7	86.0	50.0	-0.24%	-70.00%	0.03
1443-28-b	0.1051	0.0030	0.0158	0.0003	0.0484	0.0016	101.5	2.8	100.8	1.8	114.0	75.0	0.69%	-34.40%	0.06
1443-30	0.4900	0.1000	0.0174	0.0012	0.1860	0.0240	391.0	63.0	110.9	7.6	2420.0	240.0	71.64%	53.79%	0.17
1443-31	0.1280	0.0150	0.0117	0.0002	0.0783	0.0084	121.0	13.0	74.8	1.3	890.0	230.0	38.18%	67.48%	0.02
1443-32	0.0837	0.0029	0.0118	0.0003	0.0518	0.0017	81.5	2.7	75.6	1.6	254.0	74.0	7.24%	-2.16%	0.04
1443-34	0.1500	0.0210	0.0120	0.0002	0.0890	0.0120	138.0	18.0	77.0	1.4	1110.0	210.0	44.20%	63.33%	0.21
1443-35	0.0811	0.0029	0.0122	0.0003	0.0484	0.0018	79.1	2.7	78.1	1.6	108.0	81.0	1.26%	3.58%	0.03
1443-36	0.0789	0.0014	0.0119	0.0002	0.0479	0.0008	77.1	1.3	76.5	1.0	93.0	38.0	0.71%	-101.39%	0.01
1443-37	0.0865	0.0032	0.0121	0.0002	0.0517	0.0016	84.2	3.0	77.4	1.5	261.0	70.0	8.08%	-10.57%	0.20
1443-37-b	0.7600	0.1300	0.0220	0.0016	0.2380	0.0240	551.0	74.0	140.0	10.0	2980.0	170.0	74.59%	17.65%	0.33
1443-38	0.0856	0.0027	0.0122	0.0002	0.0507	0.0014	83.3	2.5	78.4	1.5	222.0	64.0	5.88%	-22.50%	0.05
1443-38-b	0.1186	0.0077	0.0161	0.0009	0.0530	0.0019	113.7	7.0	103.2	5.9	318.0	78.0	9.23%	-32.31%	0.07
1443-39	0.0766	0.0022	0.0116	0.0002	0.0478	0.0013	74.9	2.0	74.6	1.5	78.0	63.0	0.40%	-18.41%	0.02
1443-40	0.5700	0.1000	0.0178	0.0014	0.2030	0.0220	414.0	59.0	113.9	8.7	2620.0	200.0	72.49%	43.05%	0.38
1443-44	0.0936	0.0043	0.0127	0.0003	0.0534	0.0023	90.7	4.0	81.3	1.8	268.0	67.0	10.36%	-21.34%	0.07

Spot Name	207Pb / 235U Ratio	207Pb / 235U 2 SE	206Pb / 238U Ratio	206Pb / 238U 2 SE	207Pb / 206Pb Ratio	207Pb / 206Pb 2 SE	Apparent Ages (Ma) 207Pb / 235U Ma	207Pb / 235U 2 SE	206Pb / 238U Ma	206Pb / 238U 2 SE	207Pb / 206Pb Ma	207Pb / 206Pb 2 SE	Percent Discordance 207Pb/235U vs 206Pb/238U	Percent Discordance 207Pb/206Pb vs 206Pb/238U	Th/U Ratio
SMC15-05															
1505-01	0.0924	0.0016	0.0140	0.0002	0.0479	0.0009	89.7	1.5	89.6	1.2	89.0	43.0	0.12%	-108.35%	0.74
1505-02	0.1038	0.0054	0.0158	0.0008	0.0480	0.0009	100.0	4.9	100.7	5.1	97.0	44.0	-0.70%	-128.86%	1.13
1505-03A	0.0864	0.0026	0.0131	0.0002	0.0476	0.0015	84.1	2.4	83.9	1.5	83.0	67.0	0.24%	-25.22%	0.39
1505-03B	0.0829	0.0017	0.0126	0.0002	0.0483	0.0010	80.8	1.6	80.6	1.1	109.0	48.0	0.25%	-67.92%	0.57
1505-04	0.0820	0.0015	0.0126	0.0002	0.0476	0.0009	80.0	1.4	80.7	1.1	82.0	43.0	-0.81%	-87.56%	0.37
1505-05B	0.0832	0.0020	0.0129	0.0002	0.0473	0.0013	81.3	2.0	82.4	1.2	69.0	60.0	-1.37%	-37.35%	0.56
1505-05A	0.0795	0.0022	0.0118	0.0002	0.0485	0.0015	77.6	2.0	75.4	1.2	121.0	66.0	2.87%	-14.20%	0.47
1505-05C	0.0888	0.0038	0.0130	0.0002	0.0491	0.0022	86.7	3.5	83.3	1.3	146.0	95.0	3.92%	12.32%	0.16
1505-06	0.0902	0.0053	0.0137	0.0004	0.0470	0.0023	87.6	5.0	87.9	2.5	50.0	110.0	-0.34%	20.09%	0.38
1505-06-b	0.9850	0.0380	0.1123	0.0026	0.0639	0.0027	698.0	19.0	686.0	15.0	726.0	96.0	1.72%	-614.58%	1.23
1505-07	0.0888	0.0030	0.0139	0.0003	0.0464	0.0017	86.3	2.8	88.8	1.8	32.0	77.0	-2.90%	-15.32%	0.11
1505-08A	0.0816	0.0023	0.0129	0.0003	0.0464	0.0017	80.1	2.3	82.5	2.1	19.0	78.0	-3.00%	-5.77%	0.31
1505-08A-b	0.0784	0.0024	0.0121	0.0002	0.0469	0.0015	76.6	2.3	77.3	1.4	44.0	69.0	-0.91%	-12.03%	0.49
1505-08B	0.0874	0.0023	0.0130	0.0003	0.0488	0.0014	85.0	2.1	83.5	1.6	146.0	64.0	1.76%	-30.47%	0.32
1505-09B	0.1006	0.0021	0.0150	0.0003	0.0489	0.0010	97.3	1.9	95.9	2.0	138.0	44.0	1.44%	-117.95%	0.99
1505-09B-b	0.1325	0.0059	0.0190	0.0004	0.0493	0.0023	126.3	5.3	121.0	2.7	160.0	110.0	4.20%	-10.00%	0.71
1505-09A	0.0733	0.0019	0.0111	0.0002	0.0478	0.0013	71.8	1.8	71.4	1.2	83.0	59.0	0.56%	-21.02%	0.34
1505-10	0.0826	0.0019	0.0127	0.0002	0.0472	0.0012	80.5	1.8	81.3	1.4	59.0	54.0	-0.99%	-50.56%	1.03
1505-11A	0.8440	0.0470	0.0971	0.0033	0.0635	0.0036	617.0	27.0	597.0	19.0	680.0	120.0	3.24%	-397.50%	0.54
1505-11B	0.9990	0.0220	0.1173	0.0020	0.0622	0.0016	702.0	11.0	714.9	11.0	671.0	54.0	-1.84%	-1223.89%	1.70
1505-12	0.0881	0.0019	0.0136	0.0003	0.0467	0.0013	85.7	1.8	87.2	1.8	35.0	60.0	-1.75%	-45.33%	0.48

Spot Name	207Pb / 235U Ratio	207Pb / 235U 2 SE	206Pb / 238U Ratio	206Pb / 238U 2 SE	207Pb / 206Pb Ratio	207Pb / 206Pb 2 SE	Apparent Ages (Ma) 207Pb / 235U Ma	207Pb / 235U 2 SE	206Pb / 238U Ma	206Pb / 238U 2 SE	207Pb / 206Pb Ma	207Pb / 206Pb 2 SE	Percent Discordance 207Pb/235U vs 206Pb/238U	Percent Discordance 207Pb/206Pb vs 206Pb/238U	Th/U Ratio
SMC15-05															
1505-12-b	0.0763	0.0028	0.0120	0.0003	0.0460	0.0017	74.6	2.7	77.1	1.6	18.0	82.0	-3.35%	5.98%	0.41
1505-13	0.0888	0.0016	0.0133	0.0002	0.0481	0.0010	86.4	1.5	85.2	1.1	102.0	45.0	1.37%	-89.38%	0.76
1505-14	0.0795	0.0031	0.0121	0.0003	0.0470	0.0015	77.6	2.9	77.5	2.1	66.0	67.0	0.13%	-15.67%	0.45
1505-15A	0.0820	0.0014	0.0125	0.0002	0.0475	0.0009	80.0	1.4	79.8	1.4	70.0	43.0	0.25%	-85.58%	0.16
1505-15A-b	3.7700	0.1400	0.2534	0.0091	0.1071	0.0019	1582.0	29.0	1455.0	47.0	1748.0	32.0	8.03%	-4446.88%	0.08
1505-15B	0.0914	0.0014	0.0139	0.0002	0.0479	0.0009	88.8	1.3	88.7	1.3	90.0	41.0	0.11%	-116.34%	0.12
1505-16	0.0758	0.0039	0.0119	0.0003	0.0465	0.0023	74.1	3.7	76.1	2.1	20.0	100.0	-2.70%	23.90%	0.31
1505-16-b	0.0882	0.0063	0.0137	0.0005	0.0457	0.0038	85.7	5.9	87.8	2.9	0.0	170.0	-2.45%	48.35%	0.51
1505-17A	0.0882	0.0015	0.0135	0.0002	0.0473	0.0009	85.8	1.4	86.4	1.1	67.0	45.0	-0.71%	-92.02%	1.05
1505-17B	0.0782	0.0042	0.0121	0.0003	0.0470	0.0025	76.3	3.9	77.5	1.8	50.0	110.0	-1.57%	29.55%	0.45
1505-18	0.0743	0.0028	0.0112	0.0002	0.0493	0.0021	72.7	2.7	71.7	1.4	155.0	93.0	1.38%	22.90%	0.18
1505-19	0.0771	0.0024	0.0118	0.0002	0.0466	0.0015	75.4	2.3	75.9	1.3	40.0	66.0	-0.66%	-15.00%	0.41
1505-20A	0.8420	0.0150	0.0935	0.0016	0.0654	0.0016	619.3	8.5	576.0	9.3	791.0	51.0	6.99%	-1029.41%	0.45
1505-20B	0.9060	0.0190	0.1046	0.0017	0.0624	0.0014	654.1	10.0	641.1	9.9	693.0	47.0	1.99%	-1264.04%	0.38
1505-21A	0.0797	0.0026	0.0121	0.0003	0.0474	0.0015	77.8	2.4	77.2	1.7	65.0	68.0	0.77%	-13.53%	0.31
1505-21B	0.0845	0.0032	0.0124	0.0002	0.0489	0.0019	82.4	3.0	79.6	1.4	159.0	92.0	3.40%	13.48%	0.77
1505-21B-b	0.0880	0.0079	0.0143	0.0005	0.0467	0.0037	85.5	7.4	91.7	2.9	30.0	160.0	-7.25%	42.69%	0.28
1505-22	0.0814	0.0031	0.0123	0.0002	0.0478	0.0017	79.3	2.9	78.9	1.6	86.0	76.0	0.50%	-3.82%	0.40

Spot Name	207Pb / 235U Ratio	207Pb / 235U 2 SE	206Pb / 238U Ratio	206Pb / 238U 2 SE	207Pb / 206Pb Ratio	207Pb / 206Pb 2 SE	Apparent Ages (Ma) 207Pb / 235U Ma	207Pb / 235U 2 SE	206Pb / 238U Ma	206Pb / 238U 2 SE	207Pb / 206Pb Ma	207Pb / 206Pb 2 SE	Percent Discordance 207Pb/235U vs 206Pb/238U	Percent Discordance 207Pb/206Pb vs 206Pb/238U	Th/U Ratio
SMC16-09															
1609-01A	0.0884	0.0050	0.0135	0.0003	0.0464	0.0025	85.7	4.7	86.6	1.9	10.0	110.0	-1.05%	21.27%	0.14
1609-01B	0.0879	0.0048	0.0134	0.0004	0.0477	0.0029	85.3	4.5	85.9	2.5	70.0	120.0	-0.70%	28.42%	0.10
1609-02	0.1216	0.0032	0.0181	0.0005	0.0489	0.0012	116.9	2.9	115.7	2.9	138.0	56.0	1.03%	-106.61%	0.03
1609-03A	0.1288	0.0027	0.0191	0.0003	0.0490	0.0009	123.0	2.4	122.1	2.0	143.0	42.0	0.73%	-190.71%	0.02
1609-03B	0.0878	0.0055	0.0135	0.0003	0.0481	0.0033	85.2	5.1	86.4	1.8	120.0	140.0	-1.41%	38.29%	0.10
1609-04	0.1305	0.0025	0.0195	0.0003	0.0491	0.0009	124.5	2.2	124.5	1.8	146.0	44.0	0.00%	-182.95%	0.02
1609-05	0.1269	0.0025	0.0189	0.0003	0.0486	0.0009	121.3	2.3	120.9	1.8	128.0	40.0	0.33%	-202.25%	0.02
1609-06	0.1187	0.0021	0.0180	0.0003	0.0480	0.0009	113.9	1.9	115.2	1.8	98.0	43.0	-1.14%	-167.91%	0.03
1609-09	0.0894	0.0046	0.0136	0.0003	0.0485	0.0027	86.8	4.3	87.2	1.6	100.0	110.0	-0.46%	20.73%	0.09
1609-10A	0.1017	0.0022	0.0156	0.0002	0.0477	0.0011	98.3	2.0	99.6	1.5	79.0	52.0	-1.32%	-91.54%	0.03
1609-10B	0.0925	0.0027	0.0143	0.0003	0.0476	0.0013	89.7	2.5	91.3	1.8	74.0	60.0	-1.78%	-52.17%	0.11
1609-11	0.0945	0.0029	0.0145	0.0002	0.0475	0.0013	91.7	2.7	93.1	1.5	78.0	63.0	-1.53%	-47.78%	0.05
1609-12	0.1360	0.0040	0.0186	0.0003	0.0535	0.0014	129.4	3.6	118.8	1.8	338.0	57.0	8.19%	-108.42%	0.02
1609-14	0.1243	0.0022	0.0184	0.0003	0.0489	0.0009	119.0	2.0	117.7	1.9	139.0	42.0	1.09%	-180.24%	0.02
1609-15	0.1313	0.0037	0.0194	0.0004	0.0498	0.0011	125.2	3.3	123.6	2.5	183.0	50.0	1.28%	-147.20%	0.03
1609-16	0.1075	0.0049	0.0159	0.0004	0.0495	0.0024	103.5	4.5	101.6	2.4	170.0	100.0	1.84%	-1.60%	0.05
1609-16-b	0.1400	0.0100	0.0205	0.0007	0.0507	0.0033	133.1	9.1	130.8	4.1	200.0	140.0	1.73%	6.57%	0.04
1609-17	0.1195	0.0030	0.0178	0.0003	0.0484	0.0013	114.6	2.7	113.5	1.9	115.0	58.0	0.96%	-95.69%	0.03
1609-18A	0.0975	0.0055	0.0142	0.0005	0.0486	0.0033	94.4	5.1	90.7	3.0	140.0	150.0	3.92%	39.53%	0.04
1609-18A-b	0.1185	0.0033	0.0180	0.0004	0.0479	0.0012	113.7	3.0	114.8	2.2	92.0	57.0	-0.97%	-101.40%	0.02
1609-18B	0.0984	0.0021	0.0142	0.0002	0.0507	0.0012	95.3	2.0	91.1	1.4	222.0	55.0	4.41%	-65.64%	0.03

Spot Name	207Pb / 235U Ratio	207Pb / 235U 2 SE	206Pb / 238U Ratio	206Pb / 238U 2 SE	207Pb / 206Pb Ratio	207Pb / 206Pb 2 SE	Apparent Ages (Ma) 207Pb / 235U Ma	207Pb / 235U 2 SE	206Pb / 238U Ma	206Pb / 238U 2 SE	207Pb / 206Pb Ma	207Pb / 206Pb 2 SE	Percent Discordance 207Pb/235U vs 206Pb/238U	Percent Discordance 207Pb/206Pb vs 206Pb/238U	Th/U Ratio
SMC16-09															
1609-19	0.1187	0.0022	0.0179	0.0003	0.0484	0.0009	113.9	2.0	114.5	1.8	112.0	40.0	-0.53%	-186.25%	0.02
1609-20A	0.1124	0.0028	0.0168	0.0004	0.0493	0.0012	108.1	2.6	107.5	2.3	165.0	56.0	0.56%	-91.96%	0.02
1609-20A-b	0.1123	0.0050	0.0157	0.0003	0.0522	0.0024	107.9	4.6	100.3	1.7	270.0	100.0	7.04%	-0.30%	0.03
1609-20B	0.1012	0.0031	0.0151	0.0003	0.0487	0.0013	97.9	2.9	96.7	2.0	138.0	63.0	1.23%	-53.49%	0.02
1609-21A	0.0901	0.0037	0.0141	0.0004	0.0466	0.0018	87.6	3.5	90.0	2.4	31.0	81.0	-2.74%	-11.11%	0.04
1609-21B	0.1280	0.0030	0.0190	0.0004	0.0492	0.0013	122.3	2.7	121.1	2.4	165.0	57.0	0.98%	-112.46%	0.03
1609-22	0.1305	0.0033	0.0193	0.0006	0.0488	0.0012	124.5	2.9	123.1	3.9	136.0	54.0	1.12%	-127.96%	0.01
1609-22-b	0.1382	0.0027	0.0206	0.0004	0.0488	0.0010	131.7	2.4	131.2	2.2	138.0	50.0	0.38%	-162.40%	0.03
1609-23A	0.0989	0.0041	0.0148	0.0003	0.0478	0.0021	95.6	3.8	94.6	2.2	90.0	90.0	1.05%	-5.11%	0.05
1609-23A-b	0.1111	0.0050	0.0169	0.0004	0.0487	0.0021	106.9	4.5	107.9	2.8	126.0	94.0	-0.94%	-14.79%	0.02
1609-23B	0.0890	0.0016	0.0136	0.0002	0.0479	0.0009	86.6	1.5	87.3	1.3	97.0	43.0	-0.76%	-102.93%	0.02
1609-24A	0.0933	0.0018	0.0141	0.0002	0.0484	0.0010	90.7	1.7	90.4	1.3	115.0	45.0	0.32%	-100.91%	0.03
1609-24B	0.1090	0.0023	0.0166	0.0003	0.0477	0.0009	105.0	2.1	106.2	1.6	81.0	44.0	-1.14%	-141.36%	0.02
1609-26	0.1255	0.0030	0.0189	0.0004	0.0481	0.0012	120.0	2.7	120.9	2.4	98.0	55.0	-0.75%	-119.82%	0.03
1609-27	0.1112	0.0028	0.0169	0.0003	0.0474	0.0012	107.3	2.6	108.1	1.9	69.0	56.0	-0.75%	-93.04%	0.03
1609-28	0.0967	0.0048	0.0146	0.0004	0.0468	0.0022	93.6	4.5	93.4	2.5	53.0	100.0	0.21%	6.60%	0.07
1609-28-b	0.1083	0.0042	0.0163	0.0004	0.0482	0.0018	104.3	3.8	103.9	2.2	106.0	83.0	0.38%	-25.18%	0.04
1609-29	0.0927	0.0034	0.0139	0.0004	0.0479	0.0018	89.9	3.1	88.8	2.3	94.0	74.0	1.22%	-20.00%	0.07
1609-30A	0.0907	0.0034	0.0134	0.0003	0.0492	0.0019	88.0	3.1	85.8	1.9	171.0	84.0	2.50%	-2.14%	0.17
1609-30B	0.1009	0.0029	0.0152	0.0003	0.0477	0.0012	97.6	2.7	97.5	2.1	79.0	55.0	0.10%	-77.27%	0.03

Spot Name	207Pb / 235U Ratio	207Pb / 235U 2 SE	206Pb / 238U Ratio	206Pb / 238U 2 SE	207Pb / 206Pb Ratio	207Pb / 206Pb 2 SE	Apparent Ages (Ma) 207Pb / 235U Ma	207Pb / 235U 2 SE	206Pb / 238U Ma	206Pb / 238U 2 SE	207Pb / 206Pb Ma	207Pb / 206Pb 2 SE	Percent Discordance 207Pb/235U vs 206Pb/238U	Percent Discordance 207Pb/206Pb vs 206Pb/238U	Th/U Ratio
SMC16-09															
1609-31A	0.1056	0.0025	0.0157	0.0004	0.0480	0.0011	101.9	2.3	100.4	2.2	94.0	51.0	1.47%	-96.86%	0.04
1609-31B	0.1025	0.0032	0.0156	0.0004	0.0482	0.0017	99.1	2.9	100.0	2.8	101.0	75.0	-0.91%	-33.33%	0.05
1609-32	0.1303	0.0029	0.0191	0.0004	0.0494	0.0011	124.3	2.6	121.7	2.3	168.0	49.0	2.09%	-148.37%	0.02
1609-33	0.0954	0.0031	0.0141	0.0003	0.0486	0.0017	92.8	2.8	90.4	1.8	126.0	74.0	2.59%	-22.16%	0.07

Spot Name	207Pb / 235U Ratio	207Pb / 235U 2 SE	206Pb / 238U Ratio	206Pb / 238U 2 SE	207Pb / 206Pb Ratio	207Pb / 206Pb 2 SE	Apparent Ages (Ma) 207Pb / 235U Ma	207Pb / 235U 2 SE	206Pb / 238U Ma	206Pb / 238U 2 SE	207Pb / 206Pb Ma	207Pb / 206Pb 2 SE	Percent Discordance 207Pb/235U vs 206Pb/238U	Percent Discordance 207Pb/206Pb vs 206Pb/238U	Th/U Ratio
SMC16-22															
1622-05	0.0992	0.0022	0.0150	0.0003	0.0483	0.0012	96.0	2.0	96.0	2.0	109.0	56.0	0.00%	-71.43%	0.02
1622-05-b	0.1144	0.0025	0.0175	0.0003	0.0474	0.0011	109.9	2.3	112.1	2.1	70.0	52.0	-2.00%	-115.58%	0.07
1622-06	0.1072	0.0027	0.0152	0.0003	0.0515	0.0012	103.4	2.5	97.3	1.8	265.0	55.0	5.90%	-76.91%	0.10
1622-08A	0.0819	0.0016	0.0124	0.0002	0.0477	0.0011	79.9	1.5	79.4	1.3	81.0	52.0	0.63%	-52.69%	0.03
1622-08B	0.0921	0.0020	0.0138	0.0003	0.0479	0.0010	89.5	1.8	88.5	1.7	96.0	47.0	1.12%	-88.30%	0.05
1622-08C	0.1420	0.0160	0.0135	0.0003	0.0729	0.0061	133.0	13.0	86.7	1.6	870.0	130.0	34.81%	33.31%	0.03
1622-09	0.0660	0.0280	0.0133	0.0010	0.0280	0.0200	62.0	26.0	84.9	6.4	-590.0	610.0	-36.94%	86.08%	0.07
1622-10	0.1320	0.0100	0.0167	0.0005	0.0554	0.0032	124.8	8.8	106.6	2.9	319.0	69.0	14.58%	-54.49%	0.25
1622-14	0.3510	0.0210	0.0396	0.0015	0.0626	0.0024	303.0	16.0	250.1	9.5	695.0	85.0	17.46%	-194.24%	0.15
1622-15	0.1011	0.0045	0.0135	0.0004	0.0540	0.0015	97.6	4.1	86.1	2.5	350.0	57.0	11.78%	-51.05%	0.10
1622-16A	0.1022	0.0022	0.0152	0.0003	0.0488	0.0013	98.8	2.0	97.3	2.0	131.0	59.0	1.52%	-64.92%	0.06
1622-16B	0.1990	0.0200	0.0151	0.0004	0.0953	0.0093	183.0	17.0	96.5	2.2	1420.0	190.0	47.27%	49.21%	0.19
1622-18	0.0814	0.0031	0.0127	0.0005	0.0459	0.0026	79.5	2.9	81.5	3.1	0.0	120.0	-2.52%	32.08%	0.07
1622-18-b	2.7590	0.0380	0.2244	0.0031	0.0889	0.0016	1343.8	10.0	1305.0	16.0	1398.0	34.0	2.89%	-3738.24%	0.14
1622-20A	0.1248	0.0096	0.0144	0.0005	0.0611	0.0034	118.5	8.6	92.4	2.9	590.0	110.0	22.03%	16.00%	0.03
1622-20B	0.0920	0.0018	0.0139	0.0002	0.0478	0.0010	89.3	1.7	88.9	1.5	88.0	46.0	0.45%	-93.26%	0.10
1622-22	0.0969	0.0053	0.0146	0.0003	0.0482	0.0022	93.9	4.9	93.5	2.2	103.0	98.0	0.43%	4.59%	0.11
1622-22-b	3.0420	0.0740	0.1996	0.0059	0.1109	0.0019	1418.0	19.0	1173.0	32.0	1812.0	32.0	17.28%	-3565.63%	0.39
1622-23	0.0887	0.0022	0.0129	0.0002	0.0500	0.0013	86.3	2.0	82.6	1.5	187.0	56.0	4.29%	-47.50%	0.04
1622-25	0.0782	0.0073	0.0125	0.0004	0.0455	0.0041	76.4	6.9	80.3	2.5	-20.0	190.0	-5.10%	57.74%	0.08
1622-25-b	1.8570	0.0490	0.1795	0.0031	0.0749	0.0019	1066.0	17.0	1064.0	17.0	1074.0	49.0	0.19%	-2071.43%	0.22

Spot Name	207Pb / 235U Ratio	207Pb / 235U 2 SE	206Pb / 238U Ratio	206Pb / 238U 2 SE	207Pb / 206Pb Ratio	207Pb / 206Pb 2 SE	Apparent Ages (Ma) 207Pb / 235U Ma	207Pb / 235U 2 SE	206Pb / 238U Ma	206Pb / 238U 2 SE	207Pb / 206Pb Ma	207Pb / 206Pb 2 SE	Percent Discordance 207Pb/235U vs 206Pb/238U	Percent Discordance 207Pb/206Pb vs 206Pb/238U	Th/U Ratio
SMC16-22															
1622-26A	0.0954	0.0020	0.0138	0.0002	0.0501	0.0010	92.5	1.8	88.4	1.5	189.0	44.0	4.43%	-100.91%	0.08
1622-26B	0.0986	0.0022	0.0148	0.0004	0.0488	0.0012	95.5	2.0	95.0	2.2	139.0	55.0	0.52%	-72.73%	0.06
1622-27	0.0818	0.0051	0.0124	0.0006	0.0477	0.0031	79.8	4.8	79.5	3.6	80.0	140.0	0.38%	43.21%	0.11
1622-27-b	0.9030	0.0380	0.1088	0.0022	0.0602	0.0027	654.0	21.0	666.0	13.0	600.0	110.0	-1.83%	-505.45%	0.68
1622-29A	0.0880	0.0037	0.0131	0.0005	0.0485	0.0021	85.6	3.5	83.7	3.3	120.0	97.0	2.22%	13.71%	0.06
1622-29A-b	1.2900	0.1600	0.1534	0.0061	0.0616	0.0075	828.0	73.0	920.0	34.0	610.0	270.0	-11.11%	-240.74%	0.26
1622-29B	0.0922	0.0031	0.0141	0.0003	0.0475	0.0017	89.5	2.9	90.0	1.6	78.0	77.0	-0.56%	-16.88%	0.06
1622-31A	0.0913	0.0017	0.0138	0.0002	0.0481	0.0010	88.9	1.6	88.5	1.4	99.0	47.0	0.45%	-88.30%	0.02
1622-31B	0.0700	0.0020	0.0100	0.0003	0.0480	0.0011	68.7	1.9	63.9	1.6	94.0	50.0	6.99%	-27.80%	0.21
1622-31B-b	0.1801	0.0093	0.0191	0.0006	0.0689	0.0031	168.0	8.0	122.1	3.8	884.0	91.0	27.32%	-34.18%	0.21
1622-34	0.0899	0.0025	0.0137	0.0003	0.0477	0.0015	87.4	2.3	88.0	1.9	84.0	70.0	-0.69%	-25.71%	0.02
1622-34-b	0.0817	0.0028	0.0126	0.0002	0.0470	0.0016	79.7	2.7	80.5	1.3	47.0	73.0	-1.00%	-10.27%	0.01
1622-35	0.1021	0.0017	0.0144	0.0002	0.0514	0.0010	98.7	1.6	92.2	1.2	258.0	46.0	6.61%	-100.39%	0.03
1622-37	2.9500	0.3400	0.0368	0.0027	0.5610	0.0250	1361.0	89.0	232.0	17.0	4397.0	67.0	82.95%	-246.27%	0.04
1622-38	0.0900	0.0013	0.0133	0.0002	0.0490	0.0009	87.4	1.2	85.4	1.1	144.0	41.0	2.28%	-108.32%	0.05
1622-40	0.0957	0.0023	0.0147	0.0003	0.0477	0.0014	93.1	2.2	93.9	2.0	84.0	64.0	-0.86%	-46.72%	0.13
1622-40-b	0.0902	0.0029	0.0128	0.0003	0.0509	0.0019	87.7	2.7	82.2	1.8	224.0	82.0	6.27%	-0.24%	0.28
1622-41A	0.0600	0.0015	0.0087	0.0002	0.0482	0.0012	59.2	1.4	55.5	1.0	103.0	55.0	6.22%	-0.95%	0.11
1622-41A-b	0.1142	0.0053	0.0171	0.0005	0.0487	0.0019	109.7	4.8	109.3	2.9	127.0	85.0	0.36%	-28.59%	0.07
1622-41B	0.0886	0.0026	0.0132	0.0003	0.0484	0.0011	86.2	2.4	84.3	1.8	114.0	50.0	2.20%	-68.60%	0.07
1622-41B-b	0.0913	0.0023	0.0140	0.0002	0.0478	0.0010	88.6	2.2	89.3	1.5	85.0	45.0	-0.79%	-98.44%	0.29

Spot Name	207Pb / 235U Ratio	207Pb / 235U 2 SE	206Pb / 238U Ratio	206Pb / 238U 2 SE	207Pb / 206Pb Ratio	207Pb / 206Pb 2 SE	Apparent Ages (Ma) 207Pb / 235U Ma	207Pb / 235U 2 SE	206Pb / 238U Ma	206Pb / 238U 2 SE	207Pb / 206Pb Ma	207Pb / 206Pb 2 SE	Percent Discordance 207Pb/235U vs 206Pb/238U	Percent Discordance 207Pb/206Pb vs 206Pb/238U	Th/U Ratio
SMC16-22															
1622-42	0.0822	0.0034	0.0126	0.0003	0.0474	0.0018	80.1	3.2	80.4	1.6	64.0	80.0	-0.37%	-0.50%	0.78
1622-43A	0.0777	0.0084	0.0127	0.0005	0.0445	0.0049	75.8	7.9	81.3	3.0	-80.0	210.0	-7.26%	61.29%	0.04
1622-43A-b	0.0996	0.0030	0.0151	0.0003	0.0476	0.0016	96.4	2.8	96.9	1.7	76.0	72.0	-0.52%	-34.58%	0.11
1622-43B	0.0992	0.0026	0.0151	0.0004	0.0475	0.0012	96.0	2.4	96.3	2.3	71.0	57.0	-0.31%	-68.95%	0.14
1622-44	0.0880	0.0016	0.0132	0.0002	0.0483	0.0009	85.8	1.5	84.8	1.3	111.0	43.0	1.17%	-97.21%	0.07
1622-45	0.0877	0.0031	0.0131	0.0003	0.0496	0.0017	85.3	2.9	83.7	1.6	165.0	77.0	1.88%	-8.70%	0.07
1622-45-b	0.1000	0.0047	0.0153	0.0004	0.0482	0.0022	96.7	4.3	97.6	2.7	99.0	98.0	-0.93%	0.41%	0.17
1622-46	0.8260	0.0300	0.0723	0.0015	0.0833	0.0036	611.0	17.0	450.0	8.8	1270.0	85.0	26.35%	-429.41%	0.09
1622-46-b	3.3240	0.0400	0.2584	0.0034	0.0939	0.0013	1488.7	9.4	1481.0	17.0	1503.0	26.0	0.52%	-5596.15%	0.31
1622-47A	0.0615	0.0014	0.0082	0.0001	0.0509	0.0014	60.5	1.3	52.4	0.8	222.0	57.0	13.45%	8.14%	0.39
1622-47B	0.0882	0.0017	0.0129	0.0002	0.0495	0.0010	85.8	1.5	82.8	1.4	166.0	46.0	3.50%	-80.00%	0.05
1622-48	0.1061	0.0028	0.0155	0.0003	0.0491	0.0011	102.3	2.6	99.2	2.2	145.0	53.0	3.03%	-87.17%	0.26
1622-49	0.0903	0.0020	0.0136	0.0002	0.0489	0.0014	87.8	1.9	86.8	1.5	135.0	63.0	1.14%	-37.78%	0.02
1622-51A	0.0490	0.0280	0.0091	0.0014	0.0390	0.0230	47.0	28.0	58.1	8.9	-430.0	890.0	-23.62%	93.47%	0.05
1622-51A-b	0.5360	0.0120	0.0717	0.0011	0.0550	0.0013	436.2	8.2	446.0	6.8	408.0	53.0	-2.25%	-741.51%	0.60
1622-51B	0.2230	0.0220	0.0155	0.0004	0.1019	0.0084	201.0	18.0	99.0	2.3	1520.0	150.0	50.75%	34.00%	0.22
1622-52	0.0829	0.0028	0.0126	0.0004	0.0469	0.0016	80.9	2.7	81.0	2.4	47.0	75.0	-0.12%	-8.00%	0.08
1622-52-b	0.3570	0.0190	0.0504	0.0012	0.0516	0.0029	310.0	14.0	317.0	7.2	250.0	120.0	-2.26%	-164.17%	0.35
1622-53A	2.1290	0.0420	0.1920	0.0031	0.0808	0.0016	1156.0	14.0	1132.0	17.0	1214.0	39.0	2.08%	-2802.56%	0.27
1622-53B	0.1003	0.0021	0.0154	0.0003	0.0473	0.0013	97.0	1.9	98.2	2.1	64.0	59.0	-1.24%	-66.44%	0.09
1622-55	10.660	0.1200	0.4422	0.0057	0.1737	0.0025	2494.0	10.0	2360.0	25.0	2595.0	25.0	5.37%	-9340.00%	0.53

Spot Name	207Pb / 235U Ratio	207Pb / 235U 2 SE	206Pb / 238U Ratio	206Pb / 238U 2 SE	207Pb / 206Pb Ratio	207Pb / 206Pb 2 SE	Apparent Ages (Ma) 207Pb / 235U Ma	207Pb / 235U 2 SE	206Pb / 238U Ma	206Pb / 238U 2 SE	207Pb / 206Pb Ma	207Pb / 206Pb 2 SE	Percent Discordance 207Pb/235U vs 206Pb/238U	Percent Discordance 207Pb/206Pb vs 206Pb/238U	Th/U Ratio
SMC16-22															
1622-56	0.1092	0.0070	0.0155	0.0005	0.0514	0.0026	105.6	6.6	99.0	3.4	260.0	100.0	6.25%	1.00%	0.06
1622-57	0.0884	0.0044	0.0128	0.0003	0.0494	0.0025	85.9	4.1	81.8	2.2	140.0	100.0	4.77%	18.20%	0.04
1622-58	0.1067	0.0035	0.0160	0.0004	0.0477	0.0010	102.9	3.2	102.3	2.7	81.0	47.0	0.58%	-117.66%	0.10
1622-58-b	2.4380	0.0540	0.2183	0.0039	0.0815	0.0020	1257.0	14.0	1273.0	21.0	1238.0	45.0	-1.27%	-2728.89%	0.38
1622-60	0.2170	0.0200	0.0223	0.0012	0.0672	0.0058	199.0	17.0	142.2	7.6	850.0	170.0	28.54%	16.35%	0.05
1622-60-b	2.2260	0.0820	0.2018	0.0047	0.0794	0.0028	1195.0	26.0	1185.0	25.0	1194.0	72.0	0.84%	-1545.83%	0.31
1622-61A	0.0845	0.0018	0.0127	0.0002	0.0477	0.0011	82.3	1.7	81.6	1.3	87.0	51.0	0.85%	-60.00%	0.10
1622-61B	0.0894	0.0014	0.0135	0.0002	0.0478	0.0010	86.9	1.3	86.7	1.3	88.0	47.0	0.23%	-84.47%	0.08
1622-63	0.0824	0.0023	0.0127	0.0002	0.0472	0.0013	80.4	2.1	81.5	1.5	57.0	61.0	-1.37%	-33.61%	0.19
1622-65	0.0823	0.0042	0.0124	0.0003	0.0470	0.0024	80.3	4.0	79.5	2.1	80.0	120.0	1.00%	33.75%	0.10
1622-66	0.0656	0.0014	0.0093	0.0002	0.0482	0.0008	64.5	1.4	59.5	1.3	107.0	39.0	7.75%	-52.56%	0.07

REFERENCES

Abramson, I. S., 1982, On bandwidth variation in kernel estimates-a square root law: The annals of Statistics, p. 1217-1223.

Armstrong, R. L., Taubeneck, W. H., and Hales, P. O., 1977, Rb-Sr and K-Ar geochronometry of Mesozoic granitic rocks and their Sr isotopic composition, Oregon, Washington, and Idaho: Geological Society of America Bulletin, v. 88, no. 3, p. 397-411.

Bennett, E. H., 1980, Granitic rocks of Tertiary age in the Idaho batholith and their relation to mineralization: Economic Geology, v. 75, no. 2, p. 278-288.

Bennett, E. H., and Knowles, C. R., 1985, Tertiary Plutons and Related Rocks: US Geological Survey Bulletin, no. 1658-1661, p. 81.

Boehnke, P., Watson, E. B., Trail, D., Harrison, T. M., and Schmitt, A. K., 2013, Zircon saturation re-revisited: Chemical Geology, no. 351, p. 324-334.

Bons, P. D., Elburg, M. A., and Gomez-Rivas, E., 2012, A review of the formation of tectonic veins and their microstructures: Journal of Structural Geology, v. 43, p. 33-62.

Botev, Z. I., Grotowski, J. F., and Kroese, D. P., 2010, Kernel density estimation via diffusion: The annals of Statistics, v. 38, no. 5, p. 2916-2957.

Bruguier, O., Télouk, P., Cocherie, A., Fouillac, A. M., and Albarède, F., 2001, Evaluation of Pb-Pb and U-Pb Laser Ablation ICP-MSZircon Dating using Matrix-Matched Calibration Sampleswith a Frequency Quadrupled (266 nm) Nd-YAG Laser: Geostandards Newsletter, v. 25, no. 2-3, p. 361-373.

Criss, R. E., Fleck, R. J., and Taylor Jr, H. P., 1991, Tertiary meteoric hydrothermal systems and their relation to ore deposition, northwestern United States and southern British Columbia: Journal of Geophysical Research: Solid Earth, v. 96, no. B8, p. 13335-13356.

Dutrow, B., Anderson, S., Henry, D., Mueller, P., and Giaramita, M., 1995, A new Precambrian crustal province in south-central Idaho: Eos, v. 76, p. 678.

Dutrow, B., Foster, D., Mueller, P., and Ma, C., 2014, New Constraints on the Geochronology and Thermochronology of the Sawtooth Batholith, Idaho: AGU Fall Meeting Abstracts.

Foster, D. A., Mueller, P. A., Mogk, D. W., Wooden, J. L., and Vogl, J. J., 2006, Proterozoic evolution of the western margin of the Wyoming craton: Implications for the tectonic and magmatic evolution of the northern Rocky Mountains: Canadian Journal of Earth Sciences, v. 43, no. 10, p. 1601-1619.

Fukai, I., 2013, Metamorphic and geochemical signatures of calc-silicate gneisses: LSU Master's Theses, no. 1931.

Fukai, I., and Dutrow, B. L., 2017, High-grade calcareous metasediments from the Sawtooth Metamorphic Complex, Idaho, USA: evidence for passive margin strata and polymetamorphism within the Idaho batholith: International Geology Review, v. 59, no. 5-6, p. 753-778.

Gaschnig, R., Vervoort, J., Lewis, R., and Dufrane, S., 2008, Utilizing U-Pb geochronology of inherited zircon in the Atlanta lobe of the Idaho batholith as a probe of the deep crust in southern Idaho: a progress report: Northwest Geology, v. 37, p. 101-110.

Gaschnig, R. M., Vervoort, J. D., Lewis, R. S., and McClelland, W. C., 2010, Migrating magmatism in the northern US Cordillera: in situ U–Pb geochronology of the Idaho batholith: Contributions to Mineralogy and Petrology, v. 159, no. 6, p. 863-883.

Gaschnig, R. M., Vervoort, J. D., Lewis, R. S., and Tikoff, B., 2013, Probing for Proterozoic and Archean crust in the northern US Cordillera with inherited zircon from the Idaho batholith: Bulletin, v. 125, no. 1-2, p. 73-88.

Geake, J., Walker, G., Telfer, D., Mills, A., and Garlick, G., 1973, Luminescence of lunar, terrestrial, and synthesized plagioclase caused by Mn2+ and Fe3+: Lunar and Planetary Science Conference Proceedings, v. 4, p. 3181.

Götze, J., 2012, Application of cathodoluminescence microscopy and spectroscopy in geosciences: Microscopy Microanalysis, v. 18, no. 6, p. 1270-1284.

Götze, J., Habermann, D., Neuser, R. D., and Richter, D. K., 1999, High-resolution spectrometric analysis of rare earth elements-activated cathodoluminescence in feldspar minerals: Chemical Geology, v. 153, no. 1-4, p. 81-91.

Götze, J., Schertl, H.-P., Neuser, R. D., Kempe, U., and Hanchar, J. M., 2013, Optical microscope-cathodoluminescence (OM–CL) imaging as a powerful tool to reveal internal textures of minerals: Contibutions to Mineralogy and Petrology, v. 107, no. 3, p. 373-392.

Hellstrom, J., Paton, C., Woodhead, J., and Hergt, J., 2008, Iolite: Software for spatially resolved LA-(quad and MC) ICPMS analysis: Mineralogical Association of Canada Short Course v. 40.

Hoffmann, A. A., 2016, Plagioclase Corona Around Garnets: Implications of Pressure-Temperature Paths in Aluminous Gneisses: Unpublished Masters Thesis, LSU, Baton Rouge, LA.

Hyndman, D. W., 1981, Controls on source and depth of emplacement of granitic magma: Geology, v. 9, no. 6, p. 244-249.

Jackson, S. E., Pearson, N. J., Griffin, W. L., and Belousova, E. A., 2004, The application of laser ablation-inductively coupled plasma-mass spectrometry to in situ U–Pb zircon geochronology: Chemical Geology, v. 211, no. 1-2, p. 47-69.

Keppler, H., and Wyllie, P. J., 1991, Partitioning of Cu, Sn, Mo, W, U, and Th between melt and aqueous fluid in the systems haplogranite-H 2 O− HCl and haplogranite-H 2 O− HF: Contributions to Mineralogy Petrology, v. 109, no. 2, p. 139-150.

Kiilsgaard, T. H., Freeman, V. L., and Coffman, J. S., 1970, Mineral resources of the Sawtooth primitive area, Idaho: US Geological Survey Bulletin, no. 1319.

Kiilsgaard, T. H., and Lewis, R. S., 1985, Plutonic rocks of Cretaceous age and faults in the Atlanta lobe of the Idaho batholith: US Geological Survey Bulletin, v. 1658, p. 29-42.

Kylander-Clark, A. R., and Hacker, B. R., 2014, Age and significance of felsic dikes from the UHP western gneiss region: Tectonics, v. 33, no. 12, p. 2342-2360.

Le Bas, M., and Streckeisen, A. L., 1991, The IUGS systematics of igneous rocks: Journal of the Geological Society, v. 148, no. 5, p. 825-833.

Lewis, R. S., and Kiilsgaard, T. H., 1991, Eocene Plutonic Rocks in South Central Idaho: Journal of Geophysical Research-Solid Earth and Planets, v. 96, p. 13295-13311.

Lewis, R. S., Vervoort, J. D., Burmester, R. F., McClelland, W. C., and Chang, Z., 2007, Geochronological constraints on Mesoproterozoic and Neoproterozoic (?) high-grade metasedimentary rocks of north-central Idaho, USA, SEPM Special Publication, Volume 86, Society for Sedimentary Geology, p. 37-53.

Lewis, R. S., Vervoort, J. D., Burmester, R. F., and Oswald, P. J., 2010, Detrital zircon analysis of Mesoproterozoic and Neoproterozoic metasedimentary rocks of north-central Idaho: implications for development of the Belt–Purcell basin: Canadian Journal of Earth Sciences, v. 47, no. 11, p. 1383-1404.

Ludwig, K. R., 1998, On the treatment of concordant uranium-lead ages: Geochimica et Cosmochimica Acta, v. 62, no. 4, p. 665-676.

Ludwig, K. R., 2003, User's manual for isoplot 3.00, a geochronlogical toolkit for microsoft excel: Berkeley Geochronology Center Special Publication, v. 4, p. 25-32.

Lund, K., Aleinikoff, J., Evans, K., DuBray, E., Dewitt, E., and Unruh, D., 2010, SHRIMP U-Pb dating of recurrent Cryogenian and Late Cambrian–Early Ordovician alkalic magmatism in central Idaho: Implications for Rodinian rift tectonics: GSA Bulletin, v. 122, no. 3-4, p. 430-453.

Ma, C., 2015, Structure, Depositional Age, and Magmatism in the Sawtotth Metamorphic Complex, Idaho: Implications for Cordilleran Tectonics in the Northern U.S.A.: University of Florida Institutional Repository.

Ma, C., Foster, D. A., Mueller, P. A., and Dutrow, B. L., 2017, Magma-facilitated transpressional strain partitioning within the Sawtooth metamorphic complex, Idaho: A zone accommodating Cretaceous orogen-parallel translation in the Idaho batholith: Tectonics, v. 36, no. 3, p. 444-465.

Marfunin, A. d. S., 1979, Spectroscopy, luminescence and radiation centers in minerals, Springer Science & Business Media.

Metz, K., 2010, Metamorphic rocks in the Sawtooth Mountains: LSU Master's Theses, no. 2957.

Miller, C. F., McDowell, S. M., and Mapes, R. W., 2003, Hot and cold granites? Implications of zircon saturation temperatures and preservation of inheritance: Geology, v. 31, no. 6, p. 529-532.

Paces, J. B., and Miller Jr, J. D., 1993, Precise U-Pb ages of Duluth complex and related mafic intrusions, northeastern Minnesota: Geochronological insights to physical, petrogenetic, paleomagnetic, and tectonomagmatic processes associated with the 1.1 Ga midcontinent rift system: Journal of Geophysical Research: Solid Earth, v. 98, p. 13997-14013.

Paton, C., Hellstrom, J., Paul, B., Woodhead, J., and Hergt, J., 2011, Iolite: Freeware for the visualisation and processing of mass spectrometric data: Journal of Analytical Atomic Spectrometry, v. 26, no. 12, p. 2508-2518.

Paton, C., Woodhead, J. D., Hellstrom, J. C., Hergt, J. M., Greig, A., and Maas, R., 2010, Improved laser ablation U-Pb zircon geochronology through robust downhole fractionation correction: Geochemistry, Geophysics, Geosystems, v. 11, no. 3.

Petrus, J. A., Kamber, B. S. J. G., and Research, G., 2012, VizualAge: A novel approach to laser ablation ICP-MS U-Pb geochronology data reduction: Geostandards and Geoanalytical Research, v. 36, no. 3, p. 247-270.

Reid, R. R., 1963, Reconnaissance geology of the Sawtooth Range: Idaho Bureau of Mines and Geology Pamphlet, v. 37, no. 129.

Rubatto, D., 2002, Zircon trace element geochemistry: partitioning with garnet and the link between U–Pb ages and metamorphism: Chemical geology, v. 184, no. 1-2, p. 123-138.

Scholonek, C., and Augustsson, C., 2016, Can cathodoluminescence of feldspar be used as provenance indicator?: Sedimentary geology, v. 336, p. 36-45.

Sláma, J., Košler, J., Condon, D. J., Crowley, J. L., Gerdes, A., Hanchar, J. M., Horstwood, M. S., Morris, G. A., Nasdala, L., and Norberg, N., 2008, Plešovice zircon—a new natural reference material for U–Pb and Hf isotopic microanalysis: Chemical Geology, v. 249, no. 1-2, p. 1-35.

Smith, E., 2016, Metamorphic Conditions of Aluminous Gneisses in the Sawtooth: LSU Master's Theses, no. 3964.

Thackray, G. D., Rodgers, D. W., and Streutker, D., 2013, Holocene scarp on the Sawtooth fault, central Idaho, USA, documented through lidar topographic analysis: Geology, v. 41, no. 6, p. 639-642.

Vejdemo-Johansson, M., Vejdemo, S., and Ek, C.-H., 2014, Comparing distributions of color words: Pitfalls and metric choices: PloS one, v. 9, no. 2, p. e89184.

Vermeesch, P., 2012, On the visualisation of detrital age distributions: Chemical Geology, v. 312, p. 190-194.

-, 2018, IsoplotR: A free and open toolbox for geochronology: Geoscience Frontiers, v. 9, no. 5, p. 1479-1493.

Watson, E. B., and Harrison, T. M., 1983, Zircon saturation revisited: temperature and composition effects in a variety of crustal magma types: Earth and Planetary Science Letters, v. 64, no. 2, p. 295-304.

Wotzlaw, J.-F., Schaltegger, U., Frick, D. A., Dungan, M. A., Gerdes, A., and Günther, D., 2013, Tracking the evolution of large-volume silicic magma reservoirs from assembly to supereruption: Geology, v. 41, no. 8, p. 867-870.

VITA

Kyle Tollefson was born in November 1992 in Arcadia, Wisconsin. He graduated from Cochrane-Fountain City High School in May 2011 and enrolled at the University of Wisconsin-Eau Claire as a materials science student. After taking his first geology class he added geology as a major and changed his materials science emphasis area to geomaterials.

Here he found his interest in mineralogy and petrology and switched from applied materials research to characterization of watermelon tourmaline by fourier transform infrared spectroscopy (FTIR). During this time, he served as a teaching assistant for mineralogy and petrology and completed a capstone project on his tourmaline research. He completed the requirements for the materials science degree and graduated with a Bachelor of Science in geology during August 2017.

In August 2018 Kyle entered the master's program in geology at Louisiana State University. During this time, he served as a teaching assistant for igneous and metamorphic petrology, mineralogy, structural geology, and senior field camp.

Upon graduating with his MS thesis in December of 2020, Kyle will be taking time off before pursuing a doctorate.